





# **Computational Studies on the Rearrangement Reactions of Some Biologically Relevant Radicals**

von Diplom-Chemikerin

Marija Semialjac

Von der Fakultät II  
-Mathematik und Naturwissenschaften-  
der Technischen Universität Berlin  
zur Erlangung des akademischen Grades

Doktor der Naturwissenschaften  
-Dr. rer. nat.-

genehmigte Dissertation

Promotionsausschuss:

Vorsitzender: Prof. Dr. rer. nat. Jörn Müller

Berichter: Prof. Dr. rer. nat. Dr. h.c. mult. Helmut Schwarz

Prof. Dr. rer. nat. Karola Rück-Braun

Tag der mündlichen Prüfung: 2. März 2004

Berlin 2004

D 83



*mami i tati*

*(to my parents)*



## Zusammenfassung

### *Semialjac, Marija: Computational Studies on the Rearrangement Reactions of Some Biologically Relevant Radicals*

In der vorliegenden Arbeit sind intramolekulare Umlagerungen von biologischen wichtigen Radikalen mit Hilfe von theoretischen Methoden untersucht worden.

(I) Die Ionisierung von Valeramid und die sich daran anschließende Umlagerung bzw. Fragmentierung des Radikalkations wurden mit quantenchemischen Methoden untersucht. Die energetisch bevorzugte Umlagerung umfasst zunächst eine  $\gamma$ -C–H Bindungsaktivierung mit anschließender McLafferty-Umlagerung. Die anderen energetisch tiefliegenden Kanäle beginnen mit einer  $\beta$ -C–H und  $\delta$ -C–H Bindungsaktivierung und führen zu spezifischen Umlagerungen, die ebenfalls im Detail analysiert worden sind. Trotz vieler Übereinstimmungen zwischen den theoretischen und experimentellen Ergebnissen, konnten statische Rechnungen keine Erklärung für den ungewöhnlichen Temperatureffekt des Dissoziationskanals des Valeramid-Radikalkations liefern, der in massenspektrometrischen Experimenten festgestellt wurde. Deswegen wurden molekulardynamische Rechnungen nach Car-Parrinello durchgeführt, und zwei Erklärungsmöglichkeiten für den ungewöhnlichen Temperatureffekt konnten vorgeschlagen werden.

(II) Die Umlagerung von 2-Aminoethanol, die von Coenzym B<sub>12</sub>-abhängiger Ethanolamin-Ammonia-Lyase katalysiert wird, ist mit theoretischen Methoden untersucht worden. Zwei Hauptumlagerungswege, die über freie Radikale verlaufen, wurden detailliert analysiert, und nur die direkte Migration der protonierten Aminogruppe und die direkte Eliminierung des Ammoniumions haben sich als mögliche Wege der 2-Aminoethanol-Deaminierung herausgestellt. Der Einfluss des aktiven Zentrums des Enzyms auf die Energetik der Umlagerung wurde ebenfalls untersucht, wobei die Wechselwirkung zwischen dem Substrat und einigen Aminosäuren (Asp/Glu und His) modelliert wurde. Unabhängig von der Natur des die NH<sub>2</sub>-Gruppe protonierenden Moleküls, ist die intramolekulare Migration der NH<sub>3</sub>-Gruppe energetisch günstiger als die Eliminierung von NH<sub>4</sub><sup>+</sup>. Partielle Protonierung wie auch eine partielle Deprotonierung der OH-Gruppe des Substrats verlaufen „katalytisch“, da alle berechneten Aktivierungsenthalpien niedriger sind als die für die Umlagerung des „freien“ Substrats. Trotzdem überschreiten sie die Aktivierungsenthalpie des geschwindigkeitsbestimmenden Schrittes (d.h. die Wasserstoffabstraktion aus 5'-Deoxyadenosin durch das Produktradikal). Nur im Fall eines synergistischen Zusammenspiels von partieller Protonierung der NH<sub>2</sub>-Gruppe und partieller Deprotonierung der OH-Gruppe mit den zwei möglichen katalytischen Hilfsgruppen (Asp/Glu und His) ist die Aktivierungsenthalpie kompatibel mit den experimentellen Ergebnissen. Ein solches synergistisches Zusammenspiel von zwei katalytischen Gruppen ist in dem physiologisch realistischen pH-Bereich 6 – 9.5 möglich. Im Gegensatz zur oben genannten Umlagerungsreaktion ist für die die Gesamtreaktion einleitende Wasserstoffabspaltung aus 2-Aminoethanol durch das 5'-Deoxyadenosylradikal bereits eine partielle Protonierung ausreichend, um die Aktivationsbarriere genügend abzusenken.





## Abstract

### ***Semialjac, Marija: Computational Studies on the Rearrangement Reactions of Some Biologically Relevant Radicals***

Methods of computational chemistry are used to investigate rearrangement reaction of biologically relevant radicals:

(I) The ionization of valeramide, its subsequent rearrangements and further fragmentations of the radical cation are studied by quantum-chemical methods. The energetically preferred rearrangement route involves initial  $\gamma$ -C–H bond activation that proceeds into the McLafferty rearrangement. Other, low-lying channels commence via  $\beta$ -C–H and  $\delta$ -C–H bond activations, respectively, leading to specific fragmentation reactions, which are analyzed in detail. Even though these theoretical results agree nicely with the experimental data in many respects, they do not provide a rationalization for the unusual temperature effect on the dissociation pattern of ionized valeramide as observed in mass spectrometric experiments. Therefore, Car-Parrinello molecular dynamics studies of neutral and ionized valeramide were performed, which have provided two rationals for the puzzling experimental results.

(II) The rearrangement of 2-aminoethanol as catalyzed by coenzyme B<sub>12</sub> dependent ethanolamine ammonia lyase is investigated by computational means employing DFT and *ab initio* molecular orbital theory. Two major types of rearrangements involving free radical intermediates as well as their protonated forms are discussed in detail. Only the direct migration of the protonated amine group and the direct loss of an ammonium ion represent feasible pathways of 2-aminoethanol deamination as catalyzed by the enzyme. Further, the influence of the enzyme's active site on the rearrangement barrier is investigated, in that the interactions of the substrate with conceivable amino acids (Asp/Glu and His) are considered. Irrespective of the nature of the protonating species at the amino group of the substrate, intramolecular migration of the NH<sub>3</sub> group is energetically less demanding than elimination of NH<sub>4</sub><sup>+</sup>. The partial protonation as well as the partial deprotonation of the substrate's OH-group was shown to act catalytically because all computed activation enthalpies are lower than the barrier computed for the rearrangement of the "free" substrate; however, they exceed the activation enthalpy for the rate determining step, i.e. the hydrogen abstraction from 5'-deoxyadenosine by the product radical. Only for the synergistic interplay of partial protonation of the NH<sub>2</sub> group and partial deprotonation of the OH group by the two conceivable catalytic auxiliaries Asp/Glu and His, the activation enthalpy is compatible with the experimental data. This synergistic action of the two catalytic groups is expected to take place in a physiologically realistic pH range of 6 – 9.5. In contrast to the rearrangement reactions, where the synergistic effects of *two* auxiliaries are essential to pull the barrier below the upper limit, for the initial hydrogen abstraction from 2-aminoethanol by the 5'-deoxyadenosyl radical only a partial protonation of the substrate suffices.



## **Acknowledgments**

*First of all I would like to thank my supervisor, Prof. Dr. h.c. mult. Helmut Schwarz, for giving me the opportunity to do my Ph.D. in his group. I want to especially thank him for the independence in choosing my own subject of research, as well as for many fruitful discussions, which greatly contributed to my scientific work. I am as well grateful to Prof. Dr. Karola Rück-Braun for being the second examiner.*

*The Schering Research Foundation is gratefully acknowledged for a fellowship and the Konrad-Zuse Zentrum for the generous allocation of computer time.*

*In addition, I would like to thank Prof. Michele Parrinello (CSCS, Switzerland) for the opportunity to learn the Car-Parrinello molecular dynamics technique in his group and Dr. Daniel Aktah who introduced me to the CPMD method.*

*My thanks are due to Dr. Detlef Schröder for his support and many useful scientific discussions. I am very grateful to Dipl.-Chem. Jessica Loos, Dipl.-Chem. Claudia Trage and M.Sc. Mark Fitzgerald for their proofreading of this thesis. Special thanks go to Dipl.-Chem. Jessica Loos and Dr. Detlef Schröder for performing numerous mass-spectrometric experiments on valeramide that actually inspired my further theoretical investigations. Dr. Thomas Weiske's maintenance of the windows-computer systems is gratefully appreciated, as well as Dr. Martin Diefenbach's help with the Linux computers. All other members of the group I want to thank for making my graduate studies a real pleasure.*

*Last, but not least, I would like to thank my parents and Christian for all one can think of.*



## TABLE OF CONTENTS

|  |           |
|--|-----------|
| <b>1. INTRODUCTION.....</b>  | <b>1</b>  |
| <b>2. THEORETICAL APPROACH.....</b>  | <b>5</b>  |
| 2.1. QUANTUM-CHEMICAL METHODS .....  | 5         |
| 2.1.1. The Schrödinger Equation in the Born-Oppenheimer Approximation .....        | 5         |
| 2.1.2. Hartree-Fock Self-Consistent Field .....                                    | 7         |
| 2.1.3. Molecular Orbitals.....   | 9         |
| 2.1.4. Electron Correlation Methods.....   | 10        |
| 2.2. DENSITY FUNCTIONAL THEORY .....   | 12        |
| 2.2.1. The Hohenberg-Kohn Theorem.....   | 12        |
| 2.2.2. The Kohn-Sham Equations.....  | 12        |
| 2.2.3. Local Density Approximation (LDA).....                                      | 14        |
| 2.2.4. Generalized Gradient Approximation (GGA).....                               | 14        |
| 2.3. CAR-PARRINELLO MOLECULAR DYNAMICS .....                                       | 15        |
| <b>3. THEORETICAL EXPLORATION OF THE VALERAMIDE POTENTIAL-ENERGY SURFACE....</b>   | <b>21</b> |
| 3.1. BACKGROUND OF THE INVESTIGATION .....   | 21        |
| 3.2. SECTOR MASS SPECTROMETRIC AND PHOTOIONIZATION EXPERIMENTS .....               | 21        |
| 3.3. COMPUTATIONAL METHODS .....   | 23        |
| 3.4. COMPUTATIONAL ACCURACY .....  | 24        |
| 3.5. CONFORMATIONAL ANALYSIS OF NEUTRAL AND IONIZED VALERAMIDE .....               | 26        |
| 3.6. ADIABATIC AND VERTICAL IONIZATION OF VALERAMIDE .....                         | 27        |
| 3.7. UNIMOLECULAR DISSOCIATIONS OF IONIZED VALERAMIDE .....                        | 29        |
| 3.7.1. $\gamma$ -C-H Bond Activation ( $C_3$ -route) .....                         | 30        |
| 3.7.2. $\delta$ -C-H Bond Activation ( $C_2$ -route).....                          | 33        |
| 3.7.3. $\beta$ -C-H Bond Activation ( $C_1$ -route).....                           | 36        |
| 3.7.4. $\alpha$ -C-H Bond Activation (keto/enol tautomerism) .....                 | 36        |
| 3.7.5. Exit Channels.....  | 37        |
| 3.8. COMPARISON WITH LITERATURE THERMOCHEMISTRY .....                              | 40        |
| 3.9. IMPLICATIONS FOR THE FRAGMENTATION BEHAVIOR OF IONIZED VALERAMIDE .....       | 41        |
| 3.10. CONCLUSIONS.....   | 42        |
| <b>4. TEMPERATURE EFFECT ON THE DISSOCIATION PATTERN OF IONIZED VALERAMIDE ...</b> | <b>44</b> |
| 4.1. AN UNPRECEDENTED TEMPERATURE EFFECT ON THE $C_3/C_2$ BRANCHING RATIO.....     | 44        |
| 4.2. RATIONALIZATION OF THE TEMPERATURE EFFECT ON THE DISSOCIATION PATTERN:        |           |
| CAR – PARRINELLO MOLECULAR DYNAMICS STUDY .....                                    | 47        |
| 4.3. COMPUTATIONAL METHODS .....   | 48        |
| 4.4. NEUTRAL VALERAMIDE.....   | 49        |
| 4.5. VALERAMIDE RADICAL CATION.....  | 52        |
| 4.5.1. Simulations at 300 K .....  | 52        |

|  |            |
|--|------------|
| 4.5.2. Simulations at 500 K.....   | 57         |
| 4.6. CONCLUSIONS .....   | 60         |
| <b>5. REARRANGEMENT OF AMINOETHANOL AS CATALYZED BY THE VITAMIN</b>  |            |
| <b>B<sub>12</sub>-DEPENDENT ETHANOLAMINE AMMONIA LYASE.....</b>  | <b>65</b>  |
| 5.1. MIGRATION VS. ELIMINATION OF THE (PROTONATED) AMINO GROUP.....  | 65         |
| 5.2. COMPUTATIONAL METHODS .....   | 67         |
| 5.3. AMINOETHANOL.....   | 69         |
| 5.4. INTRAMOLECULAR MIGRATION .....  | 71         |
| 5.4.1. Dissociation-association Mechanism .....  | 72         |
| 5.4.2. Sequential Intramolecular Isomerizations .....  | 73         |
| 5.4.3. One-step Migration of NH <sub>2</sub> /NH <sub>3</sub> .....  | 74         |
| 5.5. DISSOCIATION PATHWAYS.....  | 75         |
| 5.5.1. Elimination of the NH <sub>x</sub> (x = 2, 3) Group as the Initial Step .....                         | 76         |
| 5.5.2. O-H Bond Cleavage as the Initial Step .....   | 77         |
| 5.5.3. Direct Ammonia/Ammonium Eliminations .....  | 77         |
| 5.6. FORMATION OF ETHANAL .....  | 79         |
| 5.7. REACTION ENTHALPIES – A COMPARISON OF CALCULATED AND EXPERIMENTAL VALUES .....                          | 81         |
| 5.7. SUMMARY AND CONCLUSIONS .....   | 82         |
| <b>6. HIS AND ASP/GLU ACTING SIMULTANEOUSLY AS CATALYTIC AUXILIARIES.....</b>                                | <b>84</b>  |
| 6.1. COMPUTATIONAL METHODS .....   | 86         |
| 6.2. MIGRATION VS. ELIMINATION .....   | 87         |
| 6.2.1. Hydroxonium and Ammonium Ions as Protonating Groups .....   | 87         |
| 6.2.2. Active Site – What is the Most Probable pH? .....   | 90         |
| 6.2.3. His Serving as a Proton Donor.....  | 92         |
| 6.2.4. Asp/Glu Serving as Proton Donors .....  | 94         |
| 6.2.5. Résumé .....  | 97         |
| 6.3. INFLUENCE OF THE OH GROUP CONFORMATION ON THE MIGRATORY APTITUDE.....                                   | 98         |
| 6.4. ACETIC ACID AND IMIDAZOLE – MORE RELIABLE MODEL SYSTEMS FOR ASP/GLU AND HIS .....                       | 102        |
| 6.5. PULL MECHANISM.....   | 104        |
| 6.6. SYNERGISTIC ACTION OF TWO CATALYTIC AUXILIARIES .....   | 107        |
| 6.7. SUMMARY AND CONCLUSIONS .....   | 110        |
| <b>7. A HYDROGEN ABSTRACTION FROM 2-AMINOETHANOL BY A MODEL SYSTEM FOR THE 5'-DEOXYADENOSYL RADICAL.....</b> | <b>113</b> |
| 7.1. COMPUTATIONAL METHODS .....   | 115        |
| 7.2. HYDROGEN ABSTRACTION SCENARIOS FROM AMINOETHANOL BY 1,5-DIDEOXYRIBOSE-5-YL RADICAL ...                  | 117        |
| 7.2.1. Non-protonated Substrate.....   | 119        |
| 7.2.2. Fully Protonated Substrate .....  | 120        |
| 7.2.3. Partially Protonated Substrate.....   | 122        |
| 7.2.4. Substrate Captured by Two Amino Acids from the Active Site.....                                       | 123        |

|  |            |
|--|------------|
| 7.3. CONCLUSIONS.....                  | 125        |
| <b>8. CONCLUSIONS AND OUTLOOK.....</b> | <b>127</b> |
| <b>9. SUPPORTING MATERIAL.....</b>     | <b>131</b> |
| APPENDIX I.....                        | 131        |
| APPENDIX II .....                      | 133        |
| APPENDIX III .....                     | 140        |
| <b>10. REFERENCES AND NOTES .....</b>  | <b>141</b> |
| <b>PUBLICATION INDEX .....</b>         | <b>155</b> |
| <b>CURRICULUM VITAE.....</b>           | <b>157</b> |





# 1. Introduction

Understanding the properties and functions of important biochemical species, ranging from small biological signaling agents up to enzymes as well as the processes in which these are involved, has been for a long time of great interest for the scientific community. The last couple of decades brought rapid methodological improvements in the ability to identify, isolate and characterize biological molecules resulting eventually in one of the most fascinating discoveries, i.e. the elucidation of the human genome. However, despite fast developments of the experimental techniques, many biologically relevant problems are very difficult if not impossible to investigate only by experimental means because of short life-times and/or high reactivities of the often elusive intermediates, especially in the case of the elucidation of detailed mechanisms of the enzymatic reactions. Recently, theoretical/computational chemistry has undergone great expansion owing to the development of more powerful computers as well as of new theoretical methods and algorithms with the consequence that computational methods present a welcome and useful complement to experiment, and in most of the cases this information is provided at much lower cost. Quite clearly, it is the synergy between theory and experiment that brings us closer in answering important (bio)chemical questions.

In this Thesis computational methods were employed in order to investigate some biologically relevant radicals and processes in which these species are involved. After a brief presentation of the theoretical methods used, in the first part of the thesis, we will deal with valeramide, which presents a model system for the investigation of higher amides (and peptides). The second part is dedicated to an interesting enzyme, the vitamin B<sub>12</sub> dependent ethanolamine ammonia lyase, and its catalytic activity in a seemingly simple rearrangement process.

The interest in *valeramide* is based on the fact that this molecule belongs to an important class of compounds, i.e. amides, and further, being a relatively small model system, it enables extensive computational investigation at relatively high levels of theory.

The presence of the -CO-NH- bond in many molecules of biological relevance makes amides a group of compounds of paramount importance for living organisms. Further, recent studies have shown that primary fatty acid amides constitute a novel class of mammalian hormones and neuromodulators.<sup>1</sup> In particular, oleamide (*cis*-9-

octadeceneamide) induces physiological sleep upon intravenous injection,<sup>2</sup> potentiates serotonin receptor subtypes,<sup>3</sup> and inhibits gap cell communication.<sup>4</sup> It is clear that fatty acid amides play a yet unknown, but important role in normal neurological processes and therefore, abnormal levels of fatty acid amides can be diagnostic for those diseases. Besides oleamide, several other fatty acid amides have been shown to exhibit hormon-like activity.<sup>5</sup>

It is well-known that, as reactive species, free radicals interact readily with many physiologically important substances in the human body, resulting in cell damage and hence various diseases.<sup>6</sup> Lipids of biological membranes, especially those from the brain cells, contain easily oxidizable polyunsaturated fatty acids, and thus are particularly affected. Moreover, free radicals are implicated in the aging process as well as in some severe afflictions such as the Alzheimer, the Parkinson disease, arthritis, myocardial infarction, arteriosclerosis, and cancer.<sup>7</sup> Because of the cellular damage caused by the free radical impact, many substances have been studied to uncover details of the radical scavenging properties, and some amides were shown to be successful in this sense as well. By varying both the acid and amine part of the amides, for example chroman amide, has been synthesized and its radical-scavenging abilities have been found to make it one of the most potent compounds.<sup>8</sup>

The elucidation of questions concerning the reaction mechanisms of amide rearrangements upon chemical activation and electron transfer might hopefully lead to a better understanding of biological systems. As a result of radiation or oxidative damage, an intramolecular hydrogen atom transfer occurs in peptide and in protein radicals.<sup>9</sup> The investigation of rearrangements of smaller amides (e.g. valeramide) may help to uncover some of the interesting molecular features and thus aid in understanding some of the processes that result in serious degenerations. In this thesis the rearrangement pathways of valeramide radical cation have been investigated by theoretical means and the results are presented in Chapters 3 and 4.

Another interesting system, which also forms a subject of this Thesis, is *ethanolamine ammonia lyase*; its catalytic activity is discussed in detail in Chapters 5, 6 and 7. Ethanolamine ammonia lyase is a coenzyme B<sub>12</sub> dependent enzyme that catalyzes the rearrangement of 2-aminethanol into ethanal and ammonia. Even though this enzyme can be found only in bacteria, because of the pronounced structural and functional similarities between all coenzyme B<sub>12</sub> dependent enzymes, the insight gained by studying

this particular system might be useful in explaining the action of other coenzyme B<sub>12</sub> dependent enzymes as well. The specific catalytic activity of these enzymes is due to the presence of a cofactor common to all of them, i.e. the coenzyme B<sub>12</sub>.

Coenzyme B<sub>12</sub> is a naturally occurring organometallic compound that contains a unique Co-C  $\sigma$ -bond, and it serves as one of the most important cofactors for enzymatic radical reactions. Since Barker's discovery in 1958 of the light sensitive coenzyme form of the vitamin B<sub>12</sub> related corrinoid for the interconversion of glutamate into 3-methylaspartate,<sup>10</sup> coenzyme B<sub>12</sub> has fascinated many scientists in various research fields by its peculiar function that itself is based on its particular structure (Figure 1.1).

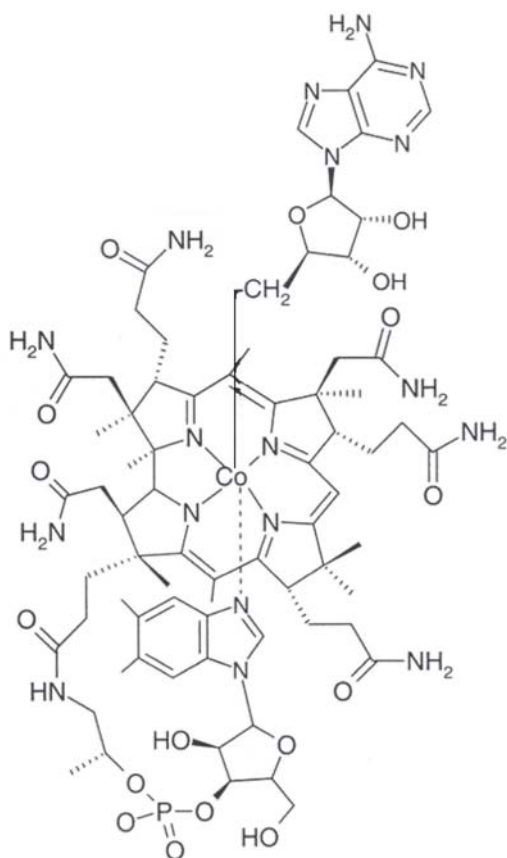
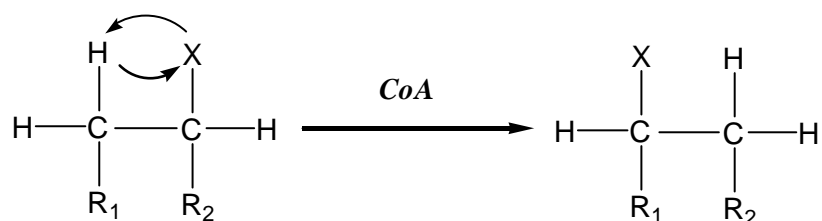


**Figure 1.1.** Coenzyme B<sub>12</sub>.

The paradigm of action of B<sub>12</sub> dependent enzymes was put forth in the 60-ties,<sup>11</sup> and about 10 enzymes requiring coenzyme B<sub>12</sub> were reported to catalyze carbon skeleton rearrangements, heteroatom eliminations and intramolecular amino group migrations. From biochemical studies on ethanolamine ammonia lyase<sup>12</sup> and diol dehydrase<sup>13</sup> a minimal mechanism of action was established, which has now been accepted as a general mechanism for other B<sub>12</sub> dependent enzymes that catalyze rearrangement reactions, and in which a hydrogen atom exchanges place with a moiety X of the substrate in a formal dyotropic rearrangement (Scheme 1.1). However, most of the essential details concerning the enzymatic catalysis remained unclear because the tree-dimensional

structures of B<sub>12</sub> dependent enzymes were not available until recently, when for some of them the X-ray structure has been determined. Nevertheless, many questions concerning catalysis and the role of the coenzyme B<sub>12</sub> remain still open, e.g. how the enzymes form radicals in the active site, and in which way they control highly reactive species like radicals in the active site. These questions are essential from the perspective of the

enzymatic mechanism not only for the coenzyme B<sub>12</sub> dependent enzymes but as well for all other enzymes that catalyze reactions in which radicals are involved.



| X                        | R <sup>1</sup>     | R <sup>2</sup> | Substrate            | Enzyme                            |
|--------------------------|--------------------|----------------|----------------------|-----------------------------------|
| CO-SCoA                  | H                  | COOH           | Methylmalonyl-CoA    | <i>Methylmalonyl-CoA mutase</i>   |
| C(=CH <sub>2</sub> )COOH | H                  | COOH           | 2-Methyleneglutarate | <i>Methyleneglutarate mutase</i>  |
| CH(NH <sub>2</sub> )COOH | H                  | COOH           | (S)-Glutamate        | <i>Glutamate mutase</i>           |
| NH <sub>2</sub>          | OH                 | H              | 2-Aminoethanol       | <i>Ethanolamine ammonia lyase</i> |
| OH                       | CH <sub>3</sub>    | OH             | Propane-1,2-diol     | <i>Diol dehydratase</i>           |
| OH                       | CH <sub>2</sub> OH | OH             | Glycerol             | <i>Glycerol dehydratase</i>       |

**Scheme 1.1.** Rearrangement reactions catalyzed by the coenzyme B<sub>12</sub> dependent enzymes.

## 2. Theoretical Approach

### 2.1. Quantum-chemical Methods<sup>14</sup>

Quantum chemical methods are based on the postulates of Quantum Mechanics, according to which a system is fully described by a wavefunction that can be found by solving the Schrödinger equation. This equation relates the stationary states of the system and their energies to the Hamiltonian operator, which can be viewed as a recipe for obtaining the energy associated with a wavefunction describing the positions of the nuclei and electrons in the system. However, in practice the Schrödinger equation cannot be solved exactly. Already for a system that contains only 3 particles approximations have to be made in order to make the method applicable. Nevertheless, the approach is called "ab initio" since it makes no use of empirical information, except for the fundamental constants of nature such as the mass of an electron, Planck's constant, etc. In spite of the necessary approximations, ab initio theory has the conceptual advantage of generality, and the practical advantage that its successes, limitations and failures are predictable.

The major disadvantage of ab initio quantum chemistry is the heavy demand on computer power. Therefore, further approximations have been applied, which led to a number of semi-empirical quantum chemical methods that can be applied to larger systems. However, compared with ab initio calculations their reliability is lower and their applicability is limited by the requirement for empirical parameters.

#### 2.1.1. The Schrödinger Equation in the Born-Oppenheimer Approximation

The energies and wavefunctions of stationary states of a system are given by the solutions of the Schrödinger Equation, Eq. (2.1):

$$\hat{H}\Psi_{e,n} = E\Psi_{e,n} \quad (2.1)$$

A wavefunction  $\Psi$  is one of the solutions of the eigenvalue equation and depends on the coordinates of the electrons and the nuclei.  $\hat{H}$  is the Hamiltonian operator, which gives the kinetic and potential energies of a system consisting of atomic nuclei and electrons. The

Hamiltonian is composed of three parts (see Eq. (2.2)): the kinetic energy of the nuclei, the kinetic energy of the electrons, and the potential energy of nuclei and electrons.

$$\hat{H} = \hat{T}_n + \hat{T}_e + \hat{V}_{e,n} \quad (2.2)$$

Two approximations are commonly made:

(i) time-independence, where only states stationary in time are concerned and relativistic effects are neglected. This is warranted unless the velocity of the electrons approaches the speed of light, which is the case only in heavy atoms.

(ii) Born-Oppenheimer approximation; which makes a separation of the motion of nuclei and electrons. The Born-Oppenheimer approximation implies the separation of nuclear and electronic wavefunctions, where the total wavefunction is presented as a product of the two parts, Eq. (2.3):

$$\Psi_{e,n} = \chi_e \Psi_n \quad (2.3)$$

The idea behind this approximation is that the electrons, being much lighter than the nuclei, can easily follow the nuclear motion. Therefore, the electronic wavefunction  $\psi_e$  can be obtained by solving the electronic Schrödinger equation (2.4):

$$\hat{H}_e(R_n)\psi(r_e) = E_e(R_n)\psi(r_e) \quad (2.4)$$

which contains positions of the nuclei, however not as variables but as parameters. The electronic Hamiltonian contains three terms: kinetic energy, electrostatic interaction between electrons and nuclei, and electrostatic repulsion between electrons, Eq. (2.5).

$$\hat{H}_e = -\frac{1}{2} \sum_{i=1}^n \Delta_i - \sum_{i=1}^n \sum_{A=1}^N \frac{Z_A}{|R_A - r_i|} + \sum_{i < j}^n \frac{1}{r_{ij}} \quad (2.5)$$

The total energy in the Born-Oppenheimer model is obtained by adding the nuclear repulsion energy to the electronic energy, Eq. (2.6):

$$E_{tot} = E_e + E_n \quad (2.6)$$

where

$$E_n = \sum_{A < B}^N \frac{Z_A Z_B}{|R_A - R_B|} \quad (2.7)$$

The total energy defines a potential energy hypersurface, which can be used to subsequently solve the Schrödinger equation for the nuclear motion, Eq. (2.8):

$$[\hat{T}_n + V(R_n)]\Phi(R_n) = \mathcal{E}_i \Phi(R_n) \quad (2.8)$$

### 2.1.2. Hartree-Fock Self-Consistent Field

The electronic Hamiltonian contains two terms that act on one electron at a time: the kinetic energy and the electron-nucleus attraction (Eq. (2.9)), and a term that describes the pairwise repulsion of electrons (Eq. (2.10)):

$$\hat{H}^1 = \sum_i^n \hat{H}_i^1 = -\frac{1}{2} \sum_{i=1}^n \Delta_i - \sum_{i=1}^n \sum_{A=1}^N \frac{Z_A}{|R_A - r_i|} \quad (2.9)$$

$$\hat{H}^2 = \sum_{i < j}^n \hat{H}_{ij}^2 = \sum_{i < j}^n \frac{1}{r_{ij}} \quad (2.10)$$

The latter depends on the coordinates of two electrons at the same time, and has turned out to be a practical computational bottleneck, which can be overcome only for very small systems. To avoid this problem the independent particle approximation is introduced, in which the interaction of each electron with all the others is treated in an average way, Eq. (2.11).

$$\hat{H}^2 = \sum_{i < j}^n \hat{H}_{ij}^2 = \sum_i^n \hat{V}_i^{av} \quad (2.11)$$

The Schrödinger equation, which initially depended on the coordinates  $\chi$  (representing spatial and spin coordinates) of all electrons, can be reduced to a set of equations (Hartree-Fock equations, Eqs. (2.12) and (2.13)):

$$\sum_{i=1}^n (\hat{H}_i^1 + \hat{V}_i^{av}) \psi(x_1, x_2, \dots, x_n) = E \psi(x_1, x_2, \dots, x_n) \quad (2.12)$$

$$(\hat{H}_i^1 + \hat{V}_i^{av}) \phi_i(x_1) = \hat{F}_i \phi_i(x_1) = \varepsilon_i \phi_i(x_1) \quad (2.13)$$

The wavefunctions  $\phi_i(x_1)$  present one-electron spin-orbitals. For each electron the potential due to all other electrons has to be determined, however it is initially unknown. In practice trial orbitals are used and iteratively modified until a self-consistent solution ("Self-Consistent Field") is obtained, which is a solution of the Hartree-Fock equations. The eigenvalues  $\varepsilon_i$  are interpreted as orbital energies.

In addition to being a solution of the electronic Schrödinger equation, the wavefunction must be normalized and must satisfy the Pauli principle. The normalization condition (Eq. (2.14)) is connected with the interpretation of the wavefunction as a distribution function, which when integrated over entire space should give a value of one:

$$\int \psi^* \psi dx = 1 \quad (2.14)$$

The Pauli principle states that the wavefunction must change sign when two independent electronic coordinates are interchanged, Eq. (2.15):

$$\psi(x_1, x_2, \dots, x_i, \dots, x_k, \dots, x_n) = -\psi(x_1, x_2, \dots, x_k, \dots, x_i, \dots, x_n) \quad (2.15)$$

An important property of the SCF method is that its solutions satisfy the Variation Principle (Eq. (2.16)), which states that the expectation value of the energy evaluated with an inexact wavefunction is always higher than the exact energy:

$$E_\psi = \frac{\langle \psi | H | \psi \rangle}{\langle \psi | \psi \rangle} \geq E_{\psi_{exact}} \quad (2.16)$$

As a consequence the lowest energy is associated with the best approximate wavefunction and therefore, the energy minimization is equivalent with the wavefunction optimization.



A common way of representing the electronic wavefunction is a Slater determinant (Eq. (2.17)) that contains spin-orbitals ( $\varphi_i$ ), which are dependent on the spatial and spin coordinates of an electron:

$$\Psi_n = n^{-1/2} \left| \varphi_1 \varphi_2 \dots \varphi_n \right| \quad (2.17)$$

The energies of Slater determinants from a Hartree-Fock calculation are readily expressed in one- and two-electron integrals and according to this notation ground state energy can be represented as:

$$E = \sum_i^{occ} H_{ii}^1 + \sum_{i<j}^{occ} [(ii|jj) - (ij|ij)] \quad (2.18)$$

where

$$H_{ii}^1 = \langle i | \hat{H}_i^1 | j \rangle = \int \varphi_i^*(x_i) \hat{H}_i^1 \varphi_j(x_i) dx_i \quad (2.19)$$

$$(ij|kl) = \iint \varphi_i^*(x_1) \varphi_j^*(x_1) \frac{1}{r_{12}} \varphi_k(x_2) \varphi_l(x_2) dx_1 dx_2 \quad (2.20)$$

The two-electron integral  $(ii|jj)$  describes the repulsion between two electrons each localized in one orbital (Coulomb integral), while for the  $(ij|ij)$  integral (exchange integral) a classical description cannot be given.

### 2.1.3. Molecular Orbitals

Molecular orbitals  $\phi_i$  are usually represented as a linear combination of atomic orbitals  $\varphi_\mu$  (LCAO), Eq. (2.21):

$$\phi_i = \sum_{\mu=1}^N c_{i\mu} \varphi_\mu \quad (2.21)$$

The expansion of the wavefunction in terms of basis functions leads to a limitation of the accuracy of the ab initio Hartree-Fock approach only because of the limited number of basis functions available. The greater the number of basis functions (provided they are well chosen) the better the wavefunction, consequently, the lower the energy. However, the

two-electron integrals (Eq. (2.20)) over atomic basis functions give rise to a major practical problem in the application of the ab initio HF method since a large number of basis functions is required for a reasonable quality calculation, resulting in a very large number of two-electron integrals. The limit of an infinite basis set is known as the Hartree-Fock limit; however, even at the Hartree-Fock limit the obtained energy is still greater than the exact energy that follows from the Hamiltonian because of the independent particle approximation that the theory assumes. In order to overcome this shortcoming, as the post Hartree-Fock methods have been introduced (see further in text).

The basis orbitals used in practical calculations are mostly atom-centered functions that resemble orbitals of isolated atoms. The radial part of such orbitals is an exponentially decaying function. Basis orbitals of this type are called Slater-type orbitals (STO; Eq. (2.22)). However, for practical calculations they have the disadvantage that evaluation of two-electron integrals involving such functions is time-consuming. Therefore, these orbitals are approximated by a linear combination of Gaussian basis functions (GTO; Eq. (2.23)):

$$\varphi^{STO} \approx \sum_{v=1}^n k_n \varphi_v^{GTO} \quad (2.22)$$

$$\varphi(r) = e^{-\alpha r^2} \quad (2.23)$$

The functional form of GTO (Gaussian-type orbital) is different from the atomic orbitals, especially in the vicinity of the nucleus and therefore, a combination of several GTO's with different exponents  $\alpha$  is necessary to give a reasonable basis orbital. The exponents  $\alpha$  and contraction coefficients  $k$  can be determined in different ways, e.g. by fitting to an STO or by optimizing the energy in ab initio calculations on atoms and small molecules. Once these values are determined, they define a standard basis set.

#### 2.1.4. Electron Correlation Methods

The Hartree-Fock method, even at its limit, has a limitation in accuracy due to the independent particle approximation that the theory uses, where the instantaneous correlation of the motions of electrons is neglected. The correlation energy, which is a

difference between the exact energy (determined by the Hamiltonian) and the HF energy, may be important in order to obtain chemically relevant answers from computations. Several approaches were developed in order to account for the correlation energy (post-HF methods), such as (i) Configuration Interaction (CI), (ii) Møller-Plesset (MP) Perturbation Theory and (iii) Multi-Configuration SCF (MCSCF or CASSCF).

(i) In the Configuration Interaction (CI) method a linear combination of Slater determinants is constructed, taking the unoccupied "virtual" orbitals from the SCF-calculation also into account. The total wavefunction is written as presented in Eq. (2.24):

$$\Psi = \phi_{HF} + \sum_{ij} c_{ij}^S \phi_i^j + \sum_{ijk} c_{ijk}^D \phi_{ij}^{kl} + \dots \quad (2.24)$$

In principle, the exact correlation energy can be obtained from a full CI calculation in which all possible configurations are taken into account. Unfortunately this is not possible but for the smallest systems only. Moreover, the problem is aggravated when the size of the basis set is increased on the way towards the Hartree-Fock limit. Thus, the theoretical limit of the exact (time-independent, non-relativistic) Schrödinger equation cannot be reached since even for small systems the number of excited configurations is enormously large. Therefore, a popular way to truncate the CI expansion is to consider only singly and doubly excited configurations (CI-SD).

(ii) A basic idea behind the Møller-Plesset Perturbation Theory is that the difference between the Fock operator and the exact Hamiltonian can be considered as a perturbation. Corrections can be made to any order of the energy (Eq. (2.25)) and the wavefunction (Eq. (2.26)).

$$E = E_{HF} + E^{(1)} + E^{(2)} + E^{(3)} + \dots \quad (2.25)$$

$$\Psi = \Psi_{HF} + \Psi^{(1)} + \Psi^{(2)} + \Psi^{(3)} + \dots \quad (2.26)$$

The most popular method, MP2, takes into account only a second level of correction.

(iii) Multiconfiguration SCF (MCSCF) and Complete Active Space SCF (CASSCF) are methods in which HF-orbitals are optimized simultaneously with a “small” CI. The MCSCF method requires considerable care in the selection of the basis set and especially the active space (orbitals). The MCSCF methods can be used to study problems where the Hartree-Fock method is inappropriate (e.g. for systems with low-lying excited states), or to generate a good starting wavefunction for a subsequent CI calculation. For processes in which transitions between potential energy surfaces occur, such as in photochemical reactions, the MCSCF methods are shown to be essential.

## 2.2. Density Functional Theory<sup>15</sup>

Density functional theory (DFT) is a powerful, in principle exact theory, which as a distinction from quantum chemical methods, is non-interacting and does not yield a correlated N-body wavefunction. In the Kohn-Sham DFT, the theory is the one-electron theory and shares many similarities with the Hartree-Fock theory. DFT has come to prominence over the last decade as a method potentially capable of providing very accurate results at low computational cost.

### 2.2.1 The Hohenberg-Kohn Theorem

The Hohenberg-Kohn theorem (2.27) states that if  $N$  interacting electrons move in an external potential  $V_{ext}$ , the ground-state electron density  $n_0$  minimizes the functional

$$E[n] = F[n] + \int n(r) V_{ext}(r) dx \quad (2.27)$$

where  $F$  is a universal functional of  $n$  and the minimum value of the functional  $E$  is  $E_0$ , the exact ground-state electronic energy.

### 2.2.2. The Kohn-Sham Equations

Kohn and Sham derived a coupled set of differential equations enabling the ground state density  $n_0$  to be found.  $F$  was separated into three distinct parts, so that the functional  $E$  becomes

$$E[n(r)] = T_s[n(r)] + \frac{1}{2} \iint \frac{n(r)n(r')}{|r-r'|} dr dr' + E_{xc}[n(r)] + \int n(r) V_{ext}(r) dr \quad (2.28)$$

where  $T_s$  is defined as the kinetic energy of a non-interacting electron gas with density  $n$ ,

$$T_s[n(r)] = -\frac{1}{2} \sum_{i=1}^N \int \psi_i^*(r) \nabla^2 \psi_i(r) dx \quad (2.29)$$

being not the kinetic energy of the real system. Introducing a normalization constraint on the electron density from Eq. (2.27) follows:

$$\frac{\delta}{\delta n(r)} [E[n(r)] - \mu \int n(r) dr] = 0 \quad (2.30)$$

where

$$\frac{\delta E[n(r)]}{\delta n(r)} = \mu \quad (2.31)$$

Equation (2.31) can be rewritten in terms of an effective potential,  $V_{eff}$

$$\frac{\delta T_s[n(r)]}{\delta n(r)} + V_{eff}(r) = \mu \quad (2.32)$$

where

$$V_{eff}(r) = V_{ext}(r) + \int \frac{n(r')}{|r-r'|} dr' + V_{xc}(r) \quad (2.33)$$

and

$$V_{xc}(r) = \frac{\delta E_{xc}[n(r)]}{\delta n(r)} \quad (2.34)$$

To find the ground state energy,  $E_0$ , and the ground state density,  $n_0$ , the one electron Schrödinger equation (Eq.(2.35)) should be solved self-consistently together with Eq. (2.32) and (2.33) and satisfying that the electron density is equal to the number of electrons in the system. A self-consistent solution is required due to the dependence of  $V_{eff}$  on  $n$ .

$$\left( -\frac{1}{2} \nabla^2 + V_{eff}(r) - \mathcal{E}_i \right) \psi_i(r) = 0 \quad (2.35)$$

The above equations provide a theoretically exact method for finding the ground state energy of an interacting system provided the form of  $E_{XC}$  is known. Unfortunately, the functional  $E_{XC}$  is in general unknown and in electronic structure calculations it is most commonly approximated within the local density approximation or generalized-gradient approximation.

### 2.2.3. Local Density Approximation (LDA)

In the local density approximation (LDA), the value of  $E_{XC}$  is approximated by the exchange-correlation energy of an electron in a homogeneous electron gas of the same density  $n(r)$ , i.e.

$$E_{XC}^{LDA}[n(r)] = \int \epsilon_{XC}(n(r))n(r)dr \quad (2.36)$$

The principle advantage of LDA-DFT over methods such as Hartree-Fock is that many experimentally relevant physical properties can be determined to a useful level of accuracy provided that the LDA performs well (correlation effects are well accounted for). The LDA is often surprisingly accurate for systems with slowly varying charge densities. However, the method has failed in treating several different cases; e.g. it has a tendency to favor more homogeneous systems and over-binds molecules and solids. In weakly bonded systems these errors are exaggerated and bond lengths are too short. The satisfactory performance of the LDA was shown to be a result of a real-space cancellation of errors in the LDA exchange and correlation energies.

### 2.2.4. Generalized Gradient Approximation (GGA)

For systems where the density varies slowly, the LDA tends to perform well. However, in strongly correlated systems, where an independent particle picture breaks down, the LDA fails. Further, the LDA does not account for van der Waals bonding, and gives a very poor description of hydrogen bonding.

An obvious approach to improve the LDA is to include gradient corrections, by making  $E_{XC}$  a functional of the density and its gradient:

$$E_{XC}^{GGA}[n(r)] = \int \varepsilon_{XC}(n(r))n(r)dr + \int F_{XC}[n(r), |\nabla n(r)|]dr \quad (2.37)$$

where  $F_{XC}$  is a correction chosen to satisfy one or several known limits for  $E_{XC}$ . Clearly, there is no unique recipe for  $F_{XC}$ , and several dozen functionals have been proposed in the literature. They do not always represent a systematic improvement over the LDA and results must be carefully compared against experimental findings. The development of improved functionals is currently a very active area of research and although incremental improvements are likely, it is far from clear whether the research will be successful in providing the substantial increase in accuracy desired.

### 2.3. Car-Parrinello Molecular Dynamics<sup>16</sup>

Ab initio molecular dynamics methods, in contrast to the effective force field methods, allow one to model chemical reactions that involve changes in the bonding in which electrons play a crucial role. For each molecular dynamics (MD) simulation, in which electrons are not being treated explicitly, a choice about the nature of the system has to be made a priori. However, if the bonding in the system changes due to changes in pressure, temperature or phase, the accuracy of the force-field suffers. In 1985 Car and Parrinello showed that it was possible to perform a molecular dynamics simulation whilst calculating the forces within density functional theory. For the first time in the molecular dynamics calculations electrons were treated explicitly in an ab initio way. The method proposed by Car and Parrinello works within the Born-Oppenheimer approximation; at any instant the state of the electronic system can be well described by the electronic ground-state that is being calculated for the ionic positions at that instant, and it responds instantaneously to changes in ionic positions.

The Car-Parrinello method makes use of the following classical Lagrangian (Eq. (2.38)):

$$L_{CP} = \sum_i \mu_i \langle \dot{\psi}_i | \dot{\psi}_i \rangle + \frac{1}{2} \sum_I M_I \dot{R}_I^2 - E[\{\psi_i\}, \{R_I\}] \quad (2.38)$$

to generate trajectories for the ionic and electronic degrees of freedom via the coupled set of equations of motion (Eqs. (2.39) and (2.40)):

$$M_I \ddot{R}_I^\alpha = - \frac{\partial E[\{\psi_i\}, \{R_I\}]}{\partial R_I^\alpha} = F_{CP}^\alpha \quad (2.39)$$

$$\mu_i \ddot{\psi}_i = - \frac{\partial E[\{\psi_i\}, \{R_I\}]}{\partial \psi_i} \quad (2.40)$$

where  $M_I$  and  $R_I$  are the mass and position, respectively, of atom  $I$ ,  $\psi_i$  are the Kohn-Sham orbitals which are allowed to evolve as classical degrees of freedom with inertial parameters  $\mu_i$ , and  $E$  is the Kohn-Sham energy functional evaluated for the set of ionic positions  $R_I$  and the set of orbitals  $\psi_i$ . The functional derivative of the Kohn-Sham energy in equation (2.40) is implicitly restricted to variations of  $\{\psi_i\}$  that preserve orthonormality.

The idea behind the CPMD method is that by putting the electrons to their ground state at a fixed set of ionic positions and then allowing the ions to move according to equation (2.39), the electronic orbitals should adiabatically follow the motion of the ions, performing small oscillations around the electronic ground state. The electronic orbitals will have a “fictitious” kinetic energy associated with their motion and the fictitious mass parameter,  $\mu_i$ . If  $\mu_i$  is small enough, then the motion of the orbitals will be very fast relative to the motion of the ions. It is generally believed that this motion consists of oscillations around the ground state and therefore, by choosing for  $\mu_i$  a value small enough, one can ensure that the frequency spectra of the electronic orbitals and the ions are well separated from one another if an energy gap exists between the occupied and unoccupied Kohn-Sham orbitals. Within a harmonic approximation, the lowest frequency of oscillation of the orbitals about the ground state may be written as:

$$\omega_0 = \left( \frac{2(\varepsilon_j - \varepsilon_i)}{\mu_i} \right)^{1/2} \quad (2.41)$$

where  $\varepsilon_i$  and  $\varepsilon_j$  are the eigenvalues of the highest occupied and the lowest unoccupied orbitals, respectively. Classical mechanics systems, which are well separated from each another in frequency, remain energetically isolated from one another. Therefore, by using for  $\mu_i$  a value small enough, the electrons are isolate energetically from the ions. In this



way it can be ensured that thermalization between electrons and ions does not occur and consequently, the electrons remain close to the electronic ground state, while the ions dynamics can be performed at the desired temperature.



## **I. PART**

### ***DISSOCIATION BEHAVIOR OF IONIZED VALERAMIDE***



### 3. Theoretical Exploration of the Valeramide Potential-Energy Surface\*

#### 3.1. Background of the Investigation

Amides are an important group of compounds for living organisms because of the -CO-NH- structural motif that can be found in many molecules of biological relevance. Consequently, there are numbers of publications on experimental and computational research aiming at the prediction of some of the physical and chemical properties of the peptide bond.<sup>17</sup> Structural studies of small amides aid in a better understanding of peptide bonds in biological molecules. Therefore, as a model molecule, valeramide, **1**, was chosen; this is a relatively small amide with a chain of only five carbon atoms, which nevertheless may mimic the behavior of larger amides with respect to intramolecular hydrogen migrations. The valeramide molecule is small enough to enable both extensive mass-spectrometric studies as well as adequate computational treatment of the dissociation process, out of which the McLafferty rearrangement seems the most interesting one. In the McLafferty rearrangement<sup>18,19</sup> an ionized carbonyl group of the substrate with a sufficient chain length gives rise to specific 1,5-hydrogen transfers followed by  $\beta$ -C-C bond cleavage affording an alkene and an enol. Thus, valeramide presents an ideal system for investigation of this important process.<sup>20</sup>

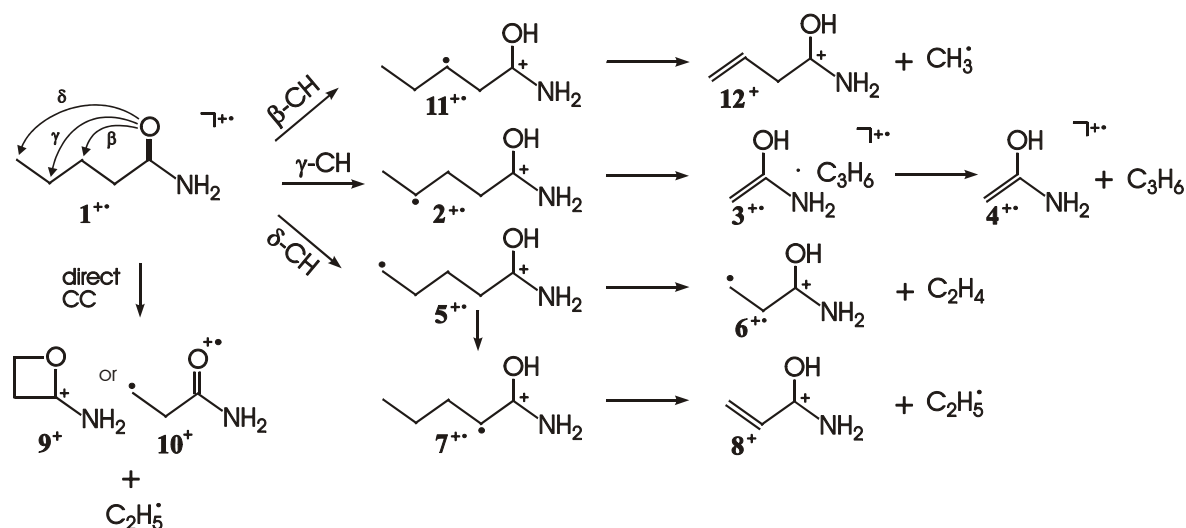
#### 3.2. Sector Mass Spectrometric and Photoionization Experiments

Unexpectedly large differences between the electron ionization and metastable ion mass spectra of hexanoic acid and also its amide has been reported by Kreft and Grützmacher.<sup>21</sup> These findings triggered further mass-spectrometric experiments aiming at a rationalization of the observed discrepancies. The dissociation behavior of ionized valeramide **1** was investigated by several experimental methods in which the electron

---

\* Results discussed in this chapter have been published in: Semialjac, M.; Loos, J.; Schröder, D.; Schwarz, H. *Int. J. Mass Spectrom.* **2002**, 214, 129.

ionization (EI), photoionization (PI), and metastable ion (MI) mass spectra were compared.<sup>22,23</sup>



**Scheme 3-1.** Dissociation pattern of ionized valeramide  $1^+$ .

Sector mass spectrometry and photoionization experiments provided an internally consistent mechanistic picture for the unimolecular dissociation of ionized valeramide. The  $\gamma$ -C-H bond activation according to the McLafferty rearrangement ( $C_3$ -route) predominates, while  $\delta$ -C-H bond activation ( $C_2$ -route) competes with it quite extensively (Scheme 3-1). At elevated energies, also  $\beta$ -C-H bond activation ( $C_1$ -route) as well as direct C(3)-C(4) bond cleavage occur. The photoionization experiments revealed that the  $C_2$ - and  $C_3$ -routes have rather low thresholds, where occurrence of the latter is observed even at the photoionization threshold. Almost all experimental results, including several mechanistic details such as the competition of direct and indirect  $C_2H_5^\bullet$  losses, are consistent within both experimental approaches. Further, the labeling distributions can be reproduced reasonably well by a kinetic modeling which explicitly includes the competition of  $C_2$ - and  $C_3$ -routes. The most interesting result of the modeling is that the kinetic isotope effects associated with the initial C-H bond activations are surprisingly small.

However, the  $C_3/C_2$  ratio shows pronounced, apparently random variations when comparing the different kinds of experiments performed. Far beyond the experimental

error margins, the  $C_3/C_2$  ratios range from almost 1 for the metastable ions formed upon EI in the sector instrument to about 4 for the metastable ions in the TPEPICO experiments.<sup>24</sup> The mechanistic analysis of both the sector-field experiments and the photoionization studies suggests that this behavior is associated with the uncoupling of these two routes.

### 3.3. Computational Methods

In order to obtain the actual energetics of the above mentioned competing processes, a theoretical insight into the behavior of ionized valeramide was desirable.

Most calculations were performed with the GAUSSIAN 98 suite of programs.<sup>25</sup> The use of density functional theory (DFT) was a natural choice because of the balance between accuracy and computational costs.<sup>26</sup> The B3LYP functional, which is a HF/DFT hybrid combining Becke's three-parameter semiempirical exchange functional (B3)<sup>27</sup> with the Lee-Yang-Parr correlation functional (LYP)<sup>28</sup>, was used throughout. Geometry optimizations were performed with Pople's polarized double- $\zeta$  6-31G\* basis set.

In order to characterize the optimized structures, frequency analysis has been performed at the same level of theory. Minima were characterized by the absence of imaginary vibrational modes, while the transition structures involved one imaginary frequency. Reaction pathways have been followed by the intrinsic reaction coordinate (IRC) calculations at the same level of theory. Because the B3LYP/6-31G\* calculations overestimate force constants, the zero-point energies (*ZPEs*) obtained at this level were scaled by 0.9805, which is the average of the factors proposed by Scott/Radom<sup>29</sup> and Wong.<sup>30</sup> The scaled *ZPEs* were used for the conversion of electronic energies to relative energies at 0 K. In order to get more reliable energetic profiles of the reactions in question, single point calculations using triple- $\zeta$  basis sets with diffuse functions included (6-311++G\*\*) were performed, and relative energies of the stationary points were calculated at the B3LYP/6-311++G\*\*//B3LYP/6-31G\* level of theory, where the *ZPEs* calculated with B3LYP/6-31G\* were used in the conversion to relative energies at 0 K.

Further, an initial screening of the conformational space of valeramide was performed with the MM2 method implemented in the Spartan program.<sup>31</sup>

### 3.4. Computational Accuracy

As far as a viable computational approach to the potential-energy surface (PES) of ionized valeramide is concerned a reasonable compromise has to be reached. Valeramide is already quite a large molecule for advanced ab initio methods, and moreover, for a proper description of the distonic ions formed as reaction intermediates the electron correlation has to be taken into account. Further, valeramide, being neutral or charged, is a rather flexible system for which a large number of energetically low-lying conformers may contribute to the chemistry observed at room temperature.

Superimposed to these more general aspect is a specific problem of amides which concerns the rotation around the C–N bond. Therefore, a brief survey about previous theoretical studies of amides is warranted. Formamide, the smallest amide, has been widely studied both experimentally and theoretically. The main interest has been focused on the planarity of the NH<sub>2</sub> group.<sup>32</sup> The microwave spectrum of formamide<sup>33</sup> is consistent with an inversion potential for the NH<sub>2</sub> group with a very shallow minimum for a non-planar structure. However, earlier experimental investigations have suggested the presence of a planar amide unit both in the gas phase and in the solid state of formamide as well as substituted amides.<sup>34</sup> While a large number of theoretical calculations has been carried out on model amides, the results are controversial.<sup>35</sup> Moreover, the solvents present in biological systems may substantially influence the abundance of non-planar (chiral) amides.<sup>36</sup> Contradictory results have been published for the conformational minima of acetamide, which can essentially assume three different types of conformations: *syn*, perpendicular, and *anti*, where the terminology proposed by Samdal<sup>37</sup> is used. B3LYP/6-311++G\*\* and B3LYP/cc-pVTZ calculations suggest that the *anti*-conformer is most stable. Helgaker *et al.*<sup>38</sup> have tested several computational methods with different basis sets for the equilibrium structures of small organic molecules. In these tests, the MP2/cc-pVTZ level of theory gave a very good agreement with the experimentally obtained equilibrium geometries. However, there is still an open question whether those methods can predict correct conformational minima and barrier heights as well. Thus, in the case of acetamide MP2/cc-pVTZ calculations predict a second stable conformational minimum, which is of a perpendicular form with the torsional angle of 30°. The energy difference between the *anti* and perpendicular structures amounts to only 3 cal/mol. Samdal tried and failed to locate the transition structure (TS) connecting these two conformers with conventional methods



of geometry optimization. For this reason, a calculation at a fixed geometry (torsional angle of  $45^\circ$ ) mimicking the transition structure has been performed and the barrier has been estimated at about 4 cal/mol. In a conformational study on acetamide, Wong and Wiberg found the perpendicular conformation to be the most stable one when MP2 and CISD methods were used.<sup>39</sup> In summary, the methods employed so far cannot give a clear answer whether the *anti* or perpendicular conformation is the most stable one.

For an extensive ab initio study, valeramide is a relatively large molecule, thereby imposing some restrictions to the computational approach applicable. Moreover, several conformers have to be considered, of which each might give rise to particularly favorable pathways. An appropriate computational description of ionized valeramide and its rearrangement reactions requires, however, a reasonably solid quantum chemical approach, which is able to adequately describe closed- and open-shell species, electron delocalization, hydrogen bonding, and transition structures in particular. In these respects, density functional theory (DFT) is successful in predicting physical properties of molecular systems, including hydrogen-bonded species, with an accuracy equal or even better than obtained by MP2 calculations,<sup>40,41</sup> but at much lower computational costs than those for higher levels of theory.<sup>42</sup> The present choice of B3LYP/6-311++G\*\*//B3LYP/6-31G\* is therefore considered as a proper level of theory to gain reliable potential-energy surfaces. In turn the computations at this level of theory are already quite demanding such that the potential-energy surface of ionized valeramide cannot be explored exhaustively. Therefore, the theoretical examination was primarily guided by the mechanistic implications derived from the experimental studies in conjunction with chemical intuition and plausibility considerations as far as the choice of low-lying conformations is concerned. Concerning a description of the distonic ion intermediates, the B3LYP/6-31G\* geometries appear to suffice, since complete geometry optimizations of a few key species at the B3LYP/6-311++G\*\* level of theory did not show large differences between the two methods neither in geometrical parameters nor in energetics (see below). Accordingly, full geometry optimizations of all species were not performed at this level of theory because the quality of the results would not change while the computational costs would increase considerably. The computational approach chosen does not ensure that all relevant conformers were covered; nevertheless, the reasonable agreement between theory and experiment obtained after all justifies the pragmatic choice of the theoretical approach used herein.

### 3.5. Conformational Analysis of Neutral and Ionized Valeramide

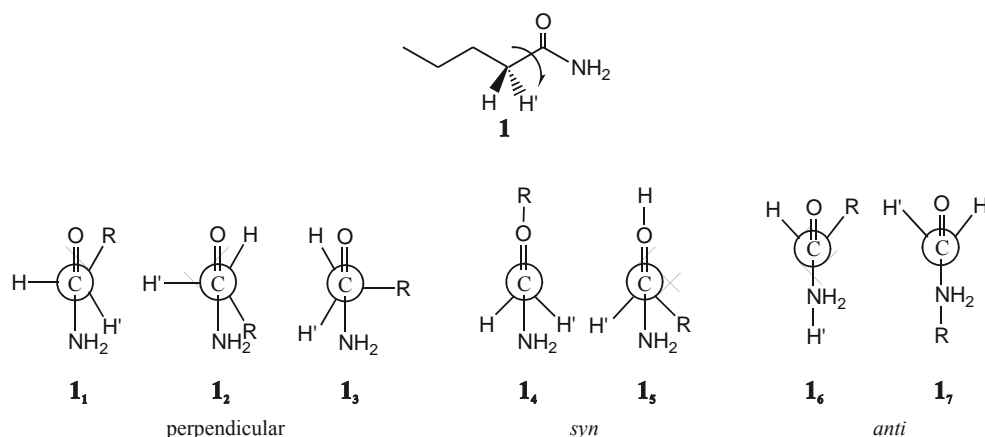


**Figure 3-1.** Newman projections along the C(1)–C(2) bond of valeramide showing the possible conformations of the amide group ( $R = n\text{-C}_3\text{H}_7$ ).

As one can infer from the work done so far on formamide and acetamide, conformational analysis can be quite demanding even for smallest amides. Turning back to valeramide as the subject of this study, it is clear that here the situation is even more complex. By analogy to the three leading conformers proposed for acetamide, one can postulate the existence of seven conformational minima for valeramide (Figure 3-1), which differ with respect to the orientations of the substituents at C(1) and C(2). In addition, the alkyl chain of valeramide may adopt several conformations. In combination with the different orientations of the amide group, a considerable number of energetically low-lying conformers evolves. For an initial screening, conformational analysis of valeramide was performed with the conformational search algorithm of the MM2 force field. More than 70 conformers were obtained within an energy range of only 3 kcal/mol. Accordingly, a manifold of conformers is expected to be sampled in experimental studies conducted at or above room temperature. For such a large number of possible conformers, an explicit consideration of all MM2 structures on the B3LYP level of theory is not practical. Because of a particular interest in different orientations of the functional group in respect to the rest of the carbone backbone, only those conformers depicted in Figure 3-1 were fully optimized at the B3LYP level of theory, while the alkyl backbone was confined to an *all-anti* conformation. Interestingly, the most stable conformer obtained in the MM2 calculations (similar to **1<sub>5</sub>**) does not even exist on the B3LYP potential energy surface, which can be attributed to the failure of molecular mechanics to describe hydrogen- and

weak-bond interactions properly. On the B3LYP level of theory, only two different conformations, **1<sub>1</sub>** and **1<sub>2</sub>** (the perpendicular conformation) were located; the latter is less stable due to steric repulsion between R and the amino group. Geometry optimizations for all the other possibilities ended in structure **1<sub>1</sub>**, suggesting this conformer as the global conformational minimum. The failure to locate the other conformations does not explicitly indicate that these conformers do not exist as minima on the PES of valeramide. Therefore, a PES scan was performed keeping the dihedral angle  $\theta_{CCCO}$  fixed while freely optimizing all other parameters. The results of the scan are consistent with structure **1<sub>1</sub>** as the global minimum (Table 3-1). The energy increase that accompanies the changes in the dihedral angle can be explained by contributions of at least two factors: (i) steric repulsion between the alkyl unit R and the amino group (basically hydrogen repulsions), and (ii) stabilization caused by the interaction of one of the C(2) hydrogens with the  $p_\pi$ -orbital on C(1), which compensates the positive charge emerging from the polarized bonds to the heteroatom

**Table 3-1.** Energetics derived from a scan of the dihedral angle  $\theta_{CCCO}$  in neutral valeramide<sup>a,b</sup> (B3LYP/6-31G\*).

| Conformer <sup>c</sup> | $\theta_{CCCO}$ <sup>b</sup> | $E_{tot}$ <sup>d</sup> | $E_{rel}$ <sup>e</sup> |
|------------------------|------------------------------|------------------------|------------------------|
| <b>1<sub>4</sub></b>   | 0                            | -327.15421             | 0.11                   |
| <b>1<sub>1</sub></b>   | 30                           | -327.15439             | 0.00                   |
| <b>1<sub>6</sub></b>   | 60                           | -327.15393             | 0.29                   |
| <b>1<sub>3</sub></b>   | 90                           | -327.15302             | 0.86                   |
| <b>1<sub>5</sub></b>   | 120                          | -327.15246             | 1.21                   |
| <b>1<sub>2</sub></b>   | 150                          | -327.15224             | 1.35                   |
| <b>1<sub>7</sub></b>   | 180                          | -327.15222             | 1.36                   |

<sup>a</sup> In these calculations,  $\theta_{CCCO}$  was kept fixed, while all other parameters were fully optimized. <sup>b</sup> Specifically, this is the dihedral angle spanned by the atoms O, C(1), C(2), and C(3). <sup>c</sup> See Figure 3-1. <sup>d</sup> Total energies in Hartree; 1 H = 627.51 kcal/mol. <sup>e</sup> Energies (in kcal/mol) relative to the most stable conformer **1<sub>1</sub>**.

substituents of C(1). The latter is most pronounced in the perpendicular conformations, in which the interacting hydrogen atom forms a dihedral angle  $\theta_{HCCO}$  of ca. 90°, thereby maximizing orbital overlap. The energetic preference of this interaction also explains why only the perpendicular conformers **1<sub>1</sub>** and **1<sub>2</sub>** exist as minima at the B3LYP level of theory.

### 3.6. Adiabatic and Vertical Ionization of Valeramide

Adiabatic and vertical ionization energies ( $IE_a$  and  $IE_v$ ) were calculated for the conformers **1<sub>1</sub>** and **1<sub>2</sub>** of neutral valeramide (Table 3-2). However, geometry optimizations

on the cation-radical PES leads to same cation structure  $\mathbf{1}_1^{+\bullet}$  for both conformers (note that the indices used for the conformations of neutral and ionized valeramide do not coincide). The difference between vertical and adiabatic ionization ( $\Delta IE_{v/a}$ ) is 0.36 eV for conformer  $\mathbf{1}_1$  and 0.28 eV for conformer  $\mathbf{1}_2$ , indicating that the structural changes upon ionization are slightly more pronounced in the former. With regard to the experimentally obtained ionization energy ( $IE = 9.40 \pm 0.03$  eV),<sup>22,43</sup> the relatively small  $\Delta IE_{v/a}$  implies that the onset for photoionization of valeramide corresponds to adiabatic ionization. Further, the energy difference of the conformers  $\mathbf{1}_1$  and  $\mathbf{1}_2$  is small, such that mixtures of at least these two conformers are likely to be sampled in the experiments. The calculated energetic difference of  $\sim 1$  kcal/mol suggests a ca. 5 : 1 ratio of  $\mathbf{1}_1$  and  $\mathbf{1}_2$  at 298 K. Relative to experiment, one notes a slight underestimation of the adiabatic  $IE_s$ , which may be attributed to a general trend of the B3LYP approach in predicting  $IE_s$  of closed-shell organic molecules.<sup>44,45</sup>

**Table 3-2.** Relative stabilities ( $E_{rel}$  in kcal/mol) of valeramide conformers, adiabatic and vertical ionization energies ( $IE_a$  and  $IE_v$ , respectively, in eV)<sup>a</sup> and their difference  $\Delta IE_{v/a}$  (in eV).

| Conformer      | Method                         | $E_{rel}$ | $IE_a$ | $IE_v$ | $\Delta IE_{v/a}$ |
|----------------|--------------------------------|-----------|--------|--------|-------------------|
| $\mathbf{1}_1$ | B3LYP/6-31G**//B3LYP/6-31G*    | 0.0       | 8.88   | 9.24   | 0.36              |
|                | B3LYP/6-311++G**//B3LYP/6-31G* | 0.0       | 9.19   | 9.55   | 0.36              |
| $\mathbf{1}_2$ | B3LYP/6-31G**//B3LYP/6-31G*    | 1.4       | 8.82   | 9.10   | 0.28              |
|                | B3LYP/6-311++G**//B3LYP/6-31G* | 1.0       | 9.15   | 9.43   | 0.28              |

<sup>a</sup> Note that adiabatic ionization of both conformers of neutral valeramide leads to the same structure for the ion, see text.

Upon ionization, geometry changes from the perpendicular into the distorted *anti*-conformation (Figure 3-2), which is similar to conformer  $\mathbf{1}_5$  of neutral valeramide, with the dihedral angles  $\theta_{RCCO} = 46.3^\circ$  and  $\theta_{HCCO} = 13.2^\circ$ . In the cation radical, the electron deficient oxygen atom orientates in such a manner that stabilization through bond delocalization from the neighboring  $\text{NH}_2$ - and  $\text{CH}_2$ - groups can occur, which is reflected in the changes of the charge distributions for neutral and ionized valeramide. Consideration of the molecular orbitals supports this picture in that the cationic species bears orbitals, which are delocalized across the C–H and N–H bonds and the carbonyl group. The changes in dihedral angles are the main cause of the difference between adiabatic and vertical ionization, while bond angles and bond lengths experience only minor variations.

The elongation of the C(1)-C(2) bond, for example, is rather small with  $r_{CC} = 1.529$  Å in the neutral compared to  $r_{CC} = 1.554$  Å in the cation radical. Concerning the planarity of amino group, the already almost planar arrangement in the neutral (the sum of the angles around nitrogen is  $358^\circ$ ) becomes perfect in the cation radical  $\mathbf{1}_1^{+\bullet}$  due to a better overlap between orbitals including the N–H bonds and the oxygen atom.

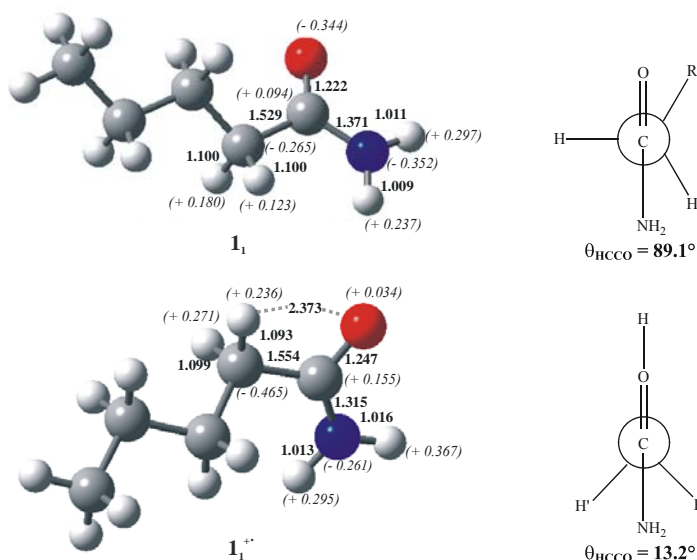


**Figure 3-2.** Optimized structures of neutral and ionized valeramide at the B3LYP/6-31G\* level of theory. Bond lengths (in Å) are given in bold, Mulliken charges in parentheses.

### 3.7. Unimolecular Dissociations of Ionized Valeramide

Detailed reaction pathways have been calculated for the five fragmentation channels of ionized valeramide deduced from the experimental studies (Scheme 3-1). The C<sub>3</sub>-route corresponds to the McLafferty rearrangement, which is initiated by a 1,5-H transfer and followed by C–C bond cleavage and formation of propene and the enol cation  $\mathbf{4}^{+\bullet}$ . The C<sub>2</sub>-route comprises three channels. Two of these have an initial 1,6-H transfer in common, i.e., the loss of C<sub>2</sub>H<sub>4</sub> to afford the  $\beta$ -distonic ion  $\mathbf{6}^{+\bullet}$  and the elimination of C<sub>2</sub>H<sub>5</sub><sup>•</sup> to form protonated acrylamide  $\mathbf{8}^+$  in a more complex process. The direct loss of the terminal ethyl group contributes to the C<sub>2</sub>-route as well. Based on the experimental findings, the C<sub>1</sub>-route is assigned to an initial 1,4-H transfer followed by loss of CH<sub>3</sub><sup>•</sup>

concomitant with formation of protonated vinylacetamide **12**<sup>+</sup>. Finally, even though the occurrence of a 1,3-H transfer, via keto/enol tautomerization, has not been inferred from experiment, it was investigated theoretically.

In perfect agreement with the interpretation of the experimental data, the barriers associated with the various hydrogen migrations in the cation radical are rather small (see below). Therefore, internal rotations around the C–C bonds play an important role in that adequate conformers need to be accessed before a particular rearrangement can occur. In fact, C–C bond rotations may contribute to or even constitute the rate-determining steps. The structural flexibility of valeramide and its cation radical makes the mechanistic study rather demanding because the rearrangements could arise from many different conformers. As a compromise between insight gained and computational resources available, the role of internal rotations prior to hydrogen migration was only investigated explicitly for the C<sub>2</sub>- and C<sub>3</sub>-routes.

### 3.7.1. $\gamma$ -C–H Bond Activation (C<sub>3</sub>-route)

In the energetically lowest-lying conformer **1**<sub>1</sub><sup>+</sup>, the distances between the oxygen atom of the carbonyl group and the hydrogens at C(4) are much too large for hydrogen migration to occur. Rotation around the C(2)–C(3) bond leads to conformer **1**<sub>3</sub><sup>+</sup>, which is 1.5 kcal/mol higher in energy than **1**<sub>1</sub><sup>+</sup> (Table 3-3).

Although the absence of imaginary modes characterizes **1**<sub>3</sub><sup>+</sup> as a real minimum at the B3LYP/6-31G\* level of theory, all attempts failed to locate a barrier associated with hydrogen migration to the distonic ion **2**<sup>+</sup> (Figure 3-3). Moreover, all computed points of a continuous scan from **1**<sub>3</sub><sup>+</sup> to **2**<sup>+</sup>, i.e., decreasing  $r_{OH}$  while optimizing all other parameters, were lower in energy than the starting point **1**<sub>3</sub><sup>+</sup>. Accordingly, the barrier associated with 1,5-H migration is rather small, if not spurious. Inspection of the computed vibrational frequencies reveals a low-lying mode at 89 cm<sup>-1</sup> of **1**<sub>3</sub><sup>+</sup> that reflects the structural changes associated with  $\gamma$ -C–H bond activation.<sup>46</sup> Further refinement might certainly be achieved with larger basis sets in the geometry optimization combined with the application of tighter convergence criteria. However, the barrier (if existing at all) would lie low in energy.

**Table 3-3.** Electronic energies ( $E_{tot}$ , in Hartree), zero-point energies ( $ZPE$ , in Hartree), and relative energies ( $E_{rel}$ , in kcal/mol)<sup>a</sup> of the stationary points on the potential-energy surface of ionized valeramide.

|  | B3LYP/6-31G*//B3LYP/6-31G* |          |                | B3LYP/6-311++G**//B3LYP/6-31G* |                 |
|--|----------------------------|----------|----------------|--------------------------------|-----------------|
|  | $E_{tot}$                  | $ZPE$    | $E_{rel}^{ab}$ | $E_{tot}$                      | $E_{rel}^{a-c}$ |
| <b>1<sub>1</sub><sup>+</sup></b>                           | -326.827971                | 0.158796 | 0.0            | -326.923706 <sup>d</sup>       | 0.0             |
| <b>1<sub>1</sub><sup>+</sup>/1<sub>2</sub><sup>+</sup></b> | -326.823143                | 0.158583 | 2.9            | -326.919235                    | 2.7             |
| <b>1<sub>2</sub><sup>+</sup></b>                           | -326.826593                | 0.158765 | 0.9            | -326.922514                    | 0.8             |
| <b>1<sub>1</sub><sup>+</sup>/1<sub>3</sub><sup>+</sup></b> | -326.821654                | 0.158462 | 3.8            | -326.917911                    | 3.5             |
| <b>1<sub>3</sub><sup>+</sup></b>                           | -326.825397                | 0.158764 | 1.6            | -326.921404                    | 1.5             |
| <b>1<sub>2</sub><sup>+</sup>/1<sub>4</sub><sup>+</sup></b> | -326.821097                | 0.158601 | 4.2            | -326.917217                    | 4.0             |
| <b>1<sub>4</sub><sup>+</sup></b>                           | -326.824067                | 0.158917 | 2.6            | -326.919870                    | 2.5             |
| <b>2<sup>+</sup></b>                                       | -326.851066                | 0.159234 | -14.2          | -326.952177                    | -17.6           |
| <b>1<sub>4</sub><sup>+</sup>/5<sub>1</sub><sup>+</sup></b> | -326.821475                | 0.158147 | 3.7            | -326.917193                    | 3.7             |
| <b>5<sub>1</sub><sup>+</sup></b>                           | -326.843174                | 0.159341 | -9.2           | -326.944120 <sup>d</sup>       | -12.4           |
| <b>5<sub>2</sub><sup>+</sup></b>                           | -326.831062                | 0.159672 | -1.4           | -326.933011                    | -5.3            |
| <b>5<sub>3</sub><sup>+</sup></b>                           | -326.829377                | 0.158749 | -0.9           | -326.932492                    | -5.5            |
| <b>5<sub>4</sub><sup>+</sup></b>                           | -326.827160                | 0.158382 | 0.3            | -326.930411                    | -4.4            |
| <b>5<sub>1</sub><sup>+</sup>/c-5<sup>+</sup></b>           | -326.819366                | 0.159789 | 6.0            | -326.920266                    | 2.8             |
| <b>c-5<sup>+</sup></b>                                     | -326.821732                | 0.159752 | 4.5            | -326.922196                    | 1.6             |
| <b>5<sub>1</sub><sup>+</sup>/6<sup>+</sup>c</b>            | -326.795501                | 0.155755 | 18.5           | -326.899203                    | 13.5            |
| <b>5<sub>3</sub><sup>+</sup>/7<sub>1</sub><sup>+</sup></b> | -326.809434                | 0.155427 | 9.6            | -326.912865                    | 4.8             |
| <b>7<sub>1</sub><sup>+</sup>f</b>                          | -326.851625                | 0.159665 | -14.3          | -326.954016                    | -18.5           |
| <b>5<sub>2</sub><sup>+</sup>/7<sub>2</sub><sup>+</sup></b> | -326.805264                | 0.155389 | 12.2           | -326.908727                    | 7.3             |
| <b>7<sub>2</sub><sup>+</sup></b>                           | -326.849834                | 0.159679 | -13.1          | -326.952205                    | -17.3           |
| <b>1<sub>1</sub><sup>+</sup>/7<sub>3</sub><sup>+</sup></b> | -326.782132                | 0.154218 | 26.0           | -326.882266                    | 23.2            |
| <b>7<sub>3</sub><sup>+</sup></b>                           | -326.854846                | 0.159999 | -16.1          | -326.957217                    | -20.3           |
| <b>1<sub>1</sub><sup>+</sup>/11<sup>+</sup></b>            | -326.819324                | 0.154831 | 3.0            | -326.916779                    | 1.9             |
| <b>11<sup>+</sup></b>                                      | -326.843288                | 0.159169 | -9.4           | -326.945129                    | -13.2           |
| <b>11<sup>+</sup>/12<sup>+</sup>c</b>                      | -326.793115                | 0.155093 | 19.6           | -326.897284                    | 14.3            |

<sup>a</sup> The lowest-lying conformer **1<sub>1</sub><sup>+</sup>** of the cation radical is used as the reference point. <sup>b</sup>  $ZPE$ s included with a scaling factor of 0.9805. <sup>c</sup>  $ZPE$ s taken from the B3LYP/6-31G\*//B3LYP/6-31G\* calculations. <sup>d</sup> Energies at B3LYP/6-311++G\*\*//B3LYP/6-311++G\*: **1<sub>1</sub><sup>+</sup>**, -326.923857 H, and **5<sub>1</sub><sup>+</sup>**, -326.9442407 H. <sup>e</sup> Barrier in the exit channel, see text. <sup>f</sup> Computed energies of neutral **7**:  $E_{tot}$ (B3LYP/6-31G\*) = -327.106796 H,  $ZPE$  = 0.159554 H,  $E_{tot}$ (B3LYP/6-311++G\*\*//B3LYP/6-31G\*) = -327.221313 H.

With regard to the interpretation of the experimental data, it is entirely sufficient that the conformational barrier associated with the formation of  $\mathbf{1}_3^{++}$  is predicted to exceed the kinetic restriction imposed by hydrogen migration. Hence, not C–H bond activation, but access to the appropriate conformation of  $\mathbf{1}^{++}$  is rate-determining for the McLafferty rearrangement. This conclusion also provides an explanation for the negligible kinetic isotope effect (*KIE*) in the McLafferty route as derived from the analysis of the experimental data. The distonic ion  $\mathbf{2}^{++}$  is 17.6 kcal/mol more stable than the lowest-lying conformer of the reactant,  $\mathbf{1}_1^{++}$ . Bond lengths and angles characterize structure  $\mathbf{2}^{++}$  as a genuine  $\gamma$ -distonic ion, rather than a loose ion/dipole complex ( $\mathbf{3}^{++}$ ) of the ionized acetamide enol interacting electrostatically with neutral propene. For example, the C(2)/C(3) and C(3)/C(4) bonds in  $\mathbf{2}^{++}$  (1.540 and 1.506 Å) almost match those in  $\mathbf{1}_1^{++}$  (1.530 and 1.555 Å).

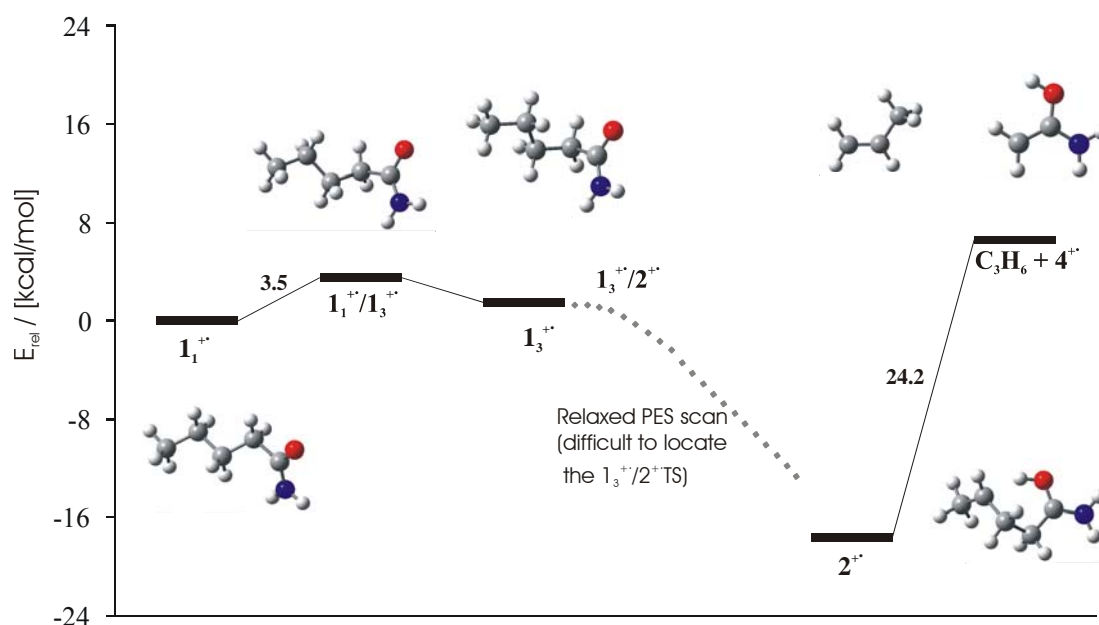


**Figure 3-3.** Potential-energy surface for the loss of  $\text{C}_3\text{H}_6$  from ionized valeramide ( $\text{C}_3$ -route) according to B3LYP6-311++G\*\*/B3LYP6-31G\* calculations.

While numerous indications for the existence of ion/dipole complexes exist in the chemistry of organic cation radicals,<sup>47</sup> all extensive attempts failed to locate a genuine minimum for  $\mathbf{3}^{++}$ , but instead always converged to  $\mathbf{2}^{++}$ . While this result should by no means dispute the possible existence of  $\mathbf{3}^{++}$ , it is entirely sufficient for the present purpose to state that structure  $\mathbf{2}^{++}$  obviously is more stable than  $\mathbf{3}^{++}$ . Dissociation of  $\mathbf{2}^{++}$  to the final



products  $\mathbf{4}^{+\bullet} + \text{C}_3\text{H}_6$  requires 24.2 kcal/mol at the B3LYP/6-311++G\*\*//B3LYP/6-31G\* level of theory, corresponding to an overall endothermicity of 6.6 kcal/mol for the reaction  $\mathbf{1}_1^{+\bullet} \rightarrow \mathbf{4}^{+\bullet} + \text{C}_3\text{H}_6$  at 0 K. A more detailed consideration of the exit channels is postponed to a separate section further below.

### 3.7.2. $\delta\text{-C-H}$ Bond Activation ( $\text{C}_2$ -route)

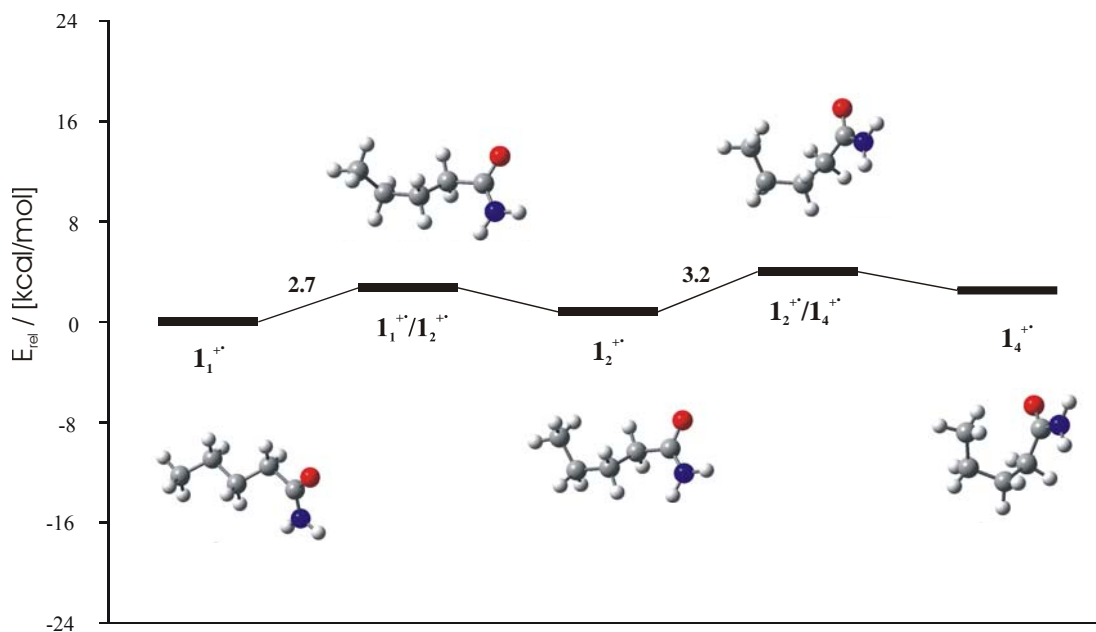


**Figure 3-4.** Conformational changes of  $\mathbf{1}^{+\bullet}$  required as a prerequisite for the access to the  $\text{C}_2$ -route according to B3LYP6-311++G\*\*//B3LYP6-31G\* calculations.

While a single C–C bond rotation is sufficient to achieve a reactive conformation for the McLafferty rearrangement, two sequential rotations  $\mathbf{1}_1^{+\bullet} \rightarrow \mathbf{1}_2^{+\bullet} \rightarrow \mathbf{1}_4^{+\bullet}$  (Figure 3-4) are required for  $\delta\text{-C-H}$  bond activation which initiates the  $\text{C}_2$ -route. Similar to the McLafferty rearrangement, the barrier associated with hydrogen migration is rather low, and the transition structure (TS)  $\mathbf{1}_4^{+\bullet}/\mathbf{5}_1^{+\bullet}$  is only 1.2 kcal/mol above  $\mathbf{1}_4^{+\bullet}$  (Figure 3-5). Again, the barrier for C–C bond rotation exceeds that associated with hydrogen migration; the difference is considerably smaller for activation of the  $\delta\text{-C-H}$  bonds, which is consistent with the small, but non-negligible *KIEs* found upon deuteration at C(5) in the experimental studies. Similar to the  $\text{C}_3$ -route, the  $\delta$ -distonic ion  $\mathbf{5}_1^{+\bullet}$  is 12.4 kcal/mol more stable than  $\mathbf{1}_1^{+\bullet}$ . In order to investigate, whether or not this effect is due to an interaction between the charge and the spin centers in  $\mathbf{5}_1^{+\bullet}$ , other conformers were considered as well,

including the seemingly ideal *all-anti* orientation of the C–C bonds. In the resulting *all-anti* conformer  $\mathbf{5}_4^{+\bullet}$ , the O–C(5) distance amounts to 6.225 Å compared to only 2.807 Å in  $\mathbf{5}_1^{+\bullet}$ . Though less strained, conformer  $\mathbf{5}_4^{+\bullet}$  is ca. 8 kcal/mol less stable than  $\mathbf{5}_1^{+\bullet}$ . A value of this magnitude is best rationalized by involving hydrogen bonding between the radical center and the hydroxy group, as also implied by the almost linear arrangement of the atoms involved ( $\alpha_{C(5)HO} = 171.8^\circ$ ) together with  $r_{C(5)H} = 1.806$  Å. In comparison, hydrogen bonding involving the amino group is energetically disfavored (conformer  $\mathbf{5}_2^{+\bullet}$ ).

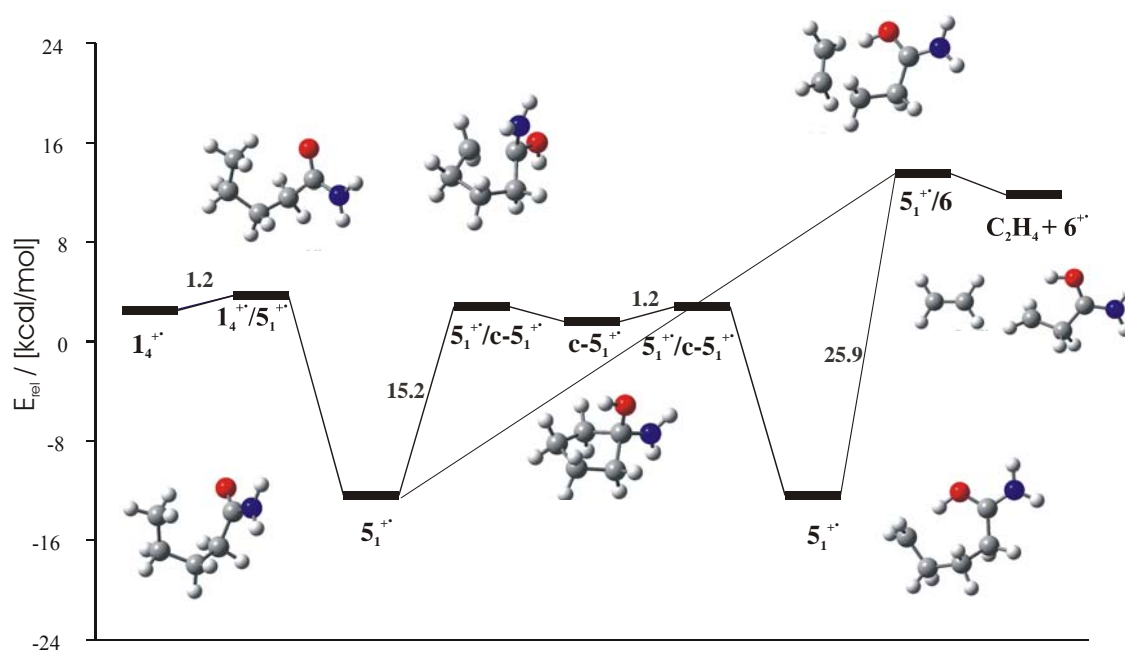


**Figure 3-5.** Potential-energy surface for the loss of  $\text{C}_2\text{H}_4$  from ionized valeramide ( $\text{C}_2$ -route) according to B3LYP6-311++G\*\*//B3LYP6-31G\* calculations.

Any conformer of  $\mathbf{5}^{+\bullet}$  can undergo C(3)–C(4) bond cleavage to afford the cation radical  $\mathbf{6}^{+\bullet}$  concomitant with neutral ethene. At the B3LYP/6-311++G\*\*//B3LYP/6-31G\* level of theory, an overall endothermicity of 11.8 kcal/mol is predicted for the reaction  $\mathbf{1}_1^{+\bullet} \rightarrow \mathbf{6}^{+\bullet} + \text{C}_2\text{H}_4$  at 0 K. Similar to the  $\delta$ -distonic ion  $\mathbf{5}_1^{+\bullet}$ , the  $\beta$ -distonic ion  $\mathbf{6}^{+\bullet}$  seems to experience stabilization by intramolecular hydrogen bonding because in the most stable conformer found the hydroxy group is oriented towards the radical site at C(3) with  $r_{C(3)O} = 2.812$  Å and  $\alpha_{C(3)HO} = 113.6^\circ$ ; however,  $r_{C(3)H(O)} = 2.269$  Å indicates that hydrogen bonding is less efficient than in  $\mathbf{5}_1^{+\bullet}$ . A conformer in which the OH group points away from the backbone ( $r_{C(3)O} = 3.019$  Å) is 4.3 kcal/mol less stable than  $\mathbf{6}^{+\bullet}$  at the B3LYP/6-311++G\*\*//B3LYP/6-31G\* level of theory. In competition with dissociation,  $\mathbf{5}_1^{+\bullet}$  can

isomerize to the cyclic structure  $c\text{-}\mathbf{5}^{+\bullet}$  where the associated TS  $\mathbf{5}_1^{+\bullet}/c\text{-}\mathbf{5}_1^{+\bullet}$  is energetically close to  $c\text{-}\mathbf{5}_1^{+\bullet}$  (Table 3-3). The relatively low energy demand of this degenerate rearrangement is in perfect agreement with the pairwise equilibration of the C(2)/C(3) and C(4)/C(5) positions as inferred from the experimental studies.

For the isomerization of the  $\delta$ -distonic ion  $\mathbf{5}^{+\bullet}$  to the ionized enol  $\mathbf{7}^{+\bullet}$  via a 1,4-hydrogen migration (Figure 3-6), a conformational change is required first. Thus, the most stable conformer  $\mathbf{5}_1^{+\bullet}$  must trade-off hydrogen bonding, giving rise to a conformer  $\mathbf{5}_3^{+\bullet}$  in which one of the hydrogens at C(2) can interact with the radical site at C(5). While the barrier associated with hydrogen migration via TS  $\mathbf{5}_3^{+\bullet}/\mathbf{7}_1^{+\bullet}$  is not very large (10.3 kcal/mol relative to  $\mathbf{5}_3^{+\bullet}$ ), the resulting energy demand in conjunction with the required conformational changes locate TS  $\mathbf{5}_3^{+\bullet}/\mathbf{7}_1^{+\bullet}$  at a relative energy of 4.8 kcal/mol above  $\mathbf{1}_1^{+\bullet}$ . Conformer  $\mathbf{7}_1^{+\bullet}$  is 18.5 kcal/mol more stable than  $\mathbf{1}_1^{+\bullet}$ ; conformer  $\mathbf{7}_2^{+\bullet}$  and the associated TS  $\mathbf{5}_2^{+\bullet}/\mathbf{7}_2^{+\bullet}$  are close in energy and primarily differ in the orientation of the functional group relative to the backbone. Any conformer of  $\mathbf{7}^{+\bullet}$  could undergo C(3)–C(4) bond scission to yield  $\mathbf{8}^+ + \text{C}_2\text{H}_5^\bullet$ , which requires 27.8 kcal/mol for conformer  $\mathbf{7}_1^{+\bullet}$ , corresponding to an overall endothermicity of 9.3 kcal/mol relative to  $\mathbf{1}_1^{+\bullet}$  at the B3LYP/6-311++G\*\*//B3LYP/6-31G\* level of theory at 0 K.

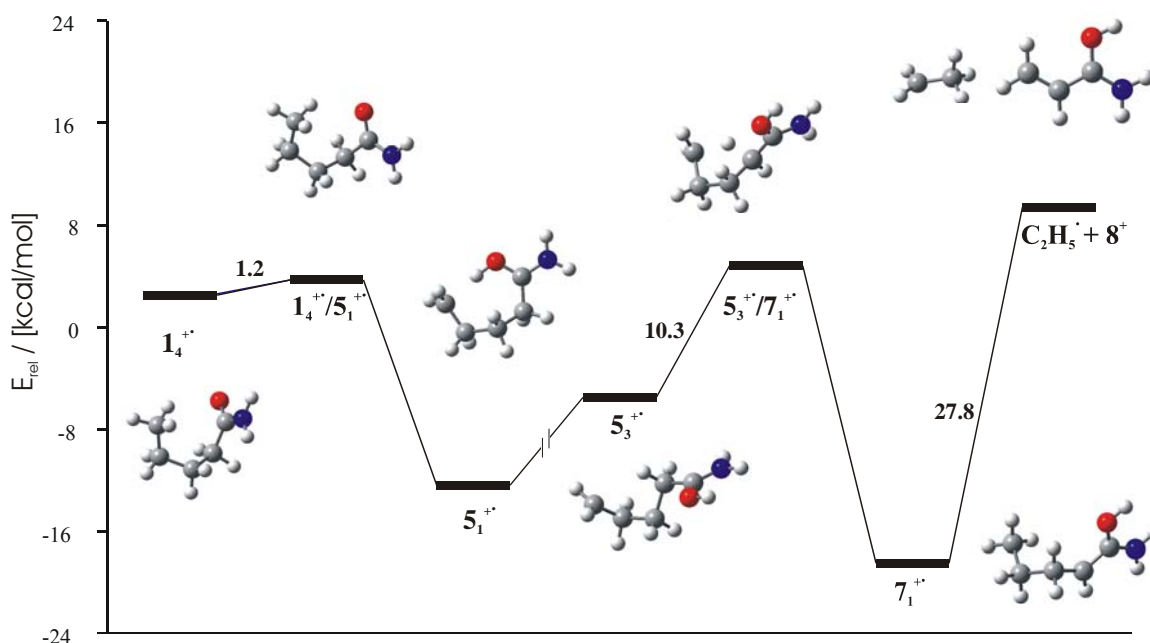


**Figure 3-6.** Potential-energy surface for the indirect loss of  $\text{C}_2\text{H}_5^\bullet$  from ionized valeramide ( $\text{C}_2$ -route) according to B3LYP6-311++G\*\*//B3LYP6-31G\* calculations.

### 7.2.3. $\beta$ -C-H Bond Activation ( $C_I$ -route)

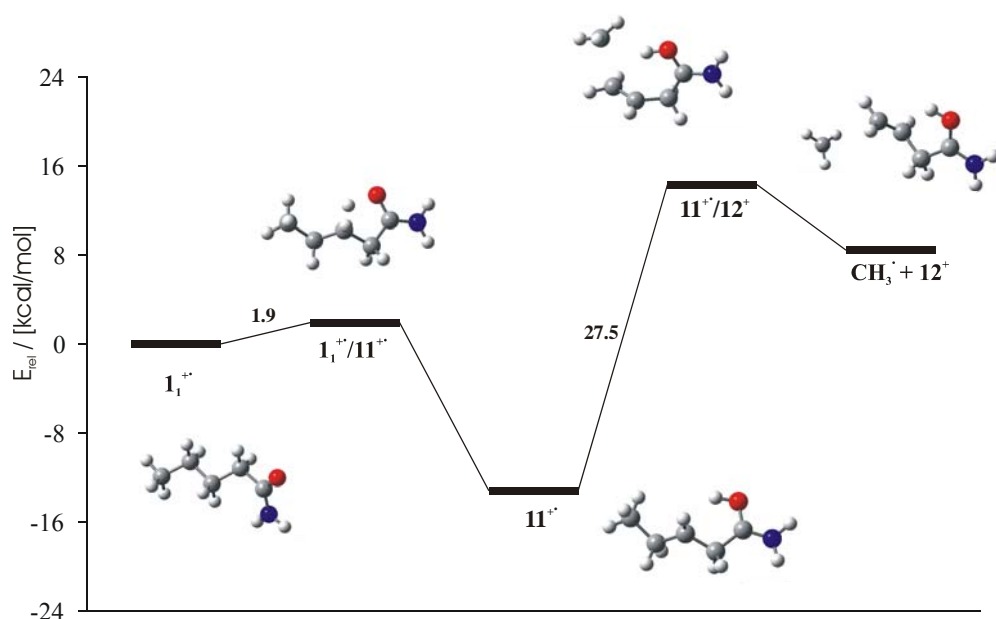


**Figure 3-7.** Potential-energy surface for the loss of  $\text{CH}_3^\bullet$  from ionized valeramide ( $C_I$ -route) according to B3LYP6-311++G\*\*//B3LYP6-31G\* calculations.

The 1,4-hydrogen transfer can directly proceed from conformer  $\mathbf{1_I^{+\bullet}}$ , and the associated TS  $\mathbf{1_I^{+\bullet}/11^{+\bullet}}$  requires only 1.9 kcal/mol (Figure 3-7). This facile hydrogen migration, besides the low barrier, can be attributed to the fact that the resulting  $\beta$ -distonic ion  $\mathbf{11^{+\bullet}}$  is 13.2 kcal/mol more stable than  $\mathbf{1_I^{+\bullet}}$ . Once more, the distonic ion formed seems to experience stabilization via hydrogen bonding, because in the computed minimum, the hydroxy group points towards the radical site with  $r_{\text{C}(3)\text{H}(\text{O})} = 2.190 \text{ \AA}$ ,  $r_{\text{C}(3)\text{O}} = 2.190 \text{ \AA}$ , and  $\alpha_{\text{C}(3)\text{HO}} = 116.4^\circ$ . Interestingly, the subsequent C(4)–C(5) bond cleavage of  $\mathbf{11^{+\bullet}}$  is associated with a significant barrier in the exit channel, TS  $\mathbf{11^{+\bullet}/12^+}$ . For the final products  $\mathbf{12^+} + \text{CH}_3^\bullet$ , an endothermicity of 8.4 kcal/mol relative to  $\mathbf{1_I^{+\bullet}}$  is predicted at the B3LYP/6-311++G\*\*//B3LYP/6-31G\* level of theory at 0 K.

### 7.2.4. $\alpha$ -C-H Bond Activation (Keto/Enol Tautomerism)

Even though the *all-anti* conformer of the ionized enol  $\mathbf{7_3^{+\bullet}}$  ( $E_{\text{rel}} = -20.3 \text{ kcal/mol}$ ) most likely corresponds to the global minimum of all cationic species examined here, the computed energy demand of 23.2 kcal/mol (Table 3-3) associated with intramolecular

keto/enol tautomerism proceeding through a 1,3-hydrogen transfer via TS  $\mathbf{1}_1^{+*}/\mathbf{7}_3^{+*}$  is much higher than those of all other hydrogen migrations investigated. This result is not at all unexpected, since previous studies have amply demonstrated that the facile keto/enol tautomerism known from the condensed phase occurs intermolecularly, whereas intramolecular keto/enol tautomerism via 1,3-hydrogen migration is associated with considerable barriers for neutral as well as cationic carbonyl compounds.<sup>48</sup> In the present case, formation of the ionized enol is indeed more likely to occur via a much more complicated, multi-step sequence  $\mathbf{1}_1^{+*} \rightarrow \mathbf{1}_2^{+*} \rightarrow \mathbf{1}_4^{+*} \rightarrow \mathbf{5}_1^{+*} \rightarrow \mathbf{5}_3^{+*} \rightarrow \mathbf{7}_1^{+*} \rightarrow \mathbf{7}_3^{+*}$  described in the context of the C<sub>2</sub>-route (see above). Consequently, the direct keto/enol tautomerism will not contribute to the dissociation behavior of ionized valeramide. The ionized enol might be involved if some neutral **7** were present in the precursor, because ionization of the enol is much easier than that of the keto isomer ( $IE_a(\mathbf{7}) = 7.19$  eV vs  $IE_a(\mathbf{1}) = 9.19$  eV; B3LYP/6-311++G\*\*//B3LYP/6-31G\*). However, at the same level of theory the neutral enol **7** is computed to be 24.9 kcal/mol less stable than neutral valeramide (**1**), such that contributions from the enol form can be excluded rigorously at 298 K. The similar stability differences have been predicted for the keto/enol tautomers of neutral acetamide.<sup>49</sup>

### 7.2.5. Exit Channels

With respect to the products formed upon dissociation of ionized valeramide, two general and one specific point need to be addressed. The first general concern is the choice of the basis sets in the computational study. Upon inspection of the data compiled in Table 3-4, it becomes obvious that the dissociation enthalpies relative to  $\mathbf{1}_1^{+*}$  show a pronounced basis set effect. The general tendency for decreasing endothermicities with increasing the size of the basis set can be attributed to a basis set superposition error. The deviations of  $\Delta E_{rel}$  are not at all uniform and most likely seem to reflect the role of electron correlation in the various fragments. For example,  $\Delta E_{rel}$  is small for the saturated, cyclic species  $\mathbf{10}^+$  and  $\mathbf{13}^+$  and large for unsaturated fragments such as  $\mathbf{4}^+$ ,  $\mathbf{6}^+$ ,  $\mathbf{8}^+$ , and  $\mathbf{12}^+$ . Irrespective of the precise origin of these effects, these trends indicate that even the larger basis set used might not suffice to describe the exit channels within a few kcal/mol. This has to be kept in mind as a note of caution for the entire PES of ionized valeramide, even though the computed data compare quite favorably with experimental data available. Nevertheless, the

use of B3LYP/6-31G\* geometries appears adequate, because exploratory geometry optimizations of  $1^{+\bullet}$ ,  $4^{+\bullet}$ , and  $5_1^{+\bullet}$  at the B3LYP/6-311++G\*\* level of theory led to differences of maximal 0.01 Å in bond lengths and maximal 0.1 kcal/mol in the relative energetics.

**Table 3-4.** Electronic energies ( $E_{tot}$ , in Hartree), zero-point energies (ZPE, in Hartree), and relative energies ( $E_{rel}$ , in kcal/mol)<sup>a</sup> of the dissociation products of ionized valeramide.

|  | B3LYP/6-31G*//B3LYP/6-31G* |          |                 | B3LYP/6-311++G**//<br>B3LYP/6-31G* |                 |                    |
|--|----------------------------|----------|-----------------|------------------------------------|-----------------|--------------------|
|  | $E_{tot}$                  | ZPE      | $E_{rel}^{a,b}$ | $E_{tot}$                          | $E_{rel}^{a-c}$ | $\Delta E_{rel}^d$ |
| $4^{+\bullet}$                             | -208.892507                | 0.073921 |                 | -208.962891 <sup>e</sup>           |                 |                    |
| C <sub>3</sub> H <sub>6</sub>              | -117.907562                | 0.080097 |                 | -117.945597 <sup>e</sup>           |                 |                    |
| $4^{+\bullet} + \text{C}_3\text{H}_6$      | -326.800069                | 0.154018 | 14.6            | 326.908488                         | 6.6             | 8.0                |
| $6^{+\bullet}$                             | -248.203109                | 0.101795 |                 | -248.283773                        |                 |                    |
| C <sub>2</sub> H <sub>4</sub>              | -78.587457                 | 0.051208 |                 | -78.615509                         |                 |                    |
| $6^{+\bullet} + \text{C}_2\text{H}_4$      | -326.790566                | 0.153003 | 19.9            | -326.899282                        | 11.8            | 8.1                |
| $8^+$                                      | -247.637169                | 0.092884 |                 | -247.717762                        |                 |                    |
| C <sub>2</sub> H <sub>5</sub> <sup>•</sup> | -79.157868                 | 0.059651 |                 | -79.185027                         |                 |                    |
| $8^+ + \text{C}_2\text{H}_5^{\bullet}$     | -326.795037                | 0.152535 | 16.8            | -326.902789                        | 9.3             | 7.5                |
| $9^+$                                      | -247.630846                | 0.094573 |                 | -247.702183                        |                 |                    |
| $9^+ + \text{C}_2\text{H}_5^{\bullet}$     | -326.788714                | 0.154224 | 21.8            | -326.887210                        | 20.1            | 1.7                |
| $10^+$                                     | -247.517747                | 0.087524 |                 | -247.591683                        |                 |                    |
| $10^+ + \text{C}_2\text{H}_5^{\bullet}$    | -326.675615                | 0.147175 | 88.3            | -326.776710                        | 84.9            | 3.4                |
| $13^{+f}$                                  | -247.617520                | 0.093827 |                 | -247.689936                        |                 |                    |
| $13^+ + \text{C}_2\text{H}_5^{\bullet}$    | -326.775388                | 0.153478 | 29.7            | -326.874963                        | 27.3            | 2.4                |
| $14^{+g}$                                  | -247.577271                | 0.088982 |                 | -247.655572                        |                 |                    |
| $14^+ + \text{C}_2\text{H}_5^{\bullet}$    | -326.735139                | 0.148633 | 52.0            | -326.840599                        | 45.9            | 6.1                |
| $12^+$                                     | -286.956919                | 0.121632 |                 | -287.048005                        |                 |                    |
| CH <sub>3</sub> <sup>•</sup>               | -39.838292                 | 0.029832 |                 | -39.855179                         |                 |                    |
| $12^+ + \text{CH}_3^{\bullet}$             | -326.795211                | 0.151464 | 16.1            | -326.903184                        | 8.4             | 7.7                |

<sup>a</sup> Relative energies can only be given for the sums of fragments having the same elemental composition as valeramide, where the lowest-lying conformer  $1_1^{+\bullet}$  of the cation radical is used as the reference point. <sup>b</sup> ZPEs included with a scaling factor of 0.9805. <sup>c</sup> ZPEs taken from the B3LYP/6-31G\* calculations. <sup>d</sup> Defined as  $\Delta E_{rel} = E_{rel}(\text{B3LYP/6-31G*}) - E_{rel}(\text{B3LYP/6-311++G**})$ .

<sup>e</sup> Energies at B3LYP/6-311++G\*\*//B3LYP/6-311++G\*\*:  $4^{+\bullet}$ , -208.9629654 H, C<sub>3</sub>H<sub>6</sub>, -117.9456353. <sup>f</sup> This structure corresponds to *N*-protonated β-propiolactame. <sup>g</sup> This structure is best described as a complex of a OCNH<sub>2</sub><sup>+</sup> cation with ethene.

The second general aspect concerns thermal contributions. In the mass spectrometric experiments, the valeramide samples were evaporated at room temperature. Therefore, the relative energies computed for 0 K and 298 K are compared with each other, where the difference  $\Delta E_{thermal}$  represents a measure for the importance of thermal contributions (Table 3-5). While thermal effects hardly change the energetics associated with the intramolecular rearrangements of ionized valeramide, all free energies of the exit channels are lowered by about 10 kcal/mol relative to  $\mathbf{1}_1^{++}$ , mostly because of entropy since two particles are formed from one. Therefore, the slightly endothermic expulsion of propene via the McLafferty route ( $E_0 = 6.6$  kcal/mol at 0 K) becomes exoergic at room temperature ( $E_0 = -4.1$  kcal/mol). Thermal contributions can thereby explain the observation of the enol fragment  $\mathbf{4}^{++}$  due to the McLafferty rearrangement right at the onset

**Table 3-5.** Relative energies ( $E_{rel}$ ,  $G_{rel}$  in kcal/mol with  $\mathbf{1}_1^{++}$  as the reference) of several points of the potential-energy surface of ionized valeramide and some the relevant dissociation channels at 0 and 298 K, respectively, and the resulting thermal contributions ( $\Delta E_{thermal}$  in kcal/mol) derived from the B3LYP/6-311++G\*\*//B3LYP/6-31G\* calculations.<sup>a</sup>

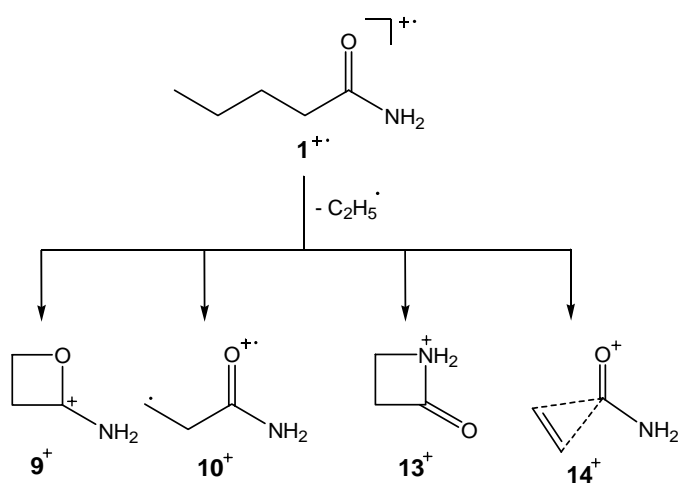
|  | $E_{rel,0}^b$ | $G_{rel,298}^c$ | $\Delta E_{thermal}^d$ |
|--|---------------|-----------------|------------------------|
| $\mathbf{1}_1^{++}/\mathbf{1}_3^{++}$          | 3.4           | 4.0             | 0.6                    |
| $\mathbf{2}_1^{++}$                            | -17.6         | -16.6           | 1.0                    |
| $\mathbf{4}^{++} + \text{C}_3\text{H}_6$       | 6.6           | -4.1            | -10.7                  |
| $\mathbf{5}_1^{++}$                            | -12.5         | -11.2           | 1.3                    |
| $\mathbf{5}_1^{++}/\mathbf{6}^{++}$            | 13.5          | 14.3            | 0.8                    |
| $\mathbf{5}_3^{++}/\mathbf{7}_1^{++}$          | 4.7           | 6.2             | 1.5                    |
| $\mathbf{6}^{++} + \text{C}_2\text{H}_4$       | 11.7          | 1.8             | -9.9                   |
| $\mathbf{7}_3^{++}$                            | -20.3         | -20.1           | 0.2                    |
| $\mathbf{8}^+ + \text{C}_2\text{H}_5^\bullet$  | 9.2           | -1.8            | -11.0                  |
| $\mathbf{9}^+ + \text{C}_2\text{H}_5^\bullet$  | 20.0          | 9.6             | -10.4                  |
| $\mathbf{11}^{++}$                             | -13.2         | -13.1           | 0.1                    |
| $\mathbf{11}^{++}/\mathbf{12}^+$               | 14.3          | 14.6            | 0.3                    |
| $\mathbf{12}^+ + \text{C}_2\text{H}_5^\bullet$ | 8.3           | -0.3            | -8.6                   |

<sup>a</sup> Unscaled frequencies used. <sup>b</sup> Relative energy at 0 K. <sup>c</sup> Relative energy at 298 K including enthalpic and entropic effects. <sup>d</sup> Defined as  $\Delta E_{thermal} = G_{rel,298} - E_{rel,0}$ .

of photoionization. Moreover, while at 0 K the indirect loss of  $\text{C}_2\text{H}_5^\bullet$  as well as the McLafferty reaction are subject to thermodynamic control due to the exit channels, both become kinetically controlled at 298 K.

The more specific aspect is related to the nature of the ionic fragment generated in the direct loss of  $\text{C}_2\text{H}_5^\bullet$ . The indirect route leads to protonated acrylamide  $\mathbf{8}^+$ , which appears to be the global minimum of the  $[\text{C}_3\text{H}_5\text{N}_2\text{O}]^+$  surface.<sup>50</sup> At the employed level of theory, the corresponding exit channel  $\mathbf{8}^+ + \text{C}_2\text{H}_5^\bullet$  is situated at  $E_{rel} = 9.2$  and  $-1.8$  kcal/mol at 0 and 298 K, respectively, and the 0 K value is used as a reference for the other options for  $\text{C}_2\text{H}_5^\bullet$  expulsions. Four different structures directly accessible from ionized valeramide were studied

theoretically. The energetically most stable of these direct products is  $9^+$  (Scheme 3-2), in which the C–C bond cleavage is assisted by simultaneous C–O bond formation. The generation of  $9^+$  is energetically more demanding than that of  $8^+$  by 10.8 kcal/mol. In contrast, direct C–C bond cleavage without formation of a new bond leads to the high-energy isomer  $10^+$  located 75.8 kcal/mol above  $8^+$ . Alternatively to assisting C–O bond formation, C–N bond formation might lead to  $13^+$ , i.e., *N*-protonated propiolactame (also known as 2-acetidinone). Isomer  $13^+$  is, however, 7.2 kcal/mol less stable than  $9^+$  and 18.0 kcal/mol disfavored compared to  $8^+$ . Finally, the computational search also revealed a minimum  $14^+$  which is best described as a complex of a  $\text{OCNH}_2^+$  cation with neutral ethene.



**Scheme 3-2.** Possible products of the direct ethyl loss from  $1^+$ .

### 3.8. Comparison with Literature Thermochemistry

Using thermochemical data bases<sup>51</sup> in combination with selected isodesmic reactions,<sup>52</sup> the heat of formation of gaseous valeramide can be estimated as  $\Delta_f H^\circ(\mathbf{1}) = -71.3 \pm 0.9$  kcal/mol. Combination with  $IE(\mathbf{1}) = 9.40 \pm 0.03$  eV, derived from the photoionization experiments, leads to  $\Delta_f H^\circ(\mathbf{1}^+) = 145.5 \pm 1.4$  kcal/mol. Next, the heat of formation of acetamide ( $-57.0 \pm 0.2$  kcal/mol) combined with its  $IE$  ( $9.69 \pm 0.07$  eV) and the stability difference of 18.9 kcal/mol in favor of the ionized enol, predicted by G2 calculations,<sup>53</sup> suggest  $\Delta_f H^\circ(\mathbf{4}^+) = 147.6 \pm 2.5$  kcal/mol.<sup>54</sup> In conjunction with  $\Delta_f H^\circ(\text{C}_3\text{H}_6) = 4.9$  kcal/mol for propene, fragmentation of  $1^+$  via the  $\text{C}_3$ -route is therefore predicted to be endothermic by  $7.0 \pm 2.9$  kcal/mol. This value compares nicely with the computed reaction enthalpy of 6.6 kcal/mol (Table 3-4).<sup>55</sup> Further, the heat of formation of



acrylamide,<sup>56</sup> its proton affinity,<sup>57</sup> and the heat of formation of ethyl radical<sup>58</sup> predict an endothermicity of  $10.0 \pm 1.6$  kcal/mol for the indirect loss of  $\text{C}_2\text{H}_5^\bullet$  via the  $\text{C}_2$ -route which fits well to the computed 9.3 kcal/mol. Literature values further suggest an endothermicity of about 10 kcal/mol<sup>59</sup> for the loss of  $\text{CH}_3^\bullet$  via the  $\text{C}_1$ -route compared to a computed value of 8.4 kcal/mol for  $\mathbf{12}^+ + \text{CH}_3^\bullet$ . Finally, the relative energetics of the  $[\text{C}_2\text{H}_5\text{N}_2\text{O}]^+$  isomers  $\mathbf{8}^+$ ,  $\mathbf{9}^+$ , and  $\mathbf{13}^+$  are qualitatively consistent with earlier computations at the HF level.

### 3.9. Implications for the Fragmentation Behavior of Ionized Valeramide

Comparing the theoretical studies with the results of the mass spectrometric experiments leads to a consistent description of the dissociation behavior of ionized valeramide. Thus, despite of the limitations of the computational approach used, the B3LYP/6-311++G\*\*//B3LYP/6-31G\* level of theory appears to describe the energetics of ionized valeramide and its rearrangement reasonably well. Moreover, the energetic order of the fragmentation channels is the same for both approaches: loss of propene is most facile and the multistep elimination of  $\text{C}_2\text{H}_5^\bullet$  can occur at slightly higher energies, while losses of  $\text{CH}_3^\bullet$  and  $\text{C}_2\text{H}_4$  as well as the direct elimination of  $\text{C}_2\text{H}_5^\bullet$  require elevated energies. For a quantitative comparison, the point of highest energy demand in each route has to be considered. At room temperature, the  $\text{C}_3$ -route is kinetically controlled via TS  $\mathbf{1}_1^+/\mathbf{1}_3^+$  in which the access to that pathway is determined by conformational changes of the cation radical  $\mathbf{1}^+$ . This situation is consistent with the negligible kinetic isotope effect upon deuteration of the C(4) position derived from experiment ( $KIE(\gamma\text{-CH}) = 1.01$ ). In contrast, the indirect loss of  $\text{C}_2\text{H}_5^\bullet$  via the  $\text{C}_2$ -route is controlled by three barriers of similar energy demands relative to  $\mathbf{1}_1^+$ : TS  $\mathbf{1}_2^+/\mathbf{1}_4^+$  (4.0 kcal/mol), TS  $\mathbf{1}_4^+/\mathbf{5}_1^+$  (3.7 kcal/mol), and TS  $\mathbf{5}_3^+/\mathbf{7}_1^+$  (4.8 kcal/mol) of which the first is a conformational barrier while the two latter are associated with hydrogen migrations. Involvement of all three TSs in the overall reaction is consistent with the more pronounced *KIEs* in this route for both, the C(2) and the C(5) positions as derived from the kinetic modeling ( $KIE(\delta\text{-CH}) = 1.32$ ). The slightly larger barriers of this route compared to the McLafferty rearrangement and the lower overall exoergicity of the  $\text{C}_2$ -route also agree favorably with the strong preference of the  $\text{C}_3$ -route in the photoionization studies. According to the calculated energy profiles, loss of

$\text{C}_2\text{H}_4$  is thermodynamically controlled by the height of the exit channel, which lies ca. 6 kcal/mol above the energy demand for loss of propene. The computations predict loss of  $\text{CH}_3^\bullet$  ( $\text{C}_1$ -route) to be subject to kinetic control due to TS **11**<sup>+</sup>/**12**<sup>+</sup> ( $E_{\text{rel}} = 14.3$  kcal/mol) operative in the exit channel. This energy demand is much larger than those of the competing channels, which is in agreement with the low abundance of  $\text{CH}_3^\bullet$  elimination in the various kinds of mass spectrometric experiments. Finally, the theoretical data shed some light on the structure of the fragment ion formed via the direct loss of  $\text{C}_2\text{H}_5^\bullet$ . Experimentally, the direct route becomes populated at about 1 eV above photoionization threshold. This amount of excess energy is clearly insufficient for the formation of **10**<sup>+</sup> as well as **14**<sup>+</sup> in the direct route, and it is therefore concluded that C–C bond cleavage is accompanied by C–O and/or C–N bond formation to yield **9**<sup>+</sup> and/or **13**<sup>+</sup>, respectively.

While all these results agree pretty well, the presented theoretical results provide no indication for the variations in the  $\text{C}_3/\text{C}_2$  branching observed in various experiments. In fact, irrespective of basis set, temperature etc., the  $\text{C}_3$ -route is always clearly preferred over the  $\text{C}_2$ -route. Accordingly, the static picture of the calculated PES of ionized valeramide in terms of minima and transition structures does not provide a rationale for the ca. 1 : 1 ratio of the  $\text{C}_2$ - and  $\text{C}_3$ -channels observed in the metastable ion studies conducted in the sector experiment. In order to bring more insight in this aspect, some molecular dynamics studies had to be performed (see Chapter 4).

### 3.10. Conclusions

The theoretical study of ionized valeramide using B3LYP leads to the construction of a potential-energy surface for the dissociation behavior of the radical cation, which is consistent with many results of the mass spectrometric studies. The calculated PES agrees with respect to the energetic ordering of the fragmentation channels observed and confirms the mechanistic schemes derived from analysis of the labeling data. In fact, even subtle details of the proposed fragmentation schemes, e.g. the pairwise equilibration of C(2)/C(3) with C(4)/C(5), as well as kinetic isotope effects are qualitatively confirmed by theory. As far as competition between the different fragmentation channels is concerned, the computed results agree qualitatively with the branching ratios obtained in the photoionization studies. Thus, the McLafferty rearrangement ( $\text{C}_3$ -route) has the lowest

energy demand, while the computed pathways for losses of  $\text{CH}_3^\bullet$ ,  $\text{C}_2\text{H}_4$ , and “indirect”  $\text{C}_2\text{H}_5^\bullet$ , respectively, are somewhat higher in energy, but of comparable magnitude. Quite remarkable is the effect of thermal contribution on the dissociation behavior, in that at 0 K all fragmentations are thermodynamically controlled by the high-energy demand of the exit channels, whereas kinetic control due to intermediate barriers is most important at 298 K or higher temperatures. The missing link between experiment and theory concerns the unusual variations in the  $\text{C}_3/\text{C}_2$  ratios observed in some of the experiments. While the theoretical results support the idea that the experimentally observed routes are uncoupled from each other, i.e., the H-migrations from various positions occur quasi-irreversibly, none of the computed properties can explain, why the  $\text{C}_3/\text{C}_2$  ratio of about 1 is observed for metastable  $\mathbf{1}^{+\bullet}$  in the sector-field instrument.

In a more general sense, the computational exploration of the potential-energy surface of the molecular ion of valeramide suggests that various kinds of C–H bond activations are possible for ionized carbonyl compounds. Instead of a kinetic control by the barrier associated with hydrogen migration, the regioselectivity of C–H bond activation seems to be determined by the accessibility of the appropriate conformations in the parent ion as well as the energetics of the associated exit channels. In fact, the present results suggest that the prevalence of the McLafferty rearrangement in the mass spectrometric fragmentation of carbonyl compounds is not primarily due to a particular preference of 1,5-hydrogen transfer, but results from the favorable energy demand of the dissociation products.

## 4. Temperature Effect on the Dissociation Pattern of Ionized Valeramide\*

### 4.1. An Unprecedented Temperature Effect on the C<sub>3</sub>/C<sub>2</sub> Branching Ratio

The metastable ion studies performed in the four-sector instrument yield C<sub>3</sub>/C<sub>2</sub> ratios close to unity. A C<sub>3</sub>/C<sub>2</sub> ratio of about  $3 \pm 1$  is derived as a mean for the metastable traces in the threshold photoelectron-photoion coincidence (TPEPICO) data between 9.8 and 10.5 eV, and for dissociative photoionization the C<sub>3</sub>/C<sub>2</sub> ratios range from ca. 5 at photon energies above 12 eV to C<sub>3</sub>/C<sub>2</sub> > 100 close to the ionization threshold of valeramide. While refined insight in most of the mechanistic details is achieved, the gross product distribution is not understood. Out of quite a few effects of various experimental parameters on the C<sub>3</sub>/C<sub>2</sub> ratio, the temperature of the ion source ( $T_s$ ) was the only difference between the two machines. The ion source of CERISES<sup>60</sup> is operated at room temperature, whereas conventional EI sources, such as the one installed in the sector instrument,<sup>22,23</sup> are usually maintained at elevated temperature (typically 200 °C) in order to reduce memory effects and to avoid temperature drifts caused by the glowing filament which effectively acts as a heater. While the temperature of the ion source is known to affect EI mass spectra<sup>61,62</sup> as well as the fragmentation patterns upon collisional activation,<sup>63,64</sup> temperature effects on intensity ratios in metastable ion spectra are usually small. Recently, a thorough study of Norrman and McMahon further corroborated these ideas.<sup>65</sup> In fact, these authors even concluded that the internal energy of metastable ions (proton-bound dimers were studied) decreases with increasing  $T_s$ . Thus, the product branching ratios typically increased by about 50 % in favor of the thermodynamically favored product when increasing  $T_s$  from 50 to 300 °C. Because a similar, or even negligible temperature behavior was also expected for ionized valeramide, a pronounced, however, *reversed* effect of the source temperature on the C<sub>3</sub>/C<sub>2</sub> ratios in the MI spectra of 1<sup>+</sup> came at a great surprise (Figure 4-1).

\* Results discussed in this chapter have been published in: (a) Schröder, D.; Loos, J.; Semialjac, M.; Weiske, T.; Schwarz, H.; Höhne, G.; Thissen, R.; Dutuit, O. *Int. J. Mass Spectrom.* **2002**, 214, 155. (b) Semialjac, M.; Schröder, D.; Schwarz, H. *Chem. Eur. J.* **2003**, 9, 4396.

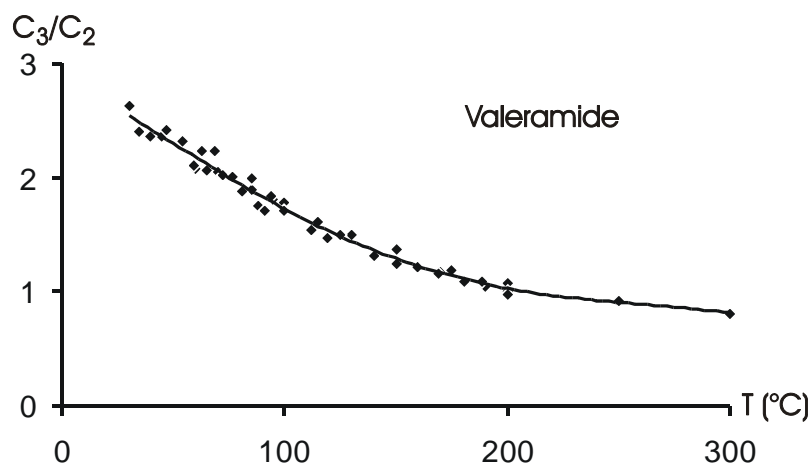


**Figure 4-1.**  $C_3/C_2$  ratios in the MI spectra of mass-selected  $1^{+*}$  as a function of the temperature of the ion source.

All experiments with the sector instrument<sup>22,23</sup> were performed at  $T_s = 200$  °C at which  $C_3/C_2$  ratios of about  $1 \pm 0.1$  were obtained in all kinds of experiments conducted with metastable  $1^{+*}$ . Upon lowering  $T_s$ , however, the  $C_3/C_2$  ratios increases notably and in fact reaches a value of ca. 3 at the lowest temperature achieved. Hence, after all it is effectively the source temperature which gives rise to the variations in the  $C_3/C_2$  ratios in the two kinds of instruments. So far no similar effect of this magnitude has been observed in previous metastable ion studies.<sup>66</sup> Compared to the results of Norrman and McMahon, the effect is much more pronounced and works in the opposite direction, i.e., the high-energy channels are favored at higher source temperatures.

For a carbonyl compound, an obvious explanation of the temperature effect is provided by invoking the involvement of keto/enol tautomerization of the neutral precursor. In fact, temperature effects have been observed in the metastable mass spectra of ionized 1,3-diones which easily undergo enolization.<sup>67</sup> For the case of valeramide, this would imply that increasing temperatures favor formation of the neutral enol **7** which is, in turn, much easier to ionize than **1** (see Chapter 3). Hence, the  $C_3/C_2$  ratio of about 1 at 200 °C might be explained by involving the formation of a mixture of  $1^{+*}$  and  $7^{+*}$  upon ionization, because the former contributes to both routes while the latter decays via the  $C_2$ -channel almost exclusively. Moreover, the enol has a significantly lower ionization energy than the keto and the corresponding cation radical  $7^{+*}$  resides in a much deeper well than

$1^{+}$ . Accordingly, an enrichment of the enol cation in the mass-selected ion beam is to be expected. Therefore, keto/enol tautomerization of the neutral would provide an intuitive and straightforward explanation for the observed temperature dependence of the MI spectra. However, the computed stability difference of ca. 25 kcal/mol in favor of  $1^{68}$  disputes involvement of neutral **7**. Even if keto/enol tautomerism is effectively catalyzed by termolecular or surface reactions, the computed energy differences suggest a keto/enol ratio of about  $10^{18}$  at room temperature, and still about  $10^{11}$  at 200 °C. These ratios appear much too large, and therefore this explanation is highly unlikely.

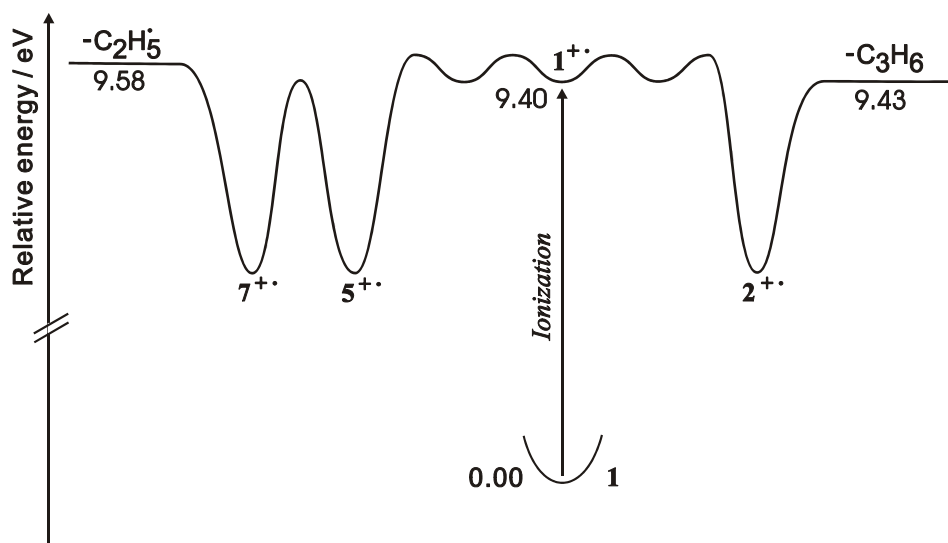


**Figure 4-2.** Simplified potential-energy surface for the competitive dissociation of  $1^{+}$  via the  $C_2$ - and  $C_3$ -routes.

Three further possible mechanistic scenarios have been proposed to account for this surprising effect:

(I) Because the regioselectivities of the initial C–H bond activations are primarily determined by the accessibility of the appropriate conformations, it is conceivable that the population of the neutral conformers required for access to the  $C_2$  route increases at elevated temperatures. A comprehensive description of such a scenario must also account for the different trajectories involved in  $\gamma$ -C–H and  $\delta$ -C–H bond activations by means of dynamic considerations.

(II) Uncoupling of the distonic intermediates  $2^{+}$  and  $5^{+}$  is expected not to affect the  $C_3/C_2$  ratio in metastable ion dissociations in any but unusual situations. In the present case, the appearance energy of the  $C_3$ -route is very close to the ionization threshold of **1**,

indicating rather low thermochemical and kinetic restrictions of this particular fragmentation (Figure 4-2). Consequently, it is conceivable that the population of intermediate  $2^{+*}$  is effectively depleted at elevated temperatures in that a significant fraction of  $2^{+*}$  formed upon ionization of **1** already dissociates before time delayed mass-selection is achieved. Thus, the unexpectedly low  $C_3/C_2$  ratio of about 1 in the experiments with metastable ions (lifetimes around few  $\mu$ s) conducted at a source temperature of 500 K could be explained through an enrichment of  $5^{+*}$  relative to  $2^{+*}$ .

(III) The third hypothesis is similar to scenario (II) but involves an enhanced propensity for the formation of long-lived  $1^{+*}$  upon ionization of neutral valeramide at low temperatures. Contribution of some amount of genuine  $1^{+*}$  to the mass-selected ion beam would result in a preference for the energetically favored  $C_3$  route. Thus, the  $C_3/C_2$  ratio would increase relatively to that observed at higher temperatures and this scenario can thereby account for the observed temperature behavior as well.

The above mentioned scenarios were taken into account and investigated further theoretically. However, yet another scenario might contribute to the temperature effect on the dissociation pattern of the ionized valeramide as well, i.e. the difference of the cross-sections for ionization of different valeramide conformers. In such a scenario depending on temperature some of the valeramide conformers could be easier ionized than the others and could give rise only to a particular rearrangement type. In order to test this scenario the whole conformational space of the neutral and ionized valeramide should be considered and such computations would be extremely time-consuming. Because of the limited computational resources available, unfortunately, this aspect could not be addressed computationally. Nevertheless, the results obtained by the Car-Parrinello molecular dynamics provided rationals for the unusual temperature effect. However, it should be kept in mind that the cross section might also contribute to the temperature effect.

## 4.2. Rationalization of the Temperature Effect on the Dissociation

### Pattern: Car – Parrinello Molecular Dynamics Study

As a natural choice for testing the above mentioned hypotheses by computational means, studies employing some of the current molecular dynamics (MD) methods are indicated. Since the electronic effects in radical cation systems most probable play a crucial role on rearrangement pathways, an ab initio MD method is deemed the only

acceptable choice for obtaining any significant results. The Car-Parrinello molecular dynamics (CPMD)<sup>69</sup> approach is the most appealing procedure because of its superb performance in chemistry and material sciences.<sup>70</sup> CPMD combines classical molecular dynamics with quantum mechanical computations of the electronic structure (ab initio part). The forces on the nuclei are obtained from the electronic ground state energy using the Hellmann-Feynman theorem, rather than from an empirical force field as common for the non-ab initio based MD methods. The Car-Parrinello procedure differs from the Born-Oppenheimer MD technique in using a dynamical optimization scheme known as simulated annealing for electronic wave function degrees of freedom, which can be treated simultaneously with Newtonian nuclear dynamics. As the parameter of inertia, called “fictitious electronic mass”, is much smaller than the nuclei masses, the wave function adapts instantaneously to the moving nuclei and keeps the electrons sufficiently close to the correct ground state (within the Born-Oppenheimer approximation).

### 4.3. Computational Methods

The Car-Parrinello molecular dynamics<sup>69</sup> simulations were performed with the CPMD program<sup>71</sup> using a plane wave basis and a spin polarized semi-local BLYP functional.<sup>27,28</sup> The wave function was expanded at the  $\Gamma$ -point in a plane wave basis set with the kinetic energy cutoff of 70 Ry and a cuboid box (dimensions [11.007 x 8.805 x 8.805] Å) was used under the periodic boundary conditions. The form of the non-local pseudo-potential according to Kleinman and Bylander was employed,<sup>72</sup> and the core electrons were described by the pseudopotentials of Trouiller and Martins.<sup>73</sup> Simulations on positively charged species were performed with the corresponding negative charge distributed uniformly in the cell.<sup>74</sup> The time step (given in a.u.; 1 a.u.  $\sim$  0.0241888 fs) for the numerical integration of the equations of motions,<sup>75</sup> according to the velocity Verlet algorithm, was adjusted to a particular system under investigation; for the neutral valeramide a time step of 4 a.u. was employed, while for the radical cation the time step equals to 3 a.u.

Some of the optimized geometries obtained in the previous theoretical study<sup>68</sup> were used as initial structures for the CPMD runs. These geometry optimizations were

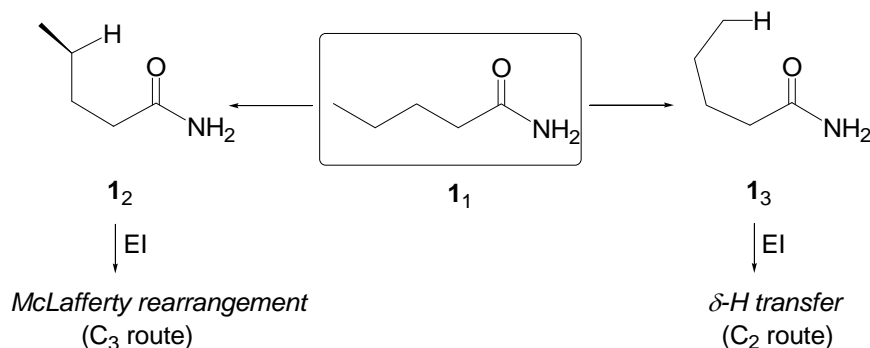


performed with the GAUSSIAN 98 suite of programs employing the B3LYP functional<sup>27,28</sup> and the 6-31G\* basis set.<sup>76</sup>

In case of the CPMD simulations, the labels do not only represent one particular structure (conformer) as was the case for the non-dynamical computations;<sup>68</sup> rather, it comprises the whole conformational subspace, although in the accompanying figures often only one representative is depicted.

In order to test the reproducibility and compare the results obtained in the previous study<sup>68</sup> (B3LYP/6-311++G\*\*//B3LYP/6-31G\*) with those computed with the CPMD (BLYP and cutoff of 70 Ry), one of the crucial transition barriers for the conformational change in valeramide radical cation has been singled out. For the conformational change  $\mathbf{1}_1^+ \rightarrow \mathbf{1}_3^+$ , the barrier equals to 3.5 kcal/mol at the B3LYP/6-311++G\*\*//B3LYP/6-31G\* level of theory, while it amounts to 4.0 kcal/mol (0 K) when computed with the BLYP functional as implemented in the CPMD program. Thus, an overall good agreement between the results obtained with the two computational methods is expected.

#### 4.4. Neutral Valeramide



**Scheme 4-1.** Conformational changes from the conformation with a relaxed carbon backbone **1**<sub>1</sub> into folded ones, that upon ionization may lead eventually to the McLafferty or the  $\delta$ -H transfer rearrangements.

A CPMD study of neutral valeramide **1** is used to address hypothesis (I), i.e. that the population of the neutral conformers required to access the C<sub>2</sub>-route increases at elevated temperatures. Therefore, CPMD simulations at an average temperature of 519 K were performed.<sup>77</sup> As an initial geometry conformer **1**<sub>1</sub> was used (Scheme 4-1), which was obtained as the (global) minimum in the previous study.<sup>68</sup> Monitoring the dihedral angle

C(1)-C(2)-C(3)-C(4) during the CPMD simulation (Figure 4-3) should indicate conformational changes of the fully extended carbon-chain conformation into folded conformers that might serve as precursors for the intramolecular H-transfers. However, during the MD simulation, which lasted for 6250 fs, no relevant conformational changes of **1** were observed (the dihedral angle C(1)-C(2)-C(3)-C(4) remains practically constant). The parameter that fluctuates most is the dihedral angle N-C(1)-C(2)-C(3) (Figure 4-3), which is associated with an internal rotation of the amide group. However, as the results of such simulations depend heavily on the initial conditions (e.g. choice of the starting conformer) and a possibility of insufficient sampling time, a note of caution is warranted. There are two ways to address the problem: either to perform a great number of MD simulations with different initial conformers, or to compute the free activation energy associated with the conformational changes crucial for the eventual hydrogen transfers. Since for valeramide more than 200 different conformers were indicated to exist,<sup>68</sup> it seems rather impractical to perform as many MD runs commencing from those conformers. Instead, the barriers associated with the conformational change starting from a conformation with the totally relaxed carbon-backbone (Scheme 4-1: encircled) into the folded ones, i.e. **1**<sub>2</sub> and **1**<sub>3</sub> were computed.

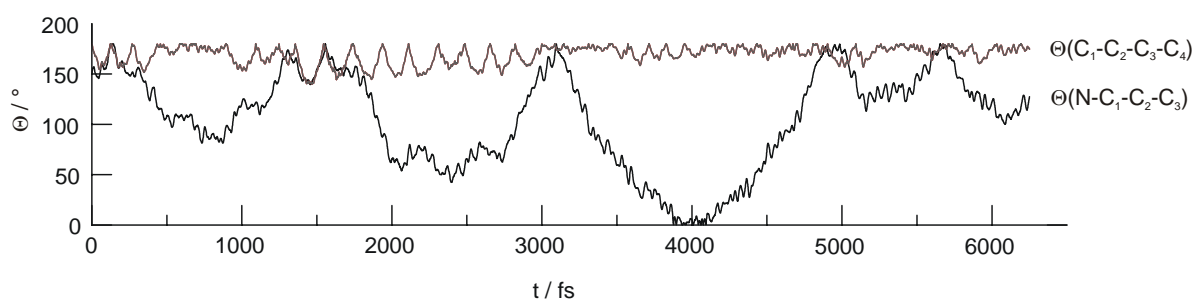


**Figure 4-3.** Changes in the dihedral angles of neutral valeramide **1** during the CPMD simulation; average temperature 519 K; trajectory sampled for 6250 fs.

The free energy profiles associated with both conformational changes were computed at approximately 500 K; in these computations the distances between the oxygen atom and a hydrogen atom attached to C(4) (crucial for the McLafferty rearrangement) or to C(5) (crucial for the  $\delta$ -H shift) were varied by performing a series of short CPMD simulations at different, fixed O-H distances (constraint parameter). For the purpose of driving the system along the reaction path it is not necessary that the constraint degree of freedom is identical with the true reaction coordinate. Rather, it suffices that the constraint

variable approximately points in the direction of the tangent of the reaction path.<sup>78</sup> The free energy profile can be determined by integrating the mean averaged force with respect to the constraint coordinate.<sup>79</sup> Therefore, short CPMD simulations (ca. 0.5 ps) were performed for a constraint O-H distance with an increment of 0.2 Å.<sup>80</sup> The free activation energy ( $\Delta G^\ddagger$ ) associated with the conformational change from the completely relaxed carbon chain (**1<sub>1</sub>**)<sup>81</sup> into the folded conformer that after ionization could lead to the McLafferty rearrangement (**1<sub>2</sub>**) amounts to 3.5 kcal/mol (Figure 4-4), while  $\Delta G^\ddagger$  for the change into a conformer, from which the  $\delta$ -H shift might commence (**1<sub>3</sub>**), equals to 5.9 kcal/mol (Figure 4-5). At average temperatures<sup>82</sup> of the simulations, the thermal energy available in the direction of the reaction coordinate equals to 0.5 kcal/mol. Thus, the conformational barriers in these endergonic reactions cannot be overcome just by thermal motion. Moreover, taking into account relative stabilities using the Boltzmann equation, one obtains an approximate composition of the conformational populations assuming that the ensemble contains only the fully relaxed carbon chain conformation (**1<sub>1</sub>**) and the two folded ones (**1<sub>2</sub>** and **1<sub>3</sub>**). This estimation results in a composition of 96.4 % **1<sub>1</sub>**, 3.3 % **1<sub>2</sub>**, and 0.3 % **1<sub>3</sub>**. Therefore, the first hypothesis can be ruled out since the conformational population of neutral valeramide at ca. 500 K consists mostly of a conformation with a fully relaxed carbon backbone **1<sub>1</sub>**. Folded conformations cannot explain the observed

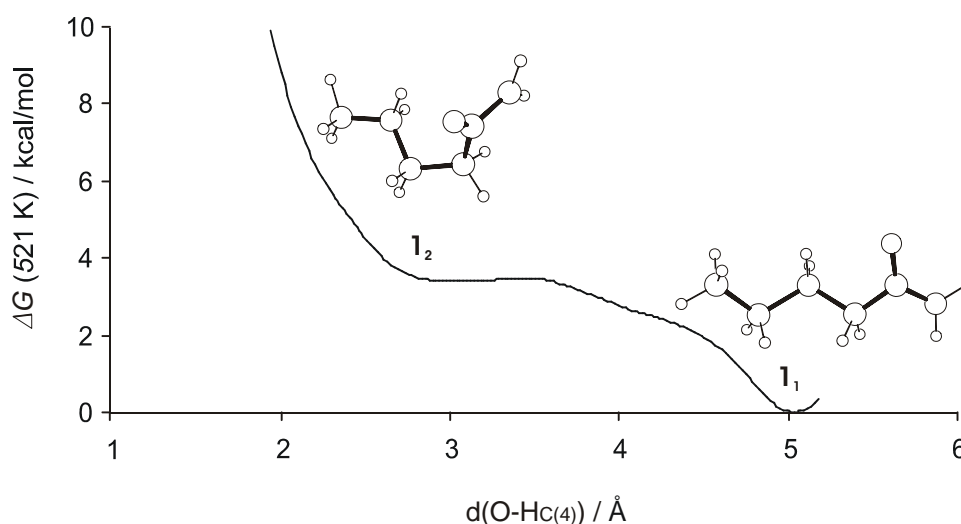


**Figure 4-4.** The free energy profile at an average temperature of 521 K for the conformational change **1<sub>1</sub>**  $\rightarrow$  **1<sub>2</sub>**; from the latter, upon ionization, the McLafferty rearrangement could commence. For the CPMD simulations the distances between the oxygen atom and a hydrogen at the C(4) center were constrained.

temperature effect on the dissociation pattern because they are not populated in sufficient amount due to the conformational barriers that cannot be surmounted by thermal motion. Thus, an explanation of the anomalous temperature effect has to be sought on the potential energy surface of the valeramide radical cation  $\mathbf{1}^{+\bullet}$ .

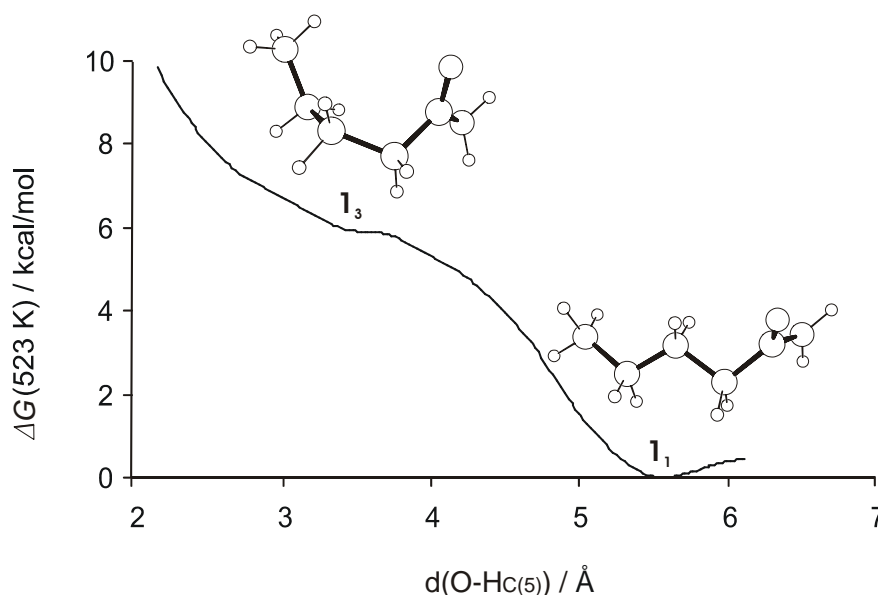


**Figure 4-5.** The free energy profile at an average temperature of 523 K for the conformational change  $\mathbf{1}_1 \rightarrow \mathbf{1}_3$ ; from the latter, upon ionization the  $\delta$ -H transfer could commence. For the CPMD simulations the distances between the oxygen atom and a hydrogen at the C(5) center were constrained.

## 4.5. Valeramide Radical Cation

### 4.5.1. Simulations at 300 K

As initial geometries for the CPMD simulations at ca. 300 K, three different conformers of the valeramide radical cation ( $\mathbf{1}_1^{+\bullet}$ ,  $\mathbf{1}_3^{+\bullet}$  and  $\mathbf{1}_4^{+\bullet}$ )<sup>83</sup> were used. Conformer  $\mathbf{1}_1^{+\bullet}$ , which contains a fully relaxed carbon backbone, corresponds to the global minimum,<sup>68</sup> and conformers  $\mathbf{1}_3^{+\bullet}$  and  $\mathbf{1}_4^{+\bullet}$  were identified as those from which the McLafferty and the  $\delta$ -H shift rearrangements commence. When  $\mathbf{1}_1^{+\bullet}$  is used as the initial geometry for the CPMD simulation, an intramolecular hydrogen transfer was not observed even after 7257 fs (see inset in Figure 4-6). Further, the dihedral angle C(1)-C(2)-C(3)-C(4) that could indicate a reaction does not change significantly during the simulations, neither does the distance between the oxygen atom and a hydrogen from the C(4)

position.<sup>84</sup> However, if the initial geometry contains already a folded carbon backbone, the McLafferty rearrangement is completed after only 392 or 1925 fs, depending whether the initial geometry for the CPMD simulation was  $\mathbf{1}_3^{+\bullet}$  or  $\mathbf{1}_4^{+\bullet}$ , respectively.

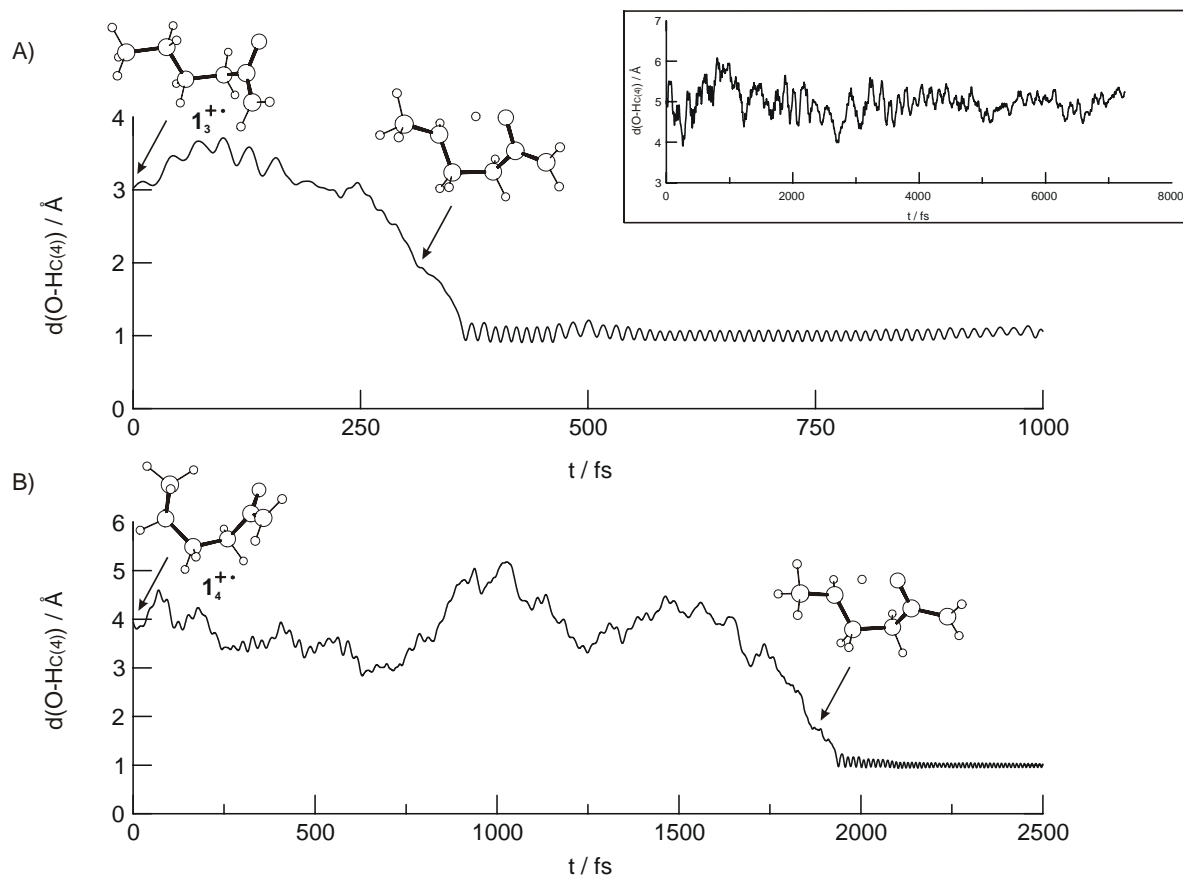


**Figure 4-6.** The CPMD simulations of  $\mathbf{1}^{+\bullet}$  at 300 K. The reaction ( $\gamma$ -H shifts) constitutes the initial phase of the McLafferty rearrangement. Two different conformers of the valeramide radical cation were used as starting geometries: A)  $\mathbf{1}_3^{+\bullet}$  and B)  $\mathbf{1}_4^{+\bullet}$ . In the inset, the CPMD simulation at 300 K is shown for the conformer  $\mathbf{1}_1^{+\bullet}$  as initial geometry; trajectory sampled for 7257 fs during which no reaction is observed.

The progress of the McLafferty reaction can be followed by monitoring the distance between the oxygen and a hydrogen atom bonded to the C(4) center (Figure 4-6). In conformer  $\mathbf{1}_3^{+\bullet}$  the oxygen-hydrogen distance is already relatively short (3.023 Å), thus facilitating the H-transfer reaction (completed within 392 fs). Even though in the non-dynamical computations conformer  $\mathbf{1}_4^{+\bullet}$  was identified as the one from which the  $\delta$ -H shift commences,<sup>68</sup> the dynamical simulation (Figure 4-6B) indicates that the McLafferty rearrangement is easily accessible from that conformation as well. Accordingly, the

McLafferty rearrangement seems more probable than the  $\delta$ -hydrogen shift. However, in order to substantiate this assumption, the  $\Delta G^\ddagger$  changes associated with both rearrangements had to be computed. Therefore, constraint molecular-dynamics simulations were performed at ca. 300 K for both rearrangements.<sup>85</sup> In order to trigger the McLafferty rearrangement, the distance between the oxygen and a hydrogen atom bonded to C(4) atom was constrained (Figure 4-7), and the competing  $\delta$ -H shift was monitored by confining the distance between the oxygen and a hydrogen at the C(5) atom (Figure 4-8).

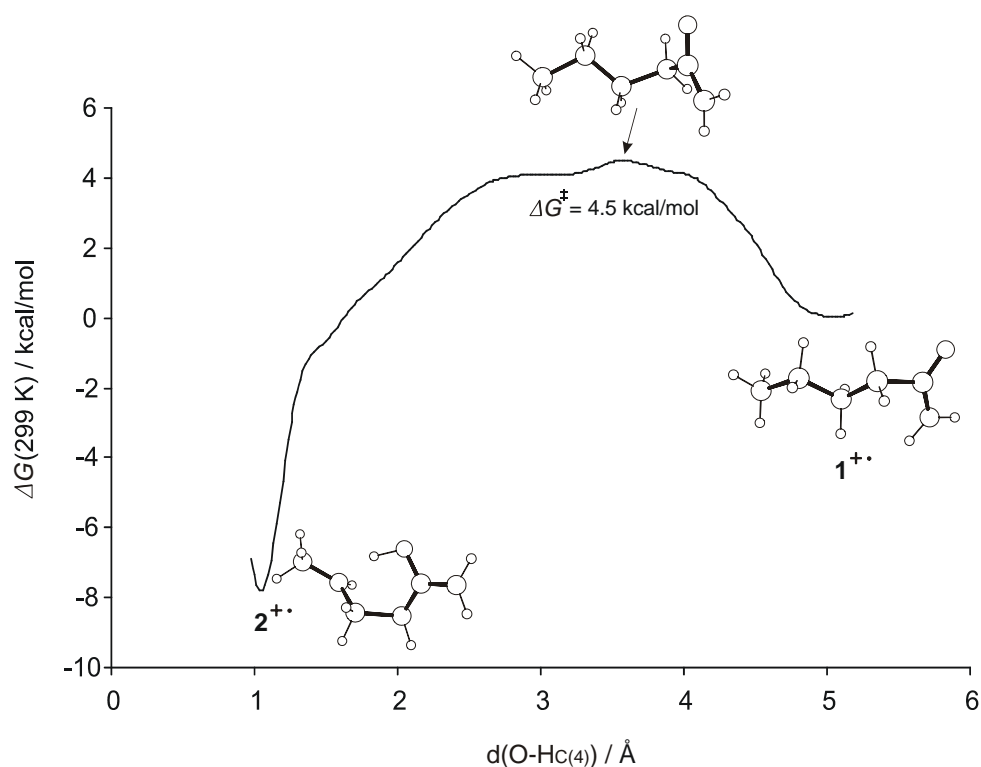


**Figure 4-7.** The free energy profile for the McLafferty rearrangement at an average temperature of 299 K, as obtained from the series of constraint CPMD simulations. The distances between the oxygen atom and a hydrogen at the C(4) center were constrained.

The activation free energy associated with the McLafferty rearrangement  $1^{+\bullet} \rightarrow 2^{+\bullet}$  amounts to 4.5 kcal/mol. As can be seen in Figure 4-7, the major amount of the activation energy is used for the conformational change (the O-H distance varies from 3 - 5 Å), while the actual hydrogen transfer does not seem to be rate determining; this scenario was already suggested in the previous experimental and theoretical studies.<sup>22,68</sup> As soon as the “correct” conformer is formed, the hydrogen transfer proceeds without any barrier to form

the distonic ion  $2^{+}$  in an exergonic reaction (-7.8 kcal/mol). This ion serves as an intermediate in the pathway in which propene ( $C_3$ -channel) is formed in an entropy-driven reaction.

The  $\delta$ -H shift is more complex due to the conformational changes that  $1^{+}$  has to overcome in order to populate a conformer from which the H transfer can proceed. Several conformational steps are indicated (see Figure 4-8) and the total activation energy prior to the H-shift activation amounts to 5.0 kcal/mol, while the free energy activation for the final step, i.e. the  $\delta$ -H transfer, equals to 2.0 kcal/mol. Thus, these CPMD computations are as well in good agreement with experimental and theoretical studies,<sup>22,68</sup> according to which the conformational changes are energetically more demanding than the actual H-transfers themselves for both competing processes. In addition, the observation that the  $C_3$  route is associated with a negligible kinetic isotope effect for hydrogen versus deuterium migration ( $KIE = 1.03$ ), whereas the  $C_2$  route bears a small, but yet significantly larger effect ( $KIE = 1.32$ )<sup>22</sup> is in accord with the present CPMD results.

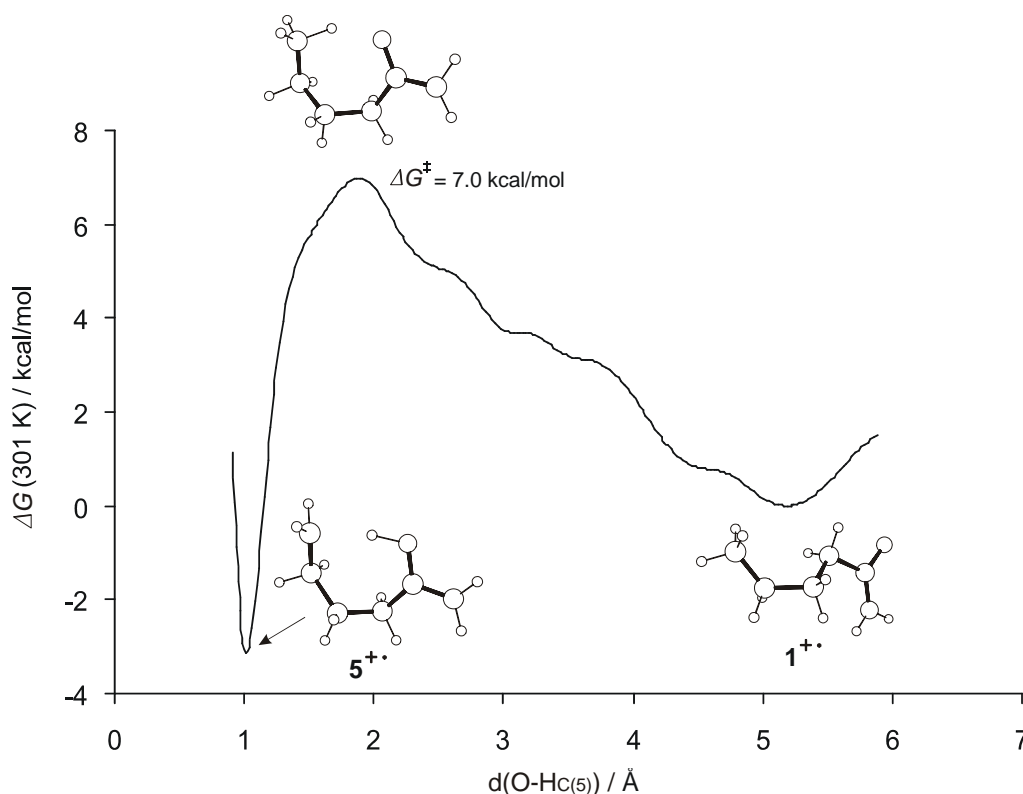


**Figure 4-8.** The free energy profile for the  $\delta$ -H transfer at an average temperature of 301 K, as obtained from the series of constraint CPMD simulations. The distances between the oxygen atom and a hydrogen at the C(5) center were constrained.

Comparison of the total  $\Delta G^\ddagger$  changes (Table 4-1) for both rearrangements reveals that the McLafferty rearrangement (4.5 kcal/mol) is energetically less demanding than the  $\delta$ -H shift (7.0 kcal/mol). Moreover, the PES associated with the McLafferty rearrangement is less complicated and the distonic ion  $2^{+\bullet}$  can immediately dissociate upon its formation thus increasing the entropy of the reaction; in contrast, the distonic ion  $5^{+\bullet}$  can enter either directly or through yet another H-shift the dissociation channel ( $C_2$ -route; see Figure 4-2). Thus, the McLafferty rearrangement seems more probable at 300 K than the  $\delta$ -hydrogen transfer. However, this does not yet explain the observed temperature effect on the dissociation pattern. Therefore, CPMD simulations at 500 K had to be performed. Nevertheless, at this point a brief comment on the third hypothesis, i.e. the role of long-lived  $1^{+\bullet}$ , is warranted. Because the conformational changes are energetically more demanding than the corresponding hydrogen transfers, conformer  $1^{+\bullet}$  is trapped by conformational barriers and can be postulated to be long-lived at ca. 300 K. In fact, no H-transfer was observed when the fully relaxed carbon backbone conformation  $1^{+\bullet}$  was taken as the initial geometry (see inset in Figure 4-6). This finding strongly suggests that in the experiments performed at lower temperatures (ca. 320 K) a larger population of  $1^{+\bullet}$  is mass-selected than at elevated temperatures, which eventually undergoes more readily the McLafferty rearrangement ( $C_3$ -route), thus increasing (relatively to the results at higher temperatures) the  $C_3/C_2$  ratio to approximately 3. Nevertheless, this explanation does not exclude the possibility that at higher temperatures the population of intermediate  $2^{+\bullet}$  is effectively depleted so that a significant fraction of  $2^{+\bullet}$ , formed upon ionization of **1**, already dissociates before mass-selection.

**Table 4-1.** Comparison between energy demands (in kcal/mol) for processes relevant for the valeramide radical cation  $1^{+\bullet}$  dissociation obtained with a non-dynamical method (B3LYP/6-311++G\*\*//B3LYP/6-31G\*) and the CPMD method.

| Activation     | Non-Dynamical<br>Method <sup>a</sup> |                      | CPMD method |                      |            |                      |
|----------------|--------------------------------------|----------------------|-------------|----------------------|------------|----------------------|
|                | 0 K                                  |                      | 300 K       |                      | 500 K      |                      |
|                | McLafferty                           | $\delta$ -H<br>shift | McLafferty  | $\delta$ -H<br>shift | McLafferty | $\delta$ -H<br>shift |
| Conformational | 3.5 <sup>b</sup>                     | 4.0                  | 4.5         | 5.0                  | 2.5        | 3.6                  |
| H-transfer     | n/a <sup>c</sup>                     | 3.7                  | 0.0         | 2.0                  | 0.0        | 2.0                  |
| Total          | 3.5                                  | 4.0                  | 4.5         | 7.0                  | 2.5        | 4.4                  |

<sup>a</sup> Values taken from ref. 68; they correspond to the most stable conformer of the particular structure. The values given present relative enthalpies at 0 K. <sup>b</sup> The BLYP as implemented in CPMD results in a barrier of 4.0 kcal/mol at 0 K. <sup>c</sup> The transition structure associated with the H-transfer could not be located.



#### 4.5.2. Simulations at 500 K

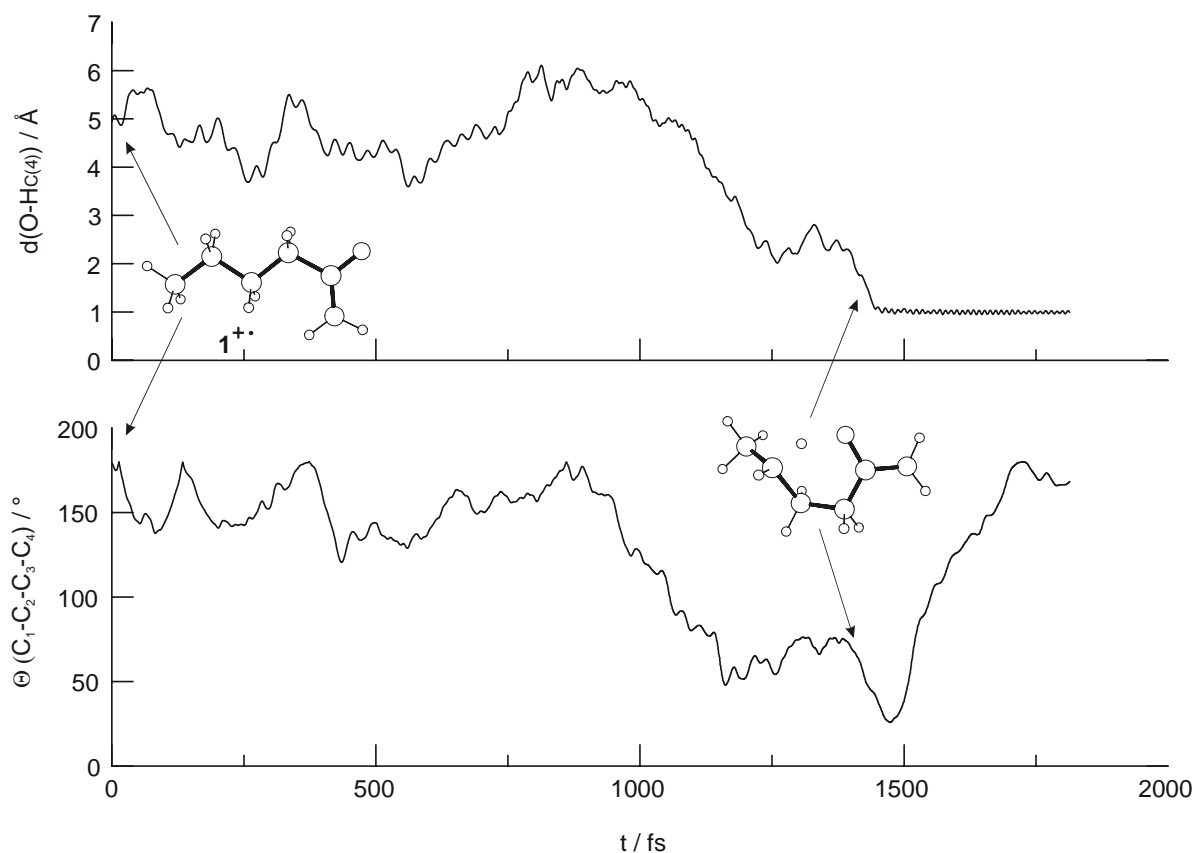
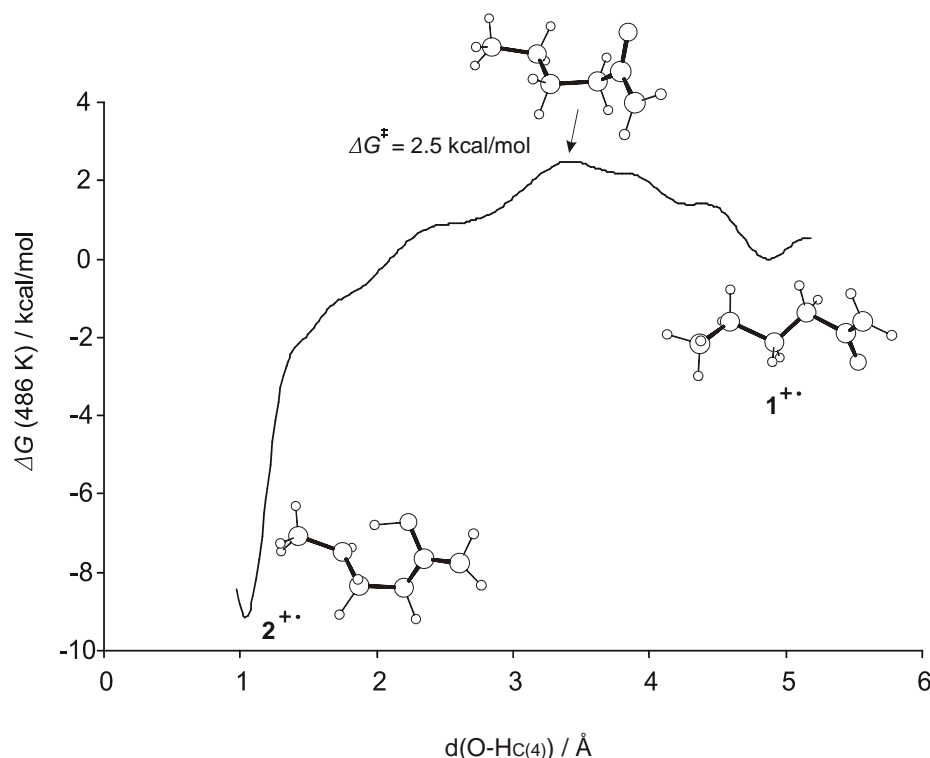


**Figure 4-9.** The CPMD simulation at an average temperature of 535 K. The reaction observed corresponds to the McLafferty rearrangement. The conformer  $1_1^{+\bullet}$  was used as initial geometry.

As the initial geometry for the CPMD simulation at ca. 500 K, conformer  $1_1^{+\bullet}$  was employed and the McLafferty rearrangement was completed already after 1444 fs (Figure 4-9). The reaction evolution can be monitored as well by following the change in the dihedral angle C(1)-C(2)-C(3)-C(4) that accompanies the H-transfer. Prior to the McLafferty rearrangement a conformational change had to occur; this is achieved within 1200 fs (see the change in the dihedral angle in Figure 4-9). Simultaneously with the hydrogen transfer, a further conformational change takes place in which the dihedral angle decreases below  $25^\circ$ . After the H-transfer has been completed, a new distonic ion is formed where the oxygen atom is protonated and the radical center is located at C(4); the resulting distonic ion undergoes yet another conformational change in order to escape from its staggered conformation.



**Figures 4-10.** The free energy profile for the McLafferty rearrangement at an average temperature of 486 K, as obtained from the series of constraint CPMD simulations. The distances between the oxygen atom and a hydrogen at the C(4) center were constrained.

In line with conclusions derived in the previous chapters, also at higher temperatures the McLafferty rearrangement seems again more probable than the  $\delta$ -H shift counterpart. Nevertheless, to be on the safe side, the free activation energy associated with both H-transfer processes has been computed. Therefore, constraint CPMD simulations<sup>85</sup> were performed at ca. 500 K with  $1^{+\bullet}$  as the initial geometry for both reaction coordinate calculations. The  $\Delta G^\ddagger$  for both rearrangements are, as expected, lower at 500 K than at 300 K. In the case of the McLafferty rearrangement (Figure 4-10), the total free activation energy equals to 2.5 kcal/mol, while the  $\delta$ -H shift is again energetically more demanding (4.4 kcal/mol; Figure 4-11). In both cases, conformational changes need to occur prior to the H-transfer. In the McLafferty rearrangement, the actual H-transfer proceeds barrierless, and the reaction takes place as soon as the right conformer is formed. Prior to the  $\delta$ -H transfer, at least two conformational barriers have to be overcome (Figure 4-11), and the activation energy associated with these steps equals to 3.6 kcal/mol, being again higher

than  $\Delta G^\ddagger$  for the H-transfer (2.0 kcal/mol) itself. Thus, the conformational changes that enable H-transfers are again rate-determining for both rearrangements.

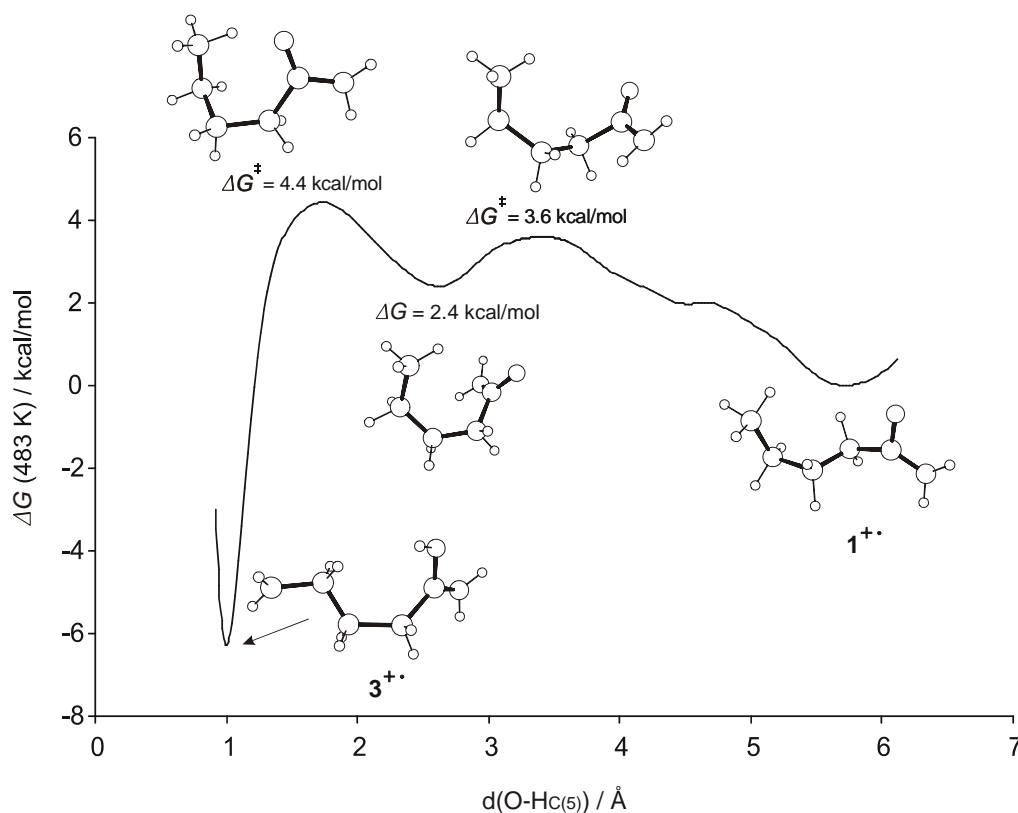


**Figure 4-11.** The free energy profile for the  $\delta$ -H transfer at an average temperature of 483 K, as obtained from the series of constraint CPMD simulations. The distances between the oxygen atom and a hydrogen at the C(5) center were constrained.

Comparing the total free activation energies associated with the two hydrogen transfers, it is clear that the McLafferty rearrangement is more probable. Moreover, such a low activation energy for the McLafferty rearrangement is expected to be easily overcome under mass-spectrometric conditions, where the appearance energy of the  $C_3$  route is very close to the ionization threshold of **1** (Figure 4-2). Therefore, it is quite likely that at elevated temperatures a significant fraction of **2**<sup>+</sup> formed upon ionization of **1** already dissociates before mass-selection is achieved; as a consequence, the actual  $C_3/C_2$  ratio drops in the experiments conducted at a source temperature of 500 K. In the mass-spectrometric experiments, the time window between the ionization and the mass-selection (some  $\mu$ s) is sufficiently large to induce the  $\gamma$ -hydrogen transfer and the dissociation of the distonic ion **2**<sup>+</sup>.<sup>22,23</sup> According to the CPMD simulation (Figure 4-9) the rearrangement is

completed after only 1444 fs. Since the subsequent dissociation of  $\mathbf{2}^{+*}$  is barrierless,<sup>68</sup> it is likely to happen immediately after the H-transfer has been completed.

## 4.6. Conclusions

CPMD studies of neutral and ionized valeramide provide a rational for the unusual temperature effects on the  $C_3/C_2$  branching ratio as observed in mass spectrometric experiments. According to the CPMD calculations, even at elevated temperatures, a conformation with the fully relaxed carbon backbone predominates (96 %) the population of the neutral valeramide. The  $\Delta G^\ddagger$  values associated with folding of the carbon backbone into conformers from which the desired H-transfers can commence, amount to 3.5 or 5.9 kcal/mol. However, these barriers cannot be surmounted just by thermal motion.

The CPMD simulations performed at ca. 300 K on the ionized valeramide reveal a substantial stability of a conformation in which the carbon backbone is fully relaxed; no reaction was observed for the trajectory that was sampled for more than 7 ps. However, when conformers with the folded carbon backbone are used as initial geometries, the McLafferty rearrangement is completed within 2 ps. Therefore, the McLafferty rearrangement seems to be more probable and is associated with a total free activation energy of 4.5 kcal/mol, while the  $\delta$ -H shift is energetically more demanding being equal to 7.0 kcal/mol.

At elevated temperature (500 K), the observed reaction (within 1.4 ps) corresponds to the McLafferty rearrangement. The estimated free activation energy associated with this process amounts to 2.5 kcal/mol, while the total free activation energy for the  $\delta$ -H transfer equals to 4.4 kcal/mol.

In accordance with the experimental<sup>22,23</sup> and theoretical studies performed on valeramide, the CPMD computations provide a rational for the observed temperature effect on the dissociation pattern of ionized valeramide. Finally, it can be concluded that the unusually low branching ratio between the two dissociation channels observed in the experiments conducted at the source temperature of ca. 500 K is most likely due to two factors:

(i) The relatively low free activation energy of the McLafferty rearrangement cause the dissociation of a substantial fraction of  $\mathbf{1}^{+*}$  or its distonic ion  $\mathbf{2}^{+*}$  prior to the time-

delayed mass selection; this reduces the  $C_3/C_2$  ratio relatively to the one observed at lower temperatures.

(ii) Since the barriers associated with conformational changes were shown to be energetically more demanding than the corresponding hydrogen transfers,  $\mathbf{1}^{+\bullet}$ , being trapped by conformational barriers, is believed to be long-lived at lower temperatures. This might indicate that in the experiments performed at room temperature a greater population of  $\mathbf{1}^{+\bullet}$  is mass-selected, which then enters easier the McLafferty rearrangement ( $C_3$ -route) increasing (relative to ratios at higher temperatures) the  $C_3/C_2$  ratio.



## **II. PART**

***VITAMIN B<sub>12</sub> DEPENDENT ETHANOLAMINE AMMONIA LYASE***





## 5. Rearrangement of Aminoethanol as Catalyzed by the Vitamin B<sub>12</sub>-dependent Ethanolamine Ammonia Lyase\*

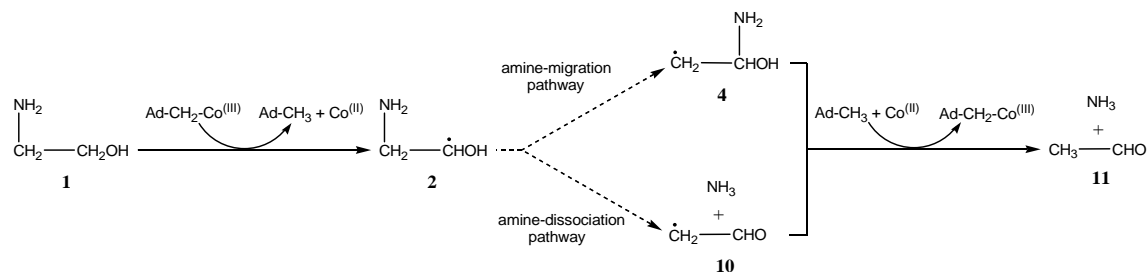
### 5.1. Migration vs. Elimination of the (Protonated) Amino Group

The vitamin B<sub>12</sub> coenzyme-dependent enzymes catalyze homolytic cleavage of the C-H bond,<sup>86,87</sup> and it is generally believed that in the subsequent 1,2-migration of hydrogen, alkyl, carbonyl, hydroxyl, or amide groups radical intermediates are involved.<sup>88</sup> Ethanolamine ammonia lyase<sup>89</sup> from bacteria metabolizes the substrate 2-aminoethanol,<sup>90</sup> **1**, to ethanal, **11**, and ammonia (Scheme 5-1).<sup>91</sup> Even though the best substrate for this reaction is **1**, the enzyme can utilize a number of other 2-aminoalcohols as well. The ethanolamine ammonia lyase requires the presence of the vitamin B<sub>12</sub> coenzyme for its catalytic activity. A central part of the catalytic role of vitamin B<sub>12</sub> stems from the relative weakness of its cobalt-carbon bond with a dissociation energy less than 30 kcal/mol.<sup>92</sup> It is assumed that the energy required for that homolysis could be delivered by a conformational change in the protein induced by binding of the substrate, and homolysis of the Co-C bond is accelerated up to a factor of 10<sup>12</sup> in the presence of an enzyme.<sup>93</sup> In the first step of the reaction, the homolytic cleavage of the C-Co(III) bond in the vitamin B<sub>12</sub> coenzyme is assumed to generate the low-spin Cob(II)alamin and the 5'-deoxyadenosyl radical, and it is the latter radical that has been proposed to abstract a hydrogen atom from aminoethanol (Scheme 5-1: **1** → **2**).<sup>94</sup> There are some indications that the protein-associated radical could participate in that step as well (see Chapter 7).<sup>95</sup> As for the initially formed intermediates involved in the subsequent rearrangement of **2**, ambiguities still exist. From experiments two basic pathways have been proposed (Scheme 5-1):<sup>96</sup> an amine-migration pathway (**2** → **4**) and an amine-dissociation pathway (**2** → **10**). Both routes yield eventually the same final products, i. e. ethanal, **11**, and ammonia; **11** itself is formed by reabstraction of a hydrogen atom from 5'-deoxyadenosine, thus regenerating the adenosyl-Cob(III)alamin and closing the catalytic cycle. As far as the rearrangement of **2** is

---

\* Results discussed in this chapter have been published in: Semialjac, M.; Schwarz, H. *J. Am. Chem. Soc.* **2002**, *124*, 8974.

concerned, despite elegant EPR experiments<sup>97</sup> and circumstantial evidence, the detailed mechanistic picture of this and related B<sub>12</sub> catalyzed transformations is the least understood aspect in the bound free-radical hypothesis.



**Scheme 5-1.** Possible rearrangement paths in the deamination of aminoethanol, **1**, by ethanolamine ammonia lyase.

The mechanistic dichotomy depicted in Scheme 5-1 seems to exist for other systems as well, and under particular conditions radical-mediated rearrangements were shown to be facile compared to those with closed-shell species. Often, the energy barriers for a carbon-heteroatom bond cleavage, caused by a neighboring radical center, decrease to half of the value for rearrangement barriers proceeding through closed-shell intermediates.<sup>98</sup> As far as gas-phase studies of aminoalkanes are concerned, for the protonated ethylamine it was shown that the ammonium ion elimination is the energetically preferred path.<sup>99</sup>

Recently, quite a few quantum-mechanical studies have been reported on B<sub>12</sub>-mediated rearrangements, and noteworthy are the following cases: methylmalonyl-CoA,<sup>100</sup> 1,2-diols,<sup>101,102,103</sup> 2-methyleneglutarate,<sup>104</sup> and the aminomutase catalyzed 1,2-amino shifts in amino acids.<sup>105</sup> The 1,2-amino migrations catalyzed by aminomutases differ from the formally related 1,2-amino shift catalyzed by ethanolamine ammonia lyase due to the fact that the former depends on the interaction of the substrate (amino acid) with another vitamin (i. e. vitamin B<sub>6</sub>) while the latter rearrangement proceeds by cooperative action of the enzyme and vitamin B<sub>12</sub> only. The intriguing concept of a partially protonated migrating group suggested by Smith, Golding, and Radom<sup>100,101,103,104</sup> seems to play an important role in the enzyme activity. Due to partial protonation, the energy barriers of the corresponding rearrangements are lowered to the extent that they get close to the energetics pertinent to enzyme catalysis.

In this chapter, several mechanistic scenarios are addressed including the concept of (partial) protonation of the substrate. The latter mode of operation is supported by the finding that in several B<sub>12</sub>-dependent enzymes the amino-acid sequence of the enzyme active site contains Asp and His residues,<sup>106</sup> which might serve as proton donors. In the case of methylmalonyl-CoA mutase catalyzed rearrangement it was concluded that His plays a role of a proton donor.<sup>107</sup> From the aminoethanol acidity ( $pK_a = 9.45$  for the conjugate acid of **1**), one can expect partial, if not complete protonation of the aminoethanol substrate embedded in the enzyme's active site. However, first only the influence of the full protonation on the rearrangement mechanisms will be investigated, while the more realistic scenario of partial protonation is being addressed in Chapter 6.

## 5.2. Computational Methods

All calculations were performed with the GAUSSIAN 98 suite of programs using the DFT and QCISD approaches. The use of the DFT formalism was a natural choice because of the balance between accuracy and computational time required by the calculations. The B3LYP functional was used.<sup>27,28</sup> It should be mentioned that in related studies<sup>108</sup> B3LYP calculations have provided good agreement with the experimental data as well as the data obtained with the high-level theoretical methods.

Geometry optimizations were performed with Pople's polarized double- $\zeta$  6-31G\* basis set. In order to characterize the optimized structures, frequency analysis has been performed at the same level of theory. Minima were characterized by the absence of imaginary vibrational frequencies, while transition structures exhibited one imaginary frequency. Computations of reaction pathways (IRC, relax PES scans) were carried out at the same level of theory.

Since the B3LYP method occasionally performs quite unsatisfactory in the case of the reaction enthalpy evaluations,<sup>109</sup> geometry reoptimizations were performed at the QCISD level of theory using Dunning's correlation-consistent double- $\zeta$  basis set cc-pVDZ<sup>110</sup> in order to obtain more accurate energetic profiles of the reactions in question, as well as the geometries of the stationary points. The CBS-RAD (QCISD, B3LYP) method<sup>111</sup> has not been applied since the computational cost would be even higher, and the energetic picture of the overall rearrangement pathways would not change dramatically. A

uniformed scaling factor of 0.9806 was used for the zero-point energy (ZPE) corrections obtained at the B3LYP level of theory. The relative energies in the text (given in kcal/mol) correspond to the enthalpies at 298 K obtained at the QCISD level of theory, unless specified otherwise. The electronic energies, ZPEs, and the enthalpies of stationary points can be found in the Appendix I of the Supporting Material.

Inclusion of solvent, e. g. water molecules, in the calculations is not indicated on the ground that hydrogen exchange has not been observed in vitamin B<sub>12</sub>-dependent rearrangements.<sup>87c</sup> While the amino-acid sequence of the enzyme has been determined,<sup>112</sup> the X-ray structure of the enzyme is not yet known. Consequently, no information is available on how the amino acids relevant for a protonation of **1** are positioned in the active site. Therefore, for the time being a comprehensive computational analysis of the isolated substrate seems to be useful of providing insight into the energetically most feasible mechanistic scenarios operating in the actual rearrangement of **2** (Scheme 5-1).

In the computations, various rearrangement possibilities of the neutral aminoethanol radical **2**, and its N-protonated counterpart **6** (Schemes 5-2, 5-4) were considered. The structure labels in Schemes 5-2 and 5-4 comprise the whole conformational space to which a structure in question belongs, while in the text, when discussing the mechanisms, a particular computationally characterized conformer is addressed. When more than one conformer was obtained during the calculations, the subscript of the label points to a specific conformer. The relative enthalpies at 298 K of the stationary points are presented in Tables 5-1 and 5-2, and the optimized geometries of minima in Figure 5-1; geometrical parameters of transition structures can be found in Figure 5-2. Comparing the radical geometries obtained at both levels of theory (Figures 5-1, 5-2), the most pronounced bond-length differences exist in the transition structures. The QCISD method is believed to provide a more accurate description of the actual geometries.<sup>113</sup> As expected, for the closed-shell species both methods give nearly identical results (Figure 5-1). As to the energetics, all B3LYP barriers are lower than the ones obtained at the QCISD level of theory; this confirms the well-known B3LYP underestimation of transition barriers for radical-mediated rearrangements.<sup>114,115</sup>

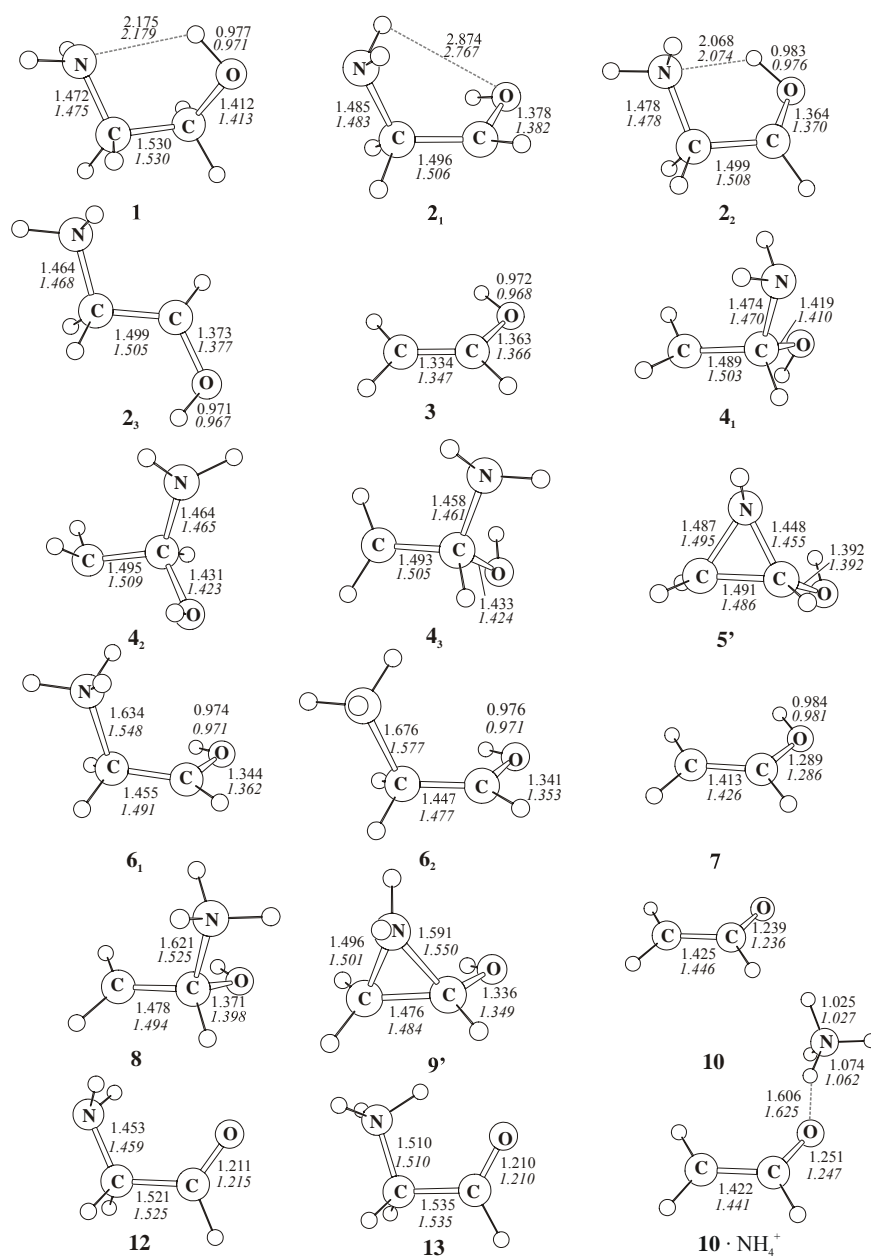


**Figure 5-1.** Optimized geometries of minima relevant for the rearrangements of **2** and **6**; bond lengths are given in Å (B3LYP results in roman and QCISD in italics).

### 5.3. Aminoethanol

The conformational analysis of aminoethanol **1** was the subject of several theoretical studies so far.<sup>116,117</sup> Out of a total of 27 conformers, a pronounced hydrogen bond bridging the two functional groups can be found in several of them. The most stable

conformer,<sup>118</sup> **1** (Figure 5-1), exhibits the strongest stabilization due to a hydrogen bond between the nitrogen atom and the hydrogen from the OH group ( $d_{\text{NH}} = 2.179 \text{ \AA}$ ).

Concerning the radical **2**, several conformers were considered for the reaction pathway calculations. The hydrogen bond is again an important factor for the structure stabilization. In the **2<sub>1</sub>** conformer (Figure 5-1) a H-bond exists between a hydrogen atom from the  $\text{NH}_2$  group and oxygen ( $d_{\text{HO}} = 2.767 \text{ \AA}$ ); this conformer corresponds to the third stable structure of aminoethanol. The conformer **2<sub>2</sub>** is structurally related to the global minimum **1**; in **2<sub>2</sub>** the N-H distance of  $2.074 \text{ \AA}$  is even shorter than in **1** ( $2.179 \text{ \AA}$ ), thus the H-bond is even stronger in the radical. The third conformer of the aminoethanol radical, i.e. **2<sub>3</sub>** (Figure 5-1), does not exhibit any stabilization through a H-bond; it is energetically less stable than the two counterparts mentioned above (by  $5.2 \text{ kcal/mol}$  relative to **2<sub>2</sub>**). While the most stable conformer **2<sub>2</sub>** may serve as a good candidate for the direct loss of ammonia (see further in text), this conformer is not likely to play a role in the amino-group migration towards the electron deficient carbon atom. For this particular rearrangement, conformers **2<sub>1</sub>** and **2<sub>3</sub>** are better candidates.

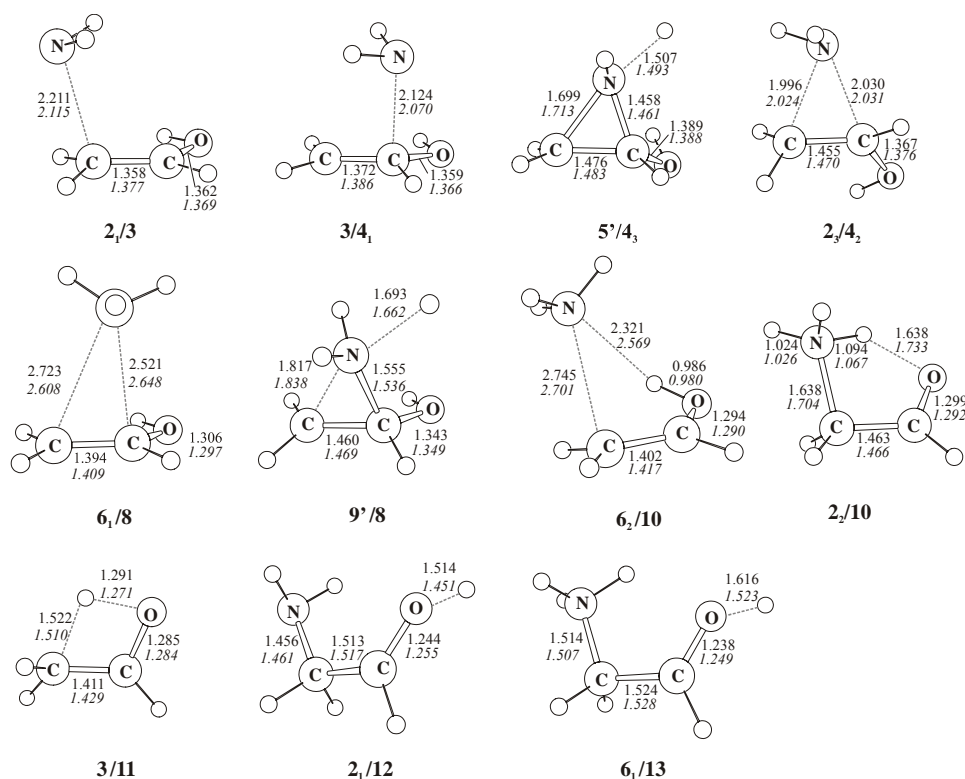
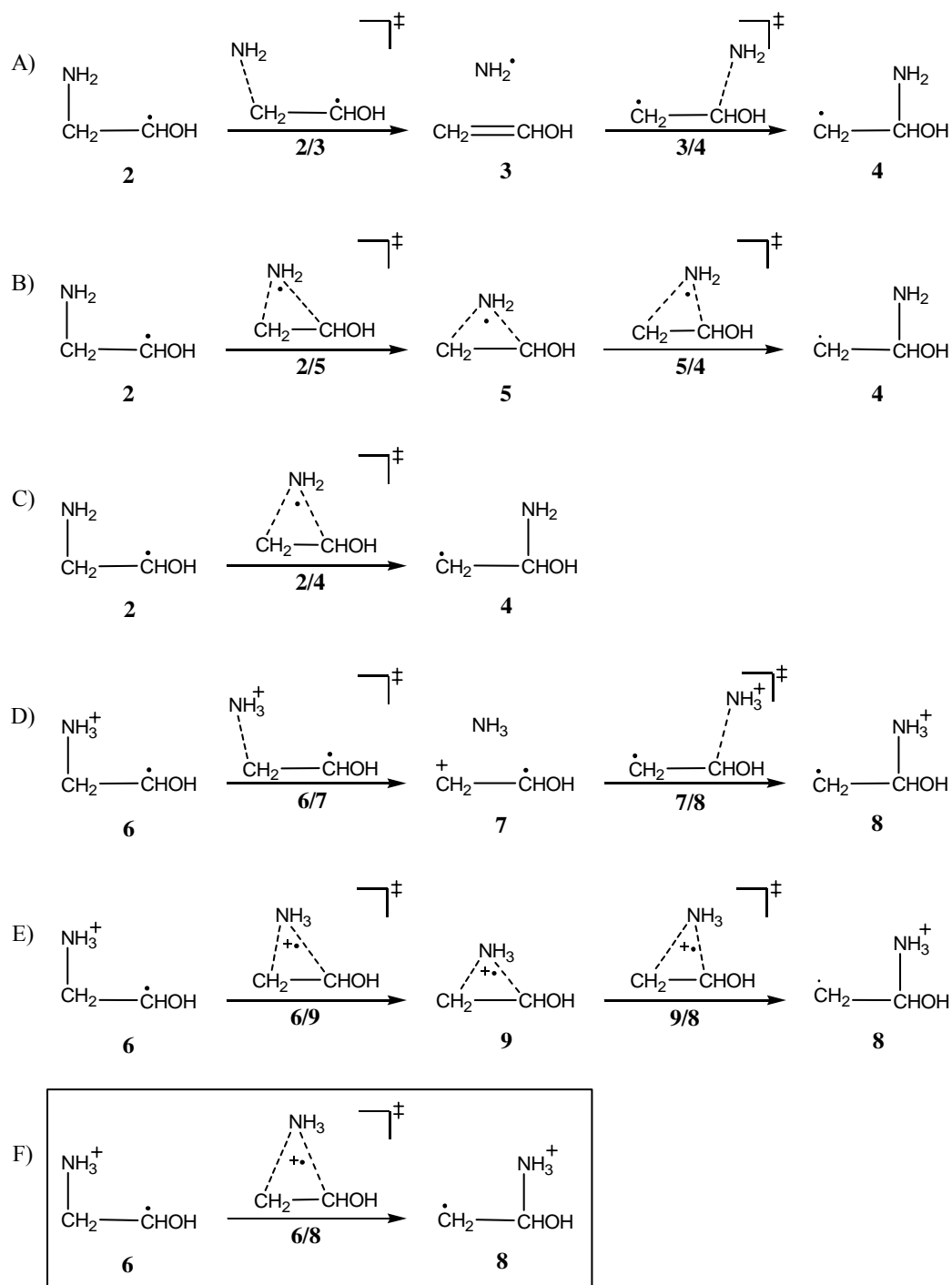


**Figure 5-2.** Optimized geometries of the transition structures involved in the rearrangements of **2** and **6**; bond lengths are given in Å (B3LYP results in roman and QCISD in italics).

## 5.4. Intramolecular Migration



**Scheme 5-2.**  $\text{NH}_x$  ( $x = 2, 3$ ) migration pathways of **2** and **6** resulting in the formation of 1-aminoethanol radical, **4**, and the N-protonated counterpart, **8**. The encircled rearrangement **6**  $\rightarrow$  **8** corresponds to the energetically preferred path.

#### 5.4.1. Dissociation-association Mechanism (Schemes 5-2A and 5-2D)

The activation enthalpy for the dissociation of the aminoethanol radical **2<sub>1</sub>** into ethenol, **3**, and NH<sub>2</sub> equals 24.1 kcal/mol; this barrier is somewhat higher than the one for the C-N bond cleavage of the aminoethyl radical. IRC calculations from the **2<sub>1</sub>/3** transition structure in the direction of the reactant resulted in the **2<sub>1</sub>** conformer. The optimization of the IRC structure in the product direction (**3** and NH<sub>2</sub>) did not indicate the existence of a complex between the two species. Instead, the structure breaks into two separate species; thus, convergence could not be achieved. Therefore, the combined energy of the products was obtained by calculating the energies of the separately optimized geometries of **3** and the NH<sub>2</sub> radical. A further possibility of the cleavage of **2<sub>1</sub>** has been considered as well: however, even permitted extensive solvation of the charged species the formation of a radical-cation **7** and an NH<sub>2</sub> anion can be excluded since the energy sum relative to **2<sub>1</sub>** equals 248.7 kcal/mol. With regard to the final rearrangement product, **4<sub>1</sub>**, the transition structure **3/4<sub>1</sub>** has been located. In analogy with the **2<sub>1</sub>/3** transition structure, the optimization of the IRC structure in a direction of the reactant could not converge. Assuming that the reaction proceeds indeed via **3** and the NH<sub>2</sub> radical, the energy required to overcome the **3/4<sub>1</sub>** transition state barrier equals 25.6 kcal/mol relative to **2<sub>1</sub>**. Obviously, path 2A is energetically too demanding to account for the enzyme-mediated rearrangement of **2**, since it is necessary for an enzymatic reaction that the energy demand for the rate-determining step falls below 20 kcal/mol.<sup>102,108</sup>

For the related reactions of the protonated radical **6** (Scheme 5-2D), the transition structures **6/7** and **7/8** were not located. Nevertheless, the combined energy of the intermediate enol radical cation **7** and ammonia (Table 5-2) is already too high to make this route a likely pathway in the rearrangement of the protonated radical **6<sub>1</sub>**. While the energy sum of the products **7** and NH<sub>3</sub> of the first rearrangement step equals 29.2 kcal/mol, relative to **6<sub>1</sub>**, this situation gets worse energetically if ethenol **3** and the radical cation NH<sub>3</sub><sup>•+</sup> are considered as a possible pair of products; the combined energy of **3** and NH<sub>3</sub><sup>•+</sup>, relative to **6<sub>1</sub>**, amounts to 47.0 kcal/mol. Clearly, this pathway is energetically not accessible for a fast enzymatic reaction, even if the enzyme might stabilize the transition states of the dissociation/association pathways 2A and 2D substantially.

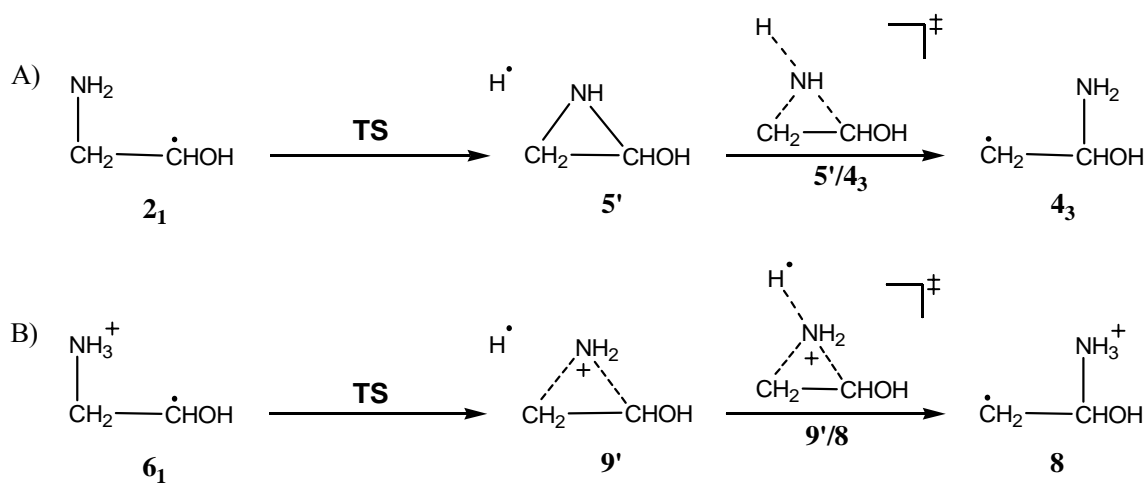


### 5.4.2. Sequential Intramolecular Isomerizations (Schemes 5-2B and 5-2E)

All attempts to locate the cyclic structure **5** as a minimum on the PES failed. During geometry optimization, one of the hydrogen atoms dissociates from the  $\text{NH}_2$  group, forming the closed-shell cyclic structure **5'** (see Scheme 5-3A). The final product **4<sub>3</sub>** (a conformer of **4** obtained with the IRC calculation from the corresponding TS **5'/4<sub>3</sub>**), can be formed through the transition structure **5'/4<sub>3</sub>**, which is associated with re-addition of the hydrogen atom (the activation enthalpy relative to **2<sub>1</sub>** equals 58.1 kcal/mol). Again, and in line with findings on related processes, the energies of all species characteristic for the sequence depicted in Scheme 5-3A are much too high to play a role in an enzymatic reaction.

A nonclassical structure proposed by George *et al.*<sup>102</sup> in the related isomerization of 1,2-ethanediol, where a hydrogen atom from an OH group bridges the C-C bond, could not be found as a stationary point of any kind for the isomerization of **2**. Similarly, in that study<sup>102</sup> a classical structure where oxygen, rather than  $\text{NH}_2$ , is the bridging group could not be located either.

Some of the problems encountered in the reaction pathway calculation discussed above were faced in the case of the protonated radical **6** as well. Instead of locating the cyclic protonated radical **9** (Scheme 5-2E), the closed-shell cyclic cation **9'** was obtained upon geometry optimization of **9**. The transition structure **9'/8** involved in the formation of **8** was found to lie 72.7 kcal/mol above **6<sub>1</sub>** (Scheme 5-3B), thus discarding this route in the isomerization of **6**.



**Scheme 5-3.**  $\text{NH}_x$  ( $x = 2, 3$ ) migration accompanied by hydrogen atom dissociation/association.

### 5.4.3. One-step Migration of $\text{NH}_2/\text{NH}_3$ (Schemes 5-2C and 5-2F)

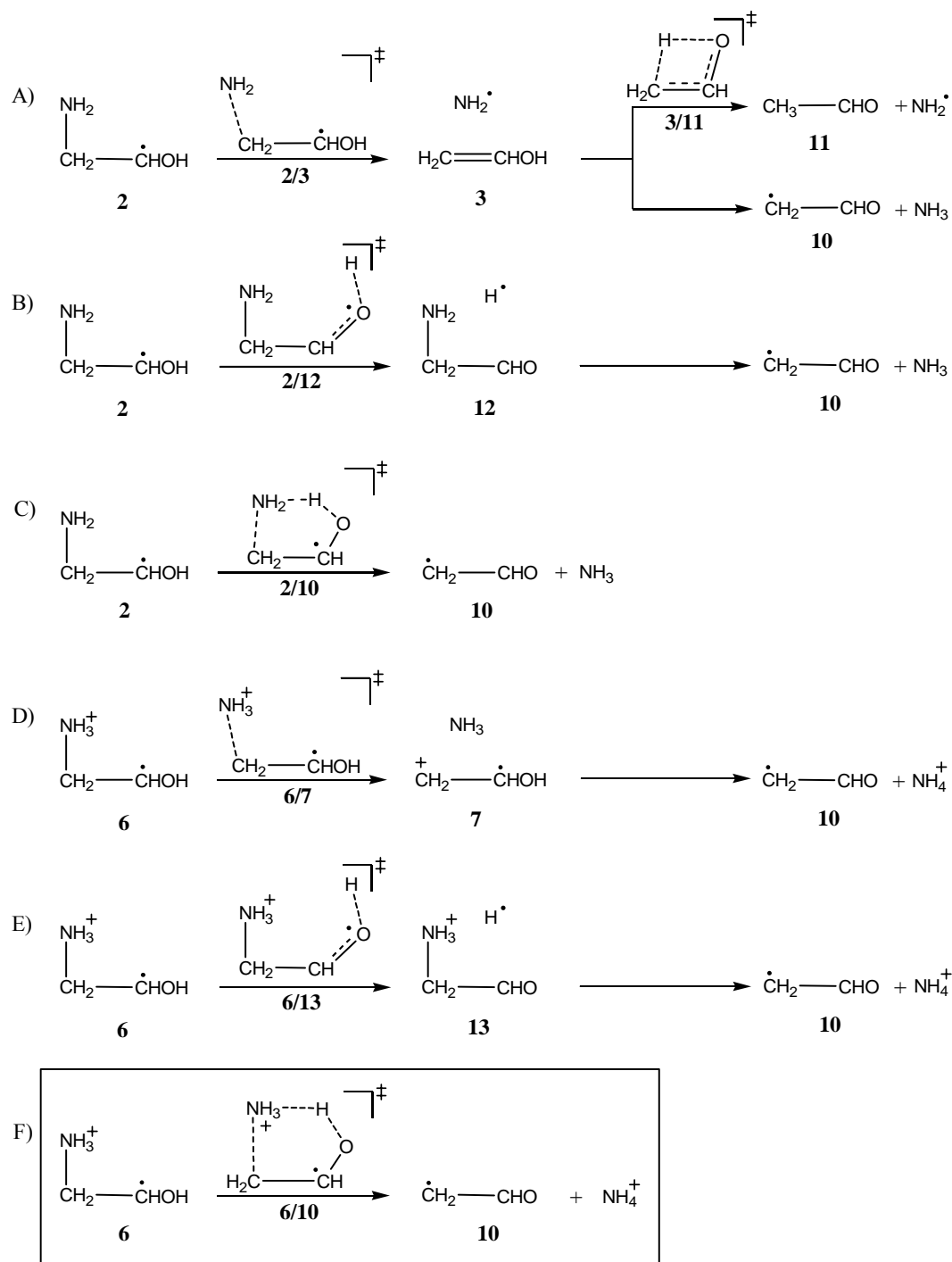
All stationary points of interest have been located on the respective PESs. The IRC calculations performed from the transition structure **2<sub>3</sub>/4<sub>2</sub>** lead to the conformers **2<sub>3</sub>** and **4<sub>2</sub>**. The barrier for a direct migration of a  $\text{NH}_2$  group amounts to 78.2 kcal/mol, and this pathway is therefore not expected to play role in the enzymatic reaction.

In contrast to the radical **2**, the activation enthalpy for the intramolecular transfer of the  $\text{NH}_3$  group starting from **6<sub>1</sub>** equals to only 10.4 kcal/mol, thus clearly falling into the energy range typical for enzyme-catalyzed reactions. The analogous barrier in the case of ammonium-ethyl radical was calculated to be 25.0 kcal/mol for the investigation of a 1,2-amino shift catalyzed by aminomutases. Obviously, the presence of the OH group at the radical terminus dramatically influences the transition state in such a way that the rearrangement is feasible even without the action of an additional cofactor, e.g.  $\text{B}_6$ , as in the case of the 1,2-amino shift catalyzed by aminomutases. Apparently, the spin delocalization through an additional heteroatom makes the migration more feasible.

The origin for the huge difference in the activation enthalpies between the migration of a neutral versus a charged group is most likely due to the bond redistribution in the two transition structures. In the case of a protonated group migration, TS **6<sub>1</sub>/8** corresponds closely to **7** and  $\text{NH}_3$ , which can be inferred from the C-N bond lengths (see Figures 5-1 and 5-2). The enol radical cation **7** is more stable than its keto counterpart due to a better spin delocalization in the C-C-O backbone;<sup>119</sup> such a spin delocalization stabilizes the transition structure as well. The slightly preferred interaction of  $\text{NH}_3$  with the C(1) center, on which the positive charge emerges, is reflected in a shorter N-C(1) distance with respect to the second C(2)-N bond. As further suggested by the calculations, the spin density at C(2) exceeds that of C(1). In contrast, in the **2<sub>3</sub>/4<sub>2</sub>** transition structure a three-center three-electron bond is present through a delocalization of electrons between nitrogen and two carbon atoms. Any significant delocalization of the spin density between C(1) and C(2), which would correspond to a partial CC double-bond formation, can be neglected due to the fact that the C-C bond in **2<sub>3</sub>/4<sub>2</sub>** is actually elongated if compared to **2<sub>3</sub>** (see Figures 5-1 and 5-2). The two C-N bonds of **2<sub>3</sub>/4<sub>2</sub>** are much shorter than in the related **6<sub>1</sub>/8** transition structure, showing a strong interaction between the  $\text{NH}_2$  group and the  $\text{C}_2$  backbone. The formation of such a strained structure with an extra electron in a high-lying orbital is obviously energetically more demanding than the corresponding **6<sub>1</sub>/8** transition structure.

## 5.5. Dissociation Pathways

Concerning the role of stepwise  $\text{NH}_x$  ( $x = 2, 3$ ) dissociation reactions, two mechanisms were considered, which differ in the details of the initial step. The reaction can commence either by the cleavage of the C-N bond (elimination of  $\text{NH}_2$  or  $\text{NH}_3$ ) or via hydrogen atom elimination from the OH group.



**Scheme 5-4.** Dissociation pathways for the formation of the 2-ethanal radical, **10**. The encircled rearrangement **6**  $\rightarrow$  **10** corresponds to the energetically preferred path.

### 5.5.1. Elimination of the $\text{NH}_x$ ( $x = 2, 3$ ) Group as the Initial Step (Schemes 5-4A and 5-4D)

These two initial steps have already been discussed in the context of dissociation-association mechanisms (see Schemes 5-2A and 5-2D), and therefore need not to be analyzed any further.

From the enol **3**, ethanal, **11**, could be formed directly through keto-enol tautomerization. The corresponding transition structure **3/11** for the unimolecular 1,3-H migration<sup>120</sup> lies 56.6 kcal/mol above **3**; thus, this symmetry-forbidden route can be discarded due to its high-energy demand. Besides, for that mechanistic proposal, the  $\text{NH}_2$  radical formed in the step **2**<sub>1</sub>  $\rightarrow$  **3** should then be capable of abstracting a hydrogen atom from 5'-deoxyadenosine; however, according to EPR experiments a hydrogen atom is abstracted by either 1-aminoethanol (**8**) or ethanal (**10**) radicals.<sup>121</sup> Formation of **10** through the homolytic bond cleavages of the O-H bond in **3** or a C-H in **11** is compatible with the expected high-energy demands, i.e. 76.9 and 90.5 kcal/mol, respectively. If one assumes that the **3**  $\rightarrow$  **10** transformation is supported by the  $\text{NH}_2$  radical formed in the previous step, then the reaction becomes exothermic (-21.1 kcal/mol relative to **3** +  $\text{NH}_2^\bullet$ ). Even though the overall reaction energetics starting from **2**<sub>1</sub> turns out to be almost thermo-neutral (3.0 kcal/mol; taking into account the energy-demanding first step and energy-releasing second one), the stepwise elimination mechanism starting with an amino-group elimination is highly unlikely as the initial step **2**<sub>1</sub>  $\rightarrow$  **3** is energetically not accessible.

If a homolytic O-H bond cleavage was to take place in structure **7** (Scheme 5-4D), a hydrogen radical and the acetyl cation<sup>122,123</sup> would be formed, and the combined energy relative to **7** equals 21.1 kcal/mol. A heterolytic O-H bond cleavage of **7** to produce **10** and a proton would be even more demanding (187.2 kcal/mol relative to **7**). In contrast, formation of an ammonium ion and **10** makes the latter reaction quite exothermic (-22.8 kcal/mol). However, once more this pathway is not very probable to play a role in the enzymatic reaction since the initial step, with an activation enthalpy higher than 29.2 kcal/mol, poses a too high barrier.

### 5.5.2. O-H Bond Cleavage as the Initial Step (Schemes 5-4B and 5-4E)

From **2<sub>1</sub>**, the homolytic O-H bond cleavage occurs through the transition structure **2<sub>1</sub>/12**. The related energy demand equals 33.9 kcal/mol, and it is unlikely that the enzyme could reduce such a high-energy barrier to make this step feasible. Nevertheless, for the sake of completeness, the whole reaction profile was investigated. The energy sum of the products, hydrogen and aminoethanal, **12**, lies 20.4 kcal/mol above the reactant structure **2<sub>1</sub>**. If a heterolytic O-H bond cleavage of **2<sub>1</sub>** were to take place, the energy of the aminoethanal radical-anion<sup>124</sup> would be, as expected, even higher (371.0 kcal/mol above **2<sub>1</sub>**). The energy demand for the homolytic C-N bond cleavage in **12** equals 73.2 kcal/mol. If this cleavage is coupled with ammonia formation the reaction enthalpy drops to -24.7 kcal/mol (relative to **12** + H<sup>•</sup>). A heterolytic C-N bond cleavage of **12** can be discarded since the energy sum of the products, NH<sub>2</sub> anion and acetyl cation,<sup>122,123</sup> lies 249.3 kcal/mol above **12**. In any case, since the first step of the reaction, the hydrogen-abstraction, is energetically quite demanding (33.9 kcal/mol), it is very unlikely that this mechanistic scenario plays a role in the enzymatic catalysis.

A homolytic O-H bond cleavage<sup>125</sup> in **6<sub>1</sub>** proceeding through the transition structure **6<sub>1</sub>/13** would require 38.1 kcal/mol, again too high for an enzymatic reaction. Consequently, the PES involving **13** needs no further detailed discussion. Rather briefly, a heterolytic C-N bond cleavage in **13** yields ammonia and the acetyl cation<sup>122,123</sup> as the products, with a combined energy of 25.3 kcal/mol relative to **13**. A homolytic C-N bond cleavage in **13** is energetically even more demanding, being equal to 98.8 kcal/mol. Even if the latter cleavage is accompanied by the N-H bond formation to generate the ammonium ion in a process that is overall exothermic (-18.6 kcal/mol relative to **13** + H<sup>•</sup>), that route can also be excluded as the barrier for the initial step **6<sub>1</sub>** → **13** cannot be overcome.

### 5.5.3. Direct Ammonia/Ammonium Eliminations (Schemes 5-4C and 5-4F)

In the **2<sub>2</sub>** conformer an intramolecular nitrogen-hydrogen interaction renders the direct elimination of NH<sub>3</sub> quite attractive. The transition structure for this path **2<sub>2</sub>/10** lies 29.6 kcal/mol above **2<sub>2</sub>**; this barrier originates from the cleavage of a strong O-H bond accompanied by the formation of a weaker N-H bond, thus resulting in a relatively high activation enthalpy of the late transition structure **2<sub>2</sub>/10** in which the N-H bond is formed

while O-H is almost completely broken (see Figure 5-2). While a complex between ammonia and the ethanal radical, **10**, has not been located on the PES, it can be postulated to exist (see next paragraph). However, once more the high activation energy makes the direct loss of ammonia not a very probable rearrangement pathway even if the barrier could become lowered somehow by enzyme catalysis.

**Table 5-1.** Relative enthalpies<sup>a</sup> (in kcal/mol) at 0 K ( $H_{rel, 0 K}$ ), and 298 K ( $H_{rel, 298 K}$ ) of the stationary points on the aminoethanol radical PES.

|                                    | B3LYP/6-31G*   |                  | QCISD/cc-pVDZ  |                  |
|------------------------------------|----------------|------------------|----------------|------------------|
|                                    | $H_{rel, 0 K}$ | $H_{rel, 298 K}$ | $H_{rel, 0 K}$ | $H_{rel, 298 K}$ |
| <b>2<sub>1</sub></b>               | 0.0            | 0.0              | 0.0            | 0.0              |
| <b>2<sub>2</sub></b>               | -4.1           | -4.4             | -4.1           | -4.4             |
| <b>2<sub>3</sub></b>               | 1.0            | 1.1              | 0.8            | 0.8              |
| <b>4<sub>1</sub></b>               | 3.7            | 3.6              | -0.8           | -0.9             |
| <b>4<sub>2</sub></b>               | 3.2            | 3.6              | 1.5            | 1.9              |
| <b>4<sub>3</sub></b>               | -0.2           | -0.1             | -1.6           | -1.6             |
| <b>2<sub>1</sub>/3</b>             | 20.4           | 20.6             | 23.9           | 24.1             |
| <b>3/4<sub>1</sub></b>             | 23.0           | 23.2             | 25.5           | 25.6             |
| <b>5'/4<sub>3</sub></b>            | 54.7           | 54.4             | 58.6           | 58.1             |
| <b>2<sub>3</sub>/4<sub>2</sub></b> | 72.5           | 72.4             | 79.1           | 79.0             |
| <b>2<sub>2</sub>/10</b>            | 16.9           | 16.4             | 25.7           | 25.2             |
| <b>2<sub>1</sub>/12</b>            | 28.0           | 28.2             | 33.7           | 33.9             |
| <b>5' + H'</b>                     | 44.6           | 45.4             | 43.2           | 43.9             |
| <b>3 + NH<sub>2</sub>'</b>         | 18.1           | 19.4             | 15.6           | 16.8             |
| <b>7 + NH<sub>2</sub>'</b>         | 241.4          | 242.8            | 247.5          | 248.7            |
| <b>10 + NH<sub>3</sub></b>         | -6.8           | -5.5             | -5.4           | -4.3             |
| <b>12 + H'</b>                     | 21.0           | 22.0             | 19.4           | 20.4             |

<sup>a</sup> For electronic energies, ZPEs, and enthalpies see Table AI-1 in the Appendix I.

through the C-C-O backbone in **6<sub>2</sub>/10** stabilizes the transition structure in contrast to **2<sub>2</sub>/10** where the spin delocalization through three centers is not achievable. A complex between the ethanal radical, **10**, and NH<sub>4</sub><sup>+</sup> has been located with a stabilization energy of 17.6 kcal/mol below **6<sub>2</sub>**. The energy requirement for a complete separation of the two building blocks amounts to 22.4 kcal/mol, indicating a strong electrostatic interaction between NH<sub>4</sub><sup>+</sup> and the carbonyl group. However, in an enzymatic environment interaction of NH<sub>4</sub><sup>+</sup> with

The activation enthalpy for the direct elimination of an ammonium ion starting from **6<sub>2</sub>** via TS **6<sub>2</sub>/10**<sup>126</sup> equals only 10.6 kcal/mol. The transition structure **6<sub>2</sub>/10** can be discussed in terms of an interaction of NH<sub>3</sub> with the stable enol radical-cation **7** (e.g. compare the bond lengths of **6<sub>2</sub>/10** and **7**; Figures 5-1 and 5-2), where a H-bond between the nitrogen atom and the hydrogen from the OH group exist ( $d_{NH} = 2.569$  Å). Further, as already mentioned, a spin delocalization

**Table 5-2.** Relative enthalpies<sup>a</sup> (in kcal/mol) at 0 K ( $H_{rel, 0 K}$ ), and 298 K ( $H_{rel, 298 K}$ ) of the stationary points on the protonated aminoethanol radical PES.

|  | B3LYP/6-31G*   |                  | QCISD/cc-pVDZ  |                  |
|--|----------------|------------------|----------------|------------------|
|  | $H_{rel, 0 K}$ | $H_{rel, 298 K}$ | $H_{rel, 0 K}$ | $H_{rel, 298 K}$ |
| <b>6<sub>1</sub></b>                   | 0.0            | 0.0              | 0.0            | 0.0              |
| <b>6<sub>2</sub></b>                   | 0.4            | 0.6              | 1.5            | 1.6              |
| <b>8</b>                               | 2.9            | 3.0              | -0.3           | -0.1             |
| <b>6<sub>1</sub>/8</b>                 | 4.7            | 4.9              | 10.2           | 10.4             |
| <b>6<sub>2</sub>/10</b>                | 8.8            | 9.1              | 12.0           | 12.2             |
| <b>9'/8</b>                            | 69.1           | 68.7             | 73.3           | 72.7             |
| <b>10 · NH<sub>4</sub><sup>+</sup></b> | -17.9          | -17.1            | -16.7          | -16.0            |
| <b>6<sub>1</sub>/13</b>                | 33.8           | 33.5             | 38.4           | 38.1             |
| <b>9' + H<sup>•</sup></b>              | 48.9           | 49.5             | 46.5           | 47.0             |
| <b>3 + NH<sub>3</sub><sup>++</sup></b> | 52.2           | 53.3             | 46.0           | 47.0             |
| <b>7 + NH<sub>3</sub></b>              | 29.3           | 30.4             | 28.2           | 29.2             |
| <b>10 + NH<sub>4</sub><sup>+</sup></b> | 6.7            | 7.7              | 5.4            | 6.4              |
| <b>13 + H<sup>•</sup></b>              | 27.7           | 28.4             | 24.3           | 25.0             |

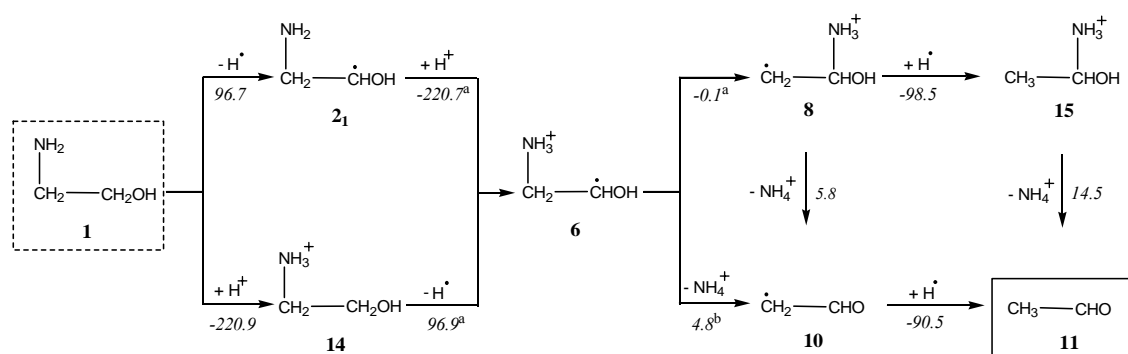
<sup>a</sup>For electronic energies, ZPEs, and enthalpies see Table A1-2 in the Appendix I.

negatively charged amino acid residues may help to pull out  $\text{NH}_4^+$  from the active site; in this case the overall rearrangement costs only 10.6 kcal/mol.

## 5.6. Formation of Ethanal

Any acceptable mechanism for ethanal formation, in the context of the ethanolamine ammonia lyase reaction, must be compatible with the rate constant for the product formation. In an ideal case of complete enzyme saturation, one could approximate  $k_{cat}$  with the rate constant of the product formation. In a realistic case, the rate of the product formation would be lower, and thus the activation enthalpy higher. Taking the value of  $k_{cat} = 55 \text{ s}^{-1}$  for the ethanolamine ammonia lyase at 295 K,<sup>127</sup> the activation enthalpy for the rate determining step can be derived from the Eyring equation. Assuming a reasonable range of activation entropy of 0 - 10 cal/mol·K, the activation enthalpy falls into the range 14.9 - 17.8 kcal/mol, respectively; thus any process with an activation enthalpy higher than ca. 16 kcal/mol can be discarded as a potential step in the deamination of aminoethanol catalyzed by the enzyme. Therefore, **4** can not serve as an intermediate in the rearrangement of **1** → **11**, since all the investigated reactions, in which **4** is involved

(Schemes 5-2 and 5-3), have activation enthalpies of their rate determining steps highly exceeding 16 kcal/mol.



**Scheme 5-5.** Conceivable pathways for the conversion of aminoethanol, **1**, into ethanal, **11**. The numbers in italics correspond to the reaction enthalpies in kcal/mol at 298 K of the corresponding reactions (<sup>a</sup>: number corresponds to a reaction in which conformer **6<sub>1</sub>** is involved; <sup>b</sup>: number corresponds to a reaction in which conformer **6<sub>2</sub>** is involved).

Possible steps for the formation of ethanal **11** from intermediates involved in these reactions, which obey the transition barrier criterion stated above, are summarized in Scheme 5-5; energies of the relevant closed-shell species are presented in Table AI-3 in the Appendix I. For example, intermediate **10** is accessible via direct loss of NH<sub>4</sub><sup>+</sup> from the protonated radical precursor **6<sub>2</sub>** (see Scheme 5-4F); here the corresponding activation enthalpy equals only 10.6 kcal/mol. Considering the energy barrier, this elimination has a high probability to occur even if full protonation of **2** in the enzymatic process has not yet been demonstrated to take place. Nevertheless, as already shown also partial protonation can result in a substantial stabilization of the transition structure thus bringing the energy demand in a region accessible to the enzymatic reaction. From **10**, ethanal, **11**, could be formed by interaction with the 5'-deoxyadenosine, while at the same time, the active form of the vitamin B<sub>12</sub> is regenerated.

Intermediate **8** can be formed either by a dissociation-association mechanism (Scheme 5-2D), or via direct migration of NH<sub>3</sub> group (Scheme 5-2F). The former path can be ruled out due to the energy barrier involved in the rearrangement (higher than 16 kcal/mol). In contrast, the latter route **6<sub>1</sub>** → **8** with an activation enthalpy of only 10.4 kcal/mol has the lowest energy barrier of all investigated rearrangement possibilities. From **8**, ethanal can be formed either by loss of an ammonium ion resulting in **10**, or by hydrogen addition from the 5'-deoxyadenosine followed by loss of an ammonium ion.



The proposal for an intramolecular  $\text{NH}_3$  migration **6**  $\rightarrow$  **8** (Scheme 5-2F) is in line with computational findings of quite similar rearrangements catalyzed by diol dehydrase,<sup>101-103,108</sup> while a dissociation pathway related to **6**  $\rightarrow$  **10** (Scheme 5-4F) is supported by solution experiments.<sup>128</sup> However, the EPR spectra do not allow to distinguish between intermediates of the rearrangements, thus leaving the question of the actual rearrangement pathway still unanswered. While the calculations slightly favor the  $\text{NH}_3$  migration pathway, with an activation-enthalpy difference between the direct  $\text{NH}_3$  migration and the  $\text{NH}_4^+$  elimination of only 0.2 kcal/mol, a definitive answer cannot be given. From the deuterium kinetic isotope effects, it was concluded, that the rate determining step in the overall reaction sequence corresponds to the hydrogen abstraction from the 5'-deoxyadenosine by the product radical.<sup>129</sup> The estimated energy barrier associated with that reaction step equals 15 kcal/mol at 298 K;<sup>130</sup> thus, both scenarios suggested by the computational work could well take place in the real enzymatic reaction. All other investigated pathways can be ruled out on energetic grounds.

## 5.7. Reaction Enthalpies – a Comparison of Calculated and Experimental Values

The reaction enthalpies for the transformation of aminoethanol radical, **2<sub>1</sub>**, into ethanal radical, **10**, and ammonia have been calculated at both levels of theory (Table 5-3). In order to obtain even more accurate reaction enthalpies, a frequency analysis of the structures in question was performed at the QCISD/cc-pVDZ level of theory as well. As the experimentally derived data for the enthalpy of the aminoethanol radical formation do not seem to exist in the literature, this figure was estimated from other data available.<sup>131</sup> Since the reliability of some of the numbers presented in thermochemical tables can be questioned, where available, the revised enthalpies<sup>132</sup> were used. For protonated aminoethanol **6** and its rearrangement into ethanal radical **10** and ammonium ion, no sufficient experimental data could be found in order to calculate the corresponding experimental enthalpy, thus only the computed values are given. The reaction enthalpies calculated at both levels of theory fall into the range of the enthalpy predicted from the experimentally available data. The uncertainty of experimentally derived enthalpies is

quite pronounced, and one can safely assume that the computationally determined values, especially at the QCISD level of theory, are even more reliable in this particular case.

**Table 5-3.** Comparison between the computed and experimentally derived reaction enthalpies (in kcal/mol).

|   | B3LYP/6-31G* <sup>a</sup> |                      | QCISD/cc-pVDZ <sup>a,b</sup> |                      | $\Delta_r H_{exp}$ |
|---|---------------------------|----------------------|------------------------------|----------------------|--------------------|
|   | $\Delta_r H (0 K)$        | $\Delta_r H (298 K)$ | $\Delta_r H (0 K)$           | $\Delta_r H (298 K)$ |                    |
| <b>2<sub>1</sub></b> → <b>10</b> + NH <sub>3</sub>              | -6.8                      | -5.5                 | -6.1                         | -4.8                 | -4.6 ± 3.2         |
| <b>6<sub>1</sub></b> → <b>10</b> + NH <sub>4</sub> <sup>+</sup> | 6.7                       | 11.9                 | 4.4                          | 5.6                  |                    |

<sup>a</sup> ZPE correction has been taken into account.

<sup>b</sup> Enthalpies obtained by performing the frequency calculations for reactants and products at the QCISD/cc-pVDZ level of theory.

## 5.7. Summary and Conclusions

The computational study of the aminoethanol rearrangement clearly discriminates between various mechanistic scenarios, thus adding in the elucidation of the actual mechanism of this important enzymatic reaction.

Due to their high activation enthalpies (more than 23 kcal/mol), and reaction mechanisms involving complete detachment of the NH<sub>2</sub>/NH<sub>3</sub> groups (dissociation-association mechanisms) can be ruled out. Further, isomerization pathways proceeding through cyclic intermediates are unrealistic as well due to the fact that such cyclic structures have not been obtained as minima on the PES neither for the protonated nor the unprotonated radical. Also, mechanisms involving a stepwise elimination of the NH<sub>3</sub>/NH<sub>4</sub><sup>+</sup> species are highly unlikely to play a role in the actual rearrangement routes due to high energy barriers involved in these pathways.

Concerning the direct transfer of the NH<sub>2</sub> group in the aminoethanol radical, that pathway can be definitively ruled out due to the exceeding high energy demand (more than 70 kcal/mol). It is inconceivable that any enzyme could reduce such a barrier for this rearrangement to become feasible. On the other hand, the activation enthalpy for a direct transfer of the NH<sub>3</sub> group in the protonated aminoethanol radical is computed to be the lowest (10.4 kcal/mol) of all rearrangement barriers investigated in this study, thus making that pathway the most probable rearrangement mechanism of the enzyme catalysis. Indeed,

this finding confirms the earlier hypothesis<sup>100,101,108</sup> that (partial) protonation of the migrating group reduces significantly the energy barrier.

The direct  $\text{NH}_3$  elimination in aminoethanol radical is not expected to be the actual rearrangement because of an energetically quite demanding barrier. On the other hand, for the protonated form of aminoethanol radical the activation enthalpy for a direct  $\text{NH}_4^+$  elimination falls into the range of enzyme catalysis (10.6 kcal/mol). However, the possible complex formation between an  $\text{NH}_4^+$  ion and the ethanal radical could present a bottleneck for that particular mechanistic route due to the high-energy demand for dissociation of the complex (22.4 kcal/mol). Nevertheless, as mentioned the enzyme surrounding could help in abstracting the  $\text{NH}_4^+$  ion from the active site, thus preventing a complex formation.

Clearly, an X-ray structure of the ethanolamine ammonia lyase or further computational investigations (see next chapter) could help in resolving the mechanistic dichotomy in distinguishing between the two mechanistic pathways (i.e. direct  $\text{NH}_3$  migration **6**  $\rightarrow$  **8** vs.  $\text{NH}_4^+$  elimination **6**  $\rightarrow$  **10**) predicted by the present model calculations as the two most probable rearrangements of aminoethanol in enzymatic reactions.

## 6. His and Asp/Glu Acting Simultaneously as Catalytic Auxiliaries\*

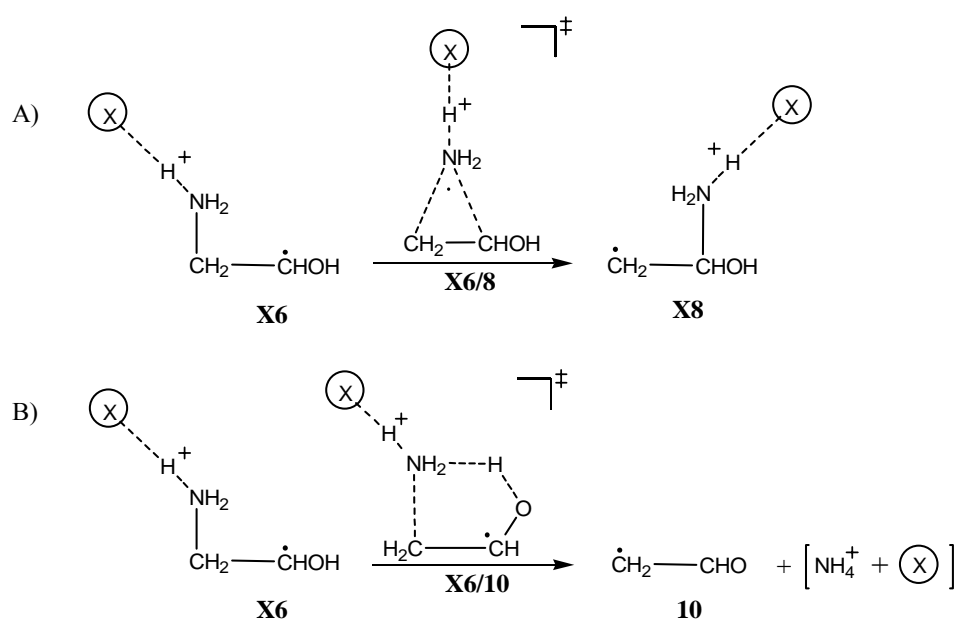
The further computational investigation aimed firstly at distinguishing between the two mechanistic scenarios identified as the most probable rearrangement pathways<sup>133</sup> discussed in the previous chapter, and will continue with a refinement of the mechanistic picture of the reaction. To this end, the more realistic concept of *partial* protonation of a migrating group introduced earlier by Smith, Golding, and Radom<sup>100,101,103,104</sup> has been applied. Further, since a push-pull mechanism as proposed by Radom and co-workers in the case of diol dehydrase<sup>134</sup> and employed in the study of ethanolamine rearrangement catalyzed by ethanolamine ammonia lyase as well,<sup>135</sup> seems to play a crucial role in the catalytic activity of ethanolamine ammonia lyase, this mechanistic variant was also taken into account. However, in contrast to the previous work,<sup>135</sup> a model that is more appropriate for mimicking the actual amino acids has been chosen. A difference between the ethanolamine ammonia lyase and the related diol dehydrase catalysis is that for the latter system K<sup>+</sup> ions were shown to play a crucial role in reducing the reaction barrier due to its interaction with the migrating group.<sup>134,136</sup>

While for the *fully* protonated substrate **6** the activation enthalpy difference for the two competing reactions as depicted in Scheme 6-1 (without X) is rather small (0.2 kcal/mol) in contrast to those involving uncharged **2**, it can be expected that *partial* protonation is likely to discriminate between the two pathways. Again, as stated earlier, inclusion of solvent, e. g. water molecules, in the calculations is not warranted on the ground that hydrogen exchange has not been observed in vitamin B<sub>12</sub>-dependent rearrangements.<sup>87c</sup> Thus, any continuum solvent model is not likely to provide more reliable data than the gas-phase calculations presented herein since the choice of dielectric constant needed for such calculations is ambiguous. As well, it was shown that the dielectric constant and the physical environment of an enzyme's active site are often closer to those in the gas phase than in bulk solution,<sup>137</sup> and furthermore, it was demonstrated that the protein backbone can substantially influence a local pH.<sup>138</sup> In several B<sub>12</sub>-dependent enzymes the amino-acid sequence of the enzyme's active site were found to contain Asp and His residues, which might serve as proton donors. In the case of the related

---

\* Results discussed in this chapter have been published in: Semialjac, M.; Schwarz, H. *J. Org. Chem.* **2003**, *68*, 6967.

methylmalonyl-CoA mutase catalyzed rearrangement it was concluded, based on mutagenesis studies, that His-244 acts as a Brønsted acid.<sup>139</sup> For example, mutation of His-244 from the wild type enzyme into Gly-244 in the mutant led to ca. 300-fold lowering in the catalytic efficiency of the enzyme. In addition, the crystal structure of methylmalonyl-CoA mutase indicated that His-244 is within hydrogen-bonding distance to the carbonyl oxygen of the carbonyl-CoA moiety.<sup>140,141</sup> Interestingly, computational studies by Wetmore *et al.* confirmed the experimental findings that His most likely partially protonates the substrate. However, recent QM/MM studies indicated that besides His-244, two additional amino acids (i.e. Gln-197, Tyr-89) might contribute as well in reducing the activation barrier.<sup>142</sup> In the case of glutamate mutase it was shown by mutagenesis studies that Glu-171 plays a role of a catalytic auxiliary,<sup>143</sup> which was confirmed later as well by theoretical studies.<sup>144</sup> While the amino-acid sequence of the ethanolamine ammonia lyase has been determined, the X-ray structure of the enzyme is not yet known, and consequently, no information is available which particular amino acids are relevant for a protonation of **1** (or **2**) and how precisely they are positioned in the active site. Therefore, several catalytic auxiliaries were considered (Scheme 6-1), including some model systems for His (X = CH<sub>2</sub>NH, imidazole) and Asp/Glu (X = HCOOH, CH<sub>3</sub>COOH). Further, the questions of the catalytic auxiliary(ies) that interact synergistically with the substrate in the enzyme's active site were addressed as well.



**Scheme 6-1.** Partially protonated aminoethanol radical **6** serving as a precursor for: A)  $\text{NH}_3$  migration, B)  $\text{NH}_4^+$  elimination (X stands for different interacting groups).

## 6.1. Computational Methods

All calculations were performed with the GAUSSIAN 98 suite of programs using the DFT and QCISD approaches. The B3LYP functional was employed.<sup>27,28</sup> Geometry optimizations were performed with Pople's polarized double- $\zeta$  6-31G\* basis set. In order to characterize the optimized structures, frequency analysis has been performed at the same level of theory. Computations of reaction pathways, i.e. intrinsic reaction coordinate (IRC) calculations and relaxed scans of the potential energy surface (PES) were carried out at the same level of theory.

Because the B3LYP method occasionally performs quite unsatisfactorily in the case of the reaction enthalpy evaluations, single point calculations and in some cases even geometry reoptimizations were performed at the QCISD level of theory using Dunning's correlation-consistent double- $\zeta$  basis set cc-pVDZ in order to obtain more accurate energetic profiles of the reactions in question. Relative energies (given in kcal/mol) discussed in the text correspond to the enthalpies at 298 K obtained at the QCISD level of theory (SP calculations),<sup>145</sup> unless specified otherwise. Electronic energies, ZPEs, and the enthalpies of stationary points are quoted in the Appendix II.

The structure labeling code employed in the previous chapter for the direct migration of an  $\text{NH}_3$  group (e.g. TS label: **6/8**) and the elimination of  $\text{NH}_4^+$  (e.g. TS label: **6/10**) was employed herein with a difference that the structures of analogous rearrangement types (migration vs. elimination) for different protonating groups  $\text{HX}^+$  are described by similar labels distinguished only in the prefix X (more on structure labeling in the Appendix III of the Supporting Material). As to the formal description of the reactions depicted in Scheme 6-1, partial protonation and its consequences for the two competing processes can be viewed as a reaction of **2** with a Brønsted acid  $\text{HX}^+$  in which, after formation of **6** the conjugated base X remains interacting with **6** throughout the whole reaction; alternatively, one may describe the rearrangement in terms of a reaction in which **2** is "sharing" a proton with  $\text{HX}^+$ . In the computations reported next the former formalism has been employed, i.e. the rearrangement commences with **6** that itself remains interacting via sharing its proton with X.

## 6.2. Migration vs. Elimination

### 6.2.1. Hydroxonium and Ammonium Ions as Protonating Groups

As the amino acids Asp, Glu and His contain in their proton donor part either an oxygen or a nitrogen atom, the protonation of **2** and the ensuing rearrangements of **6** using  $\text{NH}_4^+$  and  $\text{H}_3\text{O}^+$  as Brønsted acids were investigated first.

**Table 6-1.** Relative enthalpies<sup>a</sup> (in kcal/mol) at 0 K ( $H_{\text{rel}, 0 \text{ K}}$ ), and 298 K ( $H_{\text{rel}, 298 \text{ K}}$ ) of the stationary points on the PES of **6** interacting with  $\text{NH}_3$ .

|                            | B3LYP/6-31G*                  |                                 | QCISD/cc-pVDZ//<br>B3LYP/6-31G* |                                 | QCISD/cc-pVDZ <sup>c</sup>    |                                 |
|----------------------------|-------------------------------|---------------------------------|---------------------------------|---------------------------------|-------------------------------|---------------------------------|
|                            | $H_{\text{rel}, 0 \text{ K}}$ | $H_{\text{rel}, 298 \text{ K}}$ | $H_{\text{rel}, 0 \text{ K}}$   | $H_{\text{rel}, 298 \text{ K}}$ | $H_{\text{rel}, 0 \text{ K}}$ | $H_{\text{rel}, 298 \text{ K}}$ |
| <b>N6<sub>1</sub></b>      | 0.0                           | 0.0                             | 0.0                             | 0.0                             | 0.0                           | 0.0                             |
| <b>N6<sub>1</sub>/8</b>    | 12.8                          | 13.1                            | 19.9                            | 20.2                            | 20.2                          | 20.5                            |
| <b>N8</b>                  | 2.0                           | 2.0                             | -1.0                            | -1.0                            | -0.6                          | -0.6                            |
| <b>N6<sub>2</sub></b>      | -0.4                          | -0.7                            | -0.9                            | -1.2                            |                               |                                 |
| <b>N6<sub>2</sub>/10</b>   | 17.3                          | 17.5                            | 23.1                            | 23.3                            |                               |                                 |
| <b>N6'</b> <sup>b</sup>    | -5.5                          | -5.3                            |                                 |                                 | -5.5                          | -5.3                            |
| <b>N6'/8'</b> <sup>b</sup> | 12.6                          | 12.8                            |                                 |                                 |                               |                                 |
| <b>N8'</b> <sup>b</sup>    | 3.0                           | 3.2                             |                                 |                                 |                               |                                 |

<sup>a</sup> For electronic energies, ZPEs, and enthalpies, see Table AII-1 in the Appendix II.

<sup>b</sup> Structures contain an OH group orientation pointing away from the  $\text{NH}_3$  group (see Scheme 6-3); thus, elimination of  $\text{NH}_4^+$  is not possible for these conformers.

<sup>c</sup> Data to be discussed in the paragraph "Influence of the OH Group Conformation on the Migration".

As expected, with  $\text{NH}_4^+$  both transition structures, **N6<sub>1</sub>/8** and **N6<sub>2</sub>/10**, are energetically more demanding than when the stronger Brønsted acid  $\text{H}_3\text{O}^+$  serves as a proton donor (Tables 6-1 and 6-2). Comparing structural details of the transition structures for the reactions with the two protonating groups (see Figure 6-1), it is obvious that in the TSs proton transfer from  $\text{H}_3\text{O}^+$  is more advanced in comparison to the analogous structures with  $\text{NH}_4^+$  (see, e.g. the  $\text{H}\cdots\text{X}$  distances in **N6<sub>1</sub>/8** and **O6<sub>1</sub>/8** correspond to 1.831 Å vs. 1.898 Å). Correspondingly, the  $\text{N}\cdots\text{H}$  distance is larger for  $\text{N}\cdots\text{H}\cdots\text{X}$  when  $\text{X} = \text{NH}_3$  (1.055 Å) than for  $\text{X} = \text{H}_2\text{O}$  (1.030 Å).

**Table 6-2.** Relative enthalpies<sup>a</sup> (in kcal/mol) at 0 K ( $H_{rel, 0 K}$ ), and 298 K ( $H_{rel, 298 K}$ ) of the stationary points on the PES of **6** interacting with H<sub>2</sub>O.

|   | B3LYP/6-31G*   |                  | QCISD/cc-pVDZ//<br>B3LYP/6-31G* |                  | QCISD/cc-pVDZ <sup>c</sup> |                  |
|---|----------------|------------------|---------------------------------|------------------|----------------------------|------------------|
|   | $H_{rel, 0 K}$ | $H_{rel, 298 K}$ | $H_{rel, 0 K}$                  | $H_{rel, 298 K}$ | $H_{rel, 0 K}$             | $H_{rel, 298 K}$ |
| <b>O6<sub>1</sub></b>                                 | 0.0            | 0.0              | 0.0                             | 0.0              | 0.0                        | 0.0              |
| <b>O6<sub>1</sub>/8</b>                               | 9.9            | 10.0             | 16.6                            | 16.7             | 16.9                       | 16.9             |
| <b>O8</b>   | 2.8            | 2.7              | -0.1                            | -0.2             | 0.4                        | 0.3              |
| <b>O6<sub>2</sub></b>                                 | 0.2            | 0.3              | 0.2                             | 0.3              |                            |                  |
| <b>O6<sub>2</sub>/10</b>                              | 14.6           | 14.7             | 18.7                            | 18.8             |                            |                  |
| <b>10·NH<sub>4</sub><sup>+</sup>·H<sub>2</sub>O</b>   | -17.1          | -16.7            | -15.9                           | -15.4            |                            |                  |
| <b>10 + NH<sub>4</sub><sup>+</sup>·H<sub>2</sub>O</b> | 1.9            | 2.7              | 1.4                             | 2.2              |                            |                  |
| <b>O6'</b> <sup>b</sup>                               | -4.9           | -4.8             |                                 |                  | -5.0                       | -4.8             |
| <b>O6'/8'</b> <sup>b</sup>                            | 9.6            | 9.7              |                                 |                  |                            |                  |
| <b>O8'</b> <sup>b</sup>                               | 2.6            | 2.7              |                                 |                  |                            |                  |

<sup>a</sup> For electronic energies, ZPEs, and enthalpies, see Table AII-2 in the Appendix II.<sup>b</sup> Structures contain an OH group orientation pointing away from the NH<sub>3</sub> group (see Scheme 6-3); thus, elimination of NH<sub>4</sub><sup>+</sup> is not possible for these conformers.<sup>c</sup> Data to be discussed in the paragraph "Influence of the OH Group Conformation on the Migration".

Common to both Brønsted acids is that the transition structures **N6<sub>1</sub>/8** and **O6<sub>1</sub>/8** for a migration of the protonated amino group are energetically less demanding than for the elimination of NH<sub>4</sub><sup>+</sup> via **N6<sub>2</sub>/10** and **O6<sub>2</sub>/10**. The activation enthalpy difference between these two transition structures **X6<sub>1</sub>/8** and **X6<sub>2</sub>/10** varies slightly: it is smaller in the case of H<sub>3</sub>O<sup>+</sup> (2.1 kcal/mol) than for NH<sub>4</sub><sup>+</sup> (3.1 kcal/mol). Even though the differences in activation enthalpy between these two reactions are still rather small, they are more pronounced than in the case of the full protonation of the amino group (0.2 kcal/mol). Further, in the H<sub>3</sub>O<sup>+</sup> initiated reaction, a complex between the emerging ethanal radical, **10**, NH<sub>4</sub><sup>+</sup> and H<sub>2</sub>O was found to exist on the potential energy surface (PES; see Figure 6-1B). The energy requirement for its dissociation to liberate a free intermediate **10** equals to 17.6 kcal/mol, thus making this pathway even less probable. However, formation of such a product complex can be by-passed since the enzyme could pull out NH<sub>4</sub><sup>+</sup> upon its formation. In any case, the computational data obtained for the rearrangements of **2** with the crude model systems NH<sub>4</sub><sup>+</sup> and H<sub>3</sub>O<sup>+</sup> clearly indicate that partial protonation of the substrate results in an energetic discrimination between the two competing rearrangements.



Whether this encouraging trend continues will be tested next by employing improved amino acid-model systems.

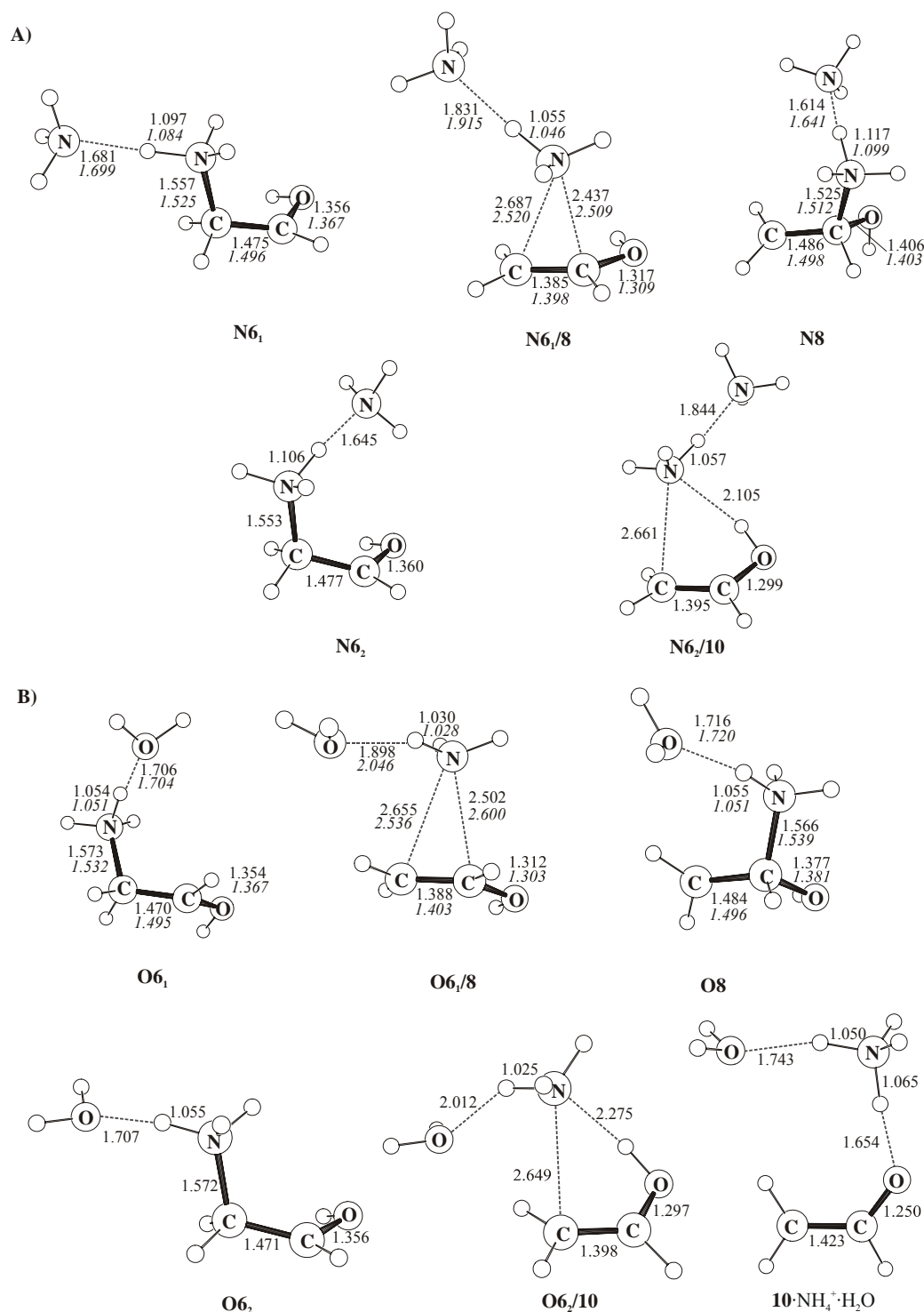


**Figure 6-1.** Optimized geometries of stationary points relevant for the rearrangements of partially protonated aminoethanol radical **6** interacting with: A) NH<sub>3</sub>; B) H<sub>2</sub>O (bond lengths are given in Å; B3LYP results in roman and QCISD in italics).

### 6.2.2. Active Site – What is the Most Probable pH?

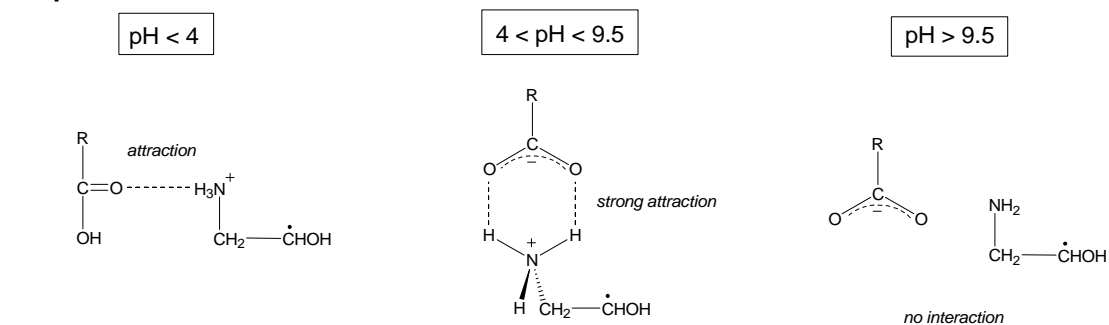
The precise pH of a reaction environment around an enzyme's active site is difficult if not impossible to predict,<sup>146</sup> even if the X-ray structure of the enzyme were known. Nevertheless, depending on the nature of the amino acids present in the active site the pH can be approximated provided the effective dielectric constant is known. As mentioned, deuterium labeling experiments suggest that solvent molecules do not have access to the active site; consequently, the effective dielectric constant depends mostly on the amino acids. However, as acidity is also affected by the molecular architecture of the actual environment (orientations of the amino acids, the protein's permanent and induced dipoles),<sup>147</sup> due to the absence of an X-ray structure, an accurate prediction of the local pH is not possible in the present case. Therefore, the discussion will be limited to several assumed pH ranges, determined by the acidity of the substrate and the amino acids Asp, Glu and His (Scheme 6-2). Aminoethanol **1** behaves as a base having a  $pK_a$  of 9.45 for its conjugated acid. For the radical **2** a similar  $pK_a$  can be reasonably assumed, as substantiated by high level ab initio calculations for the proton affinities of aminoethanol **1** and its radical **2**, which are identical. If the pH in the active site approximates the one prevailing under physiological conditions ( $pH \sim 7.5$ ),<sup>96,97,148</sup> most of the substrate **2** exists in its fully protonated form. However, partial rather than full protonation might well result through the interaction of the **2/6** couple with amino acid residues, which can serve as proton donors or as buffer reagents. As a result, substrate **2** captured in the active site would not be completely "free" but would interact with the protein backbone; clearly, such a refined picture resembles more closely enzyme-catalyzed reactions, where an enzyme through interaction with a substrate lowers the transition structure energy and thus serves as a catalyst.<sup>149</sup>

*Asp/Glu as protonating agents (Scheme 6-2A):* Assuming the amino acids Asp or Glu to act as proton donors, the pH regimes can be meaningfully divided in three regions, which are determined by the  $pK_a$  values of the Asp/Glu side chains<sup>150,151</sup> and the  $pK_a$  of the substrate. In the case of related glutamate mutase it was confirmed that Glu-171 acts as a catalytic auxiliary.<sup>143,144</sup>

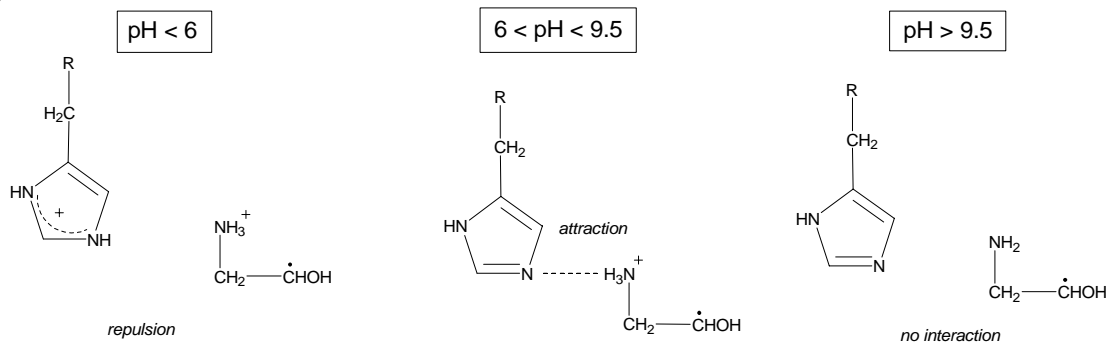
At  $pH < 4$ , amino acids exist in their non-dissociated form ( $RCOOH$ ), while substrate **2** is protonated. Nevertheless, an interaction between the amino acid and the substrate is possible through a H-bond between the basic carbonyl oxygen of the  $COOH$

group and a proton from the  $\text{NH}_3^+$  group. While that kind of interaction is expected to stabilize the structure due to a better redistribution of charge, such a low pH in the active site is not common for enzymes; however, as it cannot be discarded a priori, this scenario was investigated by computational means.

### A) Asp/Glu



### B) His



**Scheme 6-2.** Different interaction modes between the amino acid and the substrate depending on assumed pH values in the active site: A) Asp/Glu; B) His.

In the pH regime  $4 < \text{pH} < 9.5$ , both amino acids Asp/Glu exist in their carboxylate forms ( $\text{RCOO}^-$ ) while the substrate is still protonated. Therefore, a “salt bridge”-like interaction exists between the two charged species. As a consequence, the migrating  $\text{NH}_2$  group of **2** is only weakly protonated and that results in a destabilization of the corresponding transition structures. However, as this pH range is common for biological systems it presents a realistic pH scenario in the active site of the enzyme in question.

At  $\text{pH} > 9.5$ , the substrate is not protonated and the amino acids exist in their dissociated forms. An interaction between the two basic sites certainly would not contribute to a stabilization of the transition structure. As any process involving neutral **2** requires unrealistically high activation enthalpies, a further investigation of such an interaction was not taken into account. However, interactions of basic auxiliaries with the OH group of **2** will be addressed later.

*His as a protonating agent (Scheme 6-2B):* His is a common amino acid, which serves as a proton buffering agent in numerous biological systems because of its  $pK_a$  value of 6, which is close to a physiological pH. For example, in the case of the methylmalonyl-CoA mutase catalyzed rearrangement it was concluded that His-244 is the very amino acid that partially protonates a substrate and, therefore, lowers the transition barrier.<sup>139-141,144</sup>

If  $pH < 6$ , His and aminoethanol radical **2** are in their N-protonated forms, and consequently, repulsion is expected as a net effect. Clearly, such a scenario needs not to be addressed further.

In the pH regime  $6 < pH < 9.5$ , the N(3) atom of His is not protonated, while substrate **2** is expected to be protonated. Here, a H-bond between N(3) of His and a proton from the  $NH_3$  group of **6** is likely to stabilize a transition structure via charge delocalization. As mentioned, this particular pH range is common for biological systems and a computational investigation of this scenario was undertaken.

At  $pH > 9.5$ , both the substrate and His are not protonated. Since no stabilization occurs and all barriers involving **2** are high, a further investigation was not pursued.

### 6.2.3. His Serving as a Proton Donor

For the interaction of the substrate with His first the most simple imine (methanimine,  $CH_2=NH$ ) was used as a model system. Despite its limitations, methanimine is structurally closer to His than  $NH_3$  (e.g. the hybridization of the basic nitrogen atoms that is crucial for the reaction). However, the proton affinity (PA) of methanimine (203.8 kcal/mol) is similar to the PA of ammonia (204.0 kcal/mol), and both differ considerably from the PA of His (236.0 kcal/mol); consequently, an even closer model system for His had to be introduced (see further below).

As discussed above, only a pH range 6 – 9.5 needs to be taken into consideration. In this pH regime the strongest attraction between the substrate and His is expected to exist between the protonated amino group from the substrate and the imidazole  $sp^2$ -hybridized nitrogen atom from His (see Scheme 6-2B).

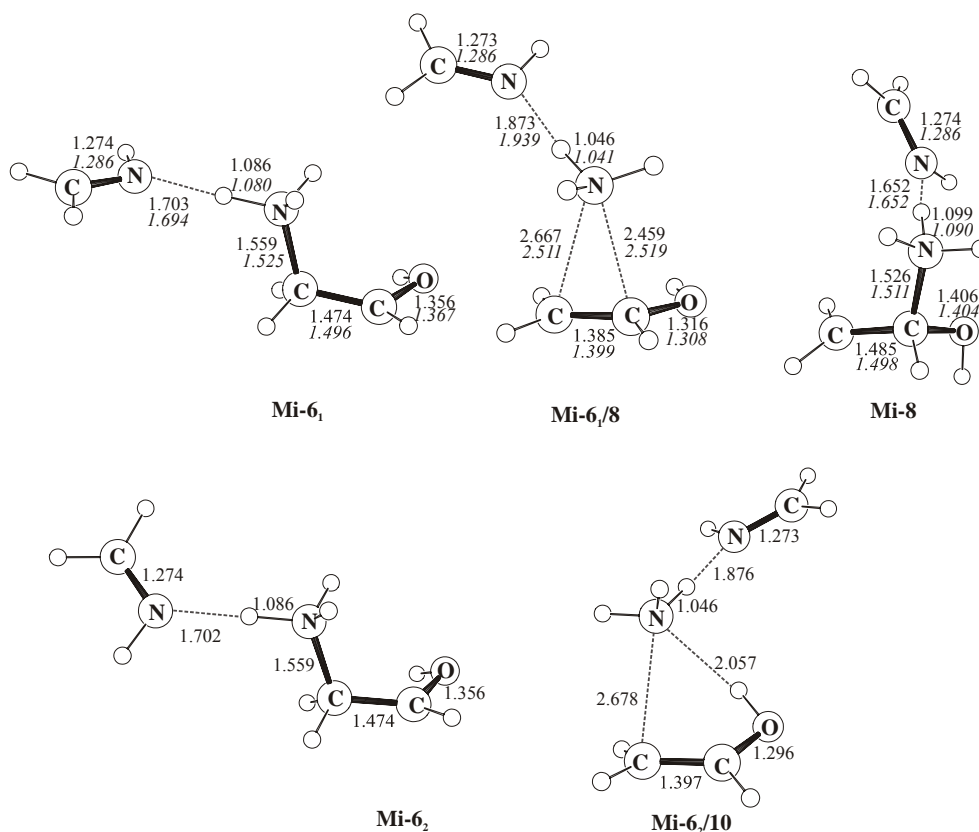


**Figure 6-2.** Optimized geometries of stationary points relevant for the rearrangements of partially protonated aminoethanol radical **6** interacting with  $\text{CH}_2=\text{NH}$  which serves as a His model system (bond lengths are given in Å; B3LYP results in roman and QCISD in italics).

In fact, the trends already observed with the most simple protonating groups ( $\text{H}_3\text{O}^+$ ,  $\text{NH}_4^+$ ) exist in the case of the His model methanimine (Mi) as well: migration of a partially protonated amino group is energetically less demanding than elimination of the ammonium ion. According to the calculations, the transition structure **Mi-6<sub>1/8</sub>** is 2.5 kcal/mol lower in energy than its **Mi-6<sub>2/10</sub>** counterpart (Table 6-3). The stabilization of the former transition structure is most probably achieved through the formation of a relatively stable planar enol radical cation moiety.<sup>152</sup> In contrast, in the **Mi-6<sub>2/10</sub>** transition structure, the enol is distorted from planarity (Figure 6-2), and already shows a trend of ethanal radical formation; for example, the C-O bond is shorter, while the C-C bond of **Mi-6<sub>2/10</sub>** is longer than corresponding bonds in **Mi-6<sub>1/8</sub>**.

Here, a brief comment on the computed values for the activation enthalpies seems warranted: for the migration of a partially protonated amino group in the system **6**/ $\text{CH}_2=\text{NH}$  this barrier height amounts to 20.0 kcal/mol, exceeding the upper limit value (ca. 15 kcal/mol). However, a final answer whether an interaction of His with the substrate is of any relevance on the migration pathway can be given only after an even more reliable

model system for His has been considered (see further in the text). Nevertheless, the migration of a partially protonated amino group is once more favored as compared to the elimination of  $\text{NH}_4^+$ .

**Table 6-3.** Relative enthalpies<sup>a</sup> (in kcal/mol) at 0 K ( $H_{\text{rel}, 0 \text{ K}}$ ), and 298 K ( $H_{\text{rel}, 298 \text{ K}}$ ) of the stationary points on the PES of **6** interacting with  $\text{CH}_2=\text{NH}$  (**Mi**) which serves as the simplest His model system.

|                              | B3LYP/6-31G*                  |                                 | QCISD/cc-pVDZ//               |                                 | QCISD/cc-pVDZ <sup>c</sup>    |                                 |
|------------------------------|-------------------------------|---------------------------------|-------------------------------|---------------------------------|-------------------------------|---------------------------------|
|                              |                               |                                 | B3LYP/6-31G*                  |                                 |                               |                                 |
|                              | $H_{\text{rel}, 0 \text{ K}}$ | $H_{\text{rel}, 298 \text{ K}}$ | $H_{\text{rel}, 0 \text{ K}}$ | $H_{\text{rel}, 298 \text{ K}}$ | $H_{\text{rel}, 0 \text{ K}}$ | $H_{\text{rel}, 298 \text{ K}}$ |
| <b>Mi-6<sub>1</sub></b>      | 0.0                           | 0.0                             | 0.0                           | 0.0                             | 0.0                           | 0.0                             |
| <b>Mi-6<sub>1</sub>/8</b>    | 12.4                          | 12.6                            | 19.8                          | 20.0                            | 20.0                          | 20.3                            |
| <b>Mi-8</b>                  | 2.1                           | 2.2                             | -0.8                          | -0.8                            | -0.4                          | -0.4                            |
| <b>Mi-6<sub>2</sub></b>      | 0.0                           | 0.0                             | 0.0                           | 0.0                             |                               |                                 |
| <b>Mi-6<sub>2</sub>/10</b>   | 16.8                          | 17.0                            | 22.3                          | 22.5                            |                               |                                 |
| <b>Mi-6'</b> <sup>b</sup>    | -5.4                          | -5.2                            |                               |                                 | -5.5                          | -5.2                            |
| <b>Mi-6'/8'</b> <sup>b</sup> | 12.1                          | 12.4                            |                               |                                 |                               |                                 |
| <b>Mi-8'</b> <sup>b</sup>    | 2.9                           | 3.1                             |                               |                                 |                               |                                 |

<sup>a</sup>For electronic energies, ZPEs, and enthalpies see Table AII-3 in the Appendix II.

<sup>b</sup> Structures contain an OH group orientation pointing away from the  $\text{NH}_3$  group (see Scheme 6-3); thus, elimination of  $\text{NH}_4^+$  is not possible for these conformers.

<sup>c</sup> Data to be discussed in the paragraph "Influence of the OH Group Conformation on the Migration".

#### 6.2.4. Asp/Glu serving as Proton Donors

Since both amino acids Asp and Glu have similar structures and comparable acidities formic acid (Fo) was used as a rather crude model to represent both of them (Figure 6-3). For the sake of shortness, in the text it will be referred only to Asp. Two pH ranges will be discussed in some detail.

At  $\text{pH} < 4$  Asp exists in its non-dissociated form and the substrate **2** is protonated. Again, the activation enthalpy for the migration involving **Fo-6<sub>1</sub>/8** is 2.4 kcal/mol lower than for the elimination proceeding through the **Fo-6<sub>2</sub>/10** transition structure (Table 6-4). While the activation enthalpy for the migration of a protonated amino group with 16.2 kcal/mol falls into the range of required activation enthalpies (ca. 15 kcal/mol), the assumed  $\text{pH} < 4$  is not common for biological systems.

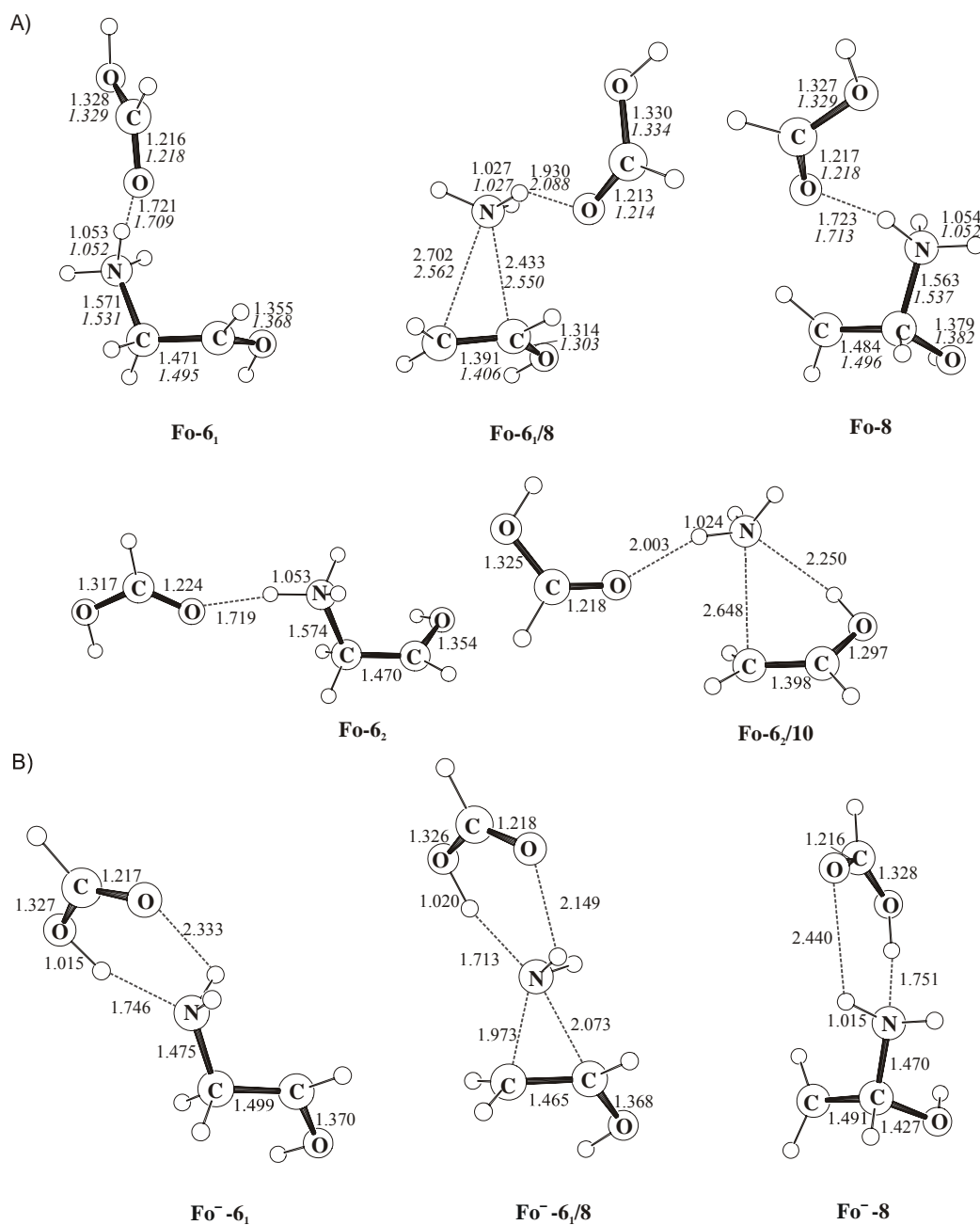


**Figure 6-3.** Optimized geometries of stationary points relevant for the rearrangements of partially protonated aminoethanol radicals **6** interacting with Asp/Glu model systems: A) HCOOH acid, B) HCOO<sup>-</sup> (bond lengths are given in Å; B3LYP results in roman and QCISD in italics).

In a pH regime of 4 – 9.5 Asp is deprotonated while the substrate still prefers the protonated form. Since solvent molecules do not have access to the active site of ethanolamine ammonia lyase,<sup>87c</sup> the overall “neutral” H-bonded complexes, which can be

viewed as structural analogues of “salt bridges”, obtained as the stationary points on the PES are believed to be more stable in the gas phase. In fact, computational studies on similar “salt bridge” complexes in biological systems showed that neutral complexes with double H-bonds between the two charged building blocks are more stable in the gas phase than their zwitter-ionic counterparts; however, the latter are clearly favored in an aqueous environment.<sup>153</sup>

**Table 6-4.** Relative enthalpies<sup>a</sup> (in kcal/mol) at 0 K ( $H_{rel, 0 K}$ ), and 298 K ( $H_{rel, 298 K}$ ) of the stationary points on the PES of **6** interacting with HCO<sub>2</sub>H (**Fo**) serving as the simplest Asp/Glu model system.

|                              | B3LYP/6-31G*   |                  | QCISD/cc-pVDZ//<br>B3LYP/6-31G* |                  | QCISD/cc-pVDZ <sup>c</sup> |                  |
|------------------------------|----------------|------------------|---------------------------------|------------------|----------------------------|------------------|
|                              | $H_{rel, 0 K}$ | $H_{rel, 298 K}$ | $H_{rel, 0 K}$                  | $H_{rel, 298 K}$ | $H_{rel, 0 K}$             | $H_{rel, 298 K}$ |
| <b>Fo-6<sub>1</sub></b>      | 0.0            | 0.0              | 0.0                             | 0.0              | 0.0                        | 0.0              |
| <b>Fo-6<sub>1</sub>/8</b>    | 9.6            | 9.8              | 16.0                            | 16.2             | 16.3                       | 16.5             |
| <b>Fo-8</b>                  | 2.5            | 2.5              | -0.3                            | -0.4             | 0.1                        | 0.1              |
| <b>Fo-6<sub>2</sub></b>      | -0.6           | -0.5             | -0.5                            | -0.4             |                            |                  |
| <b>Fo-6<sub>2</sub>/10</b>   | 14.6           | 14.9             | 18.3                            | 18.6             |                            |                  |
| <b>Fo-6'</b> <sup>b</sup>    | -4.8           | -4.8             |                                 |                  | -4.9                       | -4.8             |
| <b>Fo-6'/8'</b> <sup>b</sup> | 9.9            | 10.1             |                                 |                  |                            |                  |
| <b>Fo-8'</b> <sup>b</sup>    | 2.5            | 2.6              |                                 |                  |                            |                  |

<sup>a</sup> For electronic energies, ZPEs, and enthalpies, see Table AII-4 in the Appendix II.

<sup>b</sup> Structures contain an OH group orientation pointing away from the NH<sub>3</sub> group (see Scheme 6-3); thus, elimination of NH<sub>4</sub><sup>+</sup> is not possible for these conformers.

<sup>c</sup> Data to be discussed in the paragraph “Influence of the OH Group Conformation on the Migration”.

Here, the **Fo<sup>-</sup>-6<sub>1</sub>** structure can be interpreted as **2** interacting with the formic acid; thus in the transition structure **Fo<sup>-</sup>-6<sub>1</sub>/8** a required protonation of the migrating group NH<sub>2</sub> cannot occur and therefore, no stabilization of TS will take place. Further, the migrating group does not have a net charge and is no longer a good leaving group either (for example, the C-N bonds of **Fo<sup>-</sup>-6<sub>1</sub>/8** are shorter than in the analogous **Fo-6<sub>1</sub>/8** transition structure; Figure 6-3); thus, the transition structure **Fo<sup>-</sup>-6<sub>1</sub>/8** is energetically extremely unfavored (Table 6-5: 80.2 kcal/mol) making this reaction highly improbable. Finally, the **Fo<sup>-</sup>-6<sub>1</sub>/8** transition structure can be described in terms of a migration of the amino group in aminoethanol radical **2** only weakly interacting with the HCOOH moiety. However, as



already shown, rearrangement of unprotonated aminoethanol radical **2** is extremely demanding energetically and, consequently, the new findings do not come as any surprise.

**Table 6-5.** Relative enthalpies<sup>a</sup> (in kcal/mol) at 0 K ( $H_{rel, 0 K}$ ), and 298 K ( $H_{rel, 298 K}$ ) of the stationary points on the PES of **6** interacting with  $\text{HCO}_2^-$  (**Fo**<sup>-</sup>) as a dissociated Asp/Glu model system.

|   | B3LYP/6-31G*   |                  | QCISD/cc-pVDZ// B3LYP/6-31G* |                  |
|---|----------------|------------------|------------------------------|------------------|
|   | $H_{rel, 0 K}$ | $H_{rel, 298 K}$ | $H_{rel, 0 K}$               | $H_{rel, 298 K}$ |
| <b>Fo</b> <sup>-</sup> - <b>6</b> <sub>1</sub>            | 0.0            | 0.0              | 0.0                          | 0.0              |
| <b>Fo</b> <sup>-</sup> - <b>6</b> <sub>1</sub> / <b>8</b> | 72.8           | 72.7             | 80.3                         | 80.2             |
| <b>Fo</b> <sup>-</sup> - <b>8</b>                         | -0.4           | -0.4             | -2.3                         | -2.2             |

<sup>a</sup> For electronic energies, ZPEs, and enthalpies, see Table AII-5 in the Appendix II.

### 6.2.5. Résumé

This computational study of the aminoethanol rearrangement, including different models for a partial substrate protonation, clearly discriminates between the two most likely mechanisms (Scheme 6-1: direct  $\text{NH}_3$  migration, **6**  $\rightarrow$  **8**, vs.  $\text{NH}_4^+$  elimination, **6**  $\rightarrow$  **10**). As a result, migration of the partially protonated amino group is shown to be energetically less demanding in all investigated cases in comparison to the elimination process.

In a recently published paper, Radom and co-workers arrived at the same conclusion. Employing isodesmic reactions for the hydrogen abstraction from the 5'-deoxyadenosine model system by the putative product radicals **8** and **10**, the authors concluded that the migration **6**  $\rightarrow$  **8** constitutes a more favorable scenario since hydrogen abstraction from 5'-deoxyadenosine by **8** is calculated to be exothermic (-1.2 kcal/mol), while the same reaction, where **10** abstracts a hydrogen atom, is quite endothermic (6.2 kcal/mol). Possible barriers associated with both process have not been reported.

### 6.3. Influence of the OH Group Conformation on the Migratory Aptitude

A realistic activation enthalpy for the migration process can be estimated only if the most stable conformer of the reactant is identified. For the migration **6** → **8** different conformations of the OH group are conceivable, out of which two extreme cases will be discussed in more detail (Scheme 6-3). One of the conformations might be crucial since the (partially) protonated aminoethanol radical **6** can be stabilized through an intramolecular H-bond interaction with the lone-electron pair of the OH group (Scheme 6-3B). Interestingly, in the analogous case of non-protonated aminoethanol **2**, the orientation of the OH group towards the NH<sub>2</sub> group was found to be the most stable conformation due to the strong H-bonding between the hydrogen from OH and a nitrogen from the NH<sub>2</sub>-group. In the case of a H-bonding between the oxygen from the OH-group and a hydrogen atom from the NH<sub>3</sub> group (Scheme 6-3B), one can expect that the stability of the OH group conformation will be dictated by the strength of the proton-donating group X. Therefore, the influence of an OH group conformation on the barrier for the migration employing different protonating groups has been explored.<sup>154</sup> Structures corresponding to the OH group oriented away from the NH<sub>3</sub> group are denoted by a prime, e.g. **6'**, **8'** etc.

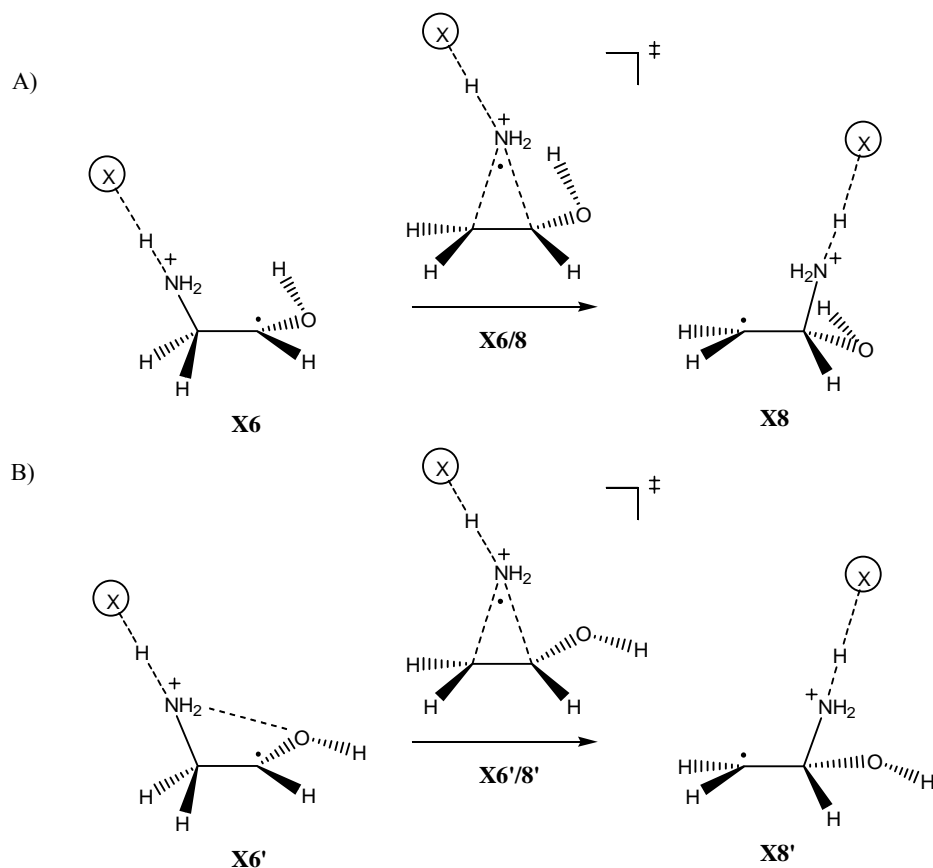
**Table 6-6.** Relative enthalpies<sup>a</sup> (in kcal/mol) at 0 K ( $H_{rel, 0 K}$ ), and 298 K ( $H_{rel, 298 K}$ ) of the stationary points on the PES of protonated aminoethanol radicals; comparison between the energetics of the migration pathways for two different orientations of the OH group in **6**.

|                                     | B3LYP/6-31G*   |                  | QCISD/cc-pVDZ  |                  |
|-------------------------------------|----------------|------------------|----------------|------------------|
|                                     | $H_{rel, 0 K}$ | $H_{rel, 298 K}$ | $H_{rel, 0 K}$ | $H_{rel, 298 K}$ |
| <b>6<sub>1</sub></b> <sup>a</sup>   | 0.0            | 0.0              | 0.0            | 0.0              |
| <b>6<sub>1</sub>/8</b> <sup>a</sup> | 4.7            | 4.9              | 10.2           | 10.4             |
| <b>8</b> <sup>a</sup>               | 2.9            | 3.0              | -0.3           | -0.1             |
| <b>6'</b> <sup>b</sup>              | -5.6           | -5.6             | -6.6           | -6.6             |
| <b>6'/8'</b> <sup>b</sup>           | 4.2            | 4.4              | 9.5            | 9.7              |
| <b>8'</b> <sup>b</sup>              | 2.8            | 2.8              | 0.5            | 0.5              |

<sup>a</sup> Energies taken from ref. 133.

<sup>b</sup> Structures contain an OH group orientation pointing away from the NH<sub>3</sub> group (see Scheme 6-3). For electronic energies, ZPEs, and enthalpies, see Table AII-6 in the Appendix II.

In order to obtain even more reliable activation enthalpies for the migration rearrangements, the reoptimizations of **X6<sub>1</sub>**, **X6<sub>1</sub>/8** and **X8** were performed at the QCISD/cc-pVDZ level of theory.



**Scheme 6-3.** Different OH group orientations in the (partially) protonated aminoethanol radical **6** and their influence on the migration pathway.

Firstly, the rearrangement of the fully protonated aminoethanol radical **6** will be addressed (Scheme 6-3 but without X); here the influence of the OH conformation should be most pronounced. According to the data in Table 6-6, conformer **6'** corresponds to the (global) minimum on the PES; this is due to a quite strong H-bond between the oxygen lone pair and a hydrogen atom from the NH<sub>3</sub> group (2.281 Å, QCISD geometry; Figure 6-4). The H-bond stabilization amounts to 6.6 kcal/mol. However, in line with the Curtin-Hammett principle<sup>155</sup> it is irrelevant energetically whether the migration proceeds directly through **6'/8'** (16.3 kcal/mol) or sequentially **6'** → **6<sub>1</sub>** (6.6 kcal/mol) and **6<sub>1</sub>/8** (10.4 kcal/mol). The resulting overall activation energy as well as the product energies are almost identical (Table 6-6).

Since for the migration processes discussed previously transition structures were located commencing from a conformer in which a H-bond between the  $\text{NH}_2\text{-H}$  and  $\text{OH}$  groups does *not* exist, in order to estimate the energy demand for the overall migration process, the transition structures **X6'8'** as well as the minima connected by the corresponding TSs for different protonating groups ( $\text{X} = \text{H}_2\text{O}$ ,  $\text{NH}_3$ ,  $\text{CH}_2\text{NH}$ ,  $\text{HCO}_2\text{H}$ ) were located at the B3LYP/6-31G\* level of theory. Next, the geometry reoptimizations of the **X6'** structures were performed at the QCISD/cc-pVDZ level of theory in order to estimate the overall migration enthalpy as stated above.

Comparing the energies of the conformers **X6<sub>1</sub>** and **X6'**, it can be seen that the stabilization gained through the H-bond interaction in the conformer **X6'** amounts to ca. 5 kcal/mol (Tables 6-1 – 6-4; QCISD/cc-pVDZ method), which implies that the overall migration pathways are  $\sim 5$  kcal/mol more demanding than previously stated. More precisely, for  $\text{X} = \text{H}_2\text{O}$ , the overall activation enthalpy for the migration equals to 21.7 kcal/mol and for  $\text{X} = \text{NH}_3$  it amounts to 25.8 kcal/mol. In case of the small amino-acid model systems the overall activation enthalpies change to 21.3 kcal/mol ( $\text{X} = \text{HCOOH}$ ) and 25.5 kcal/mol ( $\text{X} = \text{CH}_2\text{NH}$ ).

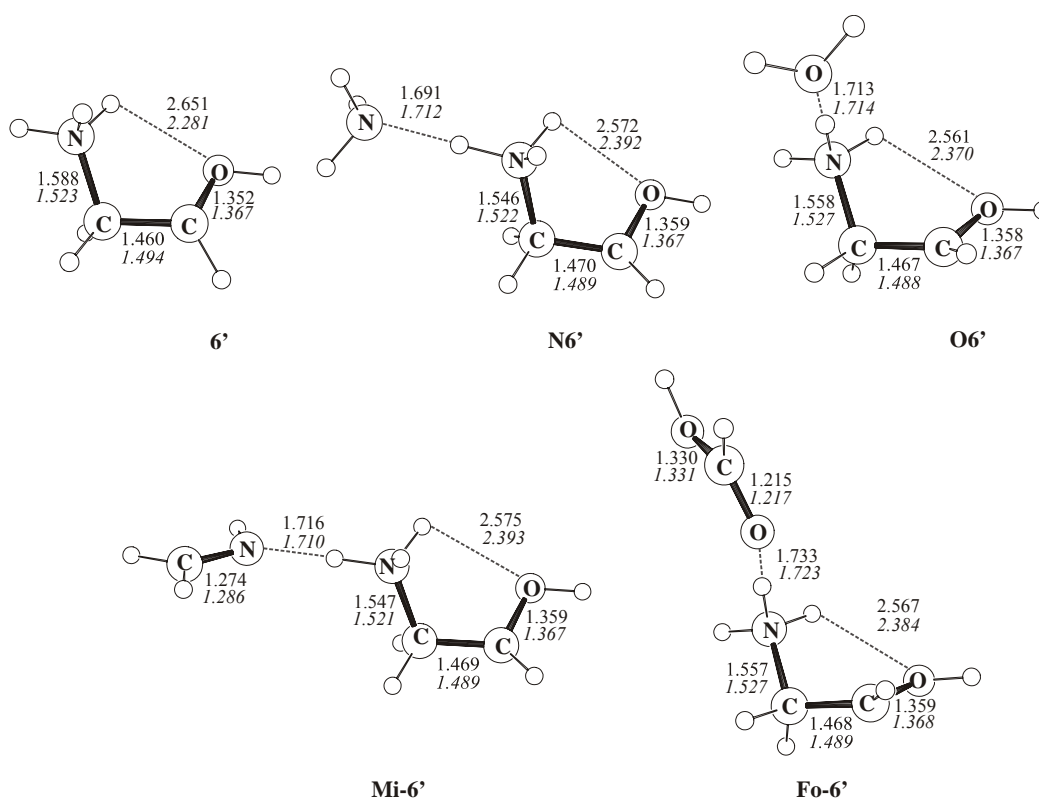


**Figure 6-4.** Optimized geometries of stationary points relevant for the rearrangements of (partially) protonated aminoethanol radicals **6'** with H-bond interaction (bond lengths are given in Å; B3LYP results in roman and QCISD in italics).

Not surprisingly, the activation enthalpy is lowest in the case of full protonation of **2**; as soon as deprotonation comes into play, the activation barrier increases substantially. However, even *partial protonation* renders the migration more favorable since the corresponding barriers for all investigated protonating groups are lower than for a completely deprotonated precursor **2**. At first sight, this statement is in disagreement with the conclusion derived by Radom and co-workers, who concluded that partial deprotonation has an anticatalytic effect based on the activation energy comparison with the rearrangement of non-protonated aminoethanol radical, **2** (23.6 kcal/mol; fragmentation – recombination mechanism<sup>156</sup>). However, for their particular case, the TS located does not commence from the most stable aminoethanol radical structure. However, the global minimum has been previously located (see Chapter 5; the structure denoted as **2<sub>2</sub>**), which is 4.4 kcal/mol more stable than the aminoethanol radical conformer located by Radom and co-workers. Keeping this in mind, the energy requirement for the rearrangement of the aminoethanol radical **2** amounts to 28 kcal/mol,<sup>157</sup> thus being higher than for any of the partially protonated precursors **X6**.

However, even if the partial protonation reduces the activation enthalpy compared to the non-protonated case, all estimated migration enthalpies still exceed the activation-enthalpy upper limit determined experimentally as acceptable for an enzymatic catalysis (ca. 15 kcal/mol). One of the possible explanations could be related to the inaccuracy of the computational method chosen. However, concerning that topic a comparison with the data reported by Radom and co-workers is warranted. The latter estimated the transition barrier **6'** → **8'** to be 15.7 kcal/mol (0 K) at the G3(MP2)-RAD(p) level of theory; this agrees pleasingly with the result derived in this study (16.1 kcal/mol at 0 K). Therefore, this computational method employed herein produces data comparable in its quality to those obtained from the computationally more demanding G3 method. Further, it is worth noting that single point calculations at the QCISD/cc-pVDZ level of theory on the B3LYP optimized geometries provide very similar relative enthalpies as the data obtained by computationally more demanding geometry reoptimizations at the QCISD level of theory (see Tables 6-1 - 6-4). Clearly, for the cases that follow it is sufficient to perform only single-point calculations at the QCISD/cc-pVDZ level of theory since these data are of the same accuracy as those that would be obtained by the geometry reoptimizations at the same level of theory.

As the method chosen cannot be the cause for an overestimation of the activation barriers, a partial protonation alone *does not* sufficiently reduce the activation enthalpy;

thus, some more refined mechanistic scenarios for the migration rearrangement have to be considered. However, before discussing some of these mechanistic variants, the migration pathways were computed using some more appropriate models for the amino acids in order to eliminate a possible overestimation of the activation enthalpy caused by employing unrealistic model systems. Thus, the migration pathway was calculated employing acetic acid (rather than formic acid) as a model system for Asp/Glu and imidazole (rather than methanimine) as a model system for His.

#### 6.4. Acetic acid and Imidazole – More Reliable Model Systems for Asp/Glu and His

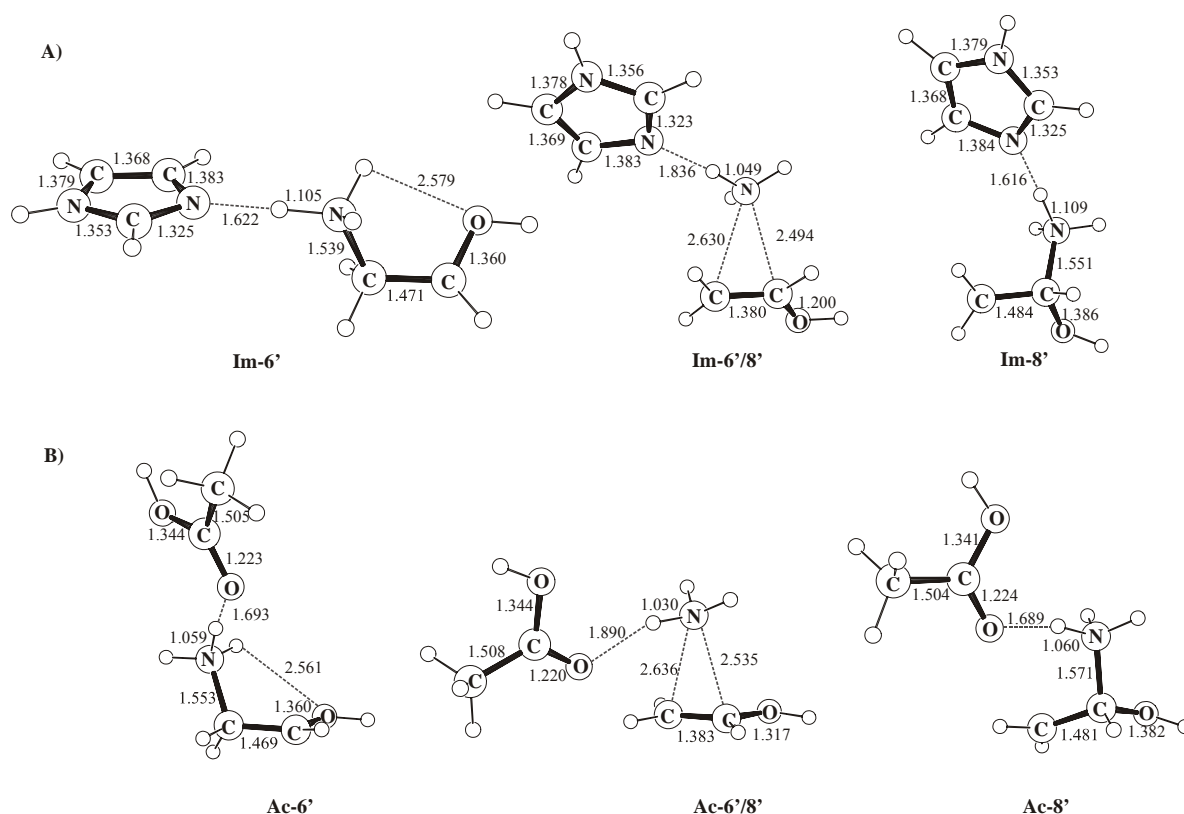


**Figure 6-5.** Optimized geometries of stationary points relevant for the rearrangements of partially protonated aminoethanol radical **6** interacting with more realistic model systems for amino acids: A) imidazole as His model system, B) acetic acid as Asp/Glu model system (bond lengths are given in Å; B3LYP results).

For both model systems, the rearrangement commences from a conformer in which an intramolecular H-bond exists (Figure 6-5); thus, the computed activation enthalpy corresponds to the final energy demand for the migration pathway. His is expected to catalytically interact with the substrate radical in the pH regime 6 – 9.5, while for Asp model system only interactions in the pH < 4 were taken into account. When imidazole interacts with the NH<sub>3</sub> group of **6**, the activation enthalpy is quite high and equals to 27.4 kcal/mol due to a higher degree of deprotonation in **Im-6'/8'** as compared to the analogous TS **Ac-6'/8'** (Figure 6-5). In case of acetic acid the activation enthalpy is somewhat lower being 24.2 kcal/mol (Table 6-7). While both models are structurally closer to the amino acids than the previously employed systems, and further, have proton affinities comparable to those of the amino acids,<sup>158</sup> the computed barriers, nevertheless, are too high to be acceptable for the enzymatic reaction. Even though partial protonation helps to lower the barrier for the rearrangement **6** → **8**, the amount gained is not sufficiently large to bring about acceleration of the enzymatic process. Clearly, in reality a more complex situation must prevail.

**Table 6-7.** Relative enthalpies<sup>a</sup> (in kcal/mol) at 0 K ( $H_{rel, 0 K}$ ), and 298 K ( $H_{rel, 298 K}$ ) of the stationary points on the PES of **6** interacting with imidazole (**Im**) as a His model system and acetic acid (**Ac**) as Asp/Glu model system.

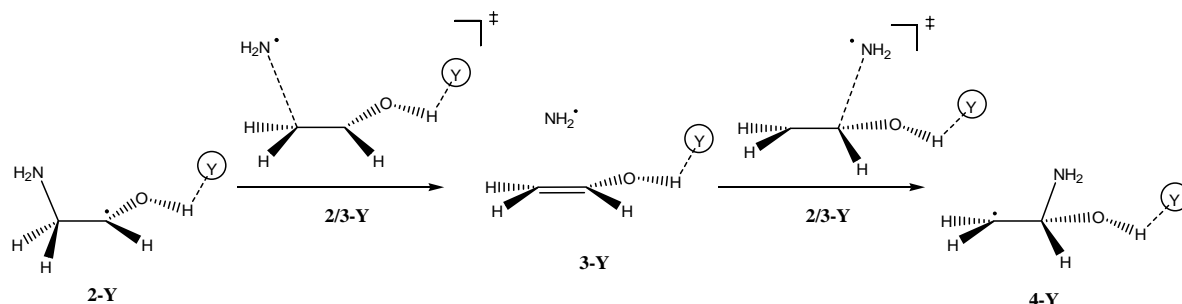
|                              | B3LYP/6-31G*   |                  | QCISD/cc-pVDZ//B3LYP/6-31G* |                  |
|------------------------------|----------------|------------------|-----------------------------|------------------|
|                              | $H_{rel, 0 K}$ | $H_{rel, 298 K}$ | $H_{rel, 0 K}$              | $H_{rel, 298 K}$ |
| <b>Im-6'</b> <sup>b</sup>    | 0.0            | 0.0              | 0.0                         | 0.0              |
| <b>Im-6'/8'</b> <sup>b</sup> | 19.1           | 19.3             | 27.2                        | 27.4             |
| <b>Im-8'</b> <sup>b</sup>    | 7.8            | 7.8              | 5.3                         | 5.3              |
| <b>Ac-6'</b> <sup>c</sup>    | 0.0            | 0.0              | 0.0                         | 0.0              |
| <b>Ac-6'/8'</b> <sup>c</sup> | 15.5           | 15.8             | 24.2                        | 24.2             |
| <b>Ac-8'</b> <sup>c</sup>    | 7.2            | 7.2              | 5.8                         | 5.9              |

<sup>a</sup> For electronic energies, ZPEs, and enthalpies, see Table AII-7 in Appendix II.

<sup>b</sup> **Im-6'** structure taken as a reference point.

<sup>c</sup> **Ac-6'** structure taken as a reference point.

## 6.5. Pull Mechanism



**Scheme 6-4.** Pull mechanism for the dissociation-association pathway.

Since **2** contains two functional groups, it is conceivable that the OH-group as well interacts with some amino acid from the active site, and by partial deprotonation of the OH group the barrier is lowered. For the non-protonated form of substrate **2** it was shown in Chapter 5 that a dissociation-association pathway is energetically least demanding; thus, this scenario was investigated for the partial deprotonation as well (Scheme 6-4). Only the first reaction step (dissociation of the  $\text{NH}_2$  group) was computed for different deprotonating groups Y, rather than computing the whole reaction profile that includes association as well. Clearly, if dissociation of the  $\text{NH}_2$ -group exceeds the activation enthalpy upper limit value, the pull mechanism alone will not play a role in the enzymatic catalysis.

First the rather small  $\text{OH}^-$  ion was used as a deprotonating agent. Even though the activation enthalpy for the dissociation process (15.2 kcal/mol, Table 6-8) falls into the range acceptable for the enzymatic catalysis, bare  $\text{OH}^-$  as a model system for Asp/Glu is quite inappropriate. Thus, the interaction at the OH-site in **2** was computed employing better model systems for the amino acids.

If the pH in the active site is higher than 4, Asp and Glu exist in their dissociated forms; thus, a carboxylate ion can partially deprotonate the OH group in **2**. The model systems employed in order to mimic these interactions were formate and acetate (see Figure 6-6). For the interaction of  $\text{HCOO}^-$  with the OH group, the activation enthalpy for the dissociation of  $\text{NH}_2$  equals to 19.7 kcal/mol. When acetate as model system for Asp/Glu was employed, the activation enthalpy is somewhat higher being equal to 20.2 kcal/mol (Table 6-8).



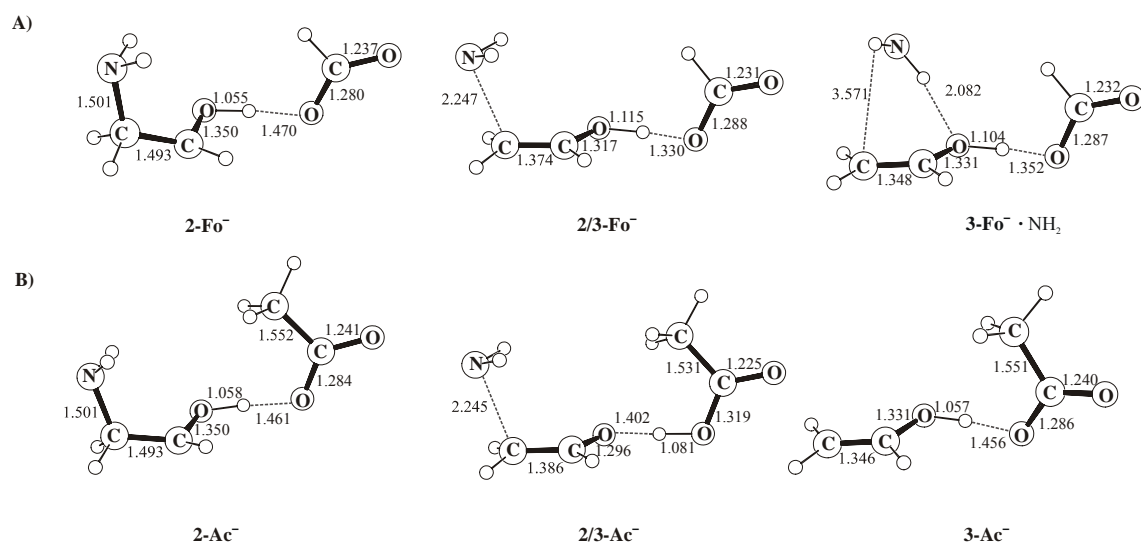


**Figure 6-6.** Pull mechanism; optimized geometries of stationary points relevant for the rearrangements of partially deprotonated aminoethanol radical **2** interacting with two His model systems: A) CH<sub>2</sub>NH, B) imidazole (bond lengths are given in Å; B3LYP results).

**Table 6-8.** Pull mechanism; relative enthalpies<sup>a</sup> (in kcal/mol) at 0 K ( $H_{rel, 0 K}$ ), and 298 K ( $H_{rel, 298 K}$ ) of the stationary points on the PES of **2** interacting with OH<sup>-</sup> (**O<sup>-</sup>**), HCO<sub>2</sub><sup>-</sup> (**Fo<sup>-</sup>**) and CH<sub>3</sub>CO<sub>2</sub><sup>-</sup> (**Ac<sup>-</sup>**) which serve as dissociated Asp/Glu model systems.

|   | B3LYP/6-31G*   |                  | QCISD/cc-pVDZ//B3LYP/6-31G* |                  |
|---|----------------|------------------|-----------------------------|------------------|
|   | $H_{rel, 0 K}$ | $H_{rel, 298 K}$ | $H_{rel, 0 K}$              | $H_{rel, 298 K}$ |
| <b>2O<sup>-</sup></b> <sup>b</sup>                    | 0.0            | 0.0              | 0.0                         | 0.0              |
| <b>2/3O<sup>-</sup></b> <sup>b</sup>                  | 8.7            | 8.9              | 15.1                        | 15.2             |
| <b>3O<sup>-</sup> · NH<sub>2</sub></b> <sup>b</sup>   | 7.7            | 8.6              | 12.8                        | 13.7             |
| <b>2-Fo<sup>-</sup></b> <sup>c</sup>                  | 0.0            | 0.0              | 0.0                         | 0.0              |
| <b>2/3-Fo<sup>-</sup></b> <sup>c</sup>                | 14.7           | 14.9             | 19.5                        | 19.7             |
| <b>3-Fo<sup>-</sup> · NH<sub>2</sub></b> <sup>c</sup> | 11.3           | 12.4             | 8.6                         | 9.7              |
| <b>2-Ac<sup>-</sup></b> <sup>d</sup>                  | 0.0            | 0.0              | 0.0                         | 0.0              |
| <b>2/3-Ac<sup>-</sup></b> <sup>d</sup>                | 14.6           | 14.8             | 20.0                        | 20.2             |
| <b>3-Ac<sup>-</sup> + NH<sub>2</sub></b> <sup>d</sup> | 19.8           | 21.0             | 17.1                        | 18.3             |

<sup>a</sup> For electronic energies, ZPEs, and enthalpies, see Table AII-8 in the Appendix II.

<sup>b</sup> **2O<sup>-</sup>** structure taken as a reference point.

<sup>c</sup> **2-Fo<sup>-</sup>** structure taken as a reference point.

<sup>d</sup> **2-Ac<sup>-</sup>** structure taken as a reference point.

His can act as a proton acceptor if the pH in the active site is higher than 6. When the smaller model system  $\text{CH}_2\text{NH}$  is used to partially deprotonate **2**, the computed activation enthalpy amounts to 24.1 kcal/mol. In the case of a more realistic model system, i.e. imidazole (Figure 6-7), the activation enthalpy is somewhat lower being equal to 23.8 kcal/mol (Table 6-9).

In general, partial deprotonation at the OH group of **2** acts catalytically as well, since in all investigated cases the activation enthalpy obtained is lower than for a non-deprotonated radical **2** (28.0 kcal/mol). However, the computed activation enthalpies for the dissociation of  $\text{NH}_2$  group still exceed the upper limit value determined from the experimental studies (ca. 15 kcal/mol); thus, the association of the  $\text{NH}_2$  radical with **3-Y** (Scheme 6-4) was not deemed necessary to be investigated computationally. Clearly, a partial deprotonation at the OH-group in **2** (pull mechanism) alone cannot sufficiently decrease the activation enthalpy. More likely, only when both interactions, i.e. partial deprotonation of the OH and partial protonation of the  $\text{NH}_2$  group, occur simultaneously, the activation enthalpy might fall below 15 kcal/mol.

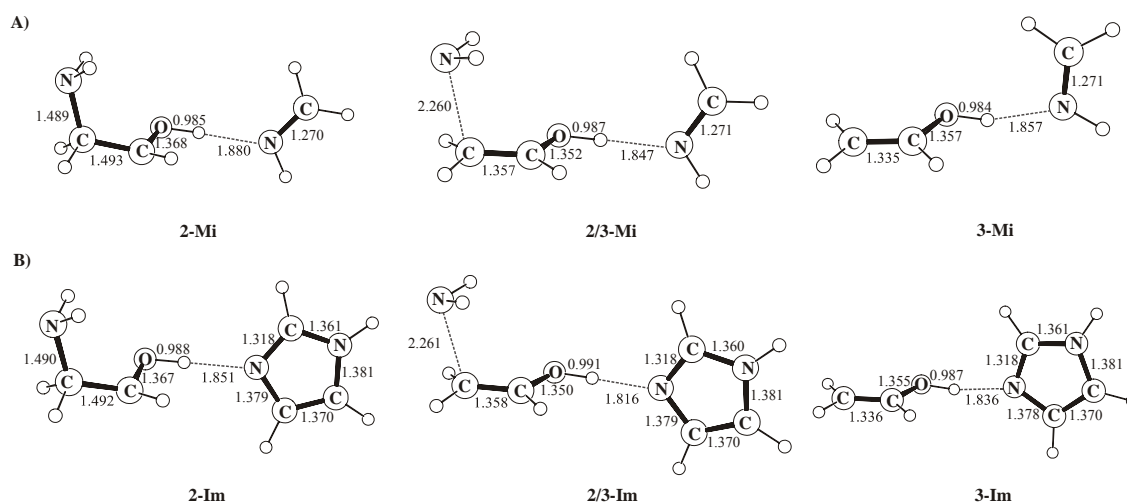


**Figure 6-7.** Pull mechanism; optimized geometries of stationary points relevant for the rearrangements of partially deprotonated aminoethanol radical **2** interacting with two His model systems: A)  $\text{CH}_2\text{NH}$ , B) imidazole (bond lengths are given in Å; B3LYP results).

**Tables 6-9.** Pull mechanism; relative enthalpies<sup>a</sup> (in kcal/mol) at 0 K ( $H_{rel, 0 K}$ ), and 298 K ( $H_{rel, 298 K}$ ) of the stationary points on the PES of **2** interacting with CH<sub>2</sub>NH (**Mi**) and imidazole (**Im**) as His model systems.

|   | B3LYP/6-31G*   |                  | QCISD/cc-pVDZ//B3LYP/6-31G* |                  |
|---|----------------|------------------|-----------------------------|------------------|
|   | $H_{rel, 0 K}$ | $H_{rel, 298 K}$ | $H_{rel, 0 K}$              | $H_{rel, 298 K}$ |
| <b>2-Mi</b> <sup>b</sup>                    | 0.0            | 0.0              | 0.0                         | 0.0              |
| <b>2/3-Mi</b> <sup>b</sup>                  | 20.9           | 21.1             | 24.0                        | 24.1             |
| <b>3-Mi</b> + NH <sub>2</sub> <sup>•b</sup> | 20.1           | 21.2             | 17.4                        | 18.5             |
| <b>2-Im</b> <sup>c</sup>                    | 0.0            | 0.0              | 0.0                         | 0.0              |
| <b>2/3-Im</b> <sup>c</sup>                  | 20.4           | 20.7             | 23.6                        | 23.8             |
| <b>3-Im</b> + NH <sub>2</sub> <sup>•c</sup> | 19.9           | 21.1             | 17.2                        | 18.4             |

<sup>a</sup> For electronic energies, ZPEs, and enthalpies, see Table AII-9 in the Appendix II.

<sup>b</sup> **2-Mi** structure taken as a reference point.

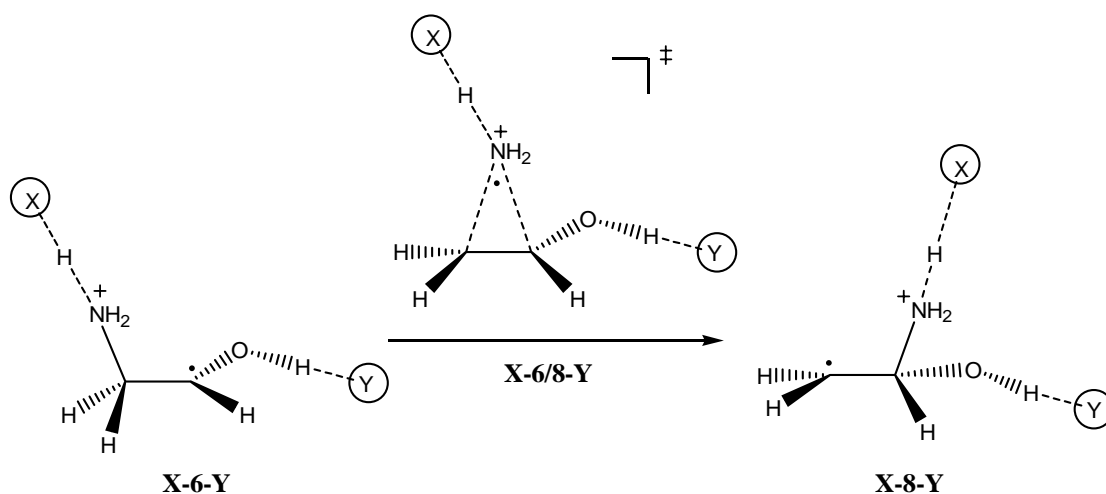
<sup>c</sup> **2-Im** structure taken as a reference point.

## 6.6. Synergistic Action of Two Catalytic Auxiliaries

One of the options by which the enzyme can reduce the activation enthalpy for the rearrangement process is the so-called push-pull mechanism proposed by Radom and co-workers in the case of diol dehydrase<sup>134</sup> and employed as well in the study of ethanolamine rearrangement catalyzed by ethanolamine ammonia lyase. Since substrate **2** exhibits acidic (OH group) and basic (NH<sub>2</sub> group) features, both sites might interact with different amino acid residues of the enzyme as depicted in Scheme 6-5. Depending on the actual pH in the enzyme's active site, interaction is possible separately at the NH<sub>2</sub> or OH group, or both sites of substrate **2** are simultaneously interacting with appropriate catalytic auxiliaries of the enzyme.

As already demonstrated by Radom and co-workers, a push-pull mechanism (Scheme 6-5) might serve as the best model for the rearrangement of aminoethanol catalyzed by ethanolamine ammonia lyase. Even though the rearrangement barriers were calculated to be lower than the upper limit value acceptable for the enzymatic reaction, one should be aware of the rather crude model systems (e.g. NH<sub>3</sub>, H<sub>2</sub>O) employed in the latter study. Therefore, the activation enthalpies were computed using rather some more realistic model systems for those amino acids that might act as catalytic auxiliaries. Clearly, these data are not only likely to result in more reliable activation enthalpies, but as well, and

perhaps even more importantly, they might help to provide a realistic picture of possible interactions in the enzyme's active site.



**Scheme 6-5.** Push-pull mechanism for a migration pathway of **6** involving a partial protonation of the  $\text{NH}_2$  group and a partial deprotonation of the OH group of the substrate.

The elucidation of the question which amino acid acts as a catalytic auxiliary at the hydroxyl and which at the amino group of **2** is related to the possible pH prevailing in the active site. Having in mind  $\text{pK}_a$  values of the potential amino acid candidates (Asp, Glu, His) and the  $\text{pK}_a$  of aminoethanol, it is clear that in the pH regime 6 - 9.5 a synergistic interaction can take place. In this pH range, Asp/Glu exist as carboxylate, His is non-protonated and the substrate **2** is protonated. In the section where aspects of partial protonation were discussed in detail, it was concluded that interaction of carboxylate with the  $\text{NH}_3$  group in **6** substantially increases the activation enthalpy and is definitely not catalytic. Thus, only His is an acceptable candidate for the interaction with the  $\text{NH}_3$  group of **6**. However, both His and Asp/Glu in this particular pH range might partially deprotonate the OH group of **6**. When discussing the pull-mechanism, it was shown that the activation enthalpy is lower when model systems for Asp/Glu were employed in comparison with model systems for His. Thus, Asp/Glu were assumed to serve as better catalytic auxiliaries at the OH-site in **6**.

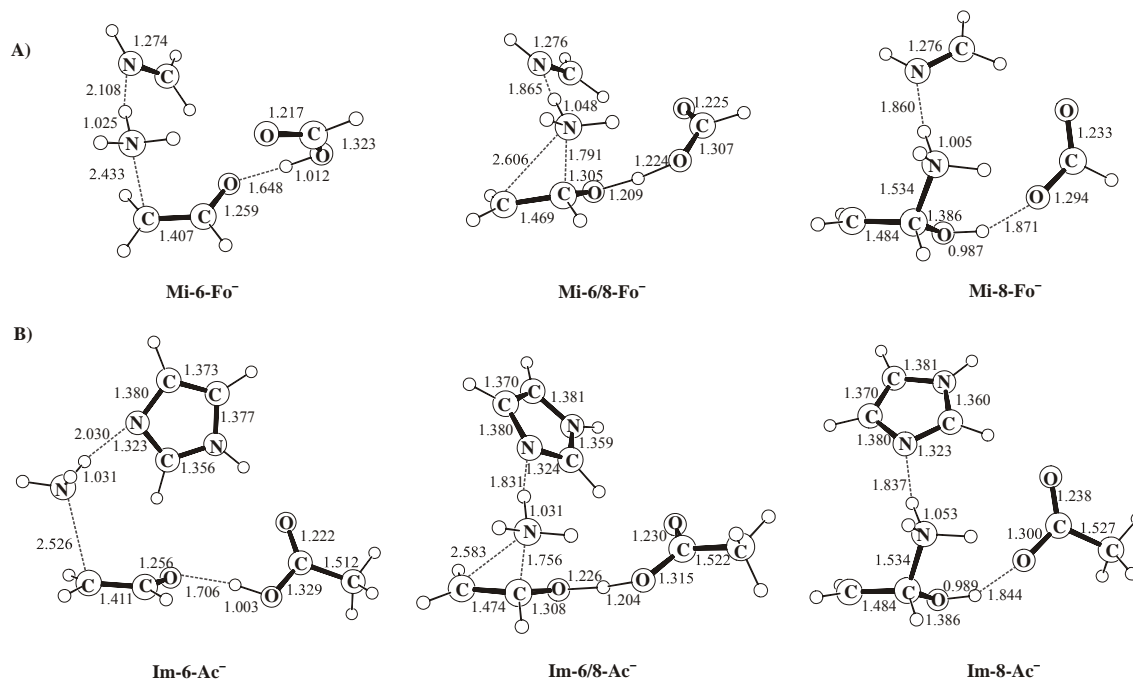


**Figure 6-8.** Push-pull mechanism; optimized geometries of stationary points relevant for the rearrangements of **6** interacting with His and Asp/Glu model systems: A) CH<sub>2</sub>NH and formate, B) imidazole and acetate (bond lengths are given in Å; B3LYP results).

In order to elucidate the push-pull mechanism in more detail two different systems were employed. First a set of smaller models for the above mentioned amino acids was employed (CH<sub>2</sub>NH for His and HCOO<sup>-</sup> for Asp/Glu; Figure 6-8A). The computed activation enthalpy amounts to 11.6 kcal/mol (Table 6-10) being lower than the upper limit value derived from the experiment. When a more realistic model for the amino acids was used (imidazole for His and CH<sub>3</sub>COO<sup>-</sup> for Asp/Glu; Figure 6-8B), the activation enthalpy is slightly higher being equal to 13.7 kcal/mol. The analysis of the structural details (Figure 6-8) reveals that the low activation enthalpies are due to both reactant destabilization and transition structure stabilization. For example, in both structures **Mi-6-Fo<sup>-</sup>** and **Im-6-Ac<sup>-</sup>** the C(2)-N bonds are extremely prolonged when compared to the ones in **Mi-6<sub>1</sub>** (Figure 6-2) or **Im-6** (Figure 6-5). At the same time, interaction of the carboxylate with the OH group of **6** results in a lengthening of the O-H bond; as a consequence, the system develops features of an ethanal structure (e.g. compare the C-C and C-O bond lengths given in Figure 6-8). The emerging radical center on C(2) is stabilized by delocalization through the developing ethanal structure. It is this subtle interplay of the two catalytic auxiliaries that makes the migration energetically less demanding than when compared to situations where

only one of the catalytic auxiliaries is in action (e.g. **Im-6/8** or **2/3-Ac<sup>-</sup>**). As a result, the activation enthalpy for the migration costs only 13.7 kcal/mol, which is lower than the upper limit value determined from the experiment (ca. 15 kcal/mol).

**Table 6-10.** Push-pull mechanism; relative enthalpies<sup>a</sup> (in kcal/mol) at 0 K ( $H_{rel, 0 K}$ ), and 298 K ( $H_{rel, 298 K}$ ) of the stationary points on the PES of **6** interacting with model systems for His and Asp/Glu (CH<sub>2</sub>NH with HCOO<sup>-</sup> and imidazole with CH<sub>3</sub>COO<sup>-</sup>).

|   | B3LYP/6-31G*   |                  | QCISD/cc-pVDZ//B3LYP/6-31G* |                  |
|---|----------------|------------------|-----------------------------|------------------|
|   | $H_{rel, 0 K}$ | $H_{rel, 298 K}$ | $H_{rel, 0 K}$              | $H_{rel, 298 K}$ |
| <b>Mi-6-Fo<sup>-</sup></b> <sup>b</sup>   | 0.0            | 0.0              | 0.0                         | 0.0              |
| <b>Mi-6/8-Fo<sup>-</sup></b> <sup>b</sup> | 13.8           | 12.8             | 12.6                        | 11.6             |
| <b>Mi-8-Fo<sup>-</sup></b> <sup>b</sup>   | 9.3            | 8.3              | 5.3                         | 4.3              |
| <b>Im-6-Ac<sup>-</sup></b> <sup>c</sup>   | 0.0            | 0.0              | 0.0                         | 0.0              |
| <b>Im-6/8-Ac<sup>-</sup></b> <sup>c</sup> | 16.9           | 15.7             | 14.9                        | 13.7             |
| <b>Im-8-Ac<sup>-</sup></b> <sup>c</sup>   | 13.0           | 11.9             | 8.7                         | 7.6              |

<sup>a</sup> For electronic energies, ZPEs, and enthalpies, see Table AII-10 in the Appendix II.

<sup>b</sup> **Mi-6-Fo<sup>-</sup>** structure taken as a reference point.

<sup>c</sup> **Im-6-Ac<sup>-</sup>** structure taken as a reference point.

## 6.7. Summary and Conclusions

The computational study of the aminoethanol rearrangement, including different models for a partial substrate protonation, clearly discriminates between the two mechanisms (direct NH<sub>3</sub> migration, **6** → **8**, vs. NH<sub>4</sub><sup>+</sup> elimination, **6** → **10**) which were identified as the most likely routes in Chapter 5. As a result, migration of the partially protonated amino group is shown to be energetically less demanding in all investigated cases in comparison to the elimination process.

However, even if realistic model systems for the amino acids His, Asp and Glu, that can act as catalytic auxiliaries and partially protonate the substrate, are employed, the computed activation enthalpies exceed the upper limit value (ca. 15 kcal/mol) determined by kinetic studies as acceptable for enzymatic catalysis. For example, when imidazole is employed as a model system for His to interact with the NH<sub>3</sub> group of substrate **6**, the activation enthalpy for the migration process amounts to 27.4 kcal/mol. If acetic acid is employed to mimic Asp or Glu interacting with NH<sub>3</sub> in **6**, the activation enthalpy is

somewhat lower, being equal to 24.2 kcal/mol. Thus, partial protonation of the amino group in the substrate alone does not sufficiently reduce the activation enthalpy for this pathway to be feasible under enzymatic conditions. However, partial protonation of the amino group still acts catalytically since all computed activation enthalpies are lower than when compared to a rearrangement of the non-protonated substrate radical **2** (28 kcal/mol).

In the case of a partial deprotonation of the substrate **2** at the OH group, the rearrangement mechanism consists of a dissociation of the NH<sub>2</sub> radical from C(2) and its association at the C(1) atom. For all investigated proton acceptors (OH<sup>-</sup>, HCOO<sup>-</sup>, CH<sub>3</sub>COO<sup>-</sup>, CH<sub>2</sub>NH, imidazole), the activation enthalpy for the dissociation step exceeds the limit value. Typical data are 20.2 kcal/mol for acetate and 23.8 kcal/mol for imidazole interacting with the OH group of **2**; thus, Asp or Glu present better candidates than His to pull a proton from the OH group of the substrate. As in the case of partial protonation of the NH<sub>2</sub> group, the partial deprotonation of the OH group acts catalytically in that it reduces the activation enthalpy, though, not sufficiently.

Obviously, a synergistic action (Scheme 6-5) of two catalytic auxiliaries in the enzyme's active site is necessary to result in a sufficient reduction of the activation enthalpy. Elucidation of the question which amino acid acts as a catalytic auxiliary at the OH (partial deprotonation) and which at the NH<sub>2</sub> group (partial protonation) of **2** depends on the possible pH in the active site. Only in a pH regime 6 - 9.5 the synergistic interaction can take place; in this pH range Asp/Glu exist as carboxylates and His is non-protonated, while the substrate is still protonated. Thus, His is a better candidate for an interaction with the NH<sub>3</sub> group in substrate **6**. However, in this particular pH range both His and Asp/Glu might partially deprotonate the OH-group in **6**. Since it was shown for the pull-mechanism (Scheme 6-4) that the activation enthalpy is lowest when model systems for Asp/Glu were employed in comparison with model systems for His, in the deprotonation step either Asp or Glu are predicted to be involved.

Details of the push-pull mechanism were calculated employing two different systems (Figure 6-8). When the smaller models for the catalytic auxiliaries His and Asp/Glu (i.e. CH<sub>2</sub>NH and HCOO<sup>-</sup>) were used, the computed activation enthalpy amounts to 11.6 kcal/mol being lower than the upper limit value determined from the experiment. For more realistic models (i.e. imidazole and CH<sub>3</sub>COO<sup>-</sup>), the activation enthalpy is slightly higher (13.7 kcal/mol), but still *lower* than the upper limit value determined experimentally (ca. 15 kcal/mol). Further, this activation enthalpy is *lower* than the barrier associated with hydrogen abstraction from the 5'-deoxyadenosine by the product radical;

this process was shown to be the rate determining step in the overall reaction sequence. In addition, the synergistic interaction of His and Asp/Glu is operative only in the pH regime of 6 - 9.5; this pH range is common in many biologically active systems.<sup>159</sup>

Finally, these computational data do not only provide reliable activation enthalpies, more importantly, they produce quite a realistic picture of possible interactions in the enzyme's active site. These findings may prove helpful in the on-going experimental attempts to structurally characterize ethanolamine ammonia lyase.



## 7. Hydrogen Abstraction from 2-Aminoethanol by a Model System for the 5'-Deoxyadenosyl Radical\*

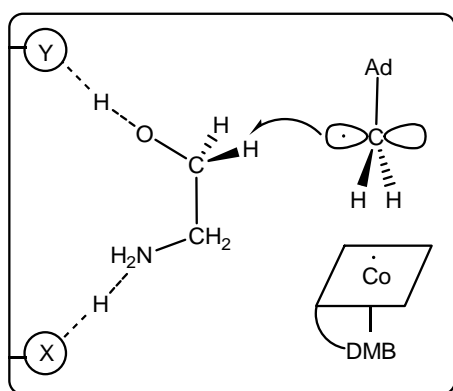
Important questions that remained unresolved for ethanolamine ammonia lyase, as well as other coenzyme B<sub>12</sub>-dependent enzymes, concern details by which these enzymes bring about the homolytic C-H bond activation and how they catalyze the cleavage of the Co-C bond; for the latter, bond homolysis is accelerated up to a factor of 10<sup>12</sup> in the presence of an enzyme. Quite a few different mechanisms have been proposed that could account for this enormous rate acceleration, i.e. enzyme induced distortion of the corrin ring to sterically labilize the Co-C bond,<sup>160</sup> enzymatic compression of the axial Co-N bond causing a weakening of the *trans*-located Co-C bond,<sup>160c,161</sup> corrin ring distortion by twisting the axial Co-N bond to rotate the 5,6-dimethylbenzimidazole,<sup>162</sup> direct bending of the Co-C bond by interaction of the adenosyl ligand with the protein,<sup>160b,d,163</sup> or, as indicated by early studies, that the substrate itself might induce weakening of the Co-C bond because in the absence of the substrate, Cob(II)alamin was not formed in significant quantity.<sup>164</sup> Direct evidence that a substrate promotes the Co-C bond homolysis has been provided for methylmalonyl-CoA mutase where it was shown that the rate of Co-C bond catalysis is sensitive on isotopic substitution in the substrate.<sup>165</sup>

In order to computationally investigate the effects that could promote the Co-C bond homolysis the whole coenzyme should be taken into account; because of the computationally extremely demanding coenzyme B<sub>12</sub> and limited computer resources that were available, this topic, unfortunately, could not be addressed. However, another intriguing aspect that is easier to tackle computationally concerns the mechanistic details by which the 5'-deoxyadenosyl radical abstracts a hydrogen atom from the substrate. In the case of ethanolamine ammonia lyase, both steady state hydrogen isotope exchange studies and EPR spectroscopy of trapped radical intermediates suggested the involvement of two different species, i.e. the 5'-deoxyadenosyl radical itself and a protein radical formed in the reaction with the former.<sup>166,167</sup> Evidence for the direct interaction of the 5'-deoxyadenosyl radical with substrate was provided by isotope exchange experiments, where the incorporation of tritium from 1-[<sup>3</sup>H]-aminoethanol into the coenzyme was demonstrated as well as the release of tritium from 5'-[<sup>3</sup>H]-adenosylcobalamin to the product radical.<sup>168</sup>

---

\* Results discussed in this chapter are in press: Semialjac, M.; Schwarz, H. *Chem. Eur. J.*

Recently, several different experiments, in particular the exchange of deuterium between the 5'-deoxyadenosyl radical and the enzyme's deactivator, electron nuclear double resonance studies and electron spin-echo envelope modulation spectroscopy provided additional support for this mechanism. However, the isotope effect observed for the incorporation of tritium from 5'-[ $^3\text{H}$ ]-deoxyadenosylcobalamin into ethanal was contradictory to the conclusion that the three hydrogen atoms at the C5'-position in 5'-deoxyadenosine (the one abstracted from the substrate and the two from the intact coenzyme) were equivalent with respect to the probability of incorporation into the product ethanal. Similar observations were made for the related diol-dehydrase.<sup>169</sup> The anomalous tritium isotope effects observed for both enzymes have been rationalized by a model that rests on the assumption the possibility that two radical species, the 5'-deoxyadenosyl radical itself and a protein radical, interact with the substrate.<sup>170</sup> In this "two-radicals" model the major part of hydrogen exchange proceeds through a protein radical, while only in ca. 11% of cases the 5'-deoxyadenosyl radical abstracts directly a hydrogen atom from the substrate. Even though the substrate and the product radicals for the ethanolamine ammonia lyase catalyzed reaction have been detected by EPR spectroscopy, a possible candidate for a protein radical has not yet been identified, in contrast to the related  $\text{B}_{12}$  dependent ribonucleotide triphosphate reductase for which the protein radical has been characterized as a cysteine thiyl radical.<sup>171</sup> However, for the base-off  $\text{B}_{12}$  dependent enzymes (class I) methylmalonyl-CoA mutase and glutamate mutase, the 5'-deoxyadenosyl radical appears to react directly with the substrate.



**Scheme 7-1.** Abstraction of a hydrogen atom by the 5'-deoxyadenosyl radical from substrate interacting with two amino acids X and Y in the active site of ethanolamine ammonia lyase.

In the present chapter the focus will be on the "non-protein radical hypothesis", i.e. assuming that the initially formed C-centered 5'-deoxyadenosyl radical acts as a hydrogen atom abstractor from substrate **1** (Scheme 7-1). In addition, the following question will be addressed: whether the substrate is "free" in the active site prior to the hydrogen abstraction or its position is fixed and the C-H bond homolysis

facilitated by interaction with some amino acids from the enzyme's active site, a scenario which seems more appropriate for an enzymatic catalysis (residue X and Y, as depicted in Scheme 7-1). The insight derived from this computational model study could be useful in a further clarification of those factors which affect the hydrogen abstraction reactions in coenzyme B<sub>12</sub> dependent enzymes.

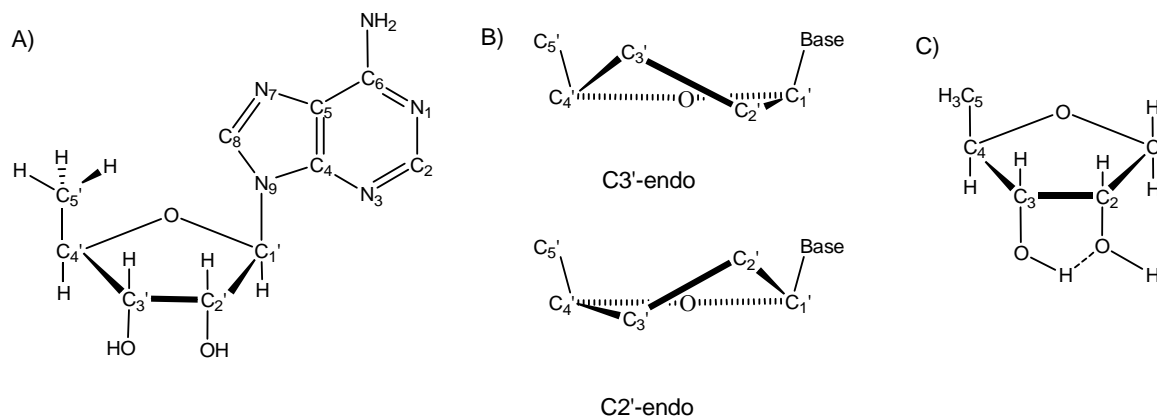
## 7.1. Computational Methods

All calculations were performed with the GAUSSIAN 98 suite of programs using both density functional theory (DFT) and an ab initio approach. The use of the DFT formalism was a natural choice because of the balance between accuracy and computational time required by the calculations, and the B3LYP functional was employed.<sup>27,28</sup> Geometry optimizations were performed with Pople's polarized double- $\zeta$  6-31G\* basis set. In order to characterize the optimized structures, frequency analysis has been performed at the same level of theory. Minima were characterized by the absence of imaginary vibrational frequencies, while transition structures exhibited one imaginary frequency. A uniform scaling factor of 0.9806 was used for the zero-point energy (ZPE) corrections calculated at the B3LYP level of theory. Computations of reaction pathways, i.e. intrinsic reaction coordinate (IRC) calculations were carried out at the same level of theory.

In order to obtain more reliable energetic profiles of the reactions in question, single point calculations using triple- $\zeta$  basis sets with diffuse functions (6-311++G\*\*) were performed employing ab initio theory (MP2). The relative energies of the stationary points were calculated at the MP2/6-311++G\*\*//B3LYP/6-31G\* level of theory, where the ZPEs calculated with B3LYP/6-31G\* were used in the conversion to relative energies at 0 K. Due to the size of the system under investigation, it had to be refrained from performing single point calculations at some more accurate level of theory, as in the studies discussed in previous chapters on related problems (i.e. QCISD).<sup>133,172</sup> However, as reported by Morokuma and co-workers,<sup>173</sup> even for the hydrogen bonding energies in the 5'-deoxyadenosyl radical the B3LYP and MP2 results are of sufficient accuracy and therefore these methods are helpful in answering the questions addressed in the present chapter.

Relative energies (given in kcal/mol) discussed in the text correspond to the enthalpies at 298 K obtained at the MP2 level of theory (single-point calculations),<sup>174</sup> unless specified otherwise.

## 7.2. Hydrogen Abstraction Scenarios from Aminoethanol by 1,5-Dideoxyribose-5-yl Radical



**Scheme 7-2.** A) 5'-deoxyadenosyl moiety, B) different ribose conformations, C) 1,5-dideoxyribose employed as a model system for the 5'-deoxyadenosyl moiety.

As already mentioned, while the amino-acid sequence of the ethanolamine ammonia lyase has been determined, the X-ray structure of the enzyme is not yet known. However, as the active sites of several coenzyme B<sub>12</sub> dependent enzymes were shown to exhibit high similarities, pertinent results obtained from the X-ray structure of B<sub>12</sub>-dependent glutamate mutase<sup>175</sup> will be used. In the active site of this enzyme two different conformers of the 5'-deoxyadenosyl moiety have been observed and the major conformational difference concerns the backbone of the ribose part. While a C2'-endo conformation is adapted by the 5'-deoxyadenosyl radical formed shortly after homolysis of the Co-C bond, a C3'-endo conformer is favored by the 5'-deoxyadenosine precursor.

Theory has characterized no less than 34 conformers of the 5'-deoxyadenosyl radical. As to the global minimum, the solid state structure<sup>176</sup> of the 5'-deoxyadenosyl moiety does not correspond to the one obtained by the computational studies. In the latter the global minimum of the free radical contains a hydrogen bond between the C2' hydroxyl group and the N3-atom from adenine. Even though the X-ray structure of the enzyme does not reveal this particular hydrogen bonding there are two water molecules situated suitably to form H-bonds with the N3-atom from adenine and the OH-group at the C2' center of ribose via a network of water molecules. Concerning the relative orientation

of the ribose and adenine moieties, the X-ray structure points to an arrangement that is disfavored by the computational work. It has been concluded that this particular orientation of the ribose and adenine ring in the solid state is a result of several stabilizing interactions between the 5'-deoxyadenosyl moiety, additional water molecules and the corrin ring. Moreover, the computationally preferred C2'-endo conformation of the ribose ring in the "liberated" 5'-deoxyadenosyl radical is triggered exactly by the H-bond interaction between the C2' hydroxyl-group and the N3-atom from adenine. In view of these conflicting results, the focus will be on calculating the energetics of the hydrogen abstraction step by employing a more simplified model system for the 5'-deoxyadenosyl radical. Clearly, QM/MM studies would represent an attractive alternative for obtaining more accurate computational results. However, as long as the X-ray structure of ethanolamine ammonia lyase remains unknown, one has to refrain from such an approach.

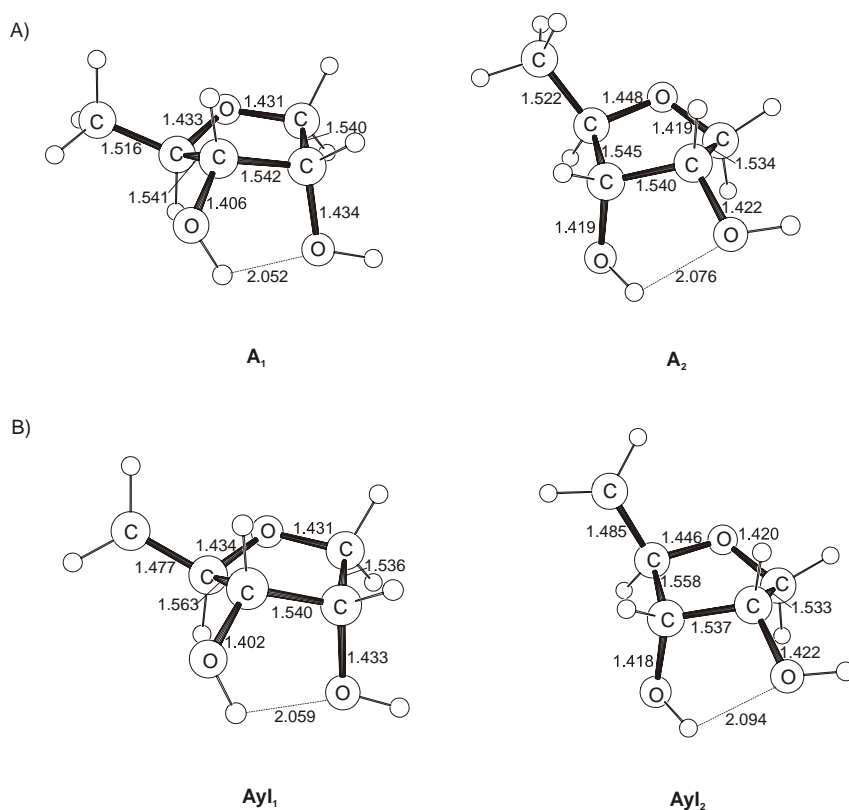


**Figure 7-1.** Optimized geometries (B3LYP/6-31G\*) of A) 1,5-dideoxyribose (C3'- and C2'-endo conformers), B) 1,5-dideoxyribose-5-yl radical (C3'- and C2'-endo conformers; bond lengths in Å).

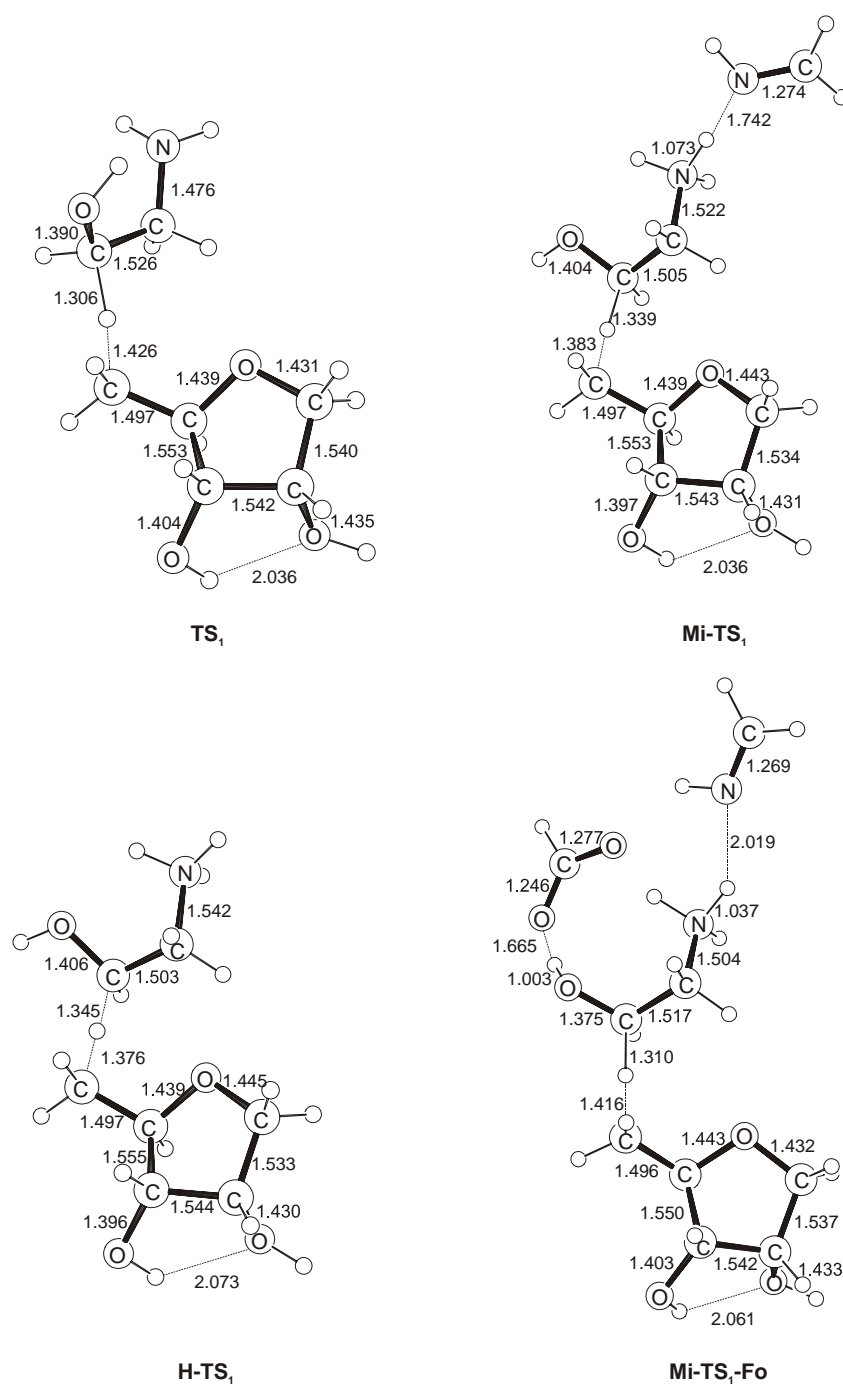


**Figure 7-2.** Optimized geometries (B3LYP/6-31G\*) of transition structures for hydrogen abstraction reaction by C3-endo conformers of 1,5-dideoxyribose-5-yl radical (bond lengths in Å).

The model chosen, i.e. 1,5-dideoxyribose<sup>177</sup> (see Scheme 7-2C), is reduced to the ribose part of 5'-deoxyadenine; the adenine fragment has not been included on the ground that its presence is not likely to affect energetically the hydrogen abstraction from substrate

**1** by the C5'-centered radical. For the 1,5-dideoxyribose a conformation that contains one intramolecular H-bond (Scheme 7-2C) was taken into account, and in the computations two different conformations of the "ribose" ring (C3-endo and C2-endo) were considered; structural details can be found in Figure 7-1.

Further, in view of the findings<sup>135,172</sup> that the energetics of the rearrangement **2** → **4** (Scheme 5-1, Chapter 5) is crucially dependent on the simultaneous operation of partially protonating and deprotonating auxiliaries X and Y, it is investigated as well whether the barrier of the hydrogen abstraction from substrate aminoethanol (**1**) is also affected by the presence or absence of amino acid residues. To this end four different scenarios have been studied: i.e. the hydrogen abstraction from the "free" substrate **1** (Scheme 7-1, without X and Y), from a fully protonated substrate (Scheme 7-1, X = H<sup>+</sup> and without Y), from a substrate interacting with a His equivalent (Scheme 7-1, X = His and without Y), and finally from a substrate interacting simultaneously with His and Asp models (Scheme 7-1, X = His and Y = Asp).

According to the computations, the C3-endo conformer of 1,5-dideoxyribose is slightly more stable (by 0.9 kcal/mol) than the C2-endo counterpart, and this difference gets even smaller (0.6 kcal/mol) for the corresponding radicals. Concerning the labeling of the stationary points, all structures having a C3-endo conformation are labeled with the subscript 1 (e.g. for 1,5-dideoxyribose **A<sub>1</sub>** and its radical **Ayl<sub>1</sub>**) in contrast to the C2-endo conformers, which carry a subscript 2 (e.g. for 1,5-dideoxyribose **A<sub>2</sub>** and its radical **Ayl<sub>2</sub>**).

### 7.2.1. Non-protonated Substrate

When a hydrogen atom is abstracted from the non-protonated substrate **1** by the two conformers **Ayl<sub>1</sub>** and **Ayl<sub>2</sub>**, the corresponding transition structures **TS<sub>1</sub>** and **TS<sub>2</sub>**, respectively, are energetically almost equivalent (17.3 and 16.7 kcal/mol). Commencing from the corresponding TSs, intrinsic reaction coordinate (IRC) computations in the direction of reactants converged into complexes between the C5'-radical and **1** (**1\*Ayl<sub>1</sub>** and **1\*Ayl<sub>2</sub>**), which are slightly less stable than the reactants, i.e. 0.9 kcal/mol for **1\*Ayl<sub>1</sub>** and 1.8 kcal/mol for **1\*Ayl<sub>2</sub>** (Table 7-1).<sup>178,179</sup> Irrespective of the conformation of the C5'-radical, the energy demands to overcome the hydrogen abstraction barrier exceed the activation enthalpy (15 kcal/mol) of the rate determining step in the whole catalytic sequence. Therefore, hydrogen abstraction from a non-protonated substrate is quite

unlikely to occur. Moreover, the  $pK_a$  value for the conjugated acid of **1** equals to 9.45 and consequently, it is reasonable to assume that **1** is (partially) protonated by some of the amino acids present in the enzyme's active site. Therefore, hydrogen abstraction from both fully and partially protonated substrates **1** will be considered next.

**Table 7-1.** Relative enthalpies (in kcal/mol) at 0 K ( $H_{rel, 0 K}$ ), and 298 K ( $H_{rel, 298 K}$ ) of the stationary points relevant for the hydrogen abstraction reaction from substrate **1**.

|                                    | B3LYP/6-31G*   |                  | MP2/6-311++G**//<br>B3LYP/6-31G* |                  |
|------------------------------------|----------------|------------------|----------------------------------|------------------|
|                                    | $H_{rel, 0 K}$ | $H_{rel, 298 K}$ | $H_{rel, 0 K}$                   | $H_{rel, 298 K}$ |
| <b>1</b> + <b>Ayl</b> <sub>1</sub> | 0.0            | 0.0              | 0.0                              | 0.0              |
| <b>1</b> * <b>Ayl</b> <sub>1</sub> | -2.8           | 1.5              | -4.4                             | 0.9              |
| <b>TS</b> <sub>1</sub>             | 10.1           | 13.6             | 15.1                             | 17.3             |
| <b>2</b> * <b>A</b> <sub>1</sub>   | -10.7          | -6.2             | -10.0                            | -4.5             |
| <b>2</b> + <b>A</b> <sub>1</sub>   | -10.2          | -6.8             | -9.1                             | -4.7             |
| <b>1</b> + <b>Ayl</b> <sub>2</sub> | 0.9            | 1.0              | 0.6                              | 0.6              |
| <b>1</b> * <b>Ayl</b> <sub>2</sub> | -1.6           | 2.6              | -3.4                             | 1.8              |
| <b>TS</b> <sub>2</sub>             | 9.7            | 13.0             | 14.4                             | 16.7             |
| <b>2</b> * <b>A</b> <sub>2</sub>   | -10.1          | -5.8             | -9.3                             | -3.6             |
| <b>2</b> + <b>A</b> <sub>2</sub>   | -10.1          | -5.8             | -8.3                             | -3.8             |

### 7.2.2. Fully Protonated Substrate

For both conformers of the 1,5-dideoxyribose-5-yl radical, transition structures for the hydrogen abstraction from the fully protonated substrate (**H-1**) were located. When compared to the separate reactants, both TSs lie very low in energy (see Table 7-2) with **H-TS**<sub>1</sub> only 2.2 kcal/mol and **H-TS**<sub>2</sub> 3.7 kcal/mol above the reactant pair **H-1**/**Ayl**<sub>1</sub>. However, from the corresponding TSs in the direction of reactants, the IRC computations converged in complexes of **H-1** with **Ayl**<sub>1</sub> or **Ayl**<sub>2</sub>. Assuming that these complexes are present in the active site, the actual activation barriers for the hydrogen abstraction amount to 13.1 kcal/mol when the **Ayl**<sub>1</sub> radical is involved and 13.8 kcal/mol for the **Ayl**<sub>2</sub> counterpart.



When compared to the hydrogen abstraction from the non-protonated substrate **1**, the decreased activation enthalpy is quite likely a result of the stabilization of the emerging radical, where in the TSs the radical center is better delocalized through the C-C bond by the presence of the electron withdrawing NH<sub>3</sub>-group. This is already indicated in some of the structural features of **TS<sub>1</sub>** versus **H-TS<sub>1</sub>** (Fig. 7-2). In the latter, the relevant C-C bond is shorter (1.503 Å) when compared to **TS<sub>1</sub>** (1.526 Å), while the C-N bond is elongated, i.e. 1.542 Å vs. 1.476 Å. For **H-TS<sub>1</sub>** the IRC computations in the direction of a product converged into a complex **6\*A<sub>1</sub>** between the protonated product radical (**6**) and **A<sub>1</sub>**.<sup>180</sup> This complex is much more stable (21.7 kcal/mol) than the separate species **6** and **A<sub>1</sub>** and extensive charge delocalization can be hold responsible for this effect.

Even though hydrogen atom abstraction from a fully protonated substrate is feasible from an energetic point of view it is quite unrealistic to expect that **1** will exist as a “free”, fully protonated species **6** in the active site. More likely is a scenario in which the substrate is captured in the enzyme’s active site and its position fixed by interaction with some amino acids that may result in *partial* protonation of the NH<sub>2</sub> group and, depending on structural details, partial deprotonation of the OH group as well. The implications of these features for the energetics of the C-H bond homolysis will be considered next.

**Table 7-2.** Relative enthalpies (in kcal/mol) at 0 K ( $H_{rel, 0 K}$ ), and 298 K ( $H_{rel, 298 K}$ ) of the stationary points relevant for the hydrogen abstraction reaction from the fully protonated substrate **H-1**.

|                              | B3LYP/6-31G*   |                  | MP2/6-311++G**//<br>B3LYP/6-31G* |                  |
|------------------------------|----------------|------------------|----------------------------------|------------------|
|                              | $H_{rel, 0 K}$ | $H_{rel, 298 K}$ | $H_{rel, 0 K}$                   | $H_{rel, 298 K}$ |
| <b>H-1 + Ayl<sub>1</sub></b> | 0.0            | 0.0              | 0.0                              | 0.0              |
| <b>H-1*Ayl<sub>1</sub></b>   | -10.2          | -10.2            | -11.8                            | -10.9            |
| <b>H-TS<sub>1</sub></b>      | -0.6           | -0.9             | 3.9                              | 2.2              |
| <b>6*A<sub>1</sub></b>       | -30.0          | -29.5            | -28.8                            | -27.4            |
| <b>6 + A<sub>1</sub></b>     | -9.6           | -9.4             | -5.9                             | -5.7             |
| <b>H-1 + Ayl<sub>2</sub></b> | 0.9            | 1.0              | 0.6                              | 0.6              |
| <b>H-1*Ayl<sub>2</sub></b>   | -9.0           | -9.1             | -11.0                            | -10.1            |
| <b>H-TS<sub>2</sub></b>      | 0.9            | 0.5              | 5.3                              | 3.7              |
| <b>6 + A<sub>2</sub></b>     | -8.4           | -8.3             | -5.1                             | -4.8             |

### 7.3. Partially Protonated Substrate

As already mentioned, the concept of partial protonation of a migrating group was shown to play an important role for several coenzyme B<sub>12</sub> dependent enzymes because it lowers the barriers for the substrate rearrangement. As a model for an amino acid that might partially protonate **1** a quite simple imine (methanimine, CH<sub>2</sub>=NH) was used to mimic His, as one of the natural choices to interact with the substrate. As shown in the previous chapter, the energetics of the reaction **2** → **4** for partially protonated **2** were almost identical for different His models employed, and to save computational time the structurally most simple system CH<sub>2</sub>NH was used here.

**Table 7-3.** Relative enthalpies (in kcal/mol) at 0 K ( $H_{rel, 0 K}$ ), and 298 K ( $H_{rel, 298 K}$ ) of the stationary points relevant for the hydrogen abstraction reaction from substrate **Mi-1** interacting with a His model system.

|                                       | B3LYP/6-31G*   |                  | MP2/6-311++G**//<br>B3LYP/6-31G* |                  |
|---------------------------------------|----------------|------------------|----------------------------------|------------------|
|                                       | $H_{rel, 0 K}$ | $H_{rel, 298 K}$ | $H_{rel, 0 K}$                   | $H_{rel, 298 K}$ |
| <b>Mi-1</b> + <b>Ayl</b> <sub>1</sub> | 0.0            | 0.0              | 0.0                              | 0.0              |
| <b>Mi-1</b> * <b>Ayl</b> <sub>1</sub> | -8.8           | -8.1             | -10.8                            | -9.1             |
| <b>Mi-TS</b> <sub>1</sub>             | 2.0            | 1.9              | 6.0                              | 4.5              |
| <b>Mi-6</b> * <b>A</b> <sub>1</sub>   | -8.6           | -15.8            | -16.5                            | -14.7            |
| <b>Mi-6</b> + <b>A</b> <sub>1</sub>   | -9.0           | -8.7             | -6.0                             | -5.7             |
| <b>Mi-1</b> + <b>Ayl</b> <sub>2</sub> | 0.9            | 1.0              | 0.6                              | 0.6              |
| <b>Mi-1</b> * <b>Ayl</b> <sub>2</sub> | -8.1           | -8.1             | -10.0                            | -9.0             |
| <b>Mi-TS</b> <sub>2</sub>             | 3.2            | 3.0              | 7.2                              | 5.8              |
| <b>Mi-6</b> + <b>A</b> <sub>2</sub>   | -7.8           | -7.6             | -5.1                             | -4.8             |

If the **Ayl**<sub>1</sub> radical abstracts the hydrogen atom from **Mi-1**, the corresponding TS (**Mi-TS**<sub>1</sub>) lies 4.5 kcal/mol above the separate reactants, i.e. **Ayl**<sub>1</sub> radical (C3-endo conformer) and **Mi-1**. **Mi-TS**<sub>2</sub> is slightly less stable lying 5.8 kcal/mol above reactants. This small difference in the stability of the two TSs **Mi-TS**<sub>1</sub> and **Mi-TS**<sub>2</sub> reflects the energetic difference that already exists for the 1,5-dideoxyribose, where the C3-endo form was found to be 0.9 kcal/mol more stable. Taking into account the existence of complexes **Mi-1**\***Ayl**<sub>1</sub> and **Mi-1**\***Ayl**<sub>2</sub>, that were obtained in the IRC computations from the

corresponding TSs in the direction of the reactants, the activation enthalpy for the hydrogen abstraction from **Mi-1** by **Ayl<sub>1</sub>** amounts to 13.6 kcal/mol and for **Ayl<sub>2</sub>** to 14.8 kcal/mol; this is only slightly higher than for the analogous reaction in which the substrate is fully protonated (13.1 kcal/mol), but still below the limiting value of 15 kcal/mol. The IRC calculations from **Mi-TS<sub>1</sub>** in the direction of a product led to a complex between **Mi-6** and **A<sub>1</sub>**,<sup>181</sup> the formation of this complex is highly exothermic (-14.7 kcal/mol) and the complex itself is 9.0 kcal/mol more stable than the separate constituents **Mi-6** and **A<sub>1</sub>**.

As to the role of substrate protonation on the activation enthalpy for the C-H bond homolysis of **1**, the computational findings clearly point to the operation of a catalytic effect. However, in view of previous findings,<sup>135,172</sup> that the synergistic operation of a simultaneous partial protonation of the NH<sub>2</sub> and a partial deprotonation of the OH group of **1** brings about a dramatic acceleration of the intramolecular rearrangement **2** → **4**, it is interesting to explore if this effect also holds true for the C-H bond activation step **1** → **2** as well.

#### 7.4. Substrate Captured by Two Amino Acids from the Active Site

In addition to His partially protonating the NH<sub>2</sub> group of **1**, Asp (in its carboxylate form) is assumed to partially deprotonate the OH group of the substrate; this kind of synergistic interaction of the two amino acids can take place in a physiologically realistic pH regime of 6 – 9.5 (discussed in details in Chapter 6). As a model system for Asp formate was employed, which was shown to serve well for the computational investigation of the rearrangement reactions. The TS involving the C3-endo conformation of the 1,5-dideoxyribose-5-yl moiety (**Mi-TS<sub>1</sub>-Fo**; 12.4 kcal/mol) is energetically 0.8 kcal/mol less demanding than the one involving the C2-endo conformer (**Mi-TS<sub>2</sub>-Fo**; 13.2 kcal/mol). While IRC computations from the TSs in the direction of reactants did not converge to the expected complexes between the reactant species, by means of exhaustive geometry optimization two relevant complexes between the reactants have been located. The complex **Mi-1-Fo\*Ayl<sub>1</sub>** lies 13.2 kcal/mol below the separate reactants, while **Mi-1-Fo\*Ayl<sub>2</sub>** is 7.7 kcal/mol more stable than the noninteracting reactants. Assuming that such complexes can be formed in the active site, the activation enthalpy for the hydrogen abstraction would amount to 25.6 kcal/mol, thus clearly exceeding the upper limit of 15 kcal/mol. Such a high activation enthalpy presumably is the result of an unfavorable

delocalization of the emerging radical center at C(1) in the presence of the partially developing negative charge on the adjacent oxygen from the OH group. A comparison of the relevant C-O and C-C bond lengths of the substrates (**Mi-1** and **Mi-1-Fo**) in the transition structures **Mi-TS<sub>1</sub>** and **Mi-TS<sub>1</sub>-Fo** (Fig. 7-2) lends qualitative support to this suggestion. Consequently, for the C-H bond activation step, the synergistic interaction of **1** does not lower the barrier; rather, the effect of only one partially protonating amino acid suffices.

IRC computations in the direction of the products result in quite stable complexes between the radical **Mi-6-Fo** and 1,5-dideoxyribose (**A<sub>1</sub>** and **A<sub>2</sub>**); assuming the existence of such complexes, hydrogen abstraction from **1** becomes highly exothermic, especially in the case of **Mi-6-Fo**\***A<sub>1</sub>** which is 21.5 kcal/mol more stable than the separate products **Mi-6-Fo** and **A<sub>1</sub>** (Table 7-4). If this product complex is really formed in the active site, the **A<sub>1</sub>** moiety being kept close to the radical **2** in the course of the subsequent amino-group migration **2** → **4** could immediately deliver a hydrogen atom back to **4** thus regenerating the 5'-deoxyadenosyl radical and closing the catalytic cycle.

**Table 7-4.** Relative enthalpies (in kcal/mol) at 0 K ( $H_{rel, 0 K}$ ), and 298 K ( $H_{rel, 298 K}$ ) of the stationary points relevant for the hydrogen abstraction reaction from substrate **Mi-1-Fo** interacting synergistically with the His and Asp model systems.

|   | B3LYP/6-31G*   |                  | MP2/6-311++G**//<br>B3LYP/6-31G* |                  |
|---|----------------|------------------|----------------------------------|------------------|
|   | $H_{rel, 0 K}$ | $H_{rel, 298 K}$ | $H_{rel, 0 K}$                   | $H_{rel, 298 K}$ |
| <b>Mi-1-Fo</b> + <b>Ayl<sub>1</sub></b> | 0.0            | 0.0              | 0.0                              | 0.0              |
| <b>Mi-1-Fo</b> * <b>Ayl<sub>1</sub></b> | -12.7          | -12.8            | -16.1                            | -13.2            |
| <b>Mi-TS<sub>1</sub>-Fo</b>             | 9.1            | 8.6              | 14.0                             | 12.4             |
| <b>Mi-6-Fo</b> * <b>A<sub>1</sub></b>   | -23.7          | -24.2            | -25.3                            | -22.1            |
| <b>Mi-6-Fo</b> + <b>A<sub>1</sub></b>   | -11.4          | -10.8            | -0.3                             | -0.6             |
| <b>Mi-1-Fo</b> + <b>Ayl<sub>2</sub></b> | 0.9            | 1.0              | 0.6                              | 0.6              |
| <b>Mi-1-Fo</b> * <b>Ayl<sub>2</sub></b> | -6.3           | -6.2             | -10.0                            | -7.7             |
| <b>Mi-TS<sub>2</sub>-Fo</b>             | 9.6            | 9.0              | 14.7                             | 13.2             |
| <b>Mi-6-Fo</b> * <b>A<sub>2</sub></b>   | -14.3          | -14.4            | -15.6                            | -13.0            |
| <b>Mi-6-Fo</b> + <b>A<sub>2</sub></b>   | -10.3          | -9.6             | 0.5                              | 0.3              |

### 7.3. Conclusions

According to the computations, the TSs in which the C3-endo conformer of 1,5-dideoxyadenosyl radical is involved are only slightly energetically less demanding than those which involve the C2-counterpart, and the energy differences in the transition structures reflect to a large extent those that already exist for the free conformers **Ayl**<sub>1</sub> and **Ayl**<sub>2</sub>. Further, since the transition structures for both 1,5-dideoxyribose-5-yl conformers in all cases investigated are energetically and structurally quite similar it is difficult (if not impossible) to decide definitively which of the C5-radical conformers actually attacks the substrate.

As to the energetics, homolysis of the C-H bond from the non-protonated substrate requires for both conformers of the model radical activation enthalpies > 16.7 kcal/mol. In contrast, all computed activation enthalpies for the hydrogen abstraction from a partially or fully protonated substrate **1** are energetically less demanding than the value associated with the rate determining step that has been experimentally derived (15 kcal/mol), i.e. the hydrogen abstraction from 5'-deoxyadenosine by the product radical. As it is realistic to assume that the quite basic 2-aminoethanol substrate is at least partially protonated in the active site, we conclude that from an energetic point of view the initially formed 5'-deoxyadenosyl radical can abstract a hydrogen atom directly from an appropriately "activated" substrate. Consequently, it does not seem necessary to invoke the role of a protein radical ("two-radicals hypothesis").

Interestingly, in case of a synergistic interaction, when substrate **1** is captured by two amino acids (e.g. His and Asp), the activation enthalpy for the hydrogen abstraction exceeds 25 kcal/mol. Therefore, it is likely that in the homolysis, in distinct contrast to the rearrangement step **2** → **4**, a synergistic interaction of **1** with two activating auxiliaries is not essential; rather partial protonation suffices.



## 8. Conclusions and Outlook

In this thesis computational methods were used in order to investigate rearrangement reactions that occur in same systems of biological relevance. The insight gained by theory was shown to be useful in answering some of the crucial questions, where the experimental methods could not provide a complete mechanistic picture of the processes under investigation. Rather, it is the synergy between theory and experiment makes it possible to elucidate complex (bio)chemical processes at the molecular level.

In the first part of this thesis the rearrangement reactions of ionized *valeramide* are computationally investigated in order to bring insight into the mechanistic pathways derived from mass-spectrometric experiments; in these experiments it was observed that the major dissociation processes correspond to competing losses of neutral propene, formed via the McLafferty rearrangement, and an ethyl radical to presumably afford protonated acrylamide; formations of a methyl radical as well as ethene occur as side reactions. According to the theoretical investigations (Chapter 3), the valeramide radical cation bears several low-lying routes for unimolecular rearrangements. The energetically preferred route involves initial  $\gamma$ -C-H bond activation according to the well-known McLafferty rearrangement. Other low-lying channels proceed via  $\beta$ -C-H and  $\delta$ -C-H bond activations, respectively, leading to specific fragmentation reactions as observed in the experiments. The theoretical results are in agreement with the experimental data as far as the relative energetic ordering of the fragmentation channels, isotope effects, and the occurrence of H/D equilibration are concerned. However, the non-dynamical calculations cannot provide a straightforward mechanistic rational for the pronounced temperature effect on the  $C_3/C_2$  branching ratios observed in the metastable ion spectra of ionized valeramide; at elevated temperatures the energetically more demanding  $C_2$ -route becomes actually as populated as the less complicated and energetically less demanding McLafferty channel ( $C_3$ -route). In order to explain this puzzling result, Car-Parrinello molecular dynamics studies of neutral and ionized valeramide were performed (Chapter 4). These dynamical computations provided two rationals for the unusually low  $C_3/C_2$  branching ratio observed in the experiments conducted at elevated temperatures: (i) The relatively low free activation energy of the McLafferty rearrangement causes the dissociation of a substantial fraction of the parent ion or its distonic counterpart at elevated temperatures.

Therefore, the McLafferty rearrangement occurs *prior* to the time-delayed mass selection and consequently, the  $C_3/C_2$  ratio observed at elevated temperatures is formally reduced. (ii) Since the barriers associated with conformational changes were shown to be energetically more demanding than the corresponding hydrogen transfers themselves, which initiate further rearrangement reactions, the parent ion is trapped by conformational barriers and is therefore, long-lived at lower temperatures. This indicates that in the experiments performed at room temperature a greater population of parent ion is mass-selected, which then enters easier the McLafferty rearrangement ( $C_3$ -route), thereby increasing (relative to higher temperatures) the  $C_3/C_2$  ratio.

The detailed insight in the mechanism of the valeramide radical-cation rearrangement holds the promise of helping to understand the rearrangement pathways of biologically important compounds containing an amide functional group upon free radical attacks. As a further research direction the combined experimental and theoretical investigations of amides with even bigger side chains or with unsaturated alkyl parts are warranted. The latter studies would be particularly interesting because a large number of the biologically active amides contain a double bond in their alkyl chain. Since many severe and yet incurable diseases are likely to be triggered by the action of free radicals, the information obtained in such studies could aid in fighting the causes of the human-cell damage induced by these diseases.

The subject of the second part of this Thesis concerns the catalytic activity of *ethanolamine ammonia lyase*, the coenzyme  $B_{12}$  dependent enzyme. First, the rearrangement of 2-aminoethanol into ethanal and ammonia is investigated (Chapter 5), where several possible mechanisms involving free radical intermediates as well as their protonated forms are considered. Two major types of rearrangements are discussed in detail, namely intramolecular migration and dissociation of the amine/ammonia groups, for both of which several scenarios are considered. The complete dissociation of the migrating group and its subsequent association constitute an unlikely route for both the protonated and the unprotonated reactant due to the high-energy barriers involved in these steps. Direct migration of the protonated amine group is far more favorable, and therefore presents the most likely candidate for the actual enzymatic reaction. The calculations further imply that the direct loss of an ammonium cation also represents a feasible pathway. Comparing the rearrangements for the aminoethanol radical and its protonated counterpart, migration of a protonated group is in general associated with lower energy



barriers, suggesting that the actual enzyme substrate quite likely corresponds to (partially) protonated aminoethanol. As the extent of the substrate protonation/deprotonation by the active site of the enzyme may vary, the actual energy barriers are expected to range between the values calculated for the two extreme cases of a substrate, i. e. the aminoethanol radical, and its fully protonated form. Further, in order to distinguish between the two most likely mechanisms, i.e. the direct intramolecular migration of the partially protonated  $\text{NH}_2$  group vs. elimination of  $\text{NH}_4^+$ , the influence of the enzyme's active site has been taken into account (Chapter 6). Three scenarios were explored, in which some of the conceivable amino acids (e.g. Asp/Glu or His) from the active site may act as catalytic auxiliaries and interact with the substrate: (i) Irrespective of the nature of the *protonating* species intramolecular migration of the  $\text{NH}_3$  group is energetically less demanding than elimination of  $\text{NH}_4^+$ . However, all computed activation enthalpies exceed the experimentally derived activation enthalpy associated with the rate determining step, i.e. the hydrogen abstraction from the 5'-deoxyadenosine by the product radical. (ii) For a *partial deprotonation* of the substrate at the OH group, the rearrangement mechanism consists of the dissociation of an  $\text{NH}_2$  radical from C(2) and its association at C(1) atom. For all investigated proton acceptors, the activation enthalpy for the dissociation step also exceeds experimentally determined limit. (iii) Only in a *synergistic action* of partial protonation of the  $\text{NH}_2$  group and partial deprotonation of the OH group by the two conceivable catalytic auxiliaries Asp/Glu and His, the activation enthalpy computed is compatible with the experimental data. Therefore this kind of "push-pull" mechanism presents most like a way of 2-aminoethanol rearrangement in the active site of the enzyme. This synergistic action is expected to take place in a physiologically realistic pH range of 6 – 9.5. In contrast to the rearrangement reactions, the energetics of the initial hydrogen abstraction from 2-aminoethanol by the 5'-deoxyadenosyl radical are lowered only by an interaction of the substrate with a protonating auxiliary (Chapter 7); the synergistic interaction does not seem necessary.

These computational findings, besides bringing an insight in the rearrangement of aminoethanol, may as well help to further characterize the yet unknown structural details of the ethanolamine ammonia lyase's active site. As a further direction of experimental research the most appealing seems the elucidation of the enzyme's X-ray structure. With this information further theoretical insight could be gained from the QM/MM studies, which would make possible to model the whole active site and all relevant interactions between the substrate, the enzyme and the coenzyme  $\text{B}_{12}$ . Since all coenzyme  $\text{B}_{12}$

dependent enzymes are structurally and functionally similar, insight gained by a detailed study of ethanolamine ammonia lyase would definitively be useful in understanding the whole class of the B<sub>12</sub> dependent enzymes that catalyze extremely important rearrangement reactions in living systems.

## 9. Supporting Material

### Appendix I

**Table AI-1.** Electronic energies ( $E_{el}$ , in  $E_h$ ), zero-point energies ( $ZPE$ , in  $E_h$ ), and enthalpies ( $H$  at 298 K, in  $E_h$ ) of the stationary points on the aminoethanol radical PES.

|                                       | B3LYP/6-31G* |          |             | QCISD/cc-pVDZ |              |
|---------------------------------------|--------------|----------|-------------|---------------|--------------|
|                                       | $E_{el}$     | $ZPE$    | $H_{298K}$  | $E_{el}$      | $H_{298K}^a$ |
| <b>2<sub>1</sub></b>                  | -209.716125  | 0.084738 | -209.625158 | -209.159075   | -209.068109  |
| <b>2<sub>2</sub></b>                  | -209.723439  | 0.085503 | -209.632144 | -209.166357   | -209.075062  |
| <b>2<sub>3</sub></b>                  | -209.714085  | 0.084362 | -209.623459 | -209.157382   | -209.066757  |
| <b>4<sub>1</sub></b>                  | -209.708955  | 0.083412 | -209.619355 | -209.159075   | -209.069475  |
| <b>4<sub>2</sub></b>                  | -209.708382  | 0.082104 | -209.619381 | -209.154141   | -209.065140  |
| <b>4<sub>3</sub></b>                  | -209.714833  | 0.083203 | -209.625342 | -209.160143   | -209.070652  |
| <b>2<sub>1</sub>/3</b>                | -209.678946  | 0.080010 | -209.592344 | -209.116344   | -209.029742  |
| <b>3/4<sub>1</sub></b>                | -209.674367  | 0.079665 | -209.588212 | -209.113413   | -209.027258  |
| <b>5'/4<sub>3</sub></b>               | -209.620566  | 0.076322 | -209.538534 | -209.057488   | -208.975456  |
| <b>2<sub>3</sub>/4<sub>2</sub></b>    | -209.595700  | 0.079801 | -209.509721 | -209.028252   | -208.942273  |
| <b>2<sub>2</sub>/10</b>               | -209.686613  | 0.082093 | -209.599064 | -209.115554   | -209.028006  |
| <b>2<sub>1</sub>/12</b>               | -209.661970  | 0.074995 | -209.580200 | -209.095786   | -209.014015  |
| NH <sub>2</sub> <sup>•</sup>          | -55.872619   | 0.018974 | -55.849865  | -55.730422    | -55.707668   |
| NH <sub>2</sub> <sup>-</sup>          | -55.840835   | 0.017657 | -55.819398  | -55.680568    | -55.659131   |
| NH <sub>3</sub>                       | -56.547948   | 0.034531 | -56.509614  | -56.398982    | -56.360648   |
| <b>3</b>                              | -153.805680  | 0.056746 | -153.744385 | -153.394950   | -153.333655  |
| <b>5'</b>                             | -209.134693  | 0.074645 | -209.054871 | -208.581116   | -208.501294  |
| <b>7</b>                              | -153.479948  | 0.056466 | -153.418883 | -153.073673   | -153.012608  |
| <b>10</b>                             | -153.171537  | 0.042733 | -153.124344 | -152.761437   | -152.714244  |
| <b>3/11</b>                           | -153.714173  | 0.050441 | -153.659457 | -153.298195   | -153.243479  |
| <b>12</b>                             | -209.171954  | 0.074025 | -209.092116 | -208.618444   | -208.538607  |
| <b>5' + H<sup>•</sup></b>             |              |          | -209.552783 |               | -208.998212  |
| <b>3 + NH<sub>2</sub><sup>•</sup></b> |              |          | -209.594250 |               | -209.041323  |
| <b>7 + NH<sub>2</sub><sup>-</sup></b> |              |          | -209.238281 |               | -208.671739  |
| <b>10 + NH<sub>3</sub></b>            |              |          | -209.633958 |               | -209.074892  |
| <b>12 + H<sup>•</sup></b>             |              |          | -209.590028 |               | -209.035524  |

<sup>a</sup> Enthalpy was calculated as a sum of enthalpy at 0 K obtained at the QCISD level of theory and the difference between enthalpies obtained at the B3LYP level of theory at 298 K and 0 K. Enthalpies at 0 K correspond to a sum of  $E_{el}$  and  $ZPE$  scaled by 0.9806.

**Table AI-2.** Electronic energies ( $E_{el}$ , in  $E_h$ ), zero-point energies ( $ZPE$ , in  $E_h$ ), and enthalpies ( $H$  at 298 K, in  $E_h$ ) of the stationary points on the protonated aminoethanol radical PES.

|  | B3LYP/6-31G* |          |             | QCISD/cc-pVDZ |              |
|--|--------------|----------|-------------|---------------|--------------|
|  | $E_{el}$     | $ZPE$    | $H_{298K}$  | $E_{el}$      | $H_{298K}^a$ |
| <b>6<sub>1</sub></b>                               | -210.081847  | 0.098289 | -209.976902 | -209.524736   | -209.419791  |
| <b>6<sub>2</sub></b>                               | -210.080807  | 0.097919 | -209.976025 | -209.522010   | -209.417228  |
| <b>8</b>   | -210.075658  | 0.096659 | -209.972070 | -209.523602   | -209.420014  |
| <b>6<sub>1</sub>/8</b>                             | -210.070428  | 0.094324 | -209.969125 | -209.504595   | -209.403292  |
| <b>6<sub>2</sub>/10</b>                            | -210.063741  | 0.094230 | -209.962428 | -209.501626   | -209.400313  |
| <b>9'/8</b>  | -209.962510  | 0.089116 | -209.867410 | -209.398995   | -209.303895  |
| <b>10 · NH<sub>4</sub><sup>+</sup></b>             | -210.106891  | 0.094873 | -210.004133 | -209.548043   | -209.445286  |
| <b>6<sub>1</sub>/13</b>                            | -210.020164  | 0.090317 | -209.923442 | -209.455758   | -209.359037  |
| NH <sub>3</sub> <sup>•+</sup>                      | -56.184377   | 0.032875 | -56.147657  | -56.048011    | -56.011291   |
| NH <sub>4</sub> <sup>+</sup>                       | -56.893889   | 0.049860 | -56.840235  | -56.749059    | -56.695405   |
| <b>9'</b>  | -209.493824  | 0.088388 | -209.400089 | -208.941701   | -208.847965  |
| <b>13</b>  | -209.528423  | 0.089082 | -209.433695 | -208.977700   | -208.882972  |
| <b>9' + H<sup>•</sup></b>                          |              |          | -209.898001 |               | -209.344883  |
| <b>3<sup>b</sup> + NH<sub>3</sub><sup>•+</sup></b> |              |          | -209.892042 |               | -209.344947  |
| <b>7<sup>b</sup> + NH<sub>3</sub><sup>b</sup></b>  |              |          | -209.928497 |               | -209.373256  |
| <b>10<sup>b</sup> + NH<sub>4</sub><sup>+</sup></b> |              |          | -209.964579 |               | -209.409649  |
| <b>13 + H<sup>•</sup></b>                          |              |          | -209.931607 |               | -209.379890  |

<sup>a</sup> Enthalpy was calculated as a sum of enthalpy at 0 K obtained at the QCISD level of theory and the difference between enthalpies obtained at the B3LYP level of theory at 298 K and 0 K. Enthalpies at 0 K correspond to a sum of  $E_{el}$  and  $ZPE$  scaled by 0.9806.

<sup>b</sup> Energy of species in Table AI-1.

**Table AI-3.** Electronic energies ( $E_{el}$ , in  $E_h$ ), zero-point energies ( $ZPE$ , in  $E_h$ ), and enthalpies ( $H$  at 298 K, in  $E_h$ ) of the closed-shell stationary points on the aminoethanol PES and its protonated counterpart.

|           | B3LYP/6-31G* |          |             | QCISD/cc-pVDZ |              |
|-----------|--------------|----------|-------------|---------------|--------------|
|           | $E_{el}$     | $ZPE$    | $H_{298K}$  | $E_{el}$      | $H_{298K}^a$ |
| <b>1</b>  | -210.379581  | 0.099062 | -210.280519 | -209.818276   | -209.719214  |
| <b>11</b> | -153.830122  | 0.055825 | -153.769456 | -153.416121   | -153.355455  |
| <b>14</b> | -210.749742  | 0.113617 | -210.629987 | -210.190933   | -210.071178  |
| <b>15</b> | -210.751489  | 0.112017 | -210.633042 | -210.192425   | -210.073978  |

<sup>a</sup> Enthalpy was calculated as a sum of enthalpy at 0 K obtained at the QCISD level of theory and the difference between enthalpies obtained at the B3LYP level of theory at 298 K and 0 K. Enthalpies at 0 K correspond to a sum of  $E_{el}$  and  $ZPE$  scaled by 0.9806.

## Appendix II

**Table AII -1.** Electronic energies ( $E_{el}$ , in  $E_h$ ), zero-point energies ( $ZPE$ , in  $E_h$ ), and enthalpies ( $H$  at 298 K, in  $E_h$ ) of the stationary points on the PES of **6** interacting with  $NH_3$ .

|   | B3LYP/6-31G* |          |             | QCISD/cc-pVDZ// B3LYP/6-31G* |              |              | QCISD/cc-pVDZ |  |  |
|---|--------------|----------|-------------|------------------------------|--------------|--------------|---------------|--|--|
|   | $E_{el}$     | ZPE      | $H_{298K}$  | $E_{el}$                     | $H_{298K}^a$ | $E_{el}$     | $H_{298K}^a$  |  |  |
| <b>N6<sub>1</sub></b>                           | -266.6720524 | 0.136178 | -266.526318 | -265.9629797                 | -265.817245  | -265.9643276 | -265.818593   |  |  |
| <b>N6<sub>2</sub></b>                           | -266.6728881 | 0.136354 | -266.527399 | -265.9645868                 | -265.819098  |              |               |  |  |
| <b>N8</b>                                       | -266.6669910 | 0.134273 | -266.523166 | -265.9626283                 | -265.818803  | -265.9633573 | -265.819532   |  |  |
| <b>N6<sub>1</sub>/8</b>                         | -266.6475330 | 0.131981 | -266.505510 | -265.927073                  | -265.785050  | -265.9279938 | -265.785971   |  |  |
| <b>N6<sub>2</sub>/10</b>                        | -266.6404667 | 0.132096 | -266.498410 | -265.9221858                 | -265.780129  |              |               |  |  |
| NH <sub>4</sub> <sup>+</sup> · H <sub>2</sub> O | -113.4952168 | 0.086454 | -113.402817 | -113.1951086                 | -113.102709  |              |               |  |  |
| NH <sub>3</sub>                                 | -56.5479480  | 0.034531 | -56.509614  | -56.3989820                  | -56.360648   |              |               |  |  |
| <b>N6</b>                                       | -266.6805301 | 0.135966 | -266.534722 |                              |              | -265.9729183 | -268.827110   |  |  |
| <b>N6/8</b>                                     | -266.6478670 | 0.131930 | -266.505848 |                              |              |              |               |  |  |
| <b>N8</b>                                       | -266.6651118 | 0.133976 | -266.521209 |                              |              |              |               |  |  |

<sup>a</sup> Enthalpy was calculated as a sum of enthalpy at 0 K obtained at the QCISD level of theory and the difference between enthalpies obtained at the B3LYP level of theory at 298 K and 0 K. Enthalpies at 0 K correspond to a sum of  $E_{el}$  and  $ZPE$  scaled by 0.9806.

**Table AII-2.** Electronic energies ( $E_{el}$ , in  $E_h$ ), zero-point energies ( $ZPE$ , in  $E_h$ ), and enthalpies ( $H$  at 298 K, in  $E_h$ ) of the stationary points on the PES of **6** interacting with  $H_2O$ .

|   | B3LYP/6-31G* |          |             | QCISD/cc-pVDZ// B3LYP/6-31G* |             |              | QCISD/cc-pVDZ |              |
|---|--------------|----------|-------------|------------------------------|-------------|--------------|---------------|--------------|
|   | $E_{el}$     | $ZPE$    | $H_{298K}$  | $E_{el}$                     | $H_{298K}$  | $E_{el}$     | $H_{298K}$    | $H_{298K}^a$ |
| <b>O6<sub>1</sub></b>                                   | -286.5241048 | 0.122854 | -286.391514 | -285.7956140                 | -285.663023 | -285.7971178 | -285.664527   |              |
| <b>O6<sub>2</sub></b>                                   | -286.5236545 | 0.122801 | -286.391023 | -285.7951739                 | -285.662542 |              |               |              |
| <b>O8</b>   | -286.5185117 | 0.121637 | -286.387252 | -285.7945845                 | -285.663325 | -285.7953298 | -285.664070   |              |
| <b>O6<sub>1</sub>/8</b>                                 | -286.5045358 | 0.119013 | -286.375634 | -285.7653657                 | -285.636464 | -285.7664262 | -285.637524   |              |
| <b>O6<sub>2</sub>/10</b>                                | -286.4969903 | 0.118998 | -286.368043 | -285.7620284                 | -285.633081 |              |               |              |
| <b>10 · NH<sub>4</sub><sup>+</sup> · H<sub>2</sub>O</b> | -286.5484570 | 0.119920 | -286.418049 | -285.8180018                 | -285.687594 |              |               |              |
| <b>10</b>   | -153.1715370 | 0.042733 | -153.124344 | -152.7614370                 | -152.714244 |              |               |              |
| NH <sub>4</sub> <sup>+</sup> · H <sub>2</sub> O         | -133.3431834 | 0.073716 | -133.262803 | -133.0255954                 | -132.945205 |              |               |              |
| NH <sub>4</sub> <sup>+</sup>                            | -56.8938890  | 0.049860 | -56.840235  | -56.7490590                  | -56.695405  |              |               |              |
| H <sub>2</sub> O  | -76.4089533  | 0.021173 | -76.384001  | -76.2383507                  | -76.213398  |              |               |              |
| <b>O6</b>   | -286.531866  | 0.122745 | -286.399144 |                              |             | -285.8049232 | -285.672201   |              |
| <b>O6/8</b>   | -286.504859  | 0.118877 | -286.376006 |                              |             |              |               |              |
| <b>O8</b>   | -286.5180944 | 0.120991 | -286.387214 |                              |             |              |               |              |

<sup>a</sup> Enthalpy was calculated as a sum of enthalpy at 0 K obtained at the QCISD level of theory and the difference between enthalpies obtained at the B3LYP level of theory at 298 K and 0 K. Enthalpies at 0 K correspond to a sum of  $E_{el}$  and  $ZPE$  scaled by 0.9806.

**Table AII-3.** Electronic energies ( $E_{el}$  in  $E_h$ ), zero-point energies ( $ZPE$ , in  $E_h$ ), and enthalpies ( $H$  at 298 K, in  $E_h$ ) of the stationary points on the PES of **6** interacting with  $\text{CH}_2=\text{NH}$  (**Mi**) as a His model system.

|   | B3LYP/6-31G* |          |             | QCISD/cc-pVDZ// B3LYP/6-31G* |              |              | QCISD/cc-pVDZ |          |              |
|---|--------------|----------|-------------|------------------------------|--------------|--------------|---------------|----------|--------------|
|   | $E_{el}$     | ZPE      | $H_{298K}$  | $E_{el}$                     | $H_{298K}^a$ | $E_{el}$     | $H_{298K}^a$  | $E_{el}$ | $H_{298K}^a$ |
| <b>Mi-6<sub>1</sub></b>                           | -304.7479143 | 0.140766 | -304.596825 | -303.9276518                 | -303.776563  | -303.9291915 | -303.778102   |          |              |
| <b>Mi-6<sub>2</sub></b>                           | -304.7479607 | 0.140785 | -304.596856 | -303.9276962                 | -303.776592  |              |               |          |              |
| <b>Mi-8</b>                                       | -304.7427092 | 0.138951 | -304.593371 | -303.9272162                 | -303.777878  | -303.9280947 | -303.778757   |          |              |
| <b>Mi-6<sub>1</sub>/8</b>                         | -304.7242018 | 0.136688 | -304.576710 | -303.8921398                 | -303.744648  | -303.8932981 | -303.745806   |          |              |
| <b>Mi-6<sub>2</sub>/10</b>                        | -304.7171600 | 0.136693 | -304.569781 | -303.8881872                 | -303.740808  |              |               |          |              |
| NH <sub>4</sub> <sup>+</sup> /CH <sub>2</sub> =NH | -151.5705787 | 0.091026 | -151.472893 | -151.1595873                 | -151.061902  |              |               |          |              |
| CH <sub>2</sub> =NH                               | -94.6272100  | 0.040060 | -94.583296  | -94.3651186                  | -94.321205   |              |               |          |              |
| <b>Mi-6</b>                                       | -304.7562856 | 0.140522 | -304.605116 |                              |              | -303.9376374 | -303.786468   |          |              |
| <b>Mi-6/8</b>                                     | -304.7246446 | 0.136643 | -304.577169 |                              |              |              |               |          |              |
| <b>Mi-8</b>                                       | -304.7412681 | 0.138724 | -304.591933 |                              |              |              |               |          |              |

<sup>a</sup> Enthalpy was calculated as a sum of enthalpy at 0 K obtained at the QCISD level of theory and the difference between enthalpies obtained at the B3LYP level of theory at 298 K and 0 K. Enthalpies at 0 K correspond to a sum of  $E_{el}$  and  $ZPE$  scaled by 0.9806.

**Table AII -4.** Electronic energies (  $E_{el}$  in  $E_h$ ), zero -point energies (  $ZPE$ , in  $E_h$ ), and enthalpies (  $H$  at 298 K, in  $E_h$ ) of the stationary points on the PES of **6** interacting with  $\text{HCO}_2\text{H}$  (**Fo**) as an Asp/Glu model system.

|                                      | B3LYP/6-31G* |          |             | QCISD/cc-pVDZ// B3LYP/6-31G* |              |              | QCISD/cc-pVDZ |              |              |
|--------------------------------------|--------------|----------|-------------|------------------------------|--------------|--------------|---------------|--------------|--------------|
|                                      | $E_{el}$     | $ZPE$    | $H_{298K}$  | $E_{el}$                     | $H_{298K}^a$ | $E_{el}$     | $E_{el}$      | $H_{298K}^a$ | $H_{298K}^a$ |
| <b>Fo-6<sub>1</sub></b>              | -399.8668539 | 0.134393 | -399.721467 | -398.8494295                 | -398.704043  | -398.8494295 | -398.8509321  | -398.705545  | -398.705545  |
| <b>Fo-6<sub>2</sub></b>              | -399.8677820 | 0.134285 | -399.722277 | -398.8501147                 | -398.704610  | -398.8501147 |               |              |              |
| <b>Fo-8</b>                          | -399.8615044 | 0.133011 | -399.717513 | -398.8486099                 | -398.704619  | -398.8486099 | -398.8493544  | -398.705363  | -398.705363  |
| <b>Fo-6<sub>1</sub>/8</b>            | -399.8474167 | 0.130156 | -399.705868 | -398.8198449                 | -398.678296  | -398.8198449 | -398.8207762  | -398.679228  | -398.679228  |
| <b>Fo-6<sub>2</sub>/10</b>           | -399.8394973 | 0.130203 | -399.697744 | -398.8161831                 | -398.674430  | -398.8161831 |               |              |              |
| $\text{NH}_4^+/\text{HCO}_2\text{H}$ | -246.6838406 | 0.085439 | -246.590389 | -246.0774511                 | -246.984000  | -246.0774511 |               |              |              |
| $\text{HCO}_2\text{H}$               | -189.7554604 | 0.033936 | -189.717424 | -189.2957234                 | -189.257687  | -189.2957234 |               |              |              |
| <b>Fo-6</b>                          | -399.8745707 | 0.134419 | -399.729037 |                              |              |              | -398.8586998  | -398.713166  | -398.713166  |
| <b>Fo-6/8</b>                        | -399.8469712 | 0.130137 | -399.705382 |                              |              |              |               |              |              |
| <b>Fo-8</b>                          | -399.8609399 | 0.132438 | -399.717286 |                              |              |              |               |              |              |

<sup>a</sup> Enthalpy was calculated as a sum of enthalpy at 0 K obtained at the QCISD level of theory and the difference between enthalpies obtained at the B3LYP level of theory at 298 K and 0 K. Enthalpies at 0 K correspond to a sum of  $E_{el}$  and  $ZPE$  scaled by 0.9806.



**Table AII-5.** Electronic energies ( $E_{el}$ , in  $E_h$ ), zero-point energies ( $ZPE$ , in  $E_h$ ), and enthalpies ( $H$  at 298 K, in  $E_h$ ) of the stationary points on the PES of **6** interacting with  $\text{HCO}_2^-$  (**Fo**<sup>-</sup>) as a dissociated Asp/Glu model system.

|   | B3LYP/6-31G* |          |             | QCISD/cc-pVDZ <sup>b</sup> |              |
|---|--------------|----------|-------------|----------------------------|--------------|
|   | $E_{el}$     | $ZPE$    | $H_{298K}$  | $E_{el}$                   | $H_{298K}^a$ |
| <b>Fo</b> <sup>-</sup> - <b>6</b> <sub>1</sub>            | -399.4924380 | 0.120882 | -399.361071 | -398.4731622               | -398.341795  |
| <b>Fo</b> <sup>-</sup> - <b>6</b> <sub>1</sub> / <b>8</b> | -399.3712215 | 0.115572 | -399.245262 | -398.3399231               | -398.213964  |
| <b>Fo</b> <sup>-</sup> - <b>8</b>                         | -399.4915734 | 0.119326 | -399.361648 | -398.4752482               | -398.345323  |
| $\text{HCO}_2^-$  | -189.1775625 | 0.020267 | -189.153385 | -188.7049686               | -188.680791  |

<sup>a</sup> Enthalpy was calculated as a sum of enthalpy at 0 K obtained at the QCISD level of theory and the difference between enthalpies obtained at the B3LYP level of theory at 298 K and 0 K. Enthalpies at 0 K correspond to a sum of  $E_{el}$  and  $ZPE$  scaled by 0.9806.

<sup>b</sup> The method used corresponds to QCISD/cc-pVDZ// B3LYP/6-31G\*.

**Table AII-6.** Electronic energies ( $E_{el}$ , in  $E_h$ ), zero-point energies ( $ZPE$ , in  $E_h$ ), and enthalpies ( $H$  at 298 K, in  $E_h$ ) of the stationary points on the PES of protonated aminoethanol.

|                       | B3LYP/6-31G* |          |             | QCISD/cc-pVDZ |              |
|-----------------------|--------------|----------|-------------|---------------|--------------|
|                       | $E_{el}$     | $ZPE$    | $H_{298K}$  | $E_{el}$      | $H_{298K}^a$ |
| <b>6'</b>             | -210.0910820 | 0.098553 | -209.985841 | -209.5355139  | -209.430273  |
| <b>6'</b> / <b>8'</b> | -210.0712105 | 0.094212 | -209.969925 | -209.5055545  | -209.404269  |
| <b>8'</b>             | -210.0757860 | 0.096585 | -209.972412 | -209.5223363  | -209.148962  |

<sup>a</sup> Enthalpy was calculated as a sum of enthalpy at 0 K obtained at the QCISD level of theory and the difference between enthalpies obtained at the B3LYP level of theory at 298 K and 0 K. Enthalpies at 0 K correspond to a sum of  $E_{el}$  and  $ZPE$  scaled by 0.9806.

**Table AII-7.** Electronic energies ( $E_{el}$ , in  $E_h$ ), zero-point energies ( $ZPE$ , in  $E_h$ ), and enthalpies ( $H$  at 298 K, in  $E_h$ ) of the stationary points on the PES of **6** interacting with imidazole (**Im**) as a His model system and acetic acid (**Ac**) as Asp/Glu model system.

|                          | B3LYP/6-31G* |          |             | QCISD/cc-pVDZ <sup>b</sup> |              |
|--------------------------|--------------|----------|-------------|----------------------------|--------------|
|                          | $E_{el}$     | $ZPE$    | $H_{298K}$  | $E_{el}$                   | $H_{298K}^a$ |
| <b>Im-6'</b>             | -436.3542789 | 0.170813 | -436.171692 | -435.1645897               | -434.982003  |
| <b>Im-6'</b> / <b>8'</b> | -436.3203434 | 0.167314 | -436.140979 | -435.1177574               | -434.973576  |
| <b>Im-8'</b>             | -436.3399806 | 0.168842 | -436.159338 | -435.1542189               | -434.938393  |
| <b>Ac-6'</b>             | -439.2049031 | 0.162167 | -439.030120 | -438.0652833               | -438.891948  |
| <b>Ac-6'</b> / <b>8'</b> | -439.1758942 | 0.157994 | -439.004960 | -438.0242586               | -437.853324  |
| <b>Ac-8'</b>             | -439.1914252 | 0.160093 | -439.018576 | -438.0553887               | -437.882540  |

<sup>a</sup> Enthalpy was calculated as a sum of enthalpy at 0 K obtained at the QCISD level of theory and the difference between enthalpies obtained at the B3LYP level of theory at 298 K and 0 K. Enthalpies at 0 K correspond to a sum of  $E_{el}$  and  $ZPE$  scaled by 0.9806.

<sup>b</sup> The method used corresponds to QCISD/cc-pVDZ// B3LYP/6-31G\*.

**Table AII-8.** Pull Mechanism; electronic energies ( $E_{el}$ , in  $E_h$ ), zero-point energies ( $ZPE$ , in  $E_h$ ), and enthalpies ( $H$  at 298 K, in  $E_h$ ) of the stationary points on the PES of **2** interacting with  $\text{OH}^-$  (**O<sup>-</sup>**),  $\text{HCO}_2^-$  (**Fo<sup>-</sup>**) and  $\text{CH}_3\text{CO}_2^-$  (**Ac<sup>-</sup>**) as dissociated Asp/Glu model systems.

|   | B3LYP/6-31G* |          |             | QCISD/cc-pVDZ//<br>B3LYP/6-31G* |              |
|---|--------------|----------|-------------|---------------------------------|--------------|
|   | $E_{el}$     | $ZPE$    | $H_{298K}$  | $E_{el}$                        | $H_{298K}^a$ |
| <b>2O<sup>-</sup></b>                             | -285.5653046 | 0.095182 | -285.461225 | -284.8252480                    | -284.721168  |
| <b>2/3O<sup>-</sup></b>                           | -285.5476777 | 0.091426 | -285.447071 | -284.7975310                    | -284.696924  |
| <b>3O<sup>-</sup>·NH<sub>2</sub><sup>·</sup></b>  | -285.5483634 | 0.090373 | -285.447592 | -284.8001656                    | -284.699394  |
| <b>2Fo<sup>-</sup></b>                            | -398.9451197 | 0.106247 | -398.828651 | -397.9145418                    | -397.798073  |
| <b>2/3Fo<sup>-</sup></b>                          | -398.9155533 | 0.100064 | -398.804904 | -397.8773851                    | -397.766736  |
| <b>3Fo<sup>-</sup>·NH<sub>2</sub><sup>·</sup></b> | -398.9195809 | 0.098596 | -398.808942 | -397.8932858                    | -397.782647  |
| <b>2Ac<sup>-</sup></b>                            | -438.2652801 | 0.134256 | -438.119360 | -437.1150659                    | -436.969146  |
| <b>2/3Ac<sup>-</sup></b>                          | -438.2366910 | 0.128771 | -438.095839 | -437.0778451                    | -436.936993  |
| <b>3Ac<sup>-</sup></b>                            | -382.3520146 | 0.106042 | -382.235957 | -381.3483441                    | -381.232287  |
| <b>NH<sub>2</sub><sup>·</sup></b>                 | -55.8726187  | 0.018974 | -55.849865  | -55.7304220                     | -55.707668   |

<sup>a</sup> Enthalpy was calculated as a sum of enthalpy at 0 K obtained at the QCISD level of theory and the difference between enthalpies obtained at the B3LYP level of theory at 298 K and 0 K. Enthalpies at 0 K correspond to a sum of  $E_{el}$  and  $ZPE$  scaled by 0.9806.

**Table AII-9.** Pull Mechanism; electronic energies ( $E_{el}$ , in  $E_h$ ), zero-point energies ( $ZPE$ , in  $E_h$ ), and enthalpies ( $H$  at 298 K, in  $E_h$ ) of the stationary points on the PES of **2** interacting with  $\text{CH}_2\text{NH}$  (**Mi**) and imidazole (**Im**) as His model systems.

|              | B3LYP/6-31G* |          |             | QCISD/cc-pVDZ//<br>B3LYP/6-31G* |              |
|--------------|--------------|----------|-------------|---------------------------------|--------------|
|              | $E_{el}$     | $ZPE$    | $H_{298K}$  | $E_{el}$                        | $H_{298K}^a$ |
| <b>2Mi</b>   | -304.3592351 | 0.126995 | -304.221727 | -303.5393790                    | -303.401871  |
| <b>2/3Mi</b> | -304.3211060 | 0.122086 | -304.188119 | -303.4963838                    | -303.363397  |
| <b>3Mi</b>   | -248.4458248 | 0.09912  | -248.338054 | -247.7725158                    | -247.664745  |
| <b>2Im</b>   | -435.9491077 | 0.157914 | -435.779537 | -434.7587607                    | -434.589190  |
| <b>2/3Im</b> | -435.9116164 | 0.152875 | -435.746627 | -434.7162543                    | -434.551265  |
| <b>3Im</b>   | -380.0358069 | 0.129769 | -379.896045 | -378.9919651                    | -378.852203  |

<sup>a</sup> Enthalpy was calculated as a sum of enthalpy at 0 K obtained at the QCISD level of theory and the difference between enthalpies obtained at the B3LYP level of theory at 298 K and 0 K. Enthalpies at 0 K correspond to a sum of  $E_{el}$  and  $ZPE$  scaled by 0.9806.

**Table AII-10.** Push-Pull Mechanism; electronic energies ( $E_{el}$ , in  $E_h$ ), zero-point energies ( $ZPE$ , in  $E_h$ ), and enthalpies ( $H$  at 298 K, in  $E_h$ ) of the stationary points on the PES of **6** interacting with model systems for His and Asp/Glu ( $CH_2NH$  and  $HCOO^-$ ; imidazole and  $CH_3COO^-$ ).

|                              | B3LYP/6-31G* |          |             | QCISD/cc-pVDZ |              |
|------------------------------|--------------|----------|-------------|---------------|--------------|
|                              | $E_{el}$     | $ZPE$    | $H_{298K}$  | $E_{el}$      | $H_{298K}^a$ |
| <b>Mi-6-Fo<sup>-</sup></b>   | -494.1428962 | 0.160288 | -493.967221 | -492.8509360  | -492.6752608 |
| <b>Mi-6/8-Fo<sup>-</sup></b> | -494.1177935 | 0.157081 | -493.946857 | -492.8276672  | -492.6567307 |
| <b>Mi-8-Fo<sup>-</sup></b>   | -494.1288556 | 0.161039 | -493.953942 | -492.8432684  | -492.6683548 |
| <b>Im-6-Ac<sup>-</sup></b>   | -665.0634295 | 0.218483 | -664.826266 | -663.2805179  | -663.0433544 |
| <b>Im-6/8-Ac<sup>-</sup></b> | -665.0337881 | 0.215666 | -664.801311 | -663.2539381  | -663.0214611 |
| <b>Im-8-Ac<sup>-</sup></b>   | -665.0437142 | 0.219521 | -664.807268 | -663.2676321  | -663.0311859 |

<sup>a</sup> Enthalpy was calculated as a sum of enthalpy at 0 K obtained at the QCISD level of theory and the difference between enthalpies obtained at the B3LYP level of theory at 298 K and 0 K. Enthalpies at 0 K correspond to a sum of  $E_{el}$  and  $ZPE$  scaled by 0.9806.

## Appendix III

### *Structure labeling code*

*Labels of different rearrangement types:*

- I) Migration of NH<sub>3</sub> group: **6** → **8**; corresponding TS **6/8**.
- II) Elimination of NH<sub>3</sub> group: **6** → **10**; corresponding TS **6/10**.
  - different conformers of the same structure type differ only in suffix number (e.g. **6<sub>1</sub>**, **6<sub>2</sub>**). In case of different OH group conformation, a prime sign is used (e.g. **6'**).
- III) Dissociation – association of NH<sub>2</sub> group: **2** → **3** + NH<sub>2</sub><sup>•</sup> → **4**; corresponding TS **2/3** and **3/4**

*Interaction at the NH<sub>3</sub>- group in 6:*

Depending on the interacting agent, different *prefix* is used:

- for NH<sub>3</sub> label N (where NH<sub>3</sub> interacts with proton from NH<sub>3</sub> group)
- for H<sub>2</sub>O label O (where H<sub>2</sub>O interacts with proton from NH<sub>3</sub> group)
- for CH<sub>2</sub>NH label Mi (where methanimine interacts with proton from NH<sub>3</sub> group)
- for HCOOH label Fo (where formic acid interacts with proton from NH<sub>3</sub> group)
- for HCOO<sup>−</sup> label Fo<sup>−</sup> (where formate interacts with proton from NH<sub>3</sub> group)
- for imidazole label Im (where imidazole interacts with proton from NH<sub>3</sub> group)
- for CH<sub>3</sub>COOH label Asp (where acetic acid interacts with proton from NH<sub>3</sub> group)

*Interaction at the OH- group in 2:*

Depending on the interacting agent, different *suffix* is used:

- for OH<sup>−</sup> label O<sup>−</sup>
- for HCOO<sup>−</sup> label Fo<sup>−</sup>
- for CH<sub>3</sub>COO<sup>−</sup> label Ac<sup>−</sup>
- for CH<sub>2</sub>NH label Mi
- for imidazole label Im

*Interactions at NH<sub>3</sub> and OH groups:*

The above code is employed simultaneously, where the prefix points to the agent interacting with the NH<sub>3</sub> group and the suffix refers to the deprotonating agent at the OH group in **6**.

## 10. References and Notes

- 1 Gee, A. J.; Groen, L. A.; Johnson, M. E. *J. Chromatogr. A* **1999**, 849, 541.
- 2 Cravatt, B. F.; Prospero-Garcia, O.; Suizdac, G.; Gilula, N. B.; Henriksen, S. J.; Boger, D. L.; Lerner, R. A. *Science* **1995**, 268, 1506.
- 3 Thomas, E. A.; Carsonh, M. J.; Neal, M. J.; Sutcliffe, J. G. *Proc. Natl. Acad. Sci. USA* **1997**, 94, 14115.
- 4 Guan, X. Cravatt, B. F. Ehring, G. R. Hall, J. E. Boger, D. L. Lerner, R. A. Gilula, N. B. *J. Cell. Biol.* **1997**, 139, 1785.
- 5 Venance, L.; Piomelli, D.; Glowinski, J.; Glaume, C. *Nature* **1995**, 376, 590.
- 6 Braugher, J. M.; Duncan, L. A.; Chase, R. L. *J. Biol. Chem.* **1986**, 261, 10282.
- 7 (a) Braugher, J. M.; Hall, E. D. *Free Radical Biol. Med.* **1989**, 6, 303. (b) Piotrowski, J. J.; Hunter, G. C.; Eskelson, C. D.; Dubick, M. A.; Bernhard, V. M. *Life Sci.* **1990**, 46, 715. (c) Rousseau, E. J.; Davison, A. J.; Dunn, B. *Free Radical Biol. Med.* **1992**, 13, 407.
- 8 Vajragupta, O.; Monthakantirat, O.; Wongkrajang, Y.; Watanabe, H.; Peungvicha, P. *Life Sci.* **2000**, 67, 1725.
- 9 Hawkins, C. L.; Davies, M. J. *Biochim. Biophys. Acta* **2001**, 1504, 196.
- 10 Barker, H. A.; Weissbach, H.; Smyth, R.D. *Proc. Natl. Acad. Sci. U.S.A.* **1958**, 44, 1093.
- 11 Eggerer, H.; Stadtman, E.R.; Overath, P.; Lynen, F. *Biochem. Z.* **1969**, 333, 1.
- 12 Babior, B. M. *Acc. Chem. Res.* **1975**, 8, 376.
- 13 Abeles, R. H.; Dolphin, D. *Acc. Chem. Res.* **1976**, 9, 114.
- 14 More about the theory and ab initio methods, presented in this chapter, can be found in the following literature: (a) Atkins, P. W. *Molecular Quantum Mechanic*, New York, Oxford University Press, **1983** (b) Hehre, W.J.; Radom, L.; Schleyer P.v.R.; Pople, J.A. *Ab Initio Molecular Orbital Theory*, New York, Wiley-VCH, **1986** (c) Szabo, A.; Ostlund, N. S. *Modern Quantum Chemistry*, New York, McGraw-Hill, **1989** (d) Levine, I. *Quantum Chemistry*, Allyn and Bacon, Boston, 4<sup>th</sup> ed., **1991**
- 15 For DFT, see: Parr, R.G.; Yang, W. *Density-Functional Theory of Atoms and Molecules*, New York, Oxford University Press, **1989**

- 16 For CPMD, see: Marx, D.; Hutter, J. *Ab-initio Molecular Dynamics: Theory and Implementation*, in *Modern Methods and Algorithms in Quantum Chemistry*, Forschungszentrum Jülich, NIC Series, Vol. 1, **2000**
- 17 Tureček, F.; Syrstand, E. A. *J. Am. Chem. Soc.* **2003**, *125*, 3353, and references cited therein.
- 18 McLafferty, F. W. *Anal. Chem.* **1956**, *28*, 306.
- 19 McLafferty, F. W. *Anal. Chem.* **1959**, *31*, 82.
- 20 Kingston, D.; Bursey, J.; Bursey, M. *Chem. Rev.* **1974**, *74*, 223.
- 21 Kreft, D. Grützmacher, H.F. *Eur. J. Mass Spectrom.* **1998**, *4*, 63.
- 22 Loos, J.; Schröder, D.; Zummack, W.; Schwarz, H.; Thissen, R.; Dutuit, O. *Int. J. Mass Spectrom.* **2002**, *214*, 105.
- 23 Schröder, D.; Loos, J.; Semialjac, M.; Weiske, T.; Schwarz, H.; Höhne, G.; Thissen, R.; Dutuit, O. *Int. J. Mass Spectrom.* **2002**, *214*, 155.
- 24 For a full description of the various mass-spectrometric experiments employed, see: ref. 22, 23.
- 25 Gaussian 98, Revision A.7, Frisch, M. J.; Trucks, G. W.; Schlegel, H. B.; Scuseria, G. E.; Robb, M. A.; Cheeseman, J. R.; Zakrzewski, V. G.; Montgomery, J. A., Jr.; Stratmann, R. E.; Burant, J. C.; Dapprich, S.; Millam, J. M.; Daniels, A. D.; Kudin, K. N.; Strain, M. C.; Farkas, O.; Tomasi, J.; Barone, V.; Cossi, M.; Cammi, R.; Mennucci, B.; Pomelli, C.; Adamo, C.; Clifford, S.; Ochterski, J.; Petersson, G. A.; Ayala, P. Y.; Cui, Q.; Morokuma, K.; Malick, D. K.; Rabuck, A. D.; Raghavachari, K.; Foresman, J. B.; Cioslowski, J.; Ortiz, J. V.; Baboul, A. G.; Stefanov, B. B.; Liu, G.; Liashenko, A.; Piskorz, P.; Komaromi, I.; Gomperts, R.; Martin, R. L.; Fox, D. J.; Keith, T.; Al-Laham, M. A.; Peng, C. Y.; Nanayakkara, A.; Gonzalez, C.; Challacombe, M.; Gill, P. M. W.; Johnson, B.; Chen, W.; Wong, M. W.; Andres, J. L.; Gonzalez, C.; Head-Gordon, M.; Replogle, E. S.; Pople, J. A.; Gaussian, Inc., Pittsburgh PA, **1998**
- 26 Koch, W.; Holthausen, M. C. *A Chemist's Guide to Density Functional Theory*, Wiley-VCH, Weinheim, **2000**
- 27 Becke, A. D. *J. Chem. Phys.* **1993**, *98*, 1372 and 5648.
- 28 Lee, C.; Yang, W.; Parr, R. G. *Phys. Rev. B* **1988**, *37*, 785.
- 29 Scott, A. P.; Radom, L. *J. Phys. Chem.* **1996**, *100*, 16502.

- 30 Wong, M. W. *Chem. Phys. Lett.* **1996**, 256, 391.
- 31 *Spartan 3.1*, Wavefunction Inc., Irvine, U. S. A., **1994**
- 32 Brown, R. D.; Godfrey, P. D.; Kleibömer, B. *J. Mol. Spectrosc.* **1987**, 124, 34.
- 33 Marstokk, K.-M.; Møllendal, H.; Samdal, S. *J. Mol. Struct.* **1996**, 376, 11.
- 34 (a) Stevens, E. D. *Acta Cryst. B* **1978**, 34, 544. (b) Ohtaki, H.; Funaki, A.; Rode, B. M.; Reibnegger, G. J. *Bull. Chem. Soc. Jpn.* **1983**, 56, 2116. (c) Olson, L. P.; Li, Y.; Houk, K. H.; Kresge, A. J.; Schaad, L. J. *J. Am. Chem. Soc.* **1995**, 117, 2992.
- 35 (a) Sugawara, Y.; Hamada, Y.; Hirakawa, A. Y.; Tsuboi, M.; Kato, S.; Morokuma, K. *Chem. Phys.* **1980**, 50, 105. (b) Wright, G. M.; Simmonds, R. J.; Parry, D. E. *J. Comput. Chem.* **1988**, 9/6, 600. (c) Wang, X.-C.; Nichols, J.; Feyereisen, M.; Gutowski, M.; Boatz, J.; Haymet, A.D.J.; Simons, J. *J. Phys. Chem.* **1991**, 95, 10419. (d) Sim, F.; St-Amant, A.; Papai, I.; Salahub, D.R. *J. Am. Chem. Soc.* **1992**, 114, 4391. (e) Dive, G.; Dehareng, D.; Ghuysen, J.M. *Theor. Chim. Acta* **1993**, 85, 409. (f) Ou, M.-C.; Chu, S.-Y. *J. Phys. Chem.* **1995**, 99, 556.
- 36 Demetropoulos, I.N.; Gerothanassis, I.P.; Vakka, C.; Kakavas, C. *J. Chem. Soc., Faraday Trans.* **1996**, 92, 921.
- 37 Samdal, S. *J. Mol. Struct.* **1998**, 440, 165.
- 38 Helgaker, T.; Gauss, J.; Jørgensen, P.; Olsen, J. *J. Chem. Phys.* **1997**, 106, 6430.
- 39 Wong, M. W.; Wiberg, K. B. *J. Phys. Chem.* **1992**, 96, 668.
- 40 Hobza, P.; Sponer, J.; Reschel, T. *J. Comput. Chem.* **1995**, 16/19, 1315.
- 41 Novoa, J.J.; Sosa, C. *J. Phys. Chem.* **1995**, 99, 15837.
- 42 See: Henry, D. J.; Radom, L. in Cioslowski, J. (Ed.), *Quantum-mechanical Prediction of Thermochemical Data*, Kluwer, Dordrecht, **2001**, p. 161.
- 43 Loos, J. *Diplomarbeit*, TU Berlin, **2000**
- 44 Curtiss, L.A.; Redfern, P.C.; Raghavachari, K.; Pople, J.A. *J. Chem. Phys.* **1998**, 109, 42.
- 45 Schröder, D.; Loos, J.; Schwarz, H.; Thissen, R.; Preda, D. V.; Scott, L.T.; Caraiman, D.; Frach, M. V.; Böhme, D.K. *Helv. Chim. Acta* **2001**, 84, 1625.
- 46 The absence of imaginary modes in  $\mathbf{1}_3^{++}$  may also result as an artifact of the limited size of the grid used in the B3LYP calculations.
- 47 (a) Frisch, M. J.; Raghavachari, K.; Pople, J.A.; Bouma, W.J.; Radom, L. *Chem. Phys.* **1983**, 75, 323. (b) Yates, B.F.; Nobes, R.H.; Radom, L. *Chem. Phys. Lett.*

- 1985**, 116, 474. (c) Heinrich, N.; Schwarz, H. in Maier, J. P (Ed.), *Ion and Cluster-Ion Spectroscopy and Structure*, Elsevier, Amsterdam, **1989**
- 48 (a) Bouma, W. J.; Radom, L. *Aust. J. Chem.* **1978**, 31, 1167. (b) Heinrich, N. Koch, W. Frenking, G. Schwarz, H. *J. Am. Chem. Soc.* **1986**, 108, 593. (c) Bertrand, W.; Bouchoux, G. *Rapid Commun. in Mass Spectrom.* **1998**, 12, 1697. (d) Mourgues, P. Chamot-Rooke, J. van der Rest, G. Nedev, H. Audier H.E., McMahon, T.B. *Int. J. Mass Spectrom.* **2001**, 210/211, 429. (e) Turecek, F. *J. Am. Chem. Soc.* **2003**, 125, 5954.
- 49 (a) Wu, C.-C.; Lien, M.H. *J. Phys. Chem.* **1996**, 100, 594. (b) Sung, K.; Tidwell, T.T. *J. Am. Chem. Soc.* **1998**, 120, 3043. (c) Sklenak, S.; Apeloig, Y.; Rappoport, Z. *J. Am. Chem. Soc.* **1998**, 120, 10359. (d) Rosenberg, R.E. *J. Org. Chem.* **1998**, 63, 5562. (e) Raspoet, G.; Nguyen, M.T.; Kelly, S.; Hegarty, A.F. *J. Org. Chem.* **1998**, 63, 9669.
- 50 Lin, C.K.; Chen, S.Y.; Lien, M.H. *J. Phys. Chem.* **1995**, 99, 1454.
- 51 (a) Lias, S.G.; Bartmess, J.E.; Liebman, J.F.; Holmes, J.L.; Levin, R.D.; Mallard, W.G. *J. Phys. Chem. Ref. Data* **1988**, 17 Suppl. 1. (b) *NIST Chemistry WebBook*, NIST Standard Reference Database Number 69, Eds. Linstrom, P.J.; Mallard, W.G. July **2001**, National Institute of Standards and Technology, Gaithersburg MD, 20899, USA (<http://webbook.nist.gov>).
- 52 In the isodesmic reactions, processes such as  $\text{RCONH}_2 + n\text{-C}_4\text{H}_9\text{COOH} \rightarrow \text{RCOOH} + n\text{-C}_4\text{H}_9\text{CONH}_2$  were assumed be thermoneutral.
- 53 Mourgues, P.; Chamot-Rooke, J.; Nedev, H.; Audier H.-E. *J. Mass Spectrom.* **2001**, 36, 102.
- 54 An average error of  $\pm 2$  kcal/mol is assigned to the G2 calculations and used in the error estimation.
- 55 Since the relative enthalpies computed at 0 K and 298 K do not differ significantly, the computed values at 0 K (Table 3-4) can be compared with the experimental values derived at the standard conditions.
- 56 Taken from ref. 51b.
- 57 Hunter, E.P.L.; Lias, S.G. *J. Phys. Ref. Data* **1998**, 27, 413.
- 58 Berkowitz, J. Ellison, G.B. Gutman, D. *J. Phys. Chem.* **1994**, 98, 2744.



- 59 No error bar is given because the estimation of the unknown proton affinity of vinylacetamide is ambiguous. Here, PA(vinylacetamide) = PA(acrylamide) = 208 kcal/mol was used.
- 60 Dutuit, O. Alcaraz, C. Gerlich, D. Guyon, P.M. Hepburn, J.W. Metayer-Zeitoun, C. Ozenne, J.B. Weng, T. *Chem. Phys.* **1996**, 209, 177.
- 61 Abebe, M.; Maccoll, A.; Bowen, R.D. *Eur. Mass Spectrom.* **1997**, 3, 197.
- 62 Vékey, K. *J. Mass Spectrom.* **1996**, 31, 445.
- 63 Mason, R.S.; Milton, D.; Harris, F. *J. Chem. Soc. Chem. Commun.* **1987**, 1453.
- 64 Mason, R.S.; Williams, C.M.; Anderson, P.D.J. *J. Chem. Soc. Chem. Commun.* **1995**, 1027.
- 65 Norrman, K.; McMahon, T.B. *Int. J. Mass Spectrom.* **1998**, 176, 87.
- 66 Medved, M.; Cooks, R.G.; Beynon, J.H. *Int. J. Mass Spectrom. Ion Phys.* **1976**, 19, 179.
- 67 Rennekamp, M.E.; Paukstelis, J.V.; Cooks, R.G. *Tetrahedron* **1971**, 27, 4407.
- 68 Semialjac, M.; Loos, J.; Schröder, D.; Schwarz, H. *Int. J. Mass Spectrom.* **2002**, 214, 129.
- 69 Car, R.; Parrinello, M. *Phys. Rev. Lett.* **1985**, 55, 2471.
- 70 (a) Haase, F.; Sauer, J. *J. Am. Chem. Soc.* **1998**, 120, 13503. (b) Rovira, C.; Parrinello, M. *Chem. Eur. J.* **1999**, 5, 250. (c) Rousseau, R.; Marx, D. *Chem. Eur. J.* **2000**, 6, 2982. (d) Dal Peraro, M.; Alber, F.; Carloni, P. *Eur. Biophys. J. Biophys.* **2001**, 30, 75. (e) Magistrato, A.; Pregosin, P.S.; Albinati, A.; Röthlisberger U. *Organometallics* **2001**, 20, 4178. (f) Costuas, K.; Parrinello, M. *J. Phys. Chem. B* **2002**, 106, 4477. (g) Piana, S.; Carloni, P.; Parrinello, M. *J. Mol. Biol.* **2002**, 319, 567. (h) Tuckerman, M. E.; Marx, D.; Parrinello, M. *Nature* **2002**, 417, 925. (i) Gervasio, F. L.; Carloni, P.; Parrinello, M. *Phys. Rev. Lett.* **2002**, 89, 108102. (j) Aktah, D.; Frank, I. *J. Am. Chem. Soc.* **2002**, 124, 3402.
- 71 Hutter, J.; Alavi, A.; Deutsch, T.; Bernasconi, M.; Goedecker, S.; Marx, D.; Tuckermann, M. E.; Parrinello, M. CPMD, version 3.5.1., IBM Research Division, Zürich and MPI für Festkörperforschung, Stuttgart, **1995-1999**.
- 72 Kleinman, L.; Bylander, D. *Phys. Rev. Lett.* **1982**, 48, 1425.
- 73 Troullier, N.; Martins, J. L. *Phy. Rev. B* **1991**, 43, 1993.
- 74 Marx, D.; Spirk, M.; Parrinello, M. *Chem. Phys. Lett.* **1997**, 273, 360.

- 75 (a) Tuckerman M. E., Parrinello M. *J. Chem. Phys.* **1994**, *101*, 1302.  
(b) Tuckerman M.E., Parrinello M. *J. Chem. Phys.* **1994**, *101*, 1316.
- 76 Hehre, W. J.; Ditchfield, R.; Pople, J. A. *J. Chem. Phys.* **1972**, *56*, 2257.
- 77 The temperature was obtained as an average during the CPMD run. Instead of using a thermostat, another common method of adjusting the system to a desired temperature is to use, as the initial temperature for the CPMD simulation, a temperature which is approximately 2 times higher than the desired one. With time evolution the system adjusts to the desired temperature and fluctuates around an average value, which in the present case equals to 519 K.
- 78 Sprik, M. *Chem. Phys.* **2000**, *258*, 139.
- 79 Sprik, M.; Ciccotti, G. *J. Chem. Phys.* **1998**, *109*, 7737.
- 80 The system was adjusted to the particular constraint value within 1000 steps of the simulation. Therefore, the first ca. 1000 steps were not taken into account for an estimation of the average force (average Lagrangian) acting on the system as a result of the constraint introduced in the system. After 1000 steps of the simulation, the average value of the Lagrangian fluctuates around some mean value that is taken for the estimation of the free energy through the integration scheme (for technical details see ref. 78, 79).
- 81 One particular structure cannot be addressed since the picture obtained from the MD simulation is dynamical; even though in the constrained CPMD one geometrical parameter is kept fixed, many different conformers are available due to internal rotations. Since these conformers have similar structures, they can be represented by one structure that corresponds to the whole conformational subspace (e.g. for the conformation with fully relaxed carbon backbone a structure with the label **1<sub>1</sub>** was used).
- 82 Average temperatures of 521 K and 523 K as obtained during the CPMD trajectories.
- 83 For details of the labeling code, see Chapter 3. Superscripts in the labeling scheme point to one specific conformer although in the case of the CPMD studies it is refrained from addressing a particular conformer because of the dynamical picture. Therefore, labeled structures without a superscript represent a conformational subspace.

- 84 A change in only one O-H distance is depicted in the inset in Figure 4-6. The distance between the other hydrogen atom attached to C(4) and oxygen was monitored resulting as well in a picture comparable to the one depicted in the inset in Figure 4-6.
- 85 The short CPMD simulations for a particular value of the constrained parameter lasted for at least 0.9 ps. The system was adjusted to the particular constraint value within ca. 3000 steps of the simulation. Therefore, the first 3000 steps were not taken into account for an estimation of the average force acting on the system as a result of the constraint introduced in the system.
- 86 (a) Frey, P. *Chem. Rev.* **1990**, *90*, 1343. (b) Kräutler, B.; Arigoni, D., Golding, B. T. *Vitamin B<sub>12</sub> and B<sub>12</sub>-Proteins*, Wiley-VCH, Weinheim, **1998**.
- 87 (a) Buckel, W.; Golding, B. T. *Chem. Soc. Rev.* **1996**, *26*, 329. (b) Golding, B. T.; Buckel, W. *Comprehensive Biological Catalysis*, Sinnott, M. L., Ed.; Academic Press, London, **1997**, Vol. 3, p 239. (c) Banerjee, R. *Biochemistry* **2001**, *40*, 6191.
- 88 (a) Eggerer, H.; Stadtman, E. R.; Overath, P.; Lynen, F. *Biochem Z.* **1960**, *333*, 1. (b) Finke, R. G.; Schiraldi, D. A.; Mayer, B. J. *Coord. Chem. Rev.* **1984**, *54*, 1. (c) Wollowitz, S.; Halpern, J. *J. Am. Chem. Soc.* **1984**, *106*, 8319. (d) Halpern, J. *Science* **1985**, *227*, 869. (e) Golding, B. T. *Chem. Br.* **1990**, *26*, 950. (f) Rétey J. *Angew. Chem. Int. Ed. Eng.* **1990**, *29*, 355. (g) Ludwig, M. L.; Matthews, R. G. *Ann. Rev. Biochem.* **1997**, *66*, 269.
- 89 The original name of the enzyme was ethanol deaminase (see ref. 91) but later it was changed to ethanolamine ammonia lyase (EC 4.3.1.7).
- 90 While the actual substrate is 2-aminoethanol, for the sake of shortness, it is abbreviated in the text as aminoethanol.
- 91 Bradbeer, C. *J. Biol. Chem.* **1965**, *240*, 4669.
- 92 Halpern, J.; Kim, S.-H.; Leung, T. W. *J. Am. Chem. Soc.* **1984**, *106*, 8317.
- 93 Hay, B. P.; Finke, R. G. *J. Am. Chem. Soc.* **1987**, *109*, 8012.
- 94 LoBrutto, R.; Bandarian, V.; Magnusson, O., Th.; Chen, X.; Schramm, V., L.; Reed, G. H. *Biochemistry* **2001**, *40*, 9., and references cited therein.
- 95 O'Brien, R. J.; Fox, J. A.; Kopczynski, M. G.; Babior, B. M. *J. Biol. Chem.* **1985**, *260*, 16131.
- 96 Warncke, K.; Ke, S.-C., *J. Am. Chem. Soc.* **1999**, *121*, 9922.

- 97 Warncke, K.; Schmidt, J. C.; Ke, S.-C., *J. Am. Chem. Soc.* **1999**, *121*, 10522.
- 98 Zipse, H. *Acc. Chem. Res.* **1999**, *32*, 571.
- 99 Bouchoux, G.; Djazi, F.; Hguyen, M. T.; Tortajada, J. *J. Phys. Chem.* **1996**, *100*, 3552.
- 100 (a) Smith, D. M.; Golding, B. T.; Radom, L. *J. Am. Chem. Soc.* **1999**, *121*, 1383.  
(b) Smith, D. M.; Golding, B. T.; Radom, L. *J. Am. Chem. Soc.* **1999**, *121*, 9388.
- 101 Smith, D. M.; Golding, B. T.; Radom, L. *J. Am. Chem. Soc.* **2001**, *123*, 5700.
- 102 George, P.; Glusker, J. P.; Bock, Ch. W., *J. Am. Chem. Soc.* **1997**, *119*, 7065.
- 103 Smith, D. M.; Golding, B. T.; Radom, L. *J. Am. Chem. Soc.* **1999**, *121*, 1664.
- 104 Smith, D. M.; Golding, B. T.; Radom, L. *J. Am. Chem. Soc.* **1999**, *121*, 1037.
- 105 Wetmore, S. D.; Smith, D. M.; Radom, L. *J. Am. Chem. Soc.* **2001**, *123*, 8678.
- 106 Banerjee, R. *Chem. Biol.* **1997**, *4*, 175.
- 107 Wetmore, S. D.; Smith, D. M.; Radom, L. *ChemBioChem.* **2001**, *2*, 919.
- 108 Smith, D. M.; Wetmore, S. D.; Radom, L. in Eriksson, L. A. (Ed.), *Theoretical Biochemistry – Processes and Properties of Biological Systems*, Elsevier Science, Amsterdam, **2001**, Chapter 5.
- 109 Henry, D. J.; Radom, L., in Cioslowski, J. (Ed.), *Quantum-Mechanical Prediction of Thermochemical Data*, Kluwer Academic Publishers, Dordrecht, **2001**, Chapter 6.
- 110 Woon, D. E.; Dunning, Jr., T. H. *J. Chem. Phys.* **1993**, *98*, 1358.
- 111 Mayer, P. M.; Parkinson, C. J.; Smith, D. M.; Radom, L. *J. Chem. Phys.* **1998**, *108*, 604.
- 112 Faust, L. P.; Connor, J. A.; Roof, D. M.; Hoch, J. A.; Babior, B. M. *J. Biol. Chem.* **1990**, *265*, 12462.
- 113 Lynch, B. J.; Truhlar, D. G. *J. Phys. Chem. A* **2001**, *105*, 2936.
- 114 Nguyen, M. T.; Creve, S.; Van Quickenborne, L. G. *J. Phys. Chem.* **1996**, *100*, 18422.
- 115 Thümmel, H. T.; Bauschlicher, Jr., C. W. *J. Phys. Chem. A* **1997**, *101*, 1188.
- 116 Chang, Y.-P.; Su, T.-M.; Li, T.-W.; Chaou, I. *J. Phys. Chem. A* **1997**, *101*, 6107.
- 117 Silva, C. F. P.; Duarte, M. L. T. S.; Fausto, R. *J. Mol. Struct.* **1999**, 482-483, 591.
- 118 The **g'Gg'** structure, as defined in ref. 117.

- 119 (a) Smit, B. J.; Nguyen, M. T.; Bouma, W. J.; Radom, L. *J. Am. Chem. Soc.* **1991**, *113*, 6452. (b) Turecek, F.; Cramer, C. J. *J. Am. Chem. Soc.* **1995**, *117*, 12243. (c) Rodríguez-Santiago, L.; Vendrell, O.; Tejero, I.; Sodupe, M.; Bertran, J. *Chem. Phys. Lett.* **2001**, *334*, 112.
- 120 Since an isotope exchange has not been observed between the substrate and the solvent in the vitamin B<sub>12</sub>-dependent rearrangements, the variant of an intermolecular keto-enol tautomerization, catalyzed by an acid or a base, need not to be considered.
- 121 According to the IUPAC rules more appropriate names for these radicals are 2-amino-2-oxoethyl and 2-oxoethyl radicals.
- 122 The  $n\text{-CH}_2\text{CHO}^+$  cation does not exist as a minimum on the PES. As already shown (see ref. 123), the global minimum on the  $\text{C}_2\text{H}_3\text{O}^+$  PES corresponds to the acetyl cation ( $\text{CH}_3\text{CO}^+$ ); thus, its formation was assumed in our investigation as well. At the B3LYP/6-31G\* level of theory the electronic energy of the acetyl cation equals  $-152.923534 E_h$  with a ZPE of  $0.044775 E_h$  and the enthalpy of  $-152.874253 E_h$  at 298 K. The electronic energy obtained by a geometry reoptimizations at the QCISD/cc-pVDZ level of theory amounts to  $-152.531426 E_h$ .
- 123 (a) Nobes, R. H.; Bouma, W. J.; Radom, L. *J. Am. Chem. Soc.* **1983**, *105*, 309. (b) Egsgaard, H.; Carlsen, L. *Chem. Phys. Lett.* **1995**, *236*, 78.
- 124 For  $\text{NH}_2\text{CH}_2\text{CHO}^\bullet$  the electronic energy at the B3LYP/6-31G\* level of theory equals  $-209.120158 E_h$  with a ZPE of  $0.070674 E_h$  and the enthalpy of  $-209.043794 E_h$  at 298 K. At the QCISD/cc-pVDZ level of theory the electronic energy amounts to  $-208.553294 E_h$ .
- 125 The alternative, heterolytic O-H bond cleavage of **6<sub>1</sub>** can be discarded, since the energy of hypervalent aminoethanal radical ( $\text{NH}_3\text{-CH}_2\text{-CH=O}^\bullet$ ; the electronic energy on the B3LYP/6-31G\* level of theory equals  $-209.723439 E_h$  with a ZPE correction of  $0.085502 E_h$  and the enthalpy of  $-209.632144 E_h$  at 298 K; at the QCISD/cc-pVDZ level of theory the electronic energy equals  $-209.166357 E_h$ ) lies 216.3 kcal/mol above **6<sub>1</sub>**.
- 126 The optimization of the IRC structure in the direction of product could not converge because of the formation of two separate species. Thus, the energy of the

- product structure was obtained by combining the energies of the separately optimized structures **10** and  $\text{NH}_4^+$ .
- 127 Faust, L. P.; Babior, B. M. *Arch. Biochem. Biophys.* **1992**, *294*, 50.
- 128 Walling, C.; Johnson, R. A. *J. Am. Chem. Soc.* **1975**, *97*, 2405.
- 129 Weisblat, D. A.; Babior, B. M. *J. Biol. Chem.* **1971**, *246*, 6064.
- 130 Babior, B. M. in Dolphin, D., (Ed.), *B<sub>12</sub>*, Wiley, New York, **1982**; Vol. 2, Chapter 10.
- 131 For  $\text{NH}_2\text{CH}_2\text{CH}_2\text{OH}$ , an experimentally determined enthalpy of formation does not seem to have been reported. In order to obtain the enthalpy of the corresponding radical, the following reaction was used:  $\text{NH}_2\text{CH}_2\text{CH}_2\text{OH} \rightarrow \text{NH}_2\text{CH}_2\text{CHOH}^\bullet + \text{H}^\bullet$ , where all other values are available except for the enthalpy of the C-H bond cleavage; the latter was approximated as the reaction enthalpy of the following reaction:  $\text{CH}_3\text{OH} \rightarrow \text{CH}_2\text{OH}^\bullet + \text{H}^\bullet$ .
- 132 Cioslowski, J.; Schimeczek, M.; Liu, G.; Stoyanov, V. *J. Chem. Phys.* **2000**, *113*, 9377.
- 133 Semialjac, M.; Schwarz, H. *J. Am. Chem. Soc.* **2002**, *124*, 8974.
- 134 Smith, D. M.; Golding, B. T.; Radom, L. *J. Am. Chem. Soc.* **2001**, *123*, 1664.
- 135 Wetmore, S. D.; Smith, D. M.; Bennett, J. T.; Radom, L. *J. Am. Chem. Soc.*, **2002**, *124*, 14054.
- 136 (a) Toraya, T.; Yoshizawa, K.; Eda, M.; Yamabe, T. *J. Biochem.* **1999**, *126*, 650. (b) Toraya, T.; Eda, M.; Kamachi, T.; Yoshizawa, K. *J. Biochem.* **2001**, *130*, 865. (c) Eda, M.; Kamachi, T.; Yoshizawa, K.; Toraya, T. *Bull. Chem. Soc. Jpn.* **2002**, *75*, 1469.
- 137 (a) Simons, T.; Archontis, G.; Karplus, M. *J. Phys. Chem. B* **1999**, *103*, 6142. (b) Czerwinski, R. M.; Harris, T. K.; Massiah, M. A.; Mildvan, A. S.; Whiteman, C. P. *Biochemistry* **2001**, *40*, 1984. (c) Cui, Q.; Karplus, M. *J. Phys. Chem. B* **2002**, *106*, 1768.
- 138 Petersson, E. J.; Choi, A.; Dahan, D. S.; Lester, H. A.; Dougherty, D. A. *J. Am. Chem. Soc.* **2002**, *124*, 12662.
- 139 Maiti, N.; Widjaja, L.; Banarjee, R. *J. Biol. Chem.* **1999**, *274*, 32733.
- 140 Mancia, F.; Keep, N. H.; Nakagawa, A.; Leadlay, P. F.; McSweeney, S.; Rasmussen, B.; Bosecke, P.; Diat, O.; Evans, P. R. *Structure* **1996**, *4*, 339.

- 141 Mancia, F., Evans, P. R. *Structure with Folding & Design* **1998**, 6, 711.
- 142 Loferer, M. J.; Webb, B. M.; Grant, G. H.; Lied, K. R. *J. Am. Chem. Soc.*, **2003**, 125, 1072.
- 143 Madhavapeddi, P.; Marsh, E. N. G. *Chem. Biol.* **2001**, 8, 1143.
- 144 Wetmore, S. D.; Smith, D. M.; Golding, B. T.; Radom, L. *J. Am. Chem. Soc.*, **2001**, 123, 7964.
- 145 The QCISD enthalpies at 298 K were computed as follows:  $\Delta H$  (QCISD; 298 K) =  $\Delta H$  (QCISD; 0 K) +  $\Delta H$  (B3LYP; 298K) –  $\Delta H$  (B3LYP; 0K), where enthalpies at 0 K include the sum of the electronic energy and ZPE corrections scaled by 0.9806.
- 146 For the sake of shortness, it is the pH of the reaction environment around the enzyme's active site which is meant when the phrase "pH in the active site" is used. For a superb discussion of this and related aspects, see: Barril, X.; Alemán, C.; Orozco, M.; Luque, F. J. *Proteins* **1998**, 32, 67.
- 147 Warshel, A. *Biochemistry* **1981**, 20, 3167.
- 148 Bandarian, V.; Reed, G. H. *Biochemistry* **1999**, 38, 12394.
- 149 (a) Pauling, L. *Chem. Eng. News* **1946**, 24, 1375. (b) Pauling, L. *Am. Sci.* **1948**, 36, 51.
- 150 (a) Dawson, R. M. C.; Elliott, D. C.; Elliott, W. H.; Jones, K. M.; *Data for Biochemical Research*, Oxford, Oxford Science Publication, 3<sup>rd</sup> Ed., **1986** (b) Perrin, D. D.; Dempsey, B.; Serjeant, E. P. *pKa Prediction for Organic Acids and Bases*, London, Chapman and Hall Publishers, **1981**.
- 151 pKa (Asp) = 3.9, pKa (Glu) = 4.1, taken from ref. 150.
- 152 (a) Smith, B. J.; Tho, N. M.; Bouma, W. J.; Radom, L. *J. Am. Chem. Soc.* **1991**, 113, 6452. (b) Turecek, F.; Cramer, C. J. *J. Am. Chem. Soc.* **1995**, 117, 12243.
- 153 (a) Campbell, S.; Rodgers, M. T.; Marzluff, E. M.; Beauchamp, J. L. *J. Am. Chem. Soc.* **1995**, 117, 12840. (b) Zheng, Y.-J.; Ornstein, R. L. *J. Am. Chem. Soc.* **1996**, 118, 11237. (c) Schnier, P. D.; Price, W. D.; Jockusch, R. A.; Williams, E. R. *J. Am. Chem. Soc.* **1996**, 118, 7175. (d) Freitas, M. A.; Marshall, A. G. *Int. J. Mass. Spectrom.* **1999**, 182/183, 221. (e) Jockusch, R. A.; Lemoff, A. S.; Williams, E. R. *J. Am. Chem. Soc.* **2001**, 123, 12255.
- 154 Conformational aspects for the interaction of **6'** with HCOO<sup>−</sup> will not be included due to the very high activation enthalpy associated with the migration pathway.

- 155 (a) Curtin, D. Y. *Rec. Chem. Prog.* **1954**, *15*, 111. (b) Winstein, S.; Holness, N. *J. J. Am. Chem. Soc.* **1955**, *77*, 5562.
- 156 In Chapter 5 this type of rearrangement was described as “dissociation - association mechanism”.
- 157 The barrier for the NH<sub>2</sub> dissociation process can be either estimated by locating a transition structure commencing from the (most) stable conformer **2<sub>2</sub>**, or equivalently, calculating the activation enthalpy for the dissociation starting from the conformer in which the H-bond interaction does not exist and adding the energy difference between the two reactant conformers. Here, the latter method was used.
- 158 PA(Asp) = 217.2 kcal/mol and PA(Glu) = 218.2 kcal/mol vs. PA(CH<sub>3</sub>COOH) = 187.3 kcal/mol, PA(HCOOH) = 177.3 kcal/mol, PA(H<sub>2</sub>O) = 165.0 kcal/mol; PA(His) vs. PA (imidazole) = 225.3 kcal/mol, PA(CH<sub>2</sub>NH) = 203.8 kcal/mol, PA(NH<sub>3</sub>) = 204.0 kcal/mol. All data taken from ref. 51b.
- 159 For example, the optimal pH for catalytic activity of related glutamate mutase falls into the range 7.5 – 8; see ref. 143.
- 160 (a) Halpern, J. *Pure Appl. Chem.* **1983**, *55*, 1059. (b) Toraya, T.; Ishida, A. *Biochemistry*, **1988**, *27*, 7677. (c) Pratt, J. M. *Pure Appl. Chem.* **1993**, *65*, 1513. (d) Waddington, M. D.; Finke, R. G. *J. Am. Chem. Soc.* **1993**, *115*, 4629. (e) Brown, K. L.; Li, J. *J. Am. Chem. Soc.* **1998**, *120*, 9466.
- 161 Marzilli, L.G.; Summers, M. F.; Bresciani-Pahor, N.; Zangrando, E.; Charland, J.-P.; Randaccio, L. *J. Am. Chem. Soc.* **1985**, *107*, 6880.
- 162 Bresciani-Pahor, N.; Forcolin, M.; Marzilli, L. G.; Randaccio, L.; Summers, M. F.; Toscano, P. J. *Coord. Chem. Rev.* **1985**, *63*, 1.
- 163 Zhu, L.; Kostic, N. M. *Inorg. Chem.* **1987**, *26*, 4194.
- 164 (a) Tamao, Y.; Blakley, R. *Biochemistry* **1973**, *12*, 24. (b) Orme-Johnson, W. H.; Beinert, H.; Blakley, R. L. *J. Biol. Chem.* **1974**, *249*, 2338. (c) Zhao, Y.; Such, P.; Retey, J. *Angew. Chem., Int. Ed. Engl.* **1992**, *31*, 215.
- 165 Padmakumar, R.; Padmakumar, R.; Banerjee, R. *Biochemistry* **1997**, *36*, 3713.
- 166 Stubbe, J.; van der Donk, W. A. *Chem. Rev.* **1998**, *98*, 705.
- 167 (a) Bandarian, V.; Poyner, R. R.; Reed, G. H. *Biochemistry* **1999**, *38*, 12403. (b) Warncke, K.; Utada, A. S. *J. Am. Chem. Soc.* **2001**, *123*, 8564.



- 168 (a) Carty, T. J.; Babior, B. M.; Abeles, R. H. *J. Biol. Chem.* **1971**, *246*, 6313. (b) Carty, T. J.; Babior, B. M.; Abeles, R. H. *J. Biol. Chem.* **1974**, *249*, 1683.
- 169 (a) Frey, P. A.; Essenberg, M. K.; Abeles, R. H. *J. Biol. Chem.* **1967**, *242*, 5369. (b) Essenberg, M. K.; Frey, P. A.; Abeles, R. H. *J. Am. Chem. Soc.* **1971**, *93*, 1242.
- 170 Cleland, W. W. *Crit. Rev. Biochem.* **1982**, *13*, 385.
- 171 (a) Booker, S.; Licht, S.; Broderick, J.; Stubbe, J. *Biochemistry* **1994**, *33*, 12676. (b) Licht, S.; Gerfen, G. J.; Stubbe, J. *Science* **1996**, *271*, 477. (c) Gerfen, G. J.; Licht, S.; Willems, J.-P.; Hoffman, B. M.; Stubbe, J. *J. Am. Chem. Soc.* **1996**, *118*, 8192. (d) Licht, S.; Booker, S.; Stubbe, J. *Biochemistry* **1999**, *38*, 1221. (e) Stubbe, J. *Chem. Comm.* **2003**, 2511.
- 172 Semialjac, M.; Schwarz, H. *J. Org. Chem.* **2003**, *68*, 6967.
- 173 Khoroshun, D. V.; Warncke, K.; Ke, S.-C.; Musaev, D. G.; Morokuma, K. *J. Am. Chem. Soc.* **2003**, *125*, 570.
- 174 The enthalpies at 298 K were computed as follows:  $\Delta H$  (MP2/6-311++G\*\*; 298 K) =  $\Delta H$  (MP2/6-311++G\*\*; 0 K) +  $\Delta H$  (B3LYP/6-31G\*; 298K) –  $\Delta H$  (B3LYP/6-31G\*; 0K), where enthalpies at 0 K include the sum of the electronic energy and ZPE corrections scaled by 0.9806.
- 175 (a) Reitzer, R.; Gruber, K.; Jogl, J.; Wagner, U. G.; Bothe, H.; Buckel, W.; Kratky, C. *Structure* **1999**, *7*, 891. (b) Gruber, K.; Reitzer, R.; Kratky, C. *Angew. Chem., Int. Ed. Engl.* **2001**, *40*, 3377. (c) Gruber, K.; Kratky, C. *Curr. Opin. Chem. Biol.* **2002**, *6*, 598.
- 176 Savage, H. F. J.; Lindley, P.F.; Finney, J. L.; Timmins, P. A. *Acta Crystallogr.* **1987**, *B43*, 280.
- 177 While the correct name for the model employed is (2S,3R,4S)-2-methyl-3,4-dihydroxytetrahydrofuran, an abbreviated version derived from the structurally related ribose, i.e. 1,5-dideoxyribose will be used. For details concerning the configurations at the C2, C3 and C4 centers (as well as the numbering of the atoms) and the nature of the intramolecular H-bond between the two OH-groups, see Scheme 7-2C.
- 178 Similarly, IRC computations from the TSs in the direction of a product led to complexes between **2** and 1,5-dideoxyribose (**2**\***A**<sub>1</sub> and **2**\***A**<sub>2</sub>; Table 7-1); these are

- slightly less stable (each 0.2 kcal/mol) than the separate species **2** and 1,5-dideoxyribose (C3- or C2-endo conformers).
- 179 Because of the pronounced structural similarities of the TSs for the reactions with the C3- and C2-endo conformers, only those involving the C3-endo conformer of the 1,5-dideoxyribose are depicted in Figure 7-2.
- 180 IRC computations commencing from **H-TS<sub>2</sub>** in the direction of a product did not converged into a complex, but because of otherwise strong similarities between the two conformers involved in this reaction, it might be postulated to exist. Since the main interest concerns the barriers of the hydrogen abstractions, it has been refrained from an exhausting search for this kind of a product complex.
- 181 Commencing from **Mi-TS<sub>2</sub>** in the direction of a product, the IRC computations did not converged into a complex. See ref. 180.

## Publication Index

1. Semialjac, M.; Loos, J.; Schröder, D.; Schwarz, H. *Int. J. Mass Spectrom.* **2002**, 214, 129.  
*Dissociation behavior of ionized valeramide. Part II: Theoretical exploration of the potential-energy surface*
2. Schröder, D.; Loos, J.; Semialjac, M.; Weiske, T.; Schwarz, H.; Höhne, G.; Thissen, R.; Dutuit, O. *Int. J. Mass Spectrom.* **2002**, 214, 155.  
*Dissociation behavior of ionized valeramide. Part III: An unprecedented temperature effect on the C<sub>3</sub>/C<sub>2</sub> branching ratio and its implications for metastable ion dissociations*
3. Semialjac, M.; Schwarz, H. *J. Am. Chem. Soc.* **2002**, 124, 8974.  
*Computational exploration of rearrangements related to the vitamin B<sub>12</sub>-dependent ethanolamine ammonia lyase catalyzed transformation*
4. Schröder, D.; Soldi-Lose, H.; Semialjac, M.; Loos, J.; Schwarz, H.; Eerdeken, G.; Arnold, F. *Int. J. Mass Spectrom.* **2003**, 228, 35.  
*On gaseous C<sub>4</sub>H<sub>6</sub>O<sub>2</sub> compounds in the Earth atmosphere: New insights from collision experiments of the protonated molecules in the laboratory and on aircraft*
5. Schröder, D.; Semialjac, M.; Schwarz, H. *Eur. J. Mass Spectrom.* **2003**, 9, 287.  
*Potential role of methyl-radical adducts with carbon dioxide in the Martian atmosphere*
6. Semialjac, M.; Schwarz, H. *J. Org. Chem.* **2003**, 68, 6967.  
*Computational study on mechanistic details of the aminoethanol rearrangement catalyzed by the vitamin B<sub>12</sub>-dependent ethanolamine ammonia lyase: His and Asp/Glu acting simultaneously as catalytic auxiliaries*
7. Semialjac, M.; Schröder, D.; Schwarz, H. *Chem. Eur. J.* **2003**, 9, 4396.  
*Car-Parrinello molecular dynamics study of the rearrangement of the valeramide radical-cation*
8. Schröder, D.; Semialjac, M.; Schwarz, H. *Int. J. Mass Spectrom.*, in press.  
*Secondary kinetic isotope effects in cation-bound dimers of acetone (C<sub>3</sub>H<sub>6</sub>O)M(C<sub>3</sub>D<sub>6</sub>O)<sup>+</sup> with M = H, Li, Na, K, Rb, Ag, and Cs*
9. Semialjac, M.; Schwarz, H. *Chem. Eur. J.*, in press.  
*Computational investigation on the hydrogen abstraction from 2-aminoethanol by 1,5-dideoxyribose-5-yl radical: A model study of a reaction occurring in the active site of ethanolamine ammonia lyase*



## Curriculum Vitae

Marija Semialjac

born on March 8<sup>th</sup> 1977 in Varaždin, Croatia

Croatian, single

## Educational Background and Previous Position

- from 02/2001 *Ph.D. student* at the Technische Universität Berlin, Institut für Chemie, in the group of Prof. Dr. Helmut Schwarz:  
Ph.D. Thesis: "Computational Studies on the Rearrangement Reactions of Some Biologically Relevant Radicals"
- 04/2002 Research stay in the group of Prof. Dr. Michele Parrinello, Swiss Center for Scientific Computing (Lugano, Switzerland)
- 10/1999 - 02/2001 *Research Assistant* at the University of Zagreb, Faculty of Science, Chemistry Department (Zagreb, Croatia)
- 10/1995 - 09/1999 Chemistry Studies at the University of Zagreb, Faculty of Science (Zagreb, Croatia)  
Diploma Thesis: "7-Norbornanone-oxime Rearrangement in Superacids"
- 09/1991 - 06/1995 Secondary chemical school (Varaždin, Croatia)
- 09/1983 - 07/1991 Primary school (Varaždin, Croatia)

## Fellowships/Awards

- 2002 - 2003 Ph.D. Fellowship of the Schering Research Foundation
- 1999 The University of Zagreb Rector's Award for the best student's research project
- 1998, 1999 The Dean's Award for the best chemistry student at the Faculty of Science
- 1998 - 1999 The fellowship of the City of Zagreb for the state's best students

## Professional Skills

Languages: English (fluent), German (very good), Croatian (mother-tongue)

Computer-operating Systems: Windows, Macintosh, Linux, Unix

Programming: Fortran

Chemical Software: Gaussian, Gamess, CPMD

## Personal Interests

literature, classical music, dancing (salsa, tango argentino), travelling

